POLITECNICO DI MILANO

PhD School of Politecnico di Milano

Doctoral Program in Environmental and Infrastructure Engineering - XXVI CYCLE

Department of Civil and Environmental Engineering – Environmental Area

HEAVY METAL REMOVAL FROM WATER: CHARACTERIZATION AND APPLICABILITY OF UNCONVENTIONAL MEDIA

Doctoral Dissertation of:

Arianna CATENACCI

PhD Advisor: Ing. Manuela *ANTONELLI*

PhD Tutor: Prof. Roberto CANZIANI

PhD Coordinator: Prof. Alberto GUADAGNINI

March 2014

Contents

Acknowledgments

To Prof. *Paolo Ferruti* and Prof. *Elisabetta Ranucci*, Department of Organic and Industrial Chemistry, Università degli Studi di Milano (IT) and to for designing and synthesizing PolyAmidoAmine Hydrogel samples.

To Prof. *Francesco Sannicolò*, Laboratori Alchemia, Milano (IT) for scaling-up the synthesis process of PolyAmidoAmine Hydrogels and providing high amounts of samples.

To Prof. *Orlando Coronell* for receiving me at the University of North Carolina at Chapel Hill (USA), as a PhD Visiting Student, and for involving me in the experimental work at the Orlando Coronell Research Group, Environmental Sciences and Engineering Department.

Abstract

Heavy metals and metalloids can have severe implications on environmental and human health: according to the World Health Organization, Cr, Ni, Cu, Pb, Hg and Zn are those of most immediate concern. The majority of toxic metal pollutants are waste products of industrial and metallurgical processes: due to the increasing diffusion and variety of heavy metals in natural water supplies, more restrictive legal limits were recently defined. Specifically-designed technologies are required to support conventional processes, such as chemical precipitation, coagulation/flocculation, ion exchange, adsorption, and membrane filtration, and improve removal efficiencies and selectivity to comply with new standards. In fact, conventional treatment techniques lack specificity, resulting in several disadvantages mainly related to low affinity and selectivity and long equilibrium processes: such conditions often produce increased costs.

Since much attention is to be focused on innovative and specific water treatment technologies, new/unconventional media for the removal of organic and inorganic micropollutants are today of great interest in the research world.

In this background, two granular media for the removal of heavy metals from water were tested at laboratory scale: PolyAmidoAmine Hydrogels (PAAH) and KDF®55 Granular Brass Media (KGBM). They both remove heavy metals from water, by using two different mechanisms of interaction with pollutants: hydrogels create complex bonds between active groups and heavy metal ions, while granular brass media, through a redox reaction, exchange electrons with contaminants, changing them into harmless components. Since few information concerning their removal abilities are provided in literature, an experimental plan for a first screening has been designed and implemented on both PAAH and KGBM, thus including kinetics, isotherms, selectivity tests and experiments for the assessment of the influence of different water constituents, aimed at both the description of the solute removal process and the achievement of information for the selection and design of water treatment processes. In order to gain these two goals, by using a strategy that moves from the microscopic to the macroscopic world and viceversa, two main features were studied:

1. the identification of chemical reactions occurring among solute and media, useful to define the field of application (type and form of contaminants) and to evaluate the influence of water characteristics (pH, interferences) on metal removal efficiency;
2. the description of the physical processes of diffusion involved in the removal of solutes in order to study the influence of process parameters (initial concentrations, dose of media) and to identify and improve suitable process units.

PAAH are synthetic polymers designed by the Department of Organic and Industrial Chemistry (Università degli Studi di Milano, IT) and characterized by the presence of amido and tertiary amine groups along the macromolecular chain. The high structural versatility of PAAH offers interesting opportunities for designing media devoted to the removal of particular contaminants; however, no engineering applications in this field have been reported so far. Two samples of PAAH, termed MBA/EDA and MBA/CYS, were synthesized and supplied into two different particle dimensions, powder ($d<1mm$) and grains ($1mm<d<2mm$). After an initial physical characterization, kinetics, isotherms and selectivity tests were performed at different doses and initial solute concentrations for two metals: copper, Cu(II) tested on both structures, and hexavalent chromium, Cr(VI) tested only on MBA/EDA structure since no significant removal has been observed for MBA/CYS. The two ions were selected because their positive and negative charges are supposed to involve different active groups along the chains of the polymers, thus resulting in different removal mechanisms. In order to gain information concerning the chemical reactions involving copper ions and PAAH active groups, the influence of pH was also investigated.

KDF Fluid Treatment Inc. manufactures (Three Rivers, Michigan 49093-9287, USA) provided the KGBM, an high-purity copper-zinc formulation. Unlike PAAH, KGBM is currently used in a variety of treatment units both at the Point-of-Entry (POE) and Point-of-Use (POU) application. Kinetics of copper removal was performed in order to define the influence of water characteristics on redox reactions involving copper and zinc. Specifically, since water constituents could result in the creation of Cu-complexes, the pH and the presence of dissolved inorganic (hydroxides, OH^- and carbonates, $CO_3^=$) and organic (EDTA, a humic acid, two different fulvic acids and a specific type of NOM, Natural Organic Matter) compounds were investigated: complexes decrease the percentage of copper dissolved in water as divalent copper ions directly available for redox reactions. Also, different types and amounts of ligands dissolved in water can affect Cu(II) removal.

Experimental results allow to quantify the main properties of the media in terms of process rates, amounts of solute removed, parameters influencing the process and interference mechanisms. As for PAAH, MBA/EDA structure, besides its considerable volume expansion, proved to be more suitable because of its affinity towards both anion and cation, faster kinetic rates and easier synthesis process. Unlike the starting solute concentration (range: 16 - 64 μM) that shows scarce influence on results, the pH and the dose of PAAH adopted determine the removal process. In regards to KGBM, both the pH, the form of contaminants and the presence of other compounds dissolved in water, greatly influence the removal rates of Cu and the process of brass corrosion, quantified by the measurement of Zn released into water.
Moving from a macroscopic to a microscopic interpretation of data, by using specific models and statistical techniques for data analysis, it's been possible to attempt a first description of the chemical and physical processes characterizing the two media, thus giving rise to new, interesting and unknown issues that would allow the achievement of a more detailed understanding of the media itself. For example, as for PAAH, both tested structures remove similar amounts of solutes but MBA/EDA is faster than MBA/CYS: the interpretation of kinetics and isotherm data with specific models suggests that the removal process involves the entire volume of particles and the diffusion of ions inside pores: because of the presence of both macropores and micropores, MBA/CYS acts slower if compared to MBA/EDA that, when in water, greatly opens its molecular chains thus facilitating the diffusion of solutes through the pores towards active groups. Differences in the removal abilities of Cu(II) and Cr(VI) are to be ascribed to steric or charge interferences that determine the diffusion of ions through pores: an in-depth analysis would allow to include in the diffusion model not only the properties of hydrogels (pore size, expansion degree) but also the characteristics of solutes (charge and dimensions of ions). As for KGBM, redox reactions occurring at the microscopic scale only partially explain the entire process. A statistical analysis on data, performed using a stepwise multiple regression, contributed: to verify the occurrence of other possible processes; to identify further constituents and range of concentrations to be further tested in order to define, on the one hand, the relationship existing between the removal of Cu and the release of Zn and to create, on the other hand, a model describing KGBM and the chemical processes characterizing its behavior in aqueous solutions.

Outline of Thesis

An introduction dealing with issues related to the increasing presence of heavy metals and metalloids and the need for further efforts in the development and characterization of new adsorbent/reactive media for the treatment of inorganic contaminated waters is reported in CHAPTER 1. It includes details on specific topics in order to provide useful information for the understanding of the experimental plan designed and the interpretation of test results: copper and chromium chemistry and occurrence in water, properties, research works and/or field applications of PolyAmidoAmine Hydrogels (PAAH) and KDF Granular Brass Media (KGBM), kinetic and isotherm models generally used for the characterization of adsorbent/reactive media.

CHAPTER 2 deals with main reasons and objectives of the research activities and introduces and explains the experimental plan designed for the two tested media, PolyAmidoAmine Hydrogels and KDF Granular Brass Media: type of tests and operating conditions selected are here summarized in order to provide an overall view of the experimental characterization of media.

Results are presented in 6 chapters, from CHAPTER 3 to CHAPTER 8: experimental methods, raw and processed data are shown in tables and figures and deeply explained in the text. Conclusions are drawn for each chapter based on the starting purpose of the experimental work. Results concerning PAAH samples are reported from CHAPTER 3 to CHAPTER 6: specifically, the first two chapters describes data on copper and chromium removal from a more practical and applicable point of view, while considerations pertaining the removal processes involved from a physical and chemical point of view are given in CHAPTERS 5 and 6. The last two chapter reports upon the kinetic studies on KGBM, separately as for the influence on copper removal of inorganic water compounds, in CHAPTER 7, and of organic compounds in CHAPTER 8 .

APPENDIXES 1 to 3 report further data and results useful to both complete the set of data and justify specific choices taken for the design of the experimental plan.

1 State of the art

The present chapter deals with the issue due to the increasing presence of heavy metals and metalloids in water. Following to a short introduction including information about international regulations on heavy metals in water (par. 1.1.1), a focus on copper and chromium chemistry and occurrence in water is reported in paragraphs 1.1.2 and 1.1.3 respectively: copper and chromium, two different charged and sized heavy metals ions, were selected to be tested for their removal from low contaminated aqueous solution, thus simulating Point-Of-Entry (POE) and Point-Of-Use (POU) applications in the drinking water treatment field. Traditional and innovative technologies for the removal of heavy metals and metalloids from water are shortly described mainly explaining advantages and disadvantages for each of them. A specific paragraph is reported pertaining recent trends in the development of new adsorbent/reactive materials (par. 1.2.2), in order to introduce the two granular media tested to achieve information about their removal abilities on copper and chromium: PolyAmidoAmine Hydrogels, PAAH (par. 1.2.2.2) and KDF Granular Brass Media, KGBM (par. 1.2.2.3). Sorption/reactive media were investigated to assess their suitability for application in the field of water pollution control: the sorption capacity and required contact time are two of the most important parameters to understand: to this purpose, par. 1.3 gives an overview on kinetic and isotherm models used to fit data and investigate the removal mechanisms involved in copper and chromium uptake by means of PAAH and KGBM.

1.1 Heavy metals and metalloids in water

Heavy metals are elements having atomic weights between 63.5 and 200.6 g/mol, and a specific gravity greater than 5.0 g/cm^3. Heavy metals are natural components of the earth's crust and exist in surface waters in colloidal, particulate and dissolved phases (Fu and Wang, 2010, Vinodh, 2011, Kennish, 1992). The colloidal and particulate metal may be found as hydroxides, oxides, silicates, sulfides or adsorbed to clay, silica and organic matter, displaying a high affinity for humic acids, organo-clays, and oxides coated with organic matter. The soluble forms are generally ions or unionized organometallic chelates or complexes, although dissolved concentrations are generally low. The solubility of trace metals in waters is mainly controlled by the water pH, the type and concentration of ligands, the oxidation state of the mineral components and the redox environment of the system (Connell et al., 1984).

Because of their high solubility in the aquatic environments, heavy metals can be absorbed by living organisms; however unlike organic contaminants, they are not biodegradable and tend to accumulate in living organisms. Once they enter the food chain, large concentrations of heavy metals may accumulate in the human body (Barakat, 2011, Fu and Wang, 2012). As a trace element, some heavy metals (e.g. selenium, cobalt, copper, iron, manganese, molybdenum, vanadium, strontium and zinc) are essential to maintain the metabolism of living organisms. However, at higher concentrations they may pose a health risk to humans and to the environment and lead to poisoning (Vinodh, 2011). Non-essential heavy metals of particular concern to surface water are cadmium, chromium, mercury, lead, arsenic, and antimony (Kennish, 1992). Also, trace metals such as lead and cadmium interfere with essential nutrients of similar appearance, such as calcium and zinc (Kurniuwan et al., 2006).

Heavy metals in surface water can originate from natural or anthropogenic sources: currently, anthropogenic inputs of metals exceed natural inputs. Sources can be furthermore divided into two categories: nonpoint and point sources. Natural inputs are generally classified as nonpoint sources: chemical and physical weathering of igneous and metamorphic rocks and soils often releases heavy metals; other contributions include the decomposition of plant and animal detritus,

precipitation or atmospheric deposition of airborne particles from volcanic activity, wind erosion, forest fire smoke, plant exudates, and oceanic spray (Kennish, 1992). Anthropogenic inputs include both nonpoint and point sources. The surface runoff from mining operations and the urban stormwater runoff containing metals from roadways and atmospheric fallout are examples for the first category, while point sources mainly consists of industrial effluents, waste sludges and domestic wastewater containing metals from metabolic wastes, corrosion of water pipes and consumer products (Connell et al., 1984).

1.1.1 International standard and guidance values for heavy metals in drinking water

Because of the rapid development of industries such as metal plating facilities, mining operations, fertilizer industries, tanneries, batteries, paper industries and pesticides, etc., heavy metals wastewaters are directly or indirectly discharged into the environment, thus affecting the quality of many water resources for drinking water supply. Faced with more and more stringent regulations, nowadays heavy metals are among the environmental priority pollutants and are becoming one of the most serious environmental problems (Fu and Wang, 2010). As a consequence, many developed countries specify standards to be applied in their own country. In Europe, this includes the European Drinking Water Directive and in the USA the United States Environmental Protection Agency (EPA) establishes standards as required by the Safe Drinking Water Act; China adopted its own drinking water standard in 2002. For countries without a legislative or administrative framework for such standards, the World Health Organization publishes guidelines on the standards ("Guideline Value") that should be achieved (WHO, 2011) forming an authoritative basis for the setting of national regulations and standards for water safety in support of public health. Table 1.1 compares guideline/standard values set by different international or national authorities for the main heavy metals or metalloids that are of health significance in drinking water.

Table 1.1. Drinking water guideline/standard concentrations for heavy metals set by the World Health Organization (WHO), the U.S. Environmental Protection Agency (USEPA), the European Union (EU) and Italian government (ITA).

CONTAMINANT	UNIT	Guideline Value (WHO)	MCL (USEPA)	Quality Standard (EU) [1]	Quality Standard (ITA) [2]
Antimony	µg/L	20	6	5	5
Arsenic	µg/L	10	10	10	10
Barium	µg/L	700	2000	*NA**	*NA*
Beryllium	µg/L	*NA*	4	*NA*	*NA*
Boron	µg/L	2400	*NA*	1000	1000
Cadmium	µg/L	3	5	5	5
Chromium (total)	µg/L	50	100	50	50
Copper (at tap)	µg/L	2000	1300	2000	1000
Lead (at tap)	µg/L	10	15	10	10
Mercury (inorganic)	µg/L	6	2	1	1
Nickel	µg/L	70	20	20	20
Selenium	µg/L	40	50	10	10
Thallium	µg/L	*NA*	2	*NA*	*NA*

[1] European Drinking Water Directive: Council Directive 98/83/EC of 3 November 1998
[2] D. Lgs. 31/2001: Legislative Decree n.31 of 2 February 2011
**NA: Not Available*

The Safe Drinking Water Act (SDWA) is the main federal law that ensures the quality of Americans' drinking water: under the SDWA, EPA sets legal limits ("MCL", Maximum Contaminant Level") that reflect both the level that protects human health and the level that water systems can achieve using the best available technology. Besides prescribing these legal limits, EPA rules set water testing schedules and methods that water systems must follow. The National Primary Drinking Water Regulations (NPDWRs or primary standards) are legally enforceable standards that apply to public water systems (USEPA, 2012).

1.1.2 Copper

Copper, a transition metal, number 29 in the periodic table of elements, is commonly found in ores. The principal ore minerals are chalcopyrite $CuFeS_2$, cuprite Cu_2O and malachite $Cu_2(CO_3)(OH)_2$. Copper occurs in the environment in three major valence states: copper metal Cu(0), monovalent (cuprous) Cu(I) and divalent (cupric) Cu(II) cations. Cu(I) usually exists in a tetrahedral arrangement, whereas Cu(II) complexes, the more stable form, most often are square planar (National Research Council, 2000; WHO, 2004).

1.1.2.1 Copper speciation

Copper, like many metals, interacts in water to form free metal cations, a variety of soluble complexes, and insoluble particles or precipitates, depending on the mineral content of the water. Typical drinking water pH and mineral content allow for the presence of free, complexed, and particulate copper. Free copper, which is the cupric ion (Cu^{2+}), is soluble and the common form at low pH levels up to 6 and when there is a lack of anionic ligands. In pure water, soluble copper hydroxide-complexes form at low and high pH values. Copper precipitates most frequently as copper hydroxide, $Cu(OH)_2$ at intermediate pH levels, typically pH in the range of 6.5-12. Precipitation is dependent on copper concentration, presence of other anions and cations, temperature, and time to thermodynamic equilibrium. Figure 1.1 shows the distribution of individual hydroxide-Cu(II)-complexes in pure water as a function of pH and identifies where copper hydroxide precipitate will form (Cuppet et al., 2006).

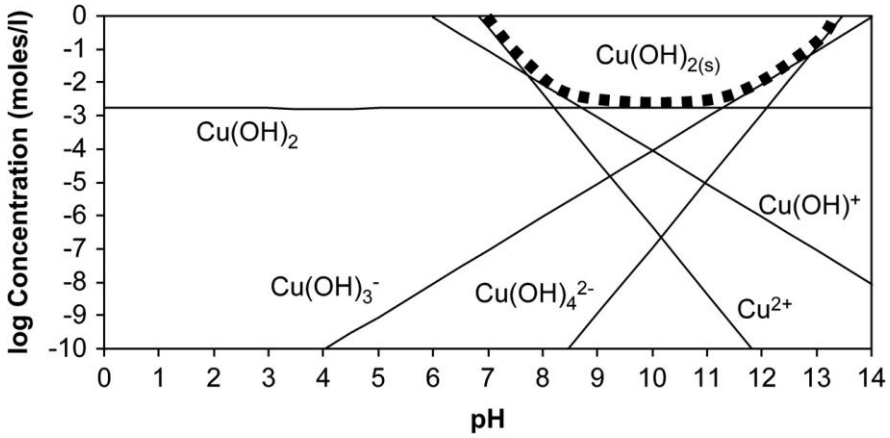

Figure 1.1. The pC-pH diagram [(-log concentration)-(-log[H^+]) diagram] for cupric solubility in pure water; dotted line shows the area where copper hydroxide precipitates in solid form (Cuppet et al., 2006).

Water constituents affects copper solubility: in rivers, copper is generally adsorbed to insoluble particles or complexed with inorganic and organic ligands while in drinking water, copper is generally free in solution. In fact, while hydroxide-complexes are always present in water, individual or combinations of anions can bind to cupric ion to form complexes based upon stability constants. Copper will form complexes with common anions, including SO_2^{-4}, OH^-, PO_3^{-4}, NO_3^-, HCO_3^- and CO_3^{2-}: in the range of pH of 6-9.3, aqueous $CuCO_3$ is prevalent, while at pH 9.3-10.7, the aqueous $[Cu(CO_3)_2]^{2-}$ ion predominates. Precipitates of these complexes form when the solubility product is exceeded: a common multianionic precipitate is malachite $[Cu_2(OH)_2(CO_3)]$, which is a blue-green Cu(II)-hydroxide-carbonate precipitate. Amine compounds and ammonia form complex tetracupric amines (e.g., $[Cu(NH_3)_4]^{2+}$) which are highly soluble in both acid and basic

solutions (Erickson et al., 1996; National Research Council, 2000; WHO, 2004; Cuppet et al., 2006). As shown, copper forms a rich variety of coordination complexes with oxidation states Cu(II) and Cu(I). The coordination chemistry of copper is dominated by Cu(II): in order to compare the affinity of a specific ligand (L) towards divalent copper ions in the formation of complexes, Table 1.2 reports the logs of equilibrium constants (β_{mlh}) corresponding to a general complexation/precipitation reaction (equation 1) between a generic metal (M) and both inorganic and organic ligands (L) (Morel and Hering, 1993; Luo et al. 2006).

$$m\cdot M + l\cdot L + h\cdot H^{+} \rightleftarrows M_m L_l H_h \qquad [\beta_{mlh}] \qquad (1)$$

Copper speciation affects toxicity and bioavailability in aquatic organisms (from algae to fish). Free copper (II) ion and mono-hydroxide Cu(II) are considered highly toxic, while other anionic complexes, especially carbonate-complexes, are less toxic to aquatic organisms. Copper is much less toxic to mammals, however, although the role of speciation of copper is known to be important in aquatic toxicity, its role in human sensory response is not well established (Kushner, 1993; Cuppet et al., 2006).

Table 1.2. Stability constants for formation of complexes from Cu^{2+} and ligands. Constants are given as logarithms of the overall formation constants, β_{mlh} for complexes at zero ionic strength and 25°C (Morel and Hering, 1993).

OH^-	**CO_3^{2-}**	**SO_4^{2-}**	**Cl^-**	**NH_3**	**PO_4^{3-}**	**CN^-**	**EDTA**	**Ethylene-diamine**
CuL 6.3	CuL 6.7	CuL 2.4	CuL 0.5	CuL 4.0	CuHL 16.5	CuL_2 16.3	CuL 20.5	CuL 10.5
CuL_2 11.8	CuL_2 10.2			CuL_2 7.5	CuH_2L 21.3	CuL_3 21.6	CuHL 23.9	CuL_2 19.6
CuL_4 16.4				CuL_3 10.3		CuL_4 23.1	CuOHL 22.6	CuOHL 11.8
Cu_2L_2 17.7				CuL_4 11.8				

1.1.2.2 Sources and concentrations of copper in water

Metallic copper is malleable, ductile and a good thermal and electrical conductor. It has many commercial uses because of its versatility which make it a preferred choice in the building industry for hot- and cold-water pipes, electrical wires, hose, nozzles, valves, fittings, coins, cooking utensils and building materials. Copper is present in munitions, alloys (brass, an alloy of copper and zinc, and bronze, an alloy of copper with about 5-10% tin) and coatings. Copper compounds are used as or in fungicides, algicides, insecticides and wood preservatives and in electroplating, azo dye manufacture, engraving, lithography, petroleum refining and pyrotechnics. Copper compounds are also used as food additives (e.g., nutrient and/or coloring agent) and sometimes added to surface water for the control of algae (Monser and Adhoum, 2002; WHO, 2004).

Human activities can release copper into the environment, especially to the land. Mining operations, along with incineration, are the main sources of copper release. Release into water occurs from weathering of soil, industrial discharge, sewage disposal and antifouling paints (Moore et al., 2013).

The concentrations of copper in drinking water can be greatly increased during the distribution of drinking water. Many pipes and plumbing fixtures contain copper, which can leach into the drinking water. Although copper metal tends not to leach in neutral solutions, organic solvents, and detergents, acid solution effectively leaches traces of the metal as cupric ions. Characteristics of the water, including increased acidity, increased temperature, and reduced hardness, can increase the leaching of copper into the water. Thus, valves in soft-drink dispensing machines are subject to the corrosive effects of carbonic acid and have been shown to be a source of toxic cupric ions. Electrolysis of copper from pipes can result from using household pipes to ground appliances. Moreover stagnation of water in pipes and plumbing fixtures containing copper and copper alloys in distribution systems and household plumbing allows leaching and increases copper to several milligrams per liter in the water. Copper concentrations in the USA surface waters range from 0.0005 to 1 mg/L, with a median value of 0.01 mg/L. Results from a number of studies from Europe, Canada and the USA indicate that copper

concentrations in drinking-water vary widely (from less than 0.005 to more than 30 mg/L) as a result of variations in water characteristics, such as pH, hardness and copper availability in the distribution system, with the primary source most often being the corrosion of interior copper plumbing (WHO, 2004).

1.1.3 Chromium

Chromium, named for its many-colored compounds, is a transition metal, number 24 in the periodic table of elements. The element is found in the combined form, mainly in chromite ores $FeCr_2O_4$, and, even if in lower abundant amounts, as crocoites ($PbCrO_4$) and chrome ochre (Cr_2O_3). Chromium exists in the oxidation states from -2 to +6, but it is essentially present in the environment in two forms, namely Cr(VI) and Cr(III). The presence of all of these species and their pH dependence pose a problem if one is interested in speciation as well as detection of a particular oxidation state. Also, though Cr(III) is biologically essential to mammals as it maintains an effective glucose, lipid and protein metabolism, Cr(VI) is highly toxic as it can diffuse as CrO_4^{2-} or $HCrO_4^-$ through cell membranes (Shupack, 1991; Sankararamakrishnan et al., 2006).

1.1.3.1 Chromium speciation

In natural aquatic environments, chromium compounds are thermodynamically stable only in the +3 and +6 states. These two ground states exist mainly in the octahedral and tetrahedral geometries respectively. Under oxidizing conditions, Cr(VI) compounds are prevalent, while under reducing conditions Cr(III) species are significant. The Eh-pH predominance diagram for aqueous chromium at 25 °C and at the total chromium concentration of 1 µM is shown in Figure 1.2, where the area of chromium hydroxide precipitation is highlighted in grey (USEPA, 1998).

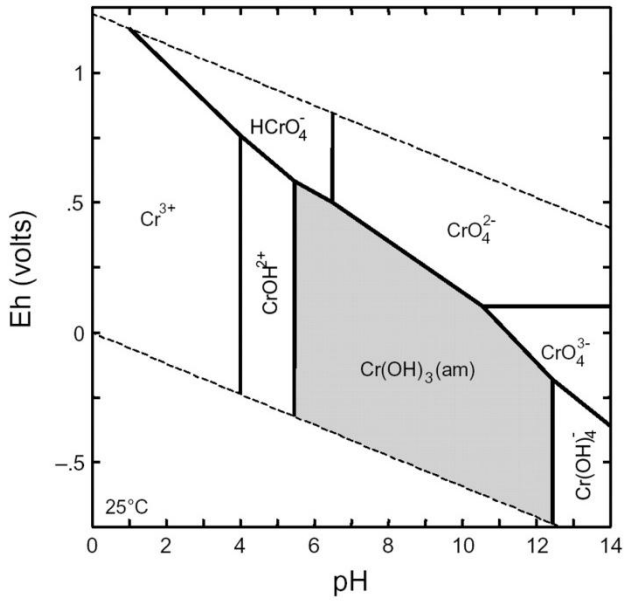

Figure 1.2. Eh-pH predominance diagram for aqueous chromium at 25 °C and Cr_{tot} = 1 µM. Inside the grey area chromium hydroxide precipitates in solid form (http://rimg.geoscienceworld.org/)

The +6 oxidation state is of great interest because it is implicated in causing cancer in man and animals. Also, since it forms anionic species with high solubility in water, which are only weakly sorbed onto inorganic surfaces, Cr(VI) has a significant mobility in soil and water (Zayed and Terry, 2003). In aqueous solution, Cr(VI) may exist either as the chromic acid neuter molecule (H_2CrO_4) or in a variety of oxospecies depending on pH, mainly the oxyanions of chromate CrO_4^{2-} and dichromate $HCrO_4^-$: the small size and large charge of the Cr(VI) engenders Cr-O double bonding. At pH < 1, the predominant species is H_2CrO_4, while at a pH between 2 and 6, the $HCrO_4^-$ oxyanion can dimerize to form the red oxyanion of dichromate $Cr_2O_7^{2-}$. Thermodynamically, the aqueous equilibria are shown in equations from 2 to 4 (Shupack, 1991; USEPA, 1998):

$H_2CrO_4 + H_2O \rightleftarrows HCrO_4^- + H^+$ K = 1.8 (2)

$HCrO_4^- + H_2O \rightleftarrows CrO_4^{-2} + H^+$ $K = 1.3 \cdot 10^{-6}$ (3)

$2CrO_4^{-2} + H^+ \rightleftarrows Cr_2O_7^{2-} + H_20$ $K = 6.3 \cdot 10^{-3}$ (4)

Polymerization to the tri- and tetrachromates occurs at very low pH: the presence of $Cr_2O_7^{2-}$ in water is usually followed by formation of the tri- and tetra-anions $Cr_3O_{10}^{-2}$ and $Cr_4O_{13}^{-2}$, respectively. $Cr_2O_7^{2-}$ becomes significant when total Cr(VI) concentration is > 52 mg/L, or even dominates when total Cr(VI) concentration is > 1.56 g/L; however, such high Cr(VI) concentrations are not found commonly in unpolluted natural waters. Therefore, since H_2CrO_4 exists only in very acidic solutions (pH<1), under environmentally relevant pH values, Cr(VI) exists only as dichromate (pH<6.5) or, for pH values higher than 6.5, as chromate. At a pH > 8 only the yellow ion CrO^{-2} exists (Shupack, 1991; WHO, 2003).

Thermodynamically, the +3 state is the most stable oxidation state of chromium, and it is represented by thousands of compounds. The main aqueous Cr(III) species are $[Cr(H_2O)_6]^{3+}$, which prevails only under acidic conditions (pH<3.6), and the Cr(III) hydrolysis products: $[Cr(H_2O)_5(OH)]^{2+}$, $[Cr(H_2O)_4(OH)_2]^{+}$, $[Cr(H_2O)_3(OH)_3]$ and $[Cr(H_2O)_2(OH)_4]^{-}$. In the presence of dissolved Fe(III) and at a pH>4, Cr(III) readily precipitates as mixed Fe(III)-Cr(III) (oxy)hydroxides. Polymeric Cr(III) species, such as $Cr_2(OH)_2^{4+}$, $Cr_3(OH)_4^{5+}$ and $Cr_4(OH)_6^{6+}$ can also be formed, but the kinetic of polymerization is slow under environmentally relevant pH and temperature values, and, therefore, polymeric Cr(III) species are never significant in natural unpolluted aquatic systems. Hence, under environmentally relevant pH values, trivalent chromium has a much lower solubility and mobility in water and soil than hexavalent chromium (WHO, 2003). The affinity of a specific inorganic or organic ligand (L) towards Cr^{3+} in the formation of complexes is reported in terms of logs of equilibrium constants (β_{mlh}) in Table 1.3 (Morel and Hering, 1993).

Table 1.3. Stability constants for formation of complexes from Cr^{3+} and ligands. Constants are given as logarithms of the overall formation constants, β_{mlh} for complexes at zero ionic strength and 25°C (Morel and Hering, 1993).

OH^-	SO_4^{2-}	Cl^-	F^-	CN^-	EDTA	Acetate
CrL 10.0	CrL 3.0	CrL 0.23	CrL 5.2	CuL_2 16.3	CrL 26.0	CrL 5.4
CrL_2 18.3			CrL_2 9.2	CuL_3 21.6	CrHL 28.2	CrL_2 8.4
CrL_3 24.0			CrL_3 12.0	CuL_4 23.1	CrOHL 32.2	CrL_3 11.2
CrL_4 28.6						
$Cr3L_4$ 47.8						

1.1.3.2 Sources and concentrations of chromium in water

Chromium and its salts are used in the manufacture of catalysts, pigments and paints, fungicides, ceramic, glass. It is also used in leather tanning industry, in photography, for chromium metal production, chrome plating and corrosion control. Cr(III) and Cr(VI) occur naturally in the environment and are present in water from the erosion of chromium deposits found in rocks and soils. At many locations, chromium compounds have been released to the environment via leakage, poor storage, or improper disposal practices. Chromium compounds are very persistent in water as sediments (WHO, 2003).

The natural total chromium content of surface waters is approximately 0.5-2 µg/L and the dissolved chromium content 0.02-0.3 µg/L. In general, the chromium content of surface waters reflects the extent of the industrial activity (levels up to 84 µg/L can be found in the USA), displaying concentrations mostly between 1 and 10 µg/L. In general, the chromium concentration in groundwater is low (<1 µg/L), but levels up to 50 µg/L have been reported in the USA; in shallow groundwater, median levels of 2-10 µg/L are reported (WHO, 2003; Zayed and Terry, 2003).

The distribution of compounds containing Cr(III) and Cr(VI) depends on the redox potential, the pH, the presence of oxidizing or reducing compounds, the kinetics of the redox reactions, the formation of Cr(III) complexes or insoluble Cr(III) salts, and the total chromium concentration. In soil, Cr(III) predominates, since Cr(VI) can easily be reduced to Cr(III) by organic matter. In water, Cr(III) is a positive ion that forms hydroxides and complexes, and is adsorbed at relatively high pH values. In surface waters, the ratio of Cr(III) to Cr(VI) varies widely, and relatively high concentrations of the latter can be found locally. In general, Cr(VI) salts are more soluble than those of Cr(III), making Cr(VI) relatively mobile (USEPA, 1998).

1.2 Heavy metal and metalloids removal from water

1.2.1 Conventional water treatment processes

Heavy metal removal from effluents can be achieved by conventional treatment processes such as chemical precipitation, flotation, ion exchange, membrane separation and adsorption on activated carbon (Barakat, 2011).

Chemical precipitation, obtained with lime and limestone by adjusting the pH to the basic conditions (pH 9-11), is the most widely used process for heavy metal removal from effluents. It can be employed to effectively treat high metal concentration of more than 1000 mg/L; other advantages of using lime precipitation include the simplicity of the process, inexpensive equipment requirement and convenient and safe operations. However, chemical precipitation is a long time process: shorter time to settle out suspended solids can be achieved by dosing coagulants, thus improving sludge settling. Nonetheless, large amounts of chemicals are needed and the production of excessive sludge amounts requires further treatment (Wang et al., 2004, Mirbagherp and Hosseini, 2004; Aziz et al., 2008).

Although it is only a kind of physical separation process, heavy metal removal by flotation has the potential for industrial application. Flotation has been employed to separate heavy metal from a liquid phase using bubble attachment, originated in mineral processing. Dissolved air flotation (DAF), ion flotation and precipitation flotation are the main flotation processes for the removal of metal ions from solution (Fu and Wang, 2011). Flotation can be employed to treat effluent with a metal concentration of less than 50 mg/L or higher than 150 mg/L. Advantages such as a better removal of small particles, shorter hydraulic retention times and low cost make flotation one of the most promising alternatives for the treatment of metal-contaminated wastewater. However, due to low removal efficiency, subsequent treatments are often required to improve the removal efficiency of heavy metal. In the last decade, the trends of research had shifted from flotation alone to a combination of flotation and other physic-chemical treatment such as filtration or powder activated carbon (Jokela and Keskitalo, 1999; Matis et al., 2003; Mavrov et al., 2003).

Ion exchange by means of synthetic organic ion exchange resins is another method used successfully in the industry for the removal of heavy metals from effluents: advantages pertain to its low sludge generation and less time consuming. The disadvantage of this method is that it cannot handle concentrated metal solution as the matrix gets easily fouled by organics and other solids in the wastewater. Moreover ion exchange is nonselective and is highly sensitive to the pH of the solution (Gode and Pehlivan, 2003; Kurniawan et al., 2006).

Membrane separation has been recently used for the treatment of effluents. Depending on the size of the particle that can be retained, various types of membrane filtration such as ultrafiltration, nanofiltration and reverse osmosis can be employed: the selection of the appropriate membrane depends on a number of factors such as the characteristics of the wastewater, the nature and concentration of materials present in the wastewater, pH and temperature. However, they are costly and prone to membrane fouling: fouling has many adverse effects on the membrane system such as flux

decline, an increase in transmembrane pressure (TMP) and the biodegradation of the membrane materials: these effects result in high operational costs for the membrane system (Qdais and Moussa, 2004; Barakat, 2011).

Activated carbon has been widely used as adsorbent in water treatment applications throughout the world. However it remains an expensive material since higher the quality of activated carbon, the greater its cost; moreover it often requires complexing agents to improve its removal performance for inorganic matters (Babel and Kurniawan, 2003).

1.2.2 New/unconventional water treatment processes

Recently, numerous approaches have been studied for the development of cheaper and more effective technologies: electrochemical treatments, photocatalitic processes and new adsorbent/reactive media of mineral, organic or biological origin represent the new trends in the physico-chemical water treatment field for the removal of inorganic contaminated waters (Barakat, 2011).

Electrochemical treatments include electrodialysis and ion-exchange electrodialysis, electrocoagulation, electroflotation, electrodeposition (Kurniawan et al., 2006). Electrodialysis offers advantages such as the ability to produce a highly concentrated stream for recovery and high separation selectivity. However, since it is a membrane process, it requires clean feed, careful operation and periodic maintenance to prevent any stack damages thus increasing process costs. Electrocoagulation, electroflotation, electrodeposition involve the plating-out of metal ions on a cathode surface and can recover metals in the elemental metal state (Fu and Wang, 2011). However, in addition to energy costs, another disadvantage lies in the corrosion that can become a significant limiting factor since electrodes have frequently to be replaced (Janssen and Koene, 2002).

Photocatalytic methods has been recently studied and developed in order to treat complex water systems containing both heavy metals and organic pollutants and overcome problems related to the presence of one species that usually impedes the removal of the other. Such methods utilize novel photocatalysts and consume cheap photons from the UV-near visible region to relay electrons from the organic substrates to metal ions, thus inducing both degradation of organic pollutants and recovery of metals in one-pot systems, operable at traces (less than ppm) of the target compounds (Barakat, 2011).

A wide range of adsorbent/reactive materials are currently studied worldwide for heavy metal removal from water: carbon nanotubes, low cost adsorbents, new synthetic polymers and redox reactive materials. The term “sorption” actually describes the transfer of heavy metals from the liquid phase to the surface of a solid, by means of physical and/or chemical interactions (Barakat, 2011; Fu and Wang, 2011). A general description of carbon nanotubes and low cost adsorbents is given in paragraph 1.2.2.1; as for the two tested media, PoliAmidoAmine Hydrogels and KDF Granular Brass Media, they are introduced and described in paragraphs 1.2.2.2 and 1.2.2.3, thus classifing them as new synthetic polymers/hydrogels and redox reactive materials, respectively.

1.2.2.1 Carbon nanotubes and low cost adsorbents

Carbon nanotubes (CNTs) have attracted great interest due to their unique morphologies leading to enhanced surface sorption properties and multi-component sorption of metal ions. CNTs are divided into two types: single-walled CNTs (SWCNTs) and multi-walled CNTs (MWCNTs). The mechanisms by which the metal ions are sorbed onto CNTs are very complicated and appear attributable to electrostatic attraction, sorption, precipitation and chemical interaction (Zhao et al., 2011). In 2009, Gao et al. found that the sorption mechanisms were governed by the surface features, ion exchange process and electrochemical potential. The latter plays a significant role in multi-component sorption where redox reactions, not only on the adsorbent surface but also among the different adsorbates, are likely to occur. The sorption capacities of metal ions by raw CNTs are very low but significantly increase if functionalized after oxidization with solutions of HNO_3, NaClO and $KMnO_4$. Researches on the removal of divalent metal ions (Cd^{2+}, Cu^{2+}, Ni^{2+}, Pb^{2+}, Zn^{2+}) from aqueous solution using various kinds of CNTs, suggested that CNTs are promising adsorbents for environmental protection

application because of the superior sorption capacity and effective desorption of divalent metal ions. However, CNTs production can be expansive and a widespread usage of CNTs will eventually be discharged to the water environment and poses a risk to humans (Fu and Wang, 2011).

Low cost and local availability adsorbents includes natural materials, modified agricultural and biological waste or industrial by-products. Some of these materials can be used as adsorbents with little processing; however, the conversion of these materials into activated carbon, which can be used as an adsorbent for water purification, would improve economic value, helping industries reduce the cost of waste disposal and providing a potential alternative to activated carbon (Kurniawan et al., 2006).

Natural materials mainly include zeolites and clay. They are both extracted from natural local deposits sited in many countries and can be later modified in order to improve their removal abilities. The mechanism of interaction with heavy metals is the exchange of ions: natural clay minerals are similar to zeolites but with higher surface area and excellent ion exchange capacities due to their high negative charge (Bailey et al., 1999; Babel and Kurniawan, 2003). The adsorption capabilities of clay result from a net negative charge on the structure of silicate minerals. This negative charge is neutralized by the adsorption of positively charged species, giving clay the ability to attract and hold cations such as heavy metals. The large surface area of clays (up to 800 m^2/g), especially that of montmorillonite, contributes to its high adsorption capacity. Removal of anions is more effective at low pH: as an example, since Cr(VI) is adsorbed in the form of $HCrO_4^-$, a positive charge is needed to attract the metal ions: above pH 2.5, SiO_2 possesses a negative charge and, generally, most of the adsorption is attributed to alumina and CaO. Clay can be modifed to improve its sorption capacity by means of different methods: by replacing the natural exchangeable cations in the clay with others (such as the organophilic cation, tetramethylammonium ion to adsorb Pb and Cr(VI)) or by coupling clay to a polymeric material thus creating the so called “clay-polymer composites” (Barakat, 2011; Solenera et al., 2008). Zeolites, naturally occurring silicate minerals, can also be produced synthetically. Clinoptilolite is probably the most abundant of more than 40 natural zeolite species. The three-dimensional structure of zeolite possesses large channels containing negatively charged sites resulting from Al^{3+} replacement of Si^{4+} in the tetrahedral (Bailey et al., 1999). Sodium, calcium, potassium and other positively charged exchangeable ions occupy the channels within the structure, and can be replaced with heavy metals. Zeolites can be modified: the process of tailoring of the zeolite results in a positively charged species, allowing for the mechanism of anion exchange for example for the removal of CrO_4^{2-}. The role of pH is very important for the selective adsorption of different heavy metal ions. Barakat (2008) reported that Cu(II) and Zn(II) were adsorbed at neutral and alkaline pH, Cr(VI) was adsorbed at acidic pH while the adsorption of Mn(IV) was achieved at high alkaline pH values. Synthetic zeolite magnetically modified with iron oxide were prepared by Nah et al. (2006) and showed high adsorption capacities for the Pb(II) ion and a good chemical resistance in a wide pH range 5-11 (Barakat, 2011).

Agricultural waste such as hazelnut shell, rice husk, almond husk, pecan shells, jackfruit, maize cob or husk can be used as an adsorbent for heavy metal uptake after chemical modification or conversion by heating into activated carbon. This process can be costly due to energy and chemicals consumption; however, chemical modification with an oxidizing agent can enlarge its surface area, thus improving its sorptive capacity and possibly compensating the cost for such a process. Waste from agricultural sources has demonstrated its ability for heavy metal removal even though an acidic pH ranging 2-6 is effective for metal removal (Bishnoi et al, 2004; Barakat, 2011). The mechanism of up-taking heavy metal involves ionic, chemical and physical adsorption: a variety of ligands such as carboxyl, amine, hydroxyl, phosphate and sulfhydryl groups are known to be involved in metal chelation thus absorbing metal ions could by complexing with negatively charged reaction sites (Igwe et al., 2005). Moreover, compared to adsorbents from other sources, those from agricultural waste possess unique characteristics such as ease of regeneration and desorption with basic or acid solutions, probably due to the presence of surface functional groups such as hydroxyl and carboxylic with high affinity for metal cations (Kurniuwan et al., 2006).

Like agricultural waste, industrial by-products are inexpensive and abundantly available and can be chemically modified to enhance removal performance: fly ash is a waste from thermal power plants; red mud is a solid by-product from alumina production; bark and sawdust from the timber industry are effective because of the high tannin content. Low rank coal, such as lignite, exchanges heavy metals ion due to its carboxylic acid and phenolic hydroxyl functional groups. The lignin is extracted from black liquor, a waste product of the paper industry; chitosan, is obtained from local fishery industries wastes (Bailey et al., 1999). As a whole, adsorbents from industrial by-products such as iron/steel slags have some

advantages for metal removal. In addition to having a wide pH range (pH 1.5-9.0) effective for metal removal, these adsorbents can be employed to treat effluents with metal concentration of less than 20 mg/L, in the range of 20-100 mg/L, or higher than 100 mg/L (Babel and Kurniuwan, 2003).

1.2.2.2 New synthetic resins/polymers: Poly Amido Amine Hydrogels (PAAH)

Synthetic resins or polymers are very often used in the removal, preconcentration and determination of various metal ions in aqueous solutions. The efficacy of the metal removal process depends on two sets of parameters: 1) the process parameters, such as type and charge of target ions and pH of the solution; 2) the properties of the resin, such as crosslinking degree, swelling under process conditions and, to a large extent, the type and structure of the ligands present in the resin structure. Since the first set of parameters is process dependent and usually cannot be changed a considerable effort is being devoted to the development of polymeric resins bearing new, more efficient types of functional groups, which are able to perform selective and efficient separations (Trochimczuk and Czerwijska, 2005). These resins can have one or more types of groups attached to their surface. The presence of two or more types of functional groups gives the possibility of taking the advantage of co-operative action of different groups on the ions present in solution. Selectivity can be increased with ligands that can coordinate or chelate with the target metal ion (Massaoud et al., 2008).

Hydrogels, which are crosslinked hydrophilic polymers, are capable of expanding their volume due to their high swelling in water (Peppas et al., 2000). Various hydrogels were synthesized and their adsorption behavior was investigated for heavy metals such as Pb(II), Cd(II), Hg(II) and metalloids like As(V) (Kesenci et al.,2002; Barakat and Sahiner, 2008). The removal is basically governed by the water diffusion into the hydrogel, carrying the heavy metals inside especially in the absence of strongly binding sites. In general, maximum binding capacity increases with pH increase to values over 6. Figure 1.3 shows the schematic representation of polymerization/crosslinking reaction that results in three-dimensional network formation of cationic hydrogel (Barakat, 2011).

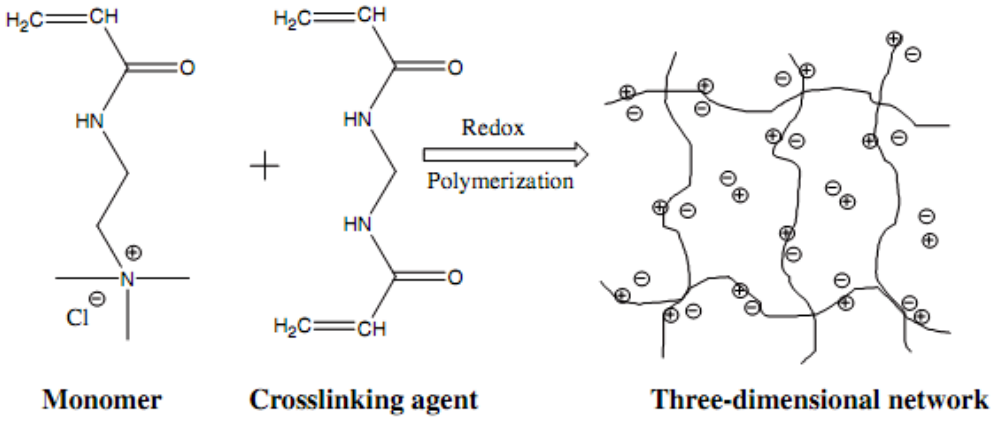

Figure 1.3. Three-dimensional network formation of cationic hydrogel (Barakat and Sahiner, 2008).

Hydrogels are often defined as “two-component systems”, since they are made of both the crosslinked polymer chains and water; such systems are able to absorb and retain high amounts of aqueous solution and the interactions responsible for the absorption of water can be mainly summarized as follows (Park et al., 2003):

- the presence, on the polymer chains, of basic or acidic groups (-OH, -COOH, -$CONH_2$, -SO_3H , -CONHO) that promote the hydration of the inner regions;
- to the phenomenon of capillarity due to the porosity of the polymer;
- to differences in osmotic pressure.

As a function of the presence of specific functional groups, hydrogels can be classified into neutral or ionic hydrogels. Neutral hydrogels swell in aqueous solution because of the osmotic force resulting from the presence of charges in the swelling solution; ionic hydrogels swell in water also because of electrostatic repulsion between the charges on the chains.

These two factors are strongly interconnected since the presence on the polymer chains of ionizable groups, anionic or cationic, makes hydrogels very sensitive to the pH of the solution: the anionic groups protonate when the pH of the solution is greater than the pKa of the group while, in presence of cationic groups protonation occurs in acidic environments. The presence of ionized groups on chains, increases the electrostatic repulsion and thus the flow of aqueous solution inside the hydrogel. In addition, the different concentration of charges of opposite sign between the inside of the matrix and the external solution, further increases the presence of aqueous solution in the hydrogel (Peppas et al., 2000; Foderà, 2005).

PoliAmidoAmines (PAAs) are a family of synthetic polymers characterized by a regular sequence of amide groups (-CO-N), and tertiary amine. PAAs may have a linear structure, as shown in Figure 1.4, or exist in complex form, either as hydrogels (PAA molecules with cross-linked structure) or dendrimers of PAAs (molecules with multiple ramifications).

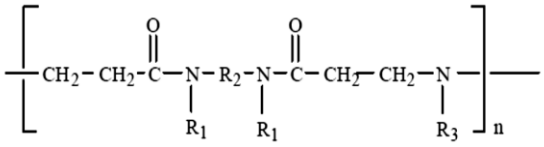

Figure 1.4. Monomeric structure for a generic PAA (Ferruti et al., 2002).

PAAs are highly functional polymers; however, further functionalization may be useful for specific purposes. During the polymerization step, active groups such as carboxylic, hydroxylic, tertiary aminic, amidic and thiolic, can be added as side substituents, thus adding specific properties to the molecules without interfering with the polymerization process. Examples of not-functionalized (a) and functionalized (b) PAAs are shown in Figure 1.5 (Caldwell et al., 1993; Ferruti et al., 2012; Jain et al., 2007).
As for their complexing ability towards heavy metals, only PAAs containing at least two aminic nitrogen atoms per repeating unit, with the exception of those derived from aminoacids, are able to coordinate heavy metal ions, such as Cu^{2+}, Co^{2+} and Ni^{2+}: nitrogen atoms with complex abilities belongs to amine groups, while amide nitrogen does not affect the removal of metals. In this mechanism, the pH is a key factor since it influences the values of the constants of complexation (Ferruti et al., 2006; Rossi, 2007).

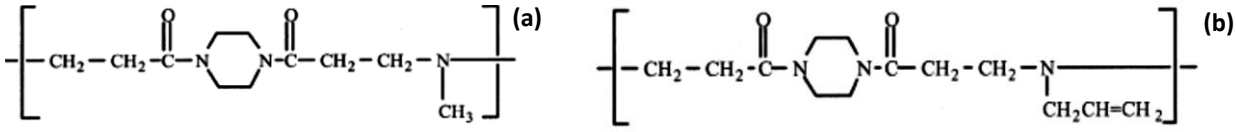

Figure 1.5. Monomeric structure for a generic PAA without (a) and with (b) functionalization (Ferruti et al., 2002).

PoliAmidoAmine Hydrogels (PAAHs) are biodegradable and biocompatible polymers, they are easily synthesized and thus often defined as "low cost polymers" (Ferruti et. al, 2002).
The chemical formula of a generic PAA hydrogel is shown in Figure 1.6: because of the presence of a tridimensional cross-linked structure, PAA hydrogels expand in water without dissolving. In general PAAHs are insoluble in water and their resistance to dissolution increases with the number of links between chains. The form of the polymer and its insolubility in water is likely to be due to the cross-linking degree: the presence, along chains, of monomers or chemical groups that are not cross-linked or insufficiently cross-linked can therefore disperse in water (Park et al., 2003). Also, PAA hydrogels absorbe water depending upon both the starting monomers used and the cross-linking degree; porosity, a property that influences the physical-chemical behavior of hydrogels in water, can be varied by changing the type of solvent used during the synthesis process (Casolaro et al., 1982, Rossi, 2007).
Water absorption mechanism can be interpreted as follows: when water gets into the polymer, polymer chains extend in an entropically unfavoured configuration and give rise to resistive forces. For an hydrogel containing acidic groups bound to their polymer chains, the H^+ comes off in basic solutions and combines with OH^- to form H_2O. Charge is compensated by

cations that enter the gel together with another OH^-. Charge neutrality is maintained. The increased cation concentration gives rise to an osmotic pressure that causes the gel to swell/deswell. Ionic gels also swell/deswell due to the general tendency of the polymer network to mix with the solution, but, typically the osmotic force is much greater than the mixing force. Equilibrium of ionic gels occurs when the elastic restoring force of the network balances the osmotic forces (Sudipto et al., 2002; Rossi, 2007).

If lowering the cross-linking degree of a polymer, its expansion and, consequently, the flexibility of chains, the number of pores and the absorption of water increases. However, it should be noted that high cross-linking degrees improve the mechanical resistance of polymers, making them less stiff and fragile against osmotic shocks. Again, the process of swelling and, consequently, the size of a hydrogel in solution depends upon numerous environmental factors including pH, concentration of salts dissolved in water, charge and size of adsorbed ions, temperature, electric field (Calucci et al., 2007).

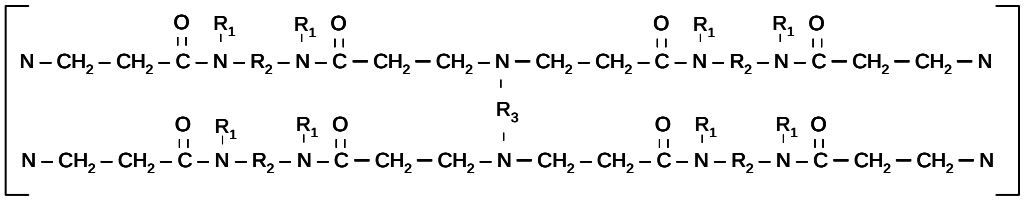

Figure 1.6. Chemical structure for a generic PAA hydrogel (Rossi, 2007).

PAA hydrogels exchange ions dissolved in water and create complexes with heavy metal ions, such as Cu^{2+}, Ni^{2+}, Co^{2+}: these two properties make such polymers of great interest for applications in the water treatment field. Their complexing ability are to be ascribed to the numerous tertiary amino groups and carboxyl groups regularly distributed along the chains, acting as ligands for heavy metals ions. The presence of further functionalization may enhance PPAH complexing abilities (Rossi, 2007, Ferruti et al., 2006).

There are currently no engineering applications of PAA hydrogels in water treatment and research is still in its preliminary stages, considering that there are no further developments after the work by Siyam et al. (1997). They studied the interactions between PAA hydrogels and copper sulfate, observing a different behavior of both the cation (Cu^{2+}) and the anion (SO_4^{2-}) as a function of the swelling degree and of the percentage content of amine groups. Further developments are needed in order to define the possibility to use PAAHs in the water treatment field.

1.2.2.3 Redox reactive materials: Zero Valent Iron (ZVI) and KDF Granular Brass Media (KGBM)

Due to low production costs and high efficiency for the removal of a wide range of contaminants, metallic iron (Fe^0) is one of the most widely studied chemical reductant for environmental applications, and it is generally used as an affordable technology for commercial soil and water remediation (Scott et al., 2011). Zero valent iron (ZVI) is not stable in aqueous media because of its susceptibility to corrosion: corrosion is nature's way of reversing an unnatural process back to a lower energy state. This electrochemical reaction involves the reduction at the cathode of the primary components available in natural waters (dissolved oxygen and water as shown in equations 5 and 6) and the dissolution of Fe^0 at the anode forming ferrous iron (Fe^{2+}); in turn, H_2 and soluble or insoluble oxides and hydroxides ($Fe(OH)_2$, $Fe(OH)_3$, FeO, FeOOH, Fe_2O_3, Fe_3O_4) are produced, as it can be seen in equations 7 and 8, and local chemically reductive conditions are achieved thus promoting the removal of contaminants (Crane and Scott, 2012; Noubactep and Schöne, 2009). As a result, ZVI particles have a core-shell structure with the core being Fe^0 and the shell as the iron oxides/hydroxides formed from the iron oxidation; specific surface and redox chemistry of this structure are unique properties for contaminant removal and transformation (Li and Zhang, 2007, Ramos et al., 2009).

$$2Fe^0_{(s)} + 4H^+_{(aq)} + O_{2(aq)} \rightleftarrows 2Fe^{2+} + 2H_2O_{(l)} \quad (5)$$

$$2Fe^0_{(s)} + 2H_2O_{(l)} \rightleftarrows 2Fe^{2+} + H_{2(g)} + 2OH^-_{(aq)} \quad (6)$$

$$2Fe^{2+}_{(s)} + 2H^+_{(aq)} + \tfrac{1}{2}O_{2(aq)} \rightleftarrows 2Fe^{3+} + H_2O_{(l)} \quad (7)$$

$$2Fe^{2+}_{(s)} + 2H_2O_{(l)} \rightleftarrows 2Fe^{3+} + H_{2(g)} + 2OH^-_{(aq)} \quad (8)$$

Because of the occurrence of multiple interactions such as reduction, (co)precipitation, complexation and sorption, ZVI particles are very effective for the removal of organic or inorganic contaminants with a variety of chemical characteristics (Dries et al., 2005). Mechanisms for heavy metal and metalloids removal by ZVI are complex and sometimes conflicting results have been reported in the literature (Li and Zhang, 2007, Noubactep and Schöne, 2009). Some authors (Li and Zhang, 2007) distinguish on the basis of the different standard potential E_0 of metal ions involved in the removal mechanisms:

- for metals, such as Zn(II) and Cd(II), with E_0 very close to or more negative than that of iron (-0.41 V), the removal mechanism is sorption/surface complex formation;
- for metals, such as Cu(II) or Ag(I) or Hg(II), with E_0 greatly more positive than iron, the removal mechanism is predominantly reduction;
- for metals, such as Ni(II) and Pb(II), with E_0 slightly more positive than iron, the removal mechanisms are both sorption and reduction.

Mainly the pH, alkalinity and the presence of dissolved oxygen (DO) but, generally, the chemical composition of water and the possibility of competitive effects, strongly influence the efficiency and the efficacy of ZVI towards specific inorganic contaminants (Bang et al., 2005).

In order to improve the removal abilities of ZVI, a logical development has been to scale down the reactive Fe^0 particulate to the nano-scale: small particle size usually offers a significant improvement in reactivity (10-1000 times greater than granular ZVI) and reaction efficacy (Scott et al., 2011; Sun et al., 2006). However, the same properties that make n-ZVI potentially useful for environmental remediation, specifically their small size and high redox reactivity, also make them potentially harmful to living organisms.

Further developments pertain to the shape of Fe^0: generally used as particles, in 2005 Chang examined the effectiveness of using thin zero valent iron wires in the treatment of wastewater generated from a metal cleaning.

Again, in order to improve the efficacy in the removal of specific contaminants and to overcome the main disadvantages in the use of metallic iron as such (for instance, the aqueous mobility in porous media), some studies were performed to synthesize new classes of ZVI-based materials: chitosan-n-ZVI beads (Liu et al., 2010), n-ZVI-Fe_3O_4 nanocomposites (Lu et al., 2012) and bentonite-supported n-ZVI (Shi et al, 2011) for the remediation of hexavalent chromium; n-ZVI supported on activated carbon for arseniate and arsenite removal from water (Zhu et al., 2009). The use of ZVI bi- and poly- metallic systems (Fe/Pd, Fe/Pt, Fe/Ag, Fe/Ni), synthesized by coating the surface of ZVI with a small amount of another metal, nobler than iron, can accelerate the reaction rate and increase the removal capacity per unit weight of ZVI: both direct electron transfer with the noble metal and the reaction with hydrogen produced by oxidation of Fe^0 occur during the chemical reduction of sorbed contaminants at the bimetallic ZVI surface (Crane and Scott, 2012). Bi-metallic n-ZVI reactivity depends on a range of factors, including nanoparticle size, physicochemistry, and the choice and quantity (%) of the noble metal. There there are still considerable concerns over the ecotoxicity of some of the noble metals chosen for alloying (for example, Ni) (Gheju, 2011).

Advantages and disadvantages in the application of ZVI technologies are related to the size of the particles used. If compared to powder/granular ZVI, n-ZVI has higher reactivity leading to an increased effectiveness towards inorganic contaminants and versatility in its environmental applications. Nevertheless, they are much more expensive because of the materials and processes needed to make them and in recent years there has been much investigation into the development of methods to produce cheap multi-kilogram quantities of n-ZVI, whilst maintaining reactivity and/or functionality. Besides further studies are needed to predict n-ZVI mobility, toxicity, fate and ecological impact (Crane and Scott, 2012). Also, drawbacks related to leakages of dissolved iron should be taken into account. Iron filing filters can leach significant (70%) quantities of iron: if the process is used in a drinking water facility, an iron removal treatment unit after the ZVI process is needed to reduce iron concentration below the legal limit: the USEPA set the Maximum Contamination Level (MCL) for iron at 0.3 mg/L (Nikolaidis et al., 2003).

In order to overcome the problem related to leakages, the possibility to use granular brass media for the removal of various contaminants from water has been developed.
Conceptually similar to ZVI particles, granular brass media are high purity copper-zinc granules that reduce contaminants in water using oxidation/reduction reactions. The exchange of electrons allows to effectively reduce and remove contaminants such as chlorine, iron, hydrogen sulfide, heavy metals, and to control microorganisms without the use of chemicals. Free chlorine, for instance, is changed into benign, water-soluble chloride, which is then carried harmlessly through the water supply. Similarly, some heavy metals such as copper, lead, mercury, chromium, nickel and others, react to plate out onto the medium's surface, thus being effectively removed from the water supply.. The interest and the advantages in its use lies in the replacement of iron with zinc leakages: zinc MCL is higher (5.0 mg/L) to that of iron. Again, in redox reactions contaminants with positive Standard Electrode Potential (E_0) values are reduced by the electron donor: Fe (E_0 = -0.44 V at 25°C) for ZVI particles, Zn (E_0 = -0.76 V at 25°C) for KDF media. Compared to iron, zinc is a highly reductant species and the reaction will proceed easier from a thermodynamic point of view (Snoeynk and Jenkins, 1980; Morel and Hering, 1993). KDF® Process Media (in the following KDF Granular Brass Media, KGBM) are widely used for a variety of pretreatment, primary water treatment, and industrial treatment processes. They are generally used to replace silver-impregnated systems and in place of, or in conjunction with, granular activated carbon filters, even carbon block or inline filters, since they extend the life of granular activated carbon (GAC) while protecting the carbon bed against fouling by bacterial growth.
In New Jersey mercury contaminated groundwaters have been removed using KDF media since 1992, in point-of-entry (POE) treatment systems producing drinking water. KDF media consistently reduce mercury from initial concentrations of 13 - 24 µg/L to concentration levels of 0.5 µg/L, below the MCL.
A typical application of the KDF media in the treatment of industrial effluents pertains the removal of lead in the circuit board manufacturer industry: lead is removed for 94.4% thus enabling the recycle of water in a closed-loop rinse-down system. When filtered through KDF media, soluble lead cations are reduced to insoluble lead atoms, which are electroplated onto the surface of the media as reported in equation 9, where zinc loses two electrons (oxidation) and goes into solution as a divalent ion, while lead gains two electrons (reduction) and plates on copper/zinc.

$$Cu/Zn^{0}_{(s)} + Pb^{2+}(NO_3)_2^{-} \rightleftarrows Zn/Cu/Pb^{0}_{(s)} + Zn^{2+} + 2NO_3^{-} \quad (9)$$

1.3 Analysis of equilibrium and kinetic processes for granular media

Two important physicochemical aspects for the evaluation of a sorption/reactive media as a unit operation are the equilibrium of the process and the kinetics. Equilibrium is established when the concentration of solute in the bulk solution is in dynamic balance with that of the interface and its achievement depends upon the solute-media interactions and the system conditions. An equilibrium analysis is a fundamental information required to evaluate the affinity or capacity of a media (Ho et al., 2000; Ho et al. 2002). In the following an overview on the isotherm and kinetic models used to fit experimental data from tests on PAAH and KGBM is reported.

1.3.1 Isotherm models

Equilibrium isotherm equations are used to describe experimental sorption data. The equation parameters and the underlying thermodynamic assumptions of these equilibrium models often provide some insight into both the removal mechanism and the surface properties and affinity of the media at a fixed temperature and pH. Thus an accurate mathematical description of the equilibrium isotherm, based on a right and proper sorption mechanism, is essential to the effective design of sorption systems (Ho et al. 2002).
When the retention of a solute on solid particles is investigated, the remaining solute concentration of the compound, *C*, can be compared with the concentration of this compound retained on solid particles, *q* (or *Q*). Figure 1.7 schematically describes sorption and desorption phenomena and shows that the final solid concentration *Q* can be calculated by

difference between the initial liquid concentration (C_{a0} or C_{b0}) and the final liquid concentration C only if the initial solid concentration (Q_{a0} or Q_{b0}) is negligible or previously measured. The relationship $q = f(C)$ is named the "sorption isotherm" and the uniqueness of this relation requires two conditions to be met: 1) the various reaction equilibria of retention/release must have been reached; (2) all other physico-chemical parameters are constant (Limousin et al., 2007).

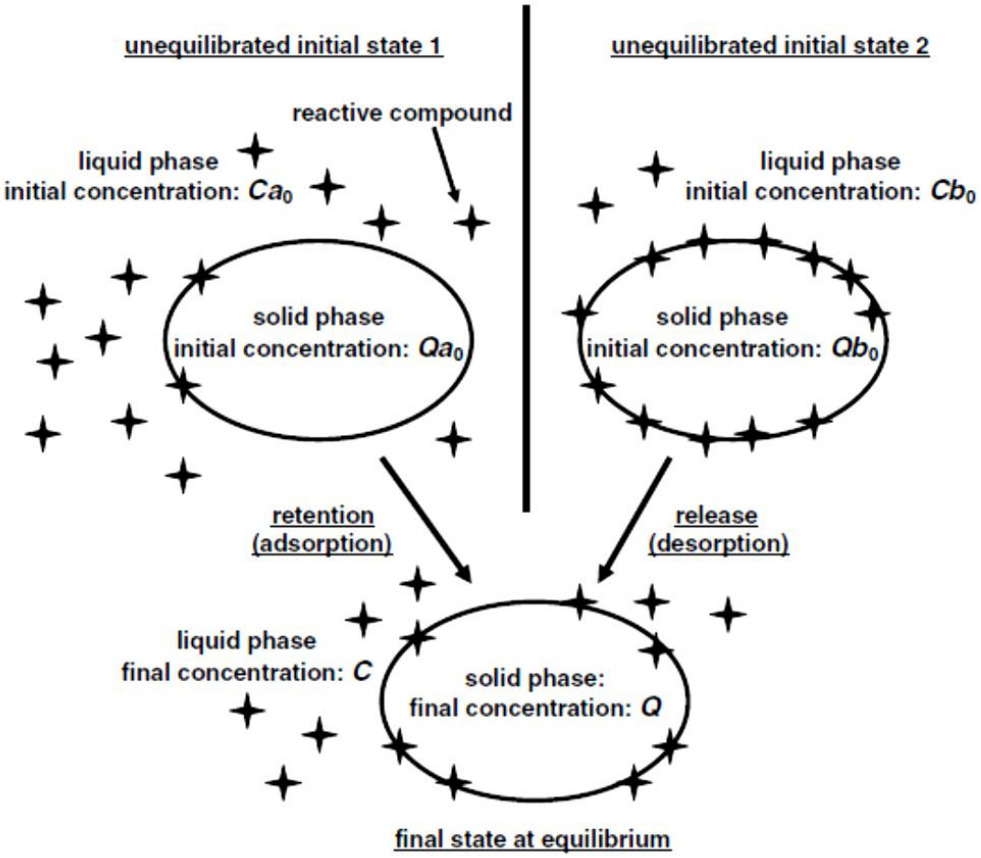

Figure 1.7. Schematic view of the sorption and desorption phenomena (Limousin et al., 2007).

If the initial solid concentration and thus the release of a compound initially present on the solid phase are negligible, the concentration of the compound retained on the solid at the generic time t (q_t) is calculated as the by difference between the initial solute concentration (C_0) and the solute concentration at time t (C_t) as shown in eq. 10, where V is the volume of solution and M is the solid mass of the sorptive/reactive media (Yang et at., 2011; Fujiki et al., 2010).

$$q_t = \frac{V}{M}(C_0 - C_t) \qquad (10)$$

Once evaluated the concentration of the compound retained on the solid phase at the equilibrium (q_{eq}), experimental data can be fitted by using different isotherm models. Giles et al. (1974) proposed a general modeling of sorption isotherms, based on four main shapes of isotherm commonly observed, as shown in Figure 1.8: the "C" isotherm, often used as an easy-to-use approximation for a narrow range of concentration or very low concentrations such as observed for trace pollutants; the "L" and "H" isotherms, where the ratio between the concentration of the compound remaining in solution and adsorbed on the solid decreases when the solute concentration increases, providing a concave curve. The "L" isotherm suggests a progressive saturation of the solid, and the curve may or not reach a strict asymptotic plateau depending if the solid has a limited or unlimited sorption capacity. The initial very high slope of the "H" isotherm suggests the presence of high affinity between the solute and the solid. Finally the "S" isotherm shows a point of inflection due to the presence of at least two opposite mechanisms (Limousin et al., 2007).

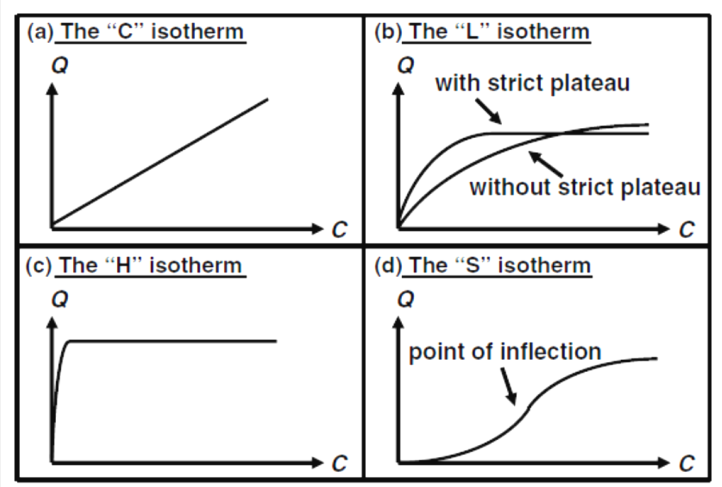

Figure 1.8. The four main types of isotherms proposed by Giles et al. (1974) (Limousin et al., 2007).

Based on the shape of experimental results, concave isotherm models type "L" or "H" were selected: Freundlich, Langmuir and Dubinin-Radushkevich isotherms are shortly described in the following.

1.3.1.1 The Freundlich isotherm

The first mathematical fit to an isotherm was published by Freundlich in 1906 and is a purely empirical formula which has shown to be suitable for describing short-term and monocomponent adsorption of metal ions by different materials. It can be applied to nonideal sorption on heterogeneous surfaces as well as multilayer sorption on microporous structure. It describes an exponential distribution of the active sites and their energies on which the adsorbed molecules are interactive. The form of the Freundlich isotherm is shown in equation 11 (Ijagbemi, 2009; Ho et al., 2002).

$$q_{eq} = k_f \cdot (C_{eq})^{1/n} \qquad (11)$$

where q_{eq} is the amount of solute on the medium surface at equilibrium, C_{eq} the solute concentration in the aqueous solution at equilibrium, k_f is a constant describing the maximum multilayer adsorption capacity and *1/n* is a characteristic constant which measures the strength of adsorption in the adsorption process: if n = 1 then the partition between the two phases is independent of the concentration; if the value of *1/n* is below 1 it indicates a normal adsorption; on the other hand, *1/n* above 1 indicates cooperative adsorption. This equation is easily linearizable (eq. 12) and a graph with $log_{10}(C_{eq})$ as x-axis versus $log_{10}(q_{eq})$ as y-axis provides a line of slope *1/n* and intercept at $log_{10}(k_f)$. According to the Freundlich equation, the isotherm does not reach a plateau as *C* increases (Ignatowicz, 2011; Limousin et al., 2007).

$$\log_{10}(q_{eq}) = \log_{10}(k_f) + \frac{1}{n}\log_{10}(C_{eq}) \qquad (12)$$

1.3.1.2 The Langmuir isotherm

In 1916 Langmuir developed a theoretical isotherm relating the amount of gas sorbed on a surface to the pressure of the gas. It describes short-term and monocomponent sorption (Ho et al., 2002; Ijagbemi, 2009). Langmuir isotherm is a model for monolayer localized physical adsorption on homogeneous surface containing a finite number of identical sites. Accordingly, equilibrium is attained once the formation of a adsorbate monolayer on the outer surface is completed and saturated, and no further adsorption takes place (Aydin and Aksoy, 2009; Ijagbemi et al., 2009; Dada et al., 2012).
Langmuir model may be extended with heterogeneity effects, lateral interactions and multilayer effects, however, in its original formulation, it is based on four assumptions (Ignatowicz, 2011):

- the surface of the adsorbent is uniform, that is, all the adsorption sites are identical, retain one molecule of the given compound and are energetically and sterically independent of the adsorbed quantity;

- adsorbed molecules do not interact;
- all adsorption occurs through the same mechanism;
- at the maximum adsorption, only one monolayer is formed: molecules of adsorbate do not deposit on other, already adsorbed, molecules of adsorbate, but only on the free surface of the adsorbent.

Thus, the solid is assumed to have a limited adsorption capacity Q_0 and a reaction of the type: free site + solute → surface complex, is considered. Since activities of adsorbed species are not clearly defined thermodynamically, the mass action law cannot be directly applied to this reaction. Nevertheless, it has been proposed to assume the surface activity coefficients equal to unity, q_{eq} as the concentration of the retained compound on the solid at equilibrium and (Q_0 - q_{eq}) as the solid concentration of the free adsorptive sites. Therefore, the Langmuir equation may be written as equation 13 and rearranged as shown in equation 14, where the constant L is related to the free energy of adsorption and corresponds to the affinity of the compound for the solid phase. A graph with C_{eq} as x-axis and q_{eq}/C_{eq} as y-axis (equation 15) provides a line of slope ($1/Q_0$) and intercepts the y-axis at ($1/Q_0 \cdot L$). According to the initial assumptions, the isotherm reaches a plateau Q_0 (contrary to the Freundlich isotherm) and the constant $Q_0 \cdot L$ is the initial slope of the isotherm (Limousin et al., 2007).

$$L = \frac{[surface\ complex]}{[solute] \cdot [freesite]} = \frac{q_{eq}}{C_{eq}(Q_o - q_{eq})} \quad (13)$$

$$q_{eq} = Q_o \cdot \frac{L \cdot C_{eq}}{1 + L \cdot C_{eq}} \quad (14)$$

$$\frac{C_{eq}}{q_{eq}} = \frac{1}{L \cdot Q_o} + \frac{q_{eq}}{Q_o} \quad (15)$$

1.3.1.3 The Dubinin-Radushkevich isotherm

Dubinin-Raduskevich (D-R) isotherm, published by Dubinin in 1960, is an empirical model initially conceived for the adsorption of subcritical vapors onto micropore solids; is more general than the Langmuir isotherm since it does not assume a homogeneous surface or constant adsorption potential (Namasivayam and Sureshkumar, 2008; Foo and Hameed, 2010). The characteristic sorption curve of the Dubinin-Raduskevich isotherm is related to the porous structure of the sorbent and is generally applied to express the adsorption mechanism with a Gaussian energy distribution onto a heterogeneous surface (Dada et al., 2012).

The approach was usually applied to distinguish the physical and chemical adsorption of solutes based on their mean free energy of sorption per mole of the sorbate, as they are it is transferred to the surface of the solid from infinite distance in the solution. This energy E can be computed by the relationship in equation 16. The isotherm constant B is therefore expressed in mol^2/kJ^2 and it can be derived along with the maximum adsorption capacity q_m by using the linearized form of the isotherm (eq. 17), as shown in equation 18 (Ho et al., 2002; Aydin and Aksoy, 2009).

$$E = \left[\frac{1}{\sqrt{2 \cdot B}} \right] \quad (16)$$

$$q_{eq} = q_m \cdot \exp(-B\varepsilon^2) \quad (17)$$

$$\ln(q_{eq}) = \ln(q_m) - B\varepsilon^2 \quad (18)$$

One of the unique features of the Dubinin-Radushkevich isotherm model lies on the fact that it is temperature dependent because of the presence of the potential Polanyi coefficient ε expressed by equation 19, where R, T and C_{eq} represent the gas constant (8.314 J/(mol·K)), absolute temperature (K) and solute equilibrium concentration, respectively. When adsorption data at different temperatures are plotted as a function of logarithm of amount adsorbed versus the square of potential energy, all suitable data would will lie on the same curve, named as the characteristic curve (Foo and Hameed, 2010).

$$\varepsilon = RT \cdot \ln(1 + 1/C_{eq}) \quad (19)$$

1.3.2 Kinetic models

Kinetic analyses are of great importance for the use of granular media in the water treatment field, since the solute uptake rate, which determines the residence time required for completion of the sorption reactions, may be established. When using granular media in field applications such as water treatment units, a sorbent and a solution are brought into contact for a limited period of time: the understanding of the nature of the kinetic process and its theoretical description are crucial for practical applications, in order to improve the equipment and the conditions for an optimum efficiency to be achieved (Kumar, 2006; Rudzinski and Plazinski, 2007).

Heterogeneous processes involving solids and fluids can be explained through several consecutive steps determining the reaction rate (Caetano et al., 2009):

- the diffusion of solute through the liquid film surrounding the particle (Liquid Film Diffusion, LFD);
- the diffusion of solute through the porous/polymeric matrix of the sorbent media/resin (Particle Diffusion, PD);
- the chemical reaction (CR).

One of these steps usually offers much greater resistance than the others and may thus be considered as the rate-limiting step of the process: the definition of the step which controls the overall rate is largely dependent on the method by which the adsorbent is contacted with water. For a batch reactor which provides a high degree of turbulence, pore diffusion is often rate-limiting. For continuous flow systems, such as columns, film diffusion is most likely rate-limiting for usually adopted flow rates (Xie et al., 2011; Weber, 1972).

The most commonly used kinetic expressions to explain the solid/liquid adsorption processes are the pseudo first-order kinetics and the pseudo second-order kinetic model: they describe the removal process as governed by the rate of the chemical reaction so that the transition from dissolved to solid state is the mechanism controlling the whole rate (Kumar, 2006; Rudzinski and Plazinski, 2006). On the other side, the Homogeneous Particle Diffusion Model (HPM) and the Intraparticle Diffusion Model (IDM) are used when diffusion processes control the solute uptake.

1.3.2.1 Pseudo first-order model (Lagergren equation)

The Lagergren rate equation (eq. 20) is the most widely used rate equation for sorption of a solute from a liquid solution and well describes reversible reactions where, generally, the solute interacts with only one reactive site of the material. The pseudo first-order model relates the rate of the process to the amount of solute removed per unit mass of media, q_t: in eq. 20, q_{eq} is the concentrations of ion in the adsorbent at equilibrium and k_1 is the pseudo first order rate constant (Ho et al., 2000).

$$\frac{dq_t}{dt} = k_1 \cdot \left(q_{eq} - q_t\right) \tag{20}$$

After integration and applying boundary conditions for the initial and end times ($t = 0$ to $t = t$ and $q_t = 0$ to $q_t = q_t$), eq. 20 may be rearranged for linearized data plotting as shown by eq. 21.

$$Log_{10}(q_{eq} - q_t) = Log_{10}(q_{eq}) - \frac{k_1}{2.303} t \tag{21}$$

In many cases, the pseudo-first order equation does not fit well with the whole range of contact time and is generally applicable over the initial stage of the sorption processes (Shehata et al., 2010). Furthermore, In some cases though the Lagergren pseudo first-order kinetics provide excellent fit with the experimental kinetic data, it failed to predict the q_e theoretically thereby deviating from the theory (Kumar, 2006).

1.3.2.2 Pseudo second-order model

The pseudo second-order kinetic explains the kinetic rate as controlled by the chemiosorption process, thus involving the reaction of more than one active site with the dissolved molecule/ion (Rudzinski and Plazinski, 2006; El-Naggar et al., 2012). The main assumptions for this model are that the adsorption may be second-order, that the rate limiting step is a chemical reaction involving valence forces through sharing or exchange of electrons, and that the adsorption follows the Langmuir equation. The pseudo second-order kinetic is reported in eq. 22 and the corresponding linearized form shown in

eq. 23 is rearranged after integrating and applying conditions for the initial and the end of the process: $t = 0$ to $t = t$ and $q_t = 0$ to $q_t = q_t$ (Qiu et al., 2009).

$$\frac{dq_t}{dt} = k_2 \cdot \left(q_{eq} - q_t\right)^2 \quad (22)$$

$$\frac{t}{q_t} = \frac{1}{k_2 \cdot q_{eq}^2} + \frac{1}{q_{eq}} t \quad (23)$$

The driving force of the process (q_{eq}-q_t), given by the difference between the amount of solute removed per unit mass of media at equilibrium and at the generic time *t*, is proportional to the available fraction of active sites; k_2 is the pseudo first order rate constant and the product $k_2 \cdot q_{eq}^2$ is the initial sorption rate (Shehata et al., 2010).

1.3.2.3 Homogeneous particle diffusion model (HPDM)

The homogeneous particle diffusion model hypothesizes the chemical reaction as explained by a chemisorption process and therefore too fast to affect the overall removal rate (Xie et al., 2011). Based on this assumption, the removal mechanism involves the diffusion of solute from the aqueous solution into the solid phase through two possible resistances: a) the diffusion of ions through the liquid film surrounding the particle, liquid film diffusion, or b) the diffusion of ions into the sorbent beads or particle diffusion mechanism (Caetano et al., 2009). Nernst-Plank equation, which takes into account both concentration and electrical gradients of exchanging ions into the flux equation, was used to establish the HPDM equations (Shehata et al., 2010).

With diffusion rate controlling the solute uptake on particles of spherical shape, a solution of the simultaneous set of differential and algebraic equations was proposed, once: defined *X(t)*, the fractional attainment of equilibrium at time *t*; assumed spherical particles with average radius *r*; used Vermeulen approximation for the whole range $0 < X(t) < 1$. *X(t)* is evaluated by means of eq. 24, where q_t and q_e are solute loading on the solid phase at time *t* and when equilibrium is attained, respectively (Valderrama et al., 2008).

$$X(t) = \frac{q_t}{q_e} \quad (24)$$

If the diffusion of ions through the adsorbent beads is the slowest step, the particle diffusion will be the rate-determining step and the particle diffusion model could apply to calculate the diffusion coefficients. Then, the rate equation is expressed by eq. 25, that can be used for calculating the effective particle diffusivity in terms of the diffusion coefficient of solute in the solid phase D_p (m^2/s).

$$-\ln(1 - X^2(t)) = K_P \cdot t \qquad \text{where} \quad K_P = \frac{\pi^2 \cdot D_p}{r^2} \quad (25)$$

If liquid film diffusion controls the rate of exchange, the analogous expression of eq. 26 can be used, where *C* and C_r are the equilibrium concentrations of the ion in solution and solid phases, respectively, D_l the diffusion coefficient in the liquid phase (m^2/s) and δ the thickness of the liquid film (Caetano et al., 2009; Xie et al., 2011; El-Naggar et al., 2012).

$$-\ln(1 - X(t)) = K_L \cdot t \qquad \text{where} \quad K_L = \frac{3 \cdot D_l \cdot C}{r \cdot \delta \cdot C_r} \quad (26)$$

1.3.2.4 Intraparticle diffusion model

According to Weber and Morris, if the rate limiting step is particle diffusion, a plot of solute sorbed against square root of contact time should yield a straight line passing through the origin (Weber and Morris, 1963). Weber-Morris found that in many adsorption cases, solute uptake q_t varies almost proportionally with $t^{1/2}$ as shown in eq. 27, where k_P is the intraparticle diffusion rate constant. For Weber-Morris model, it is essential for the q_t - $t^{1/2}$ plot to go through the origin if the intraparticle diffusion is the sole rate-limiting step. However, it is not always the case and adsorption kinetics may be controlled by film diffusion and intraparticle diffusion simultaneously. Thus, the slope is not equal to zero as shown in

eq. 28, where *D* is a constant that gives an indication of the thickness of the boundary layer: the higher the value of *D is*, the greater the boundary layer effect are (Qiu et al., 2009; Wu et al., 2009; El-Naggar et al., 2012).

$$q_t = k_P \cdot t^{1/2} \quad (27)$$

$$q_t = k_P \cdot t^{1/2} + D \quad (28)$$

In such cases, it is assumed that the external resistance to mass transfer surrounding the particles is significant only in the early stages of sorption. This can be seen in the initially steeper linear. The second linear portion is the gradual sorption stage in which intraparticle diffusion dominates (Valderrama et al., 2008).

Furthermore multi-linearity in qt vs. t1/2 plot is considered, that is, two or three steps are involved to follow the whole process. In this form, an external surface adsorption or instantaneous adsorption occurs in the first step, then the presence of pores of different sizes determines a gradual adsorption, where the solute moves slowly from larger pores to micro-pores causing a slow adsorption rate (Valderrama et al., 2008, Wu et al., 2009).

1.4 References

1. Aydın Y. A., N. D. Aksoy (2009). Adsorption of chromium on chitosan: optimization, kinetics and thermodynamics. Chemical Engineering Journal 151, 188-194.
2. Aziz H.A., M.N. Adlan, K.S. Ariffin (2008). Heavy metals (Cd, Pb, Zn, Ni, Cu and Cr(III)) removal from water in Malaysia: post treatment by high quality limestone. Bioresource Technology 99, 1578-1583.
3. Babel S. and T.A. Kurniawan (2003). Low-cost adsorbents for heavy metals uptake from contaminated water: a review. Journal of Hazardous Materials B 97, 219-243.
4. Bailey S.E., T.J. Olin, R.M. Bricka, D.D. Adrian (1999). A review of potentially low-cost sorbents for heavy metals Water Research 33(11), 2469-2479.
5. Barakat M.A. (2008). Adsorption of heavy metals from aqueous solutions on synthetic zeolite. Research Journal of Environmental Sciences 2(1), 13-22.
6. Barakat M.A. (2011). New trends in removing heavy metals from industrial wastewater. Arabian Journal of Chemistry 4, 361-377.
7. Barakat M.A. and N. Sahiner (2008). Cationic hydrogels for toxic arsenate removal from aqueous environment. Journal of Environmental Management 88, 955-961.
8. Bishnoi N.R., M. Bajaj, N. Sharma, A. Gupta (2004). Adsorption of Cr(VI) on activated rice husk carbon and activated alumina. Bioresource Technology 91(3), 305-307.
9. Caetano M., Valderrama C., Farrán A., Cortina J.L (2009). Phenol removal from aqueous solution by adsorption and ion exchange mechanisms onto polymeric resins. Journal of Colloid and Interface Science, 338(2), 402-409.
10. Caldwell G., E. W. Neuse, A. Stephanou (1993). Synthesis of water-soluble polyamidoamines for biomedical applications. II. Polymers possessing intrachain-type secondary amino groups suitable for side-chain attachment. Journal of Applied Polymer Science, 50: 393-401.
11. Calucci L., Forte C., Ranucci E. (2007). Water/polymer interactions in a poly(amidoamine) hydrogel studied by NMR spectroscopy. Biomacromolecules 8(9), 2936-2942.
12. Casolaro M., P. Ferruti, C. Bertoglio Riolo, T. Soldi, M. Pesavento, R. Barbucci, M. C. Beni (1982). Applied macroinorganics. II. Protonation and heavy metal ions complex-formation behavior of three crosslinked resins of

poly(amido-amine) structure. Journal of Applied Polymer Science 27(6), 2239-2248.

13. Chang L. Y. (2005). Chromate reduction in wastewater at different pH levels using thin iron wires - A laboratory study. *Environmental Progress* 24(3), 305-316.
14. Council Directive 98/83/EC of 3 November 1998 on the quality of water intended for human consumption. Official Journal of the European Communities.
15. Crane R.A.,T.B. Scott (2012). Nanoscale zero-valent iron: future prospects for an emerging water treatment technology. Journal of Hazardous Materials 211-212, 112-125.
16. Cuppett J. D., S. E. Duncan, A. M. Dietrich (2006). Evaluation of copper speciation and water quality factors that affect aqueous copper tasting response. Chem. Senses 31, 689-697.
17. Dada A.O., A.P. Olalekan, A.M. Olatunya, O. Dada (2012). Langmuir, Freundlich, Temkin and Dubinin–Radushkevich isotherms studies of equilibrium sorption of Zn^{2+} unto phosphoric acid modified rice husk. Journal of Applied Chemistry 3(1), 38-45.
18. Dries J., L. Bastiaens, D. Springael, S. N. Agathos, L. Diels (2005). Combined removal of chlorinated ethenes and heavy metals by zerovalent iron in batch and continuous flow column systems. Environmental Science & Technology 39 (21), 8460-8465.
19. El-Naggar I.M., E.S. Zakaria, I.M. Ali, M. Khalil, M.F. El-Shahat (2012). Kinetic modeling analysis for the removal of cesium ions from aqueous solutions using polyaniline titanotungstate Arabian Journal of Chemistry, 5, 109-119.
20. Erickson R.J., D. A. Benoit, V. R. Mattson, E. N. Leonard, H. P. Nelson Jr. (1996). The effects of water chemistry on the toxicity of copper to fathead minnows. Environmental Toxicology and Chemistry 15(2), 181-193.
21. Ferruti P., E. Ranucci, A. Manfredi, N. Mauro, E. Ferrari, R. Bruni, F. Colombo, P. Mussini, M. Rossi (2012). L-lysine and EDTA polymer mimics as resins for the quantitative and reversible removal of heavy metal ion water pollutants. Journal of Polymer Science, Part A: Polym. Chem. 50(24), 5000-5010.
22. Ferruti P., M. A. Marchisio, R. Duncan (2002). Poly(amido-amine)s: Biomedical Applications. Macromolecular Rapid Communications 23(5-6), 332-355.
23. Ferruti P., Ranucci E., Bianchi S., Falciola L., Mussini P.R., Rossi M. (2006). Novel polyamidoamine-based hydrogel with an innovative molecular architecture as a Co2+, Ni2+, and Cu2+ sorbing material: cyclovoltammetry and extended X-Ray absorption fine structure studies. Journal of Polymer Science, Part A: Polym. Chem. 44(7), 2316-2327.
24. Foderà V. (2005). Studio sperimentale sulle potenziali applicazioni di idrogeli polimerici come “drug delivery systems”. Tesi di laurea: Università degli studi di Palermo.
25. Foo K.Y., B.H. Hameed (2010). Insights into the modeling of adsorption isotherm systems. Chemical Engineering Journal 156, 2-10.
26. Fu F., Q. Wang (2011). Removal of heavy metal ions from wastewaters: A review. Journal of Environmental Management 92, 407-418.
27. Fujiki J., N. Sonetaka, K.P. Ko, E. Furuya (2010). Experimental determination of intraparticle diffusivity and fluid film mass transfer coefficient using batch contactors. Chemical Engineering Journal 160, 683-690.
28. Gao Z., T.J. Bandosz, Z. Zhao, M. Han, J. Qiu (2009). Investigation of factors affecting adsorption of transition metals on oxidized carbon nanotubes. Journal of Hazardous Materials 167, 357-365.
29. Gheju M. (2011). Hexavalent chromium reduction with zero-valent iron (ZVI) in aquatic systems. Water Air & Soil Pollution 222, 103-148.
30. Giles C.H., D. Smith, A. Huitson (1974). A general treatment and classification of the solute adsorption isotherm. I. Theoretical Journal of Colloid and Interface Science 47, 755-765.

31. Gode F., E. Pehlivan (2003). A comparative study of two chelating ion-exchange resins for the removal of chromium(III) from aqueous solution. Journal of Hazardous Material 100(1-3), 231-243.

32. Ho Y.S., J.C.Y. Ng, G. McKay (2000). Kinetics of pollutant sorption by biosorbents: review. Separation and purification methods 29(2), 189-232.

33. Ho Y.S., J.C.Y. Ng, G. McKay (2000). Kinetics of pollutant sorption by biosorbents: review. Separation and purification methods 29(2), 189-232.

34. Ho Y.S., J.F. Porter, G. McKay (2002). Equilibrium isotherm studies for the sorption of divalent metal ions onto peat: copper, nickel and lead single component systems. Water, Air, and Soil Pollution 141, 1-33.

35. Ignatowicz K. (2011). A mass transfer model for the adsorption of pesticide on coconut shell based activated carbon. International Journal of Heat and Mass Transfer 54, 4931-4938.

36. Igwe J.C., D.N. Ogunewe, A.A. Abia (2005). Competitive adsorption of Zn(II), Cd(II) and Pb(II) ions from aqueous and non-aqueous solution by maize cob and husk. African Journal of Biotechnology 4(10), 1113-1116.

37. Ijagbemi C.O., M.H. Baek, D.S. Kim (2009). Montmorillonite surface properties and sorption characteristics for heavy metal removal from aqueous solutions. Journal of Hazardous Materials 166, 538-546.

38. Jain R., S. M. Standley, J. M. J. Frèchet (2007). Synthesis and Degradation of pH-Sensitive Linear Poly(amidoamine)s. Macromolecules, 40: 452-457.

39. Janssen L.J.J., L. Koene (2002). The role of electrochemistry and electrochemical technology in environmental protection, Chemical Engineering Journal 85, 137-146.

40. Jokela P., P. Keskitalo (1999). Plywood mill water system closure by dissolved air flotation treatment. Water Science & Technology 40(11/12), 33-42.

41. Kennish L. (1992). Toxicity of heavy metals: effects of Cr and Se on humans health. Journal of Indian Public Health Education 2, 36-64.

42. Kesenci, K., R. Say, A. Denizli (2002). Removal of heavy metal ions from water by using poly(ethyleneglycol dimethacrylate-co-acryl-amide) beads. European Polymer Journal 38, 1443-1448.

43. Kumar K. V. (2006). Linear and non-linear regression analysis for the sorption kinetics of methylene blue onto activated carbon. Journal of Hazardous Materials, 137(3), 1538–1544.

44. Kumar K. V. (2006). Linear and non-linear regression analysis for the sorption kinetics of methylene blue onto activated carbon. Journal of Hazardous Materials, 137(3), 1538-1544.

45. Kurniawan T.A., G.Y.S. Chan, W. Lo, S. Babel (2006a). Comparisons of low-cost adsorbents for treating wastewaters laden with heavy metals. Science of the Total Environment 366, 409- 426.

46. Kurniawan T.A., G.Y.S. Chan, W.H. Lo, S. Babel (2006b). Physicochemical treatment techniques for wastewater laden with heavy metals. Chemical Engineering Journal 118, 83-98.

47. Kushner D.J. (1993). Effects of Speciation of Toxic Metals on their Biological Activity. Water Pollution. Res. J. Canada 28(1), 111-128.

48. Li X., W. Zhang (2007). Sequestration of metal cations with zerovalent iron nanoparticles. A study with high resolution X-ray Photoelectron Spectroscopy (HR-XPS). Journal of Physical Chemistry C 111, 6939-6946.

49. Limousin G., J.P. Gaudet, L. Charlet, S. Szenknect, V. Barthès, M. Krimissa (2007). Sorption isotherms: a review on physical bases, modeling and measurement . Applied Geochemistry 22, 249-275.

50. Liu T., L. Zhao, D. Sun, X. Tan (2010). Entrapment of nanoscale zero-valent iron in chitosan beads for hexavalent chromium removal from wastewater. Journal of Hazardous Materials 184, 724-730.

51. Lu X., J. Xu, G. Jiang, J. Tang, X. Xu (2012). Highly active nanoscale zero-valent iron (nZVI)–Fe3O4 nanocomposites for the removal of chromium(VI) from aqueous solutions. Journal of Colloid and Interface Science 369, 460-469.

52. Luo Y., S. Sander, K. A Hunter (2010). Removal of Copper and Copper-Binding Organic Ligands During Potable Water Treatment. Environmental Technology 26, 75-83.

53. Massaoud A.A., H.A. Hanafi, T. Siyam, Z.A. Saleh, F.A. Ali (2008). Separation of Ga(III) from Cu(II), Ni(II) and Zn(II) in Aqueous Solution using Synthetic Polymeric Resins. Central European Journal of Chemistry 6(1), 39-45.

54. Matis K.A., A.I. Zouboulis, N.K. Lazaridis, I.C. Hancock (2003). Sorptive flotation for metal ions recovery. International Journal Mineral Process 70, 99-108.

55. Mavrov V., T. Erwe, C. Blöcher, H. Chmiel (2003). Study of new integrated processes combining adsorption, membrane separation and flotation for heavy metal removal from wastewater. Desalination 157, 97-104.

56. Mirbagherp S.A., S.N. Hosseini (2004). Pilot plant investigation on petrochemical wastewater treatment for the removal of copper and chromium with the objective of reuse. Desalination 171, 85-93.

57. Monser L. and N. Adhoum (2002). Modified activated carbon for the removal of copper, zinc, chromium and cyanide from wastewater. Separation and Purification Technology 26, 137-146.

58. Moore L.R., J. R. Durand, F. Strickland (2013). Copper removal from mine effluents: from lab to field evaluations. Mine Water Environ 32, 239-246.

59. Morel F.M.M., J.G. Hering (1993). Principles and applications of aquatic chemistry. New York: Wiley, 1993.

60. Nah I.W., K.Y. Hwang, C. Jeon, H.B. Choi (2006). Removal of Pb ion from water by magnetically modified zeolite. Minerals Engineering 19(14), 1452-1455.

61. Namasivayam C., M.V. Sureshkumar (2008). Removal of chromium(VI) from water and wastewater using surfactant modified coconut coir pith as a biosorbent. Bioresource Technology 99, 2218-2225.

62. National Research Council (2000). Copper in Drinking Water. Washington, DC: The National Academies Press, 2000.

63. Nikolaidis N. P., G. M. Dobbs, J. A. Lackovic (2003). Arsenic removal by zero-valent iron: field, laboratory and modeling studies. *Water Research* 37, 1417-142.

64. Noubactep C., A. Schöner (2009). Fe0-based alloys for environmental remediation: thinking outside the box. Journal of Hazardous Materials 165, 1210-1214.

65. Park K. R., Y. C. Nho (2003). Preparation and characterization by radiation of poly(vinylalcohol) and poly(N-vinylpirrolidone) hydrogels containing aloe vera. Journal of Applied Polymer Science, 90: 1477-1485.

66. Peppas N., P. Bures, W. Leobandug, H. Ichikawa (2000). Hydrogels in pharmaceutical formulations. European Journal of Pharmaceutics and Biopharmaceutics, 50: 27-46.

67. Qdais H.A., H. Moussa (2004). Removal of heavy metals from wastewater by membrane processes: a comparative study. Desalination 164(2), 105-110.

68. Qiu H., L. Lv, B.C. Pan, Q.J. Zhang, W.M. Zhang, Q.X. Zhang (2009). Critical review in adsorption kinetic models. Journal of Zhejiang University SCIENCE A 10(5), 716-724.

69. Ramos M. A. V., W. Yan, X. Li, B. E. Koel, W. Zhang (2009). Simultaneous oxidation and reduction of arsenic by zero-valent iron nanoparticles: understanding the significance of the core-shell structure. Journal of Physical Chemistry C 113(33), 14591-14594.

70. Rossi M. (2007). Electroanalysis for Physico-Chemical Characterization and Molecular Design of Polymers of Biomedical Interest: Poly(amidoamine)s. Tesi di Dottorato: Università degli studi di Milano.

71. Rudzinski W., W. Plazinski (2006). Kinetics of solute adsorption at solid/solution interfaces: a theoretical development

of the empirical pseudo-first and pseudo-second order kinetic rate equations, based on applying the statistical rate theory of interfacial transport. J. Phys. Chem. B, 110, 16514-16525.

72. Sankararamakrishnan N., A.Dixit, L. Iyengar, R. Sanghi (2006). Removal of hexavalent chromium using a novel cross linked xanthated chitosan. Bioresource Technology 97, 2377-2382.

73. Scott T.B., I.C. Popescu, R.A. Crane, C. Noubactep (2011). Nano-scale metallic iron for the treatment of solutions containing multiple inorganic contaminants. Journal of Hazardous Materials 186, 280-287.

74. Shehata F.A., M.F. Attallah, E.H. Borai, M.A. Hilal, M.M. Abo-Aly (2010). Sorption reaction mechanism of some hazardous radionuclides from mixed waste by impregnated crown ether onto polymeric resin. Applied Radiation and Isotopes 68, 239-249.

75. Shi L., X. Zhang, Z. Chen (2011). Removal of Chromium (VI) from wastewater using bentonite-supported nanoscale zero-valent iron. Water Research 45, 886-892.

76. Siyam T., H. A. Youssef, I. M. El-Naggar (1997). Adsorption studies of copper sulfate on hydrogels of Poly(amido-amines). Journal of macromolecular science. Pure and applied chemistry , 34: 2379-2388.

77. Snoeynk V.L., D. Jenkins. Water chemistry. New York: Wiley, 1980.

78. Solenera M., S. Tunalib, A.S. Ozcan, A. Ozcanc, T. Gedikbey (2008). Adsorption characteristics of lead(II) ions onto the clay/poly(methoxyethyl)acrylamide (PMEA) composite from aqueous solutions. Desalination 223, 308-322.

79. Sudipto K., N. R. Aluru, B. Johnson, W.Crone, D. J. Beebe, J. Moore (2002). Equilibrium swelling and kinetics of pH-responsive hydrogels: models, experiments and simulation. Journal of Microelettromechanical Systems, 11: 544-555.

80. Sun Y., X. Li, J. Cao, W. Zhang, H. P. Wang (2006). Characterization of zero-valent iron nanoparticles. Advances in Colloid and Interface Science 120, 47-56.

81. Trochimczuk A.W. and S. Czerwijska (2005). In(III) and Ga(III) sorption by polymeric resins with substituted phenylphosphinic acid ligands. Reactive & Functional Polymers 63, 215-220.

82. USEPA (1998). Toxicological review of hexavalent chromium. U.S. Environmental Protection Agency, Washington DC, 1998.

83. USEPA (2012). 2012 Edition of the Drinking Water Standards and Health Advisories. U.S. Environmental Protection Agency, Washington DC, 2012.

84. Valderrama C., Gamisans X., de las Heras X., Farrán A., Cortina J.L. (2008). Sorption kinetics of polycyclic aromatic hydrocarbons removal using granular acrivated carbon: intraparticle diffusion coefficients. Journal of Hazardous Materials, 157(2-3), 386-396.

85. Wang L.K., Y.T. Hung, D.A. Vaccari, Y. Li, N.K. Shammas (2004). Chemical precipitation. Physicochemical Treatment Processes 31, 141-198.

86. Weber W.J. and J.C. Morris (1963). Kinetics of Adsorption on Carbon from Solution, Journal of the Sanitary Engineering Division, American Society of Chemical Engineering 89, 31-59.

87. WHO (2003). Chromium in Drinking-water. Background document for development of WHO Guidelines for Drinking-water Quality. World Health Organization, Geneva, 2003.

88. WHO (2004). Copper in Drinking-water. Background document for development of WHO Guidelines for Drinking-water Quality. World Health Organization, Geneva, 2003.

89. WHO (2011). Guidelines for Drinking-water Quality, 4th edition. World Health Organization, Geneva, 1996.

90. Wu F.C., R.L. Tseng, R.S. Juang (2009). Initial behavior of intraparticle diffusion model used in the description of adsorption kinetics. Chemical Engineering Journal 153(1-3), 1-8.

91. Yang Q., J. Zhang, Q. Yang, X. Tang, Y. Yu, G. Yang (2011). Determination of diffusion coefficient and analysis of diffusion factors of Cr(VI) ion in clay soil. Transactions of Tianjin University 17, 051-056.

92. Zayed A. M. and N. Terry (2003). Chromium in the environment: factors affecting biological remediation. Plant and Soil 249, 139-156.

93. Zhao G., X. Wu, X. Tan, X. Wang (2011). Sorption of Heavy Metal Ions from Aqueous Solutions: A Review. The Open Colloid Science Journal (4), 19-31.

94. Zhu H., Y. Jia, X. Wu, H. Wang (2009). Removal of arsenic from water by supported nano zero-valent iron on activated carbon. Journal of Hazardous Materials 172, 1591-1596.

95. http://rimg.geoscienceworld.org/

96. http://www.kdfft.com/

2 Design of the research

2.1 Introduction and aim of the research

New, unconventional media to be used in water treatment units for the removal of organic and inorganic micropollutants are of great interest because of the need for increased properties of selectivity and efficiency in the removal processes. The study of such features plays a key role for both the description of the solute removal process and the achievement of information for the selection and design of water treatment processes.

For this purpose, two media for the removal of heavy metals from water were tested at laboratory scale: PolyAmidoAmine Hydrogels (PAAHs) and KDF®55 Granular Brass Media (KGBM). They both remove heavy metals from water, by using two different mechanisms of interaction with pollutants: hydrogels create complex bonds between active groups and heavy metal ions, while granular brass media, through a redox reaction, exchange electrons with contaminants, changing them into harmless components. Main information concerning PolyAmidoAmine Hydrogels and KDF®55 Granular Brass Media are provided in the next paragraph (par. 2.2), in order to point out properties, similarities and differences influencing the identification of experimental tests and conditions. However, few data are provided in literature concerning their removal abilities: kinetic rates and processes, equilibrium conditions achieved, selectivity features and influencing parameters in the removal process. Such characterization would allow, for each studied media:

- the identification of the best fields and mode of application;
- the selection of process parameters optimizing removal efficiencies and rates;
- the description of solute removal mechanisms involved, from a chemical (reactions involved) and physical (diffusion processes) point of view.

Based on such knowledge, a comparison among new generation and traditional media conceived for the removal of heavy metals from water would enable to identify strengths and weak features and to help in the selection of suitable media or processes for a specific contamination issue. On the other hand, by using specific models or statistical techniques for data analysis, a first attempt in the description of the removal processes characterizing the media, would give rise to new, interesting and unknown issues in order to achieve a more detailed understanding of the media themselves. Figure 2.1 shows a simplified scheme useful for the selection and the development of an appropriate experimental plan.

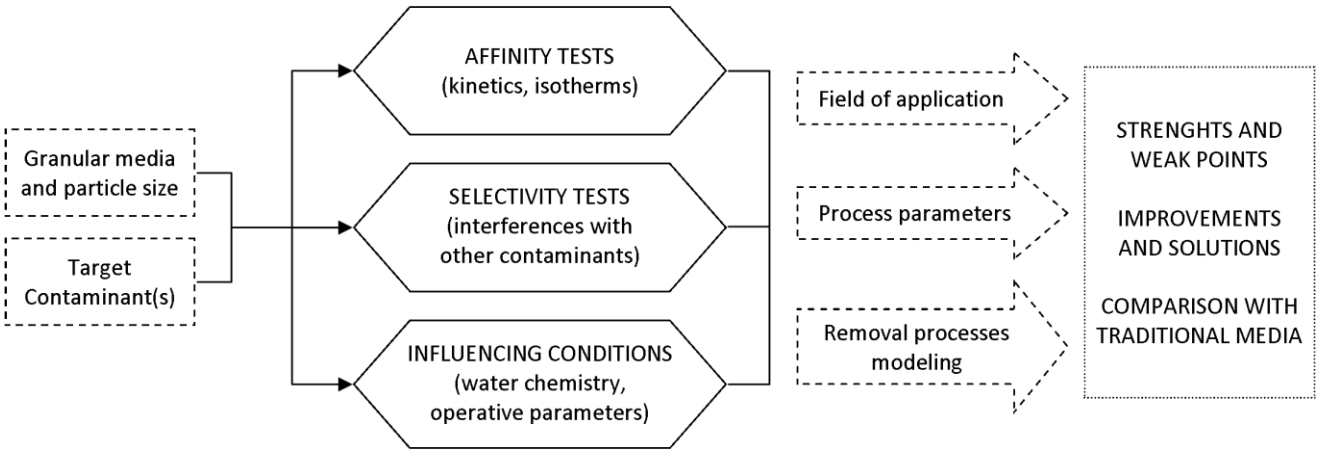

Figure 2.1. Scheme for the development of the experimental plan.

An experimental plan for a first screening has been designed and performed on both PAAHs and KGBM, thus including kinetics, isotherms, selectivity tests and experiments for the assessment of the influence of different water constituents. It is reported along with a brief explanation as for the type of test selected and the parameters adopted (par. 2.3).
Obviously, further investigations based on these results are needed to complete and focus on a deeper characterization of the two media, and consequently define upsides and drawbacks using a precise and specific approach.

2.2 Characteristics of tested media

2.2.1 PolyAmidoAmine Hydrogels (PAAH)

PolyAmidoAmine Hydrogels are synthetic polymers designed by the Department of Organic and Industrial Chemistry (Università degli Studi di Milano, IT) and characterized by the presence of amido and tertiary amine groups regularly arranged along the macromolecular chain. Their chemistry is very versatile, since they are easily cross-linked and, in addition, by employing suitably functionalized monomers, virtually any kind of functions may be introduced as pendant groups along their backbone [Calucci et al., 2007; Ferruti et al., 2002]. Hydrogels have a tri-dimensional molecular architecture and, consequently, are insoluble in water. However, they are capable of absorbing and storing large amounts of water leading to a volumetric expansion [Casolaro et al., 1982]. The complexing ability of amine and carboxyl groups and, in some instances, of other functions bonded to the main structure, enables PAAHs to create coordination complexes with heavy metal ions such as Cu^{2+}, Ni^{2+}, Co^{2+} [Ferruti et al., 2006; Ferruti et al., 2012].
The high structural versatility of PAAHs offers interesting opportunities for designing resins specifically devoted to the removal of particular contaminants; however, no engineering applications of PAA hydrogels in this field have been reported so far. Two samples of PAA hydrogels were synthesized and supplied by the Department of Organic and Industrial Chemistry: they are termed according to the starting polymers employed during the synthesis process and differ in functionalization: MBA/EDA (MethyleneBisAcrylamide/EthyleneDiAmine), besides aminic nitrogen, has no specific functional groups, while MBA/CYS (MethyleneBisAcrylamide/CYStamine) is further functionalized with disulphide groups -SS-. Chemical formulas are reported in Figure 2.2. They were both provided into two different particle dimensions, powder (d<1mm) and grains (1mm<d<2mm), as shown in Figure 2.3.

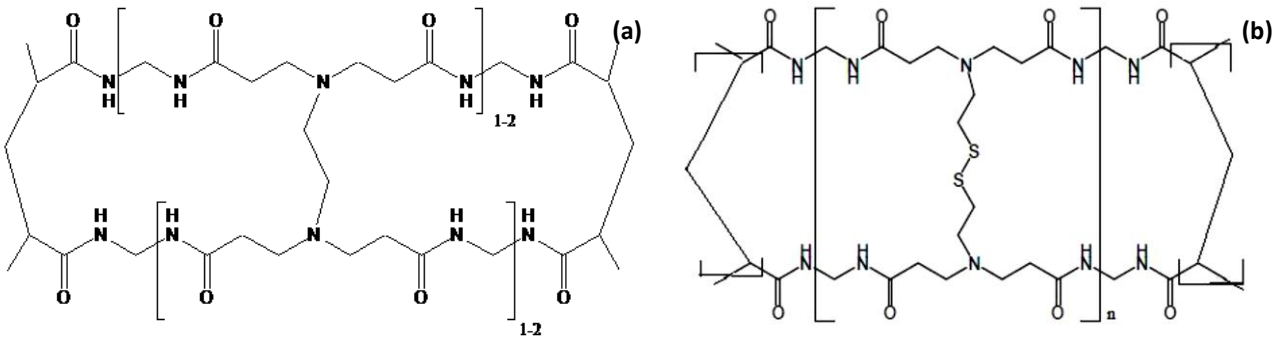

Figure 2.2. Chemical formulas of the two PAAH tested structures: MBA/EDA (a) and MBA/CYS (b).

Figure 2.3. PAAH samples: MBA/EDA - d<1mm (a), MBA/EDA - 1mm<d<2mm (b), MBA/CYS - d<1mm (c), MBA/CYS - 1mm<d<2mm (d).

Since the synthesis process at the laboratory scale allowed the production of just few tens of grams of hydrogels, an attempt to scale-up the synthesis process was carried out by a company, namely Laboratori Alchemia (Milan, IT), that provided hundreds of grams of two PAAH structures in both particle sizes. Chemical and physical characteristics were thus evaluated, in order to verify the synthetic process scale-up. No significant differences were observed: Table 2.1 summarizes the average values of the main properties of MBA/EDA and MBA/CYS samples in the form of powder and grain, measured and provided by Laboratori Alchemia.

Table 2.1. Properties of MBA/CYS and MBA/EDA samples measured and provided by Laboratori Alchemia (Milan, IT) for both powders (d<1mm) and grains (1mm<d<2mm).

	Elemental Analysis				Bulk Density ρ [g/cm^3]	Humidity U [%]*	Particle size analysis D_{50} [µm] **
	C [%]	H [%]	N [%]	S [%]			
MBA/EDA - d<1mm	44.04	7.03	17.38	-	0.816	6.9	618.4
MBA/EDA - 1mm<d<2mm	44.94	7.03	17.38	-	0.714	8.3	1405
MBA/CYS - d<1mm	37.17	6.15	13.56	13.39	0.828	4.8	685.9
MBA/CYS - 1mm<d<2mm	37.17	6.15	13.56	13.39	0.797	5.4	1378

**LOD (Loss on Drying) Method*

***Techniques used: Sieve Analysis for grains and Laser Diffraction for powders.*

The distribution point D_{50}, is the diameter corresponding to the 50% of the distribution with a smaller particle size

2.2.2 KDF55® Granular Brass Media (KGBM)

KDF Fluid Treatment Inc. manufactures (Three Rivers, Michigan 49093-9287, USA) provided the granulated KDF®55 media, an high-purity copper-zinc formulation, containing no chemical additives that reduce contaminants in water using an oxidation/reduction (redox) reaction. KDF®55 is designed specifically for removing or reducing up to 98% of heavy metals, such as lead, mercury, nickel, chromium. In addition, it controls chlorine, lime scale, bacteria and algae, even in hot water thus allowing applications in problematic circumstances like showers and tubs (http://www.kdfft.com/).
Unlike PAAHs, they are currently used for a variety of pretreatment, primary water treatment, and industrial treatment processes, both for Point-of-Entry (POE) and Point-of-Use (POU) applications. They are generally used in place of, or in conjunction with, granular activated carbon filters, since they extend the life of granular activated carbon (GAC) while protecting the carbon bed against fouling by bacterial growth. They are also used to replace silver-impregnated carbon filters, used to control bacterial growth, since they are less expensive and not toxic. Finally they can be used to protect Reverse Osmosis, Deionization and Ion Exchange systems from chlorine degradation and bacterial contamination, resulting in less fouling, longer life and reduced maintenance costs (http://www.kdfft.com/).
Main properties measured on a sample of the tested KDF®55 Granular Brass Media are summarized in Table 2.2 and the physical aspect of its granules can be observed in Figure 2.4.

Table 2.2. KDF®55 Granular Brass Media properties and measurement methods adopted.

PARAMETER	VALUE	MEASURMENT METHOD
Bulk Zn/Cu ratio elemental ratio	0.40	Measurement of Cu and Zn concentrations in solution by using Inductively Coupled Plasma Mass Spectrometry (ICP-MS). The solution was prepared by dissolving 0.1 g of KGBM in 5 mL of 6 M HNO_3 for 10 minutes, and then diluting it with ultrapure water to a final volume of 500 mL for 48 hours
Size range of granules	149-2000 μm	Scanning Electron Microscopy (SEM) *
Specific surface area	0.0149 m^2/g	Brunauer Emmett Teller (BET) multi-point surface area analysis
Density	2.75 g/cm^3	-

** The advertized value supplied by KDF Fluid Treatment Inc. manufactures was confirmed by SEM analysis*

Figure 2.4. KDF®55 Granular Brass Media just as used for tests.

2.3 Experimental plan

Table 2.3 and Table 2.4 summarize the experimental plan designed for PolyAmidoAmine Hydrogels and for KDF Granular Brass Media, respectively. Experiments on KDF Granular Brass Media, were performed at the University of North Carolina at Chapel Hill (USA), Orlando Coronell Research Group, Environmental Sciences and Engineering Department.

In Table 2.3, the experimental conditions adopted to perform different tests on PAAH samples are listed. Particle sizes ("d<1mm" and "1mm<d<2mm") and batches of production ("B1" and "B2") are specified in the acronyms used to identify PAAH samples. Tap water was used to prepare contaminated aqueous solutions.
The Swelling Degree of polymers in water was measured on each PAAH sample over time: this physical property of hydrogels is of importance for both the definition of effective volumes involved in a specific treatment unit and for a deeper understanding of diffusion processes occurring in particles matrix.
Kinetics and isotherms on a jar test device were performed at different solid/liquid ratios (S/L ratio) and solute concentrations. Two inorganic micro-pollutants were tested separately on hydrogels: copper Cu^{2+}, on both MBA/EDA and MBA/CYS, and hexavalent chromium, dissolved in water as CrO_4^{2-} or $HCrO^{4-}$, only on MBA/EDA structure, since preliminary experiments resulted in no significant removal for MBA/CYS. The two ions were selected because their positive and negative charges are supposed to involve different active groups along the chains of the polymers, thus resulting in different removal mechanisms. As for copper, in order to describe the contribution of each stages determining the overall kinetic rate of the process, both kinetic tests on a mechanical shaker and stirring rate experiments on a jar test device allowed to identify the hydrodynamic conditions necessary to control the diffusion mechanisms involved in copper removal.
Selectivity tests on Cu(II), Ni(II), Cd(II) and Zn(II) and on Cu(II) and Cr(VI) at specific operating conditions were performed in order to define positive and/or negative interference mechanisms of various ions differently charged and sized. The influence of pH was also investigated, and information concerning the chemical reactions between copper ions and PAAH active groups were drawn from results.

Table 2.4 reports the experimental plan and the operating conditions selected for each type of test. Kinetics of copper removal were performed in order to define the influence of water characteristics on redox reactions involving copper and zinc. Specifically, the pH and the presence of dissolved inorganic and organic compounds were investigated: in fact, water constituents could result in the creation of copper complexes, thus decreasing the percentage of copper dissolved in water as divalent copper ions. To this purpose, ultrapure water added with specific compounds was used.
Four pH values were tested in absence of any kind of complexes while, concerning inorganic ligands experiments, hydroxides [OH^-] and carbonates [$CO_3^{=}$] were tested adopting experimental conditions that produce in water defined starting percentages of hydroxides and carbonate complexes.
Organic ligands experiments were carried out on five organic compounds: Ethylenediaminetetraacetic acid (EDTA), Fulvic Acid (FA), Humic Acid (HA), Suwanee River Fulvic Acid (SRFA) and Suwanee River Natural Organic Matter (SRNOM). Tests on EDTA at different organic concentration were useful to define the influence of organic complex percentages, while experiments at the same value of the equivalent ratio between copper and carbon (ER) enabled to compare the effect of the ligand itself. Finally, tests performed on organic compounds both at the same DOC concentration and organic concentration (M_{OC}) explain how different types and amounts of organics dissolved in water influence copper removal.

2.4 Content of the Thesis

Results are presented in the following 6 chapters: from Chapter 3 to 6 data from tests on PAAHs are described, while Chapters 7 and 8 reports upon the kinetic studies on KGBM.

- CHAPTER 3 quantitatively describes the uptake of copper by means of MBA/EDA and MBA/CYS PAAH structures, and provides the main process parameters such as equilibrium contact times, removal efficiencies and amounts of copper removed. The effect of pH variations is also investigated along with the study of the reactions involved between copper and active groups. Furthermore, interference tests were performed on Cu(II), Zn(II), Ni(II) and Cd(II).

- CHAPTER 4 focuses on the removal of Cr(VI) by means of MBA/EDA hydrogel: results from kinetic, isotherm and interference tests with copper are used to evaluate the process parameters (contact time, residual concentration, chromium removed per unit mass of polymer) and to better understand the type of reactions or mechanisms of interactions occurring between PAAH active groups and solutes in the form of cations (copper) and anions (chromium).

- CHAPTER 5 deals with a physical explanation of the kinetic processes involved in Cu(II) and Cr(VI) removal. Based on different hypothesis as for the mechanisms of interaction and diffusion of the solute through a generic porous media, three models were selected and used to fit experimental data collected on both MBA/EDA and MBA/CYS. Because of the mixing conditions adopted, the diffusion through the particle matrix controls the overall kinetic: a detailed study on intraparticle diffusion through hydrogels is proposed.

- CHAPTER 6 analyzes data from Cu(II) kinetic tests performed on a mechanical shaker by using models selected in Chapter 5. In this case, the contact mode chosen determines the overall rate to be controlled by the diffusion through the liquid film surrounding particles. A description of copper removal by PAAHs by using a saturation kinetic model was proposed along with a comparison between the results obtained on hydrogels in the form of powder and grains.

- CHAPTER 7 introduces a kinetic study on KDF granular media aimed at the identification of the main reactions involved in copper removal. The influence water characteristics is investigated on both copper removal and zinc release, focusing on pH and on the presence of dissolved inorganic constituents that could result in copper complexes, specifically hydroxides [OH^-] and carbonates [$CO_3^=$].

- CHAPTER 8 describes results obtained from kinetics on KDF granular media in presence of 5 different organic compounds dissolved in water at different concentrations. The influence on copper removal was studied considering both the creation of organo-complexes with copper ions, and the presence of huge organic molecules in water that could interfere with the diffusion mechanisms of the copper towards KDF particles.

Further results that complete the set of data are reported in three Appendixes useful for the comprehension of specific choices taken in the design of the experimental plan. Specifically:

- APPENDIX 1 details the results obtained from preliminary tests performed in order to define the washing procedure of PAAH samples. A washing procedure is needed to remove the residues of synthesis reagents, thus minimizing alterations of water composition during tests, and to get polymers acquainted of aqueous solutions.

- APPENDIX 2 shows results obtained from preliminary tests performed to assess the applicability of PAA hydrogels in water treatment units, specifically filtration processes in column or in cross-flow systems.

- APPENDIX 3 reports procedures, formulas and complex and solubility constants for the quantitative estimation of copper speciation in water at varying of pH and inorganic water constituents. Based on these results, experimental conditions to be used for tests on KGBM have been defined.

Table 2.3. Experimental plan on PAAH: tested PAAH samples and boundary conditions used for each type of experiment.

TYPE OF TEST	PAAH SAMPLE	EXPERIMENTAL CONDITIONS					
		pH	Pollutant(s) Concentration	Reactor Volume	Dose of PAAH	Contact Time	Mixing rate
SWELLING DEGREE OVER TIME batch and static conditions	MBA/EDA - d<1mm (B1, B2) MBA/EDA - 1mm<d<2mm (B1, B2) MBA/CYS - d<1mm (B1, B2) MBA/CYS - 1mm<d<2mm (B1, B2)	pH of water	-	-	-	7 to 10 values from 5 min to 24 h	-
KINETICS - Cu(II) batch and dynamic conditions (mechanical shaker)	MBA/EDA - d<1mm (B1) MBA/EDA - 1mm<d<2mm (B1) MBA/CYS - d<1mm (B1) MBA/CYS - 1mm<d<2mm (B1)	pH of water (6.0 - 8.5)	2 mg_{Cu}/L (32 µM)	0.5 L	6.7 - 3.3 - 1.67 g/L	6 to 8 values from 15 min to 72 h	150 swinging per minute
KINETICS - Cu(II) batch and dynamic conditions (jar test apparatus)	MBA/EDA - d<1mm (B1, B2) MBA/CYS - d<1mm (B1, B2)	pH of water (7.0 - 8.5)	2 mg_{Cu}/L (32 µM)	0.5 L	3.3 g/L	7 to 10 values from 5 min to 16 h	120 rpm
KINETICS - Cr(VI) batch and dynamic conditions (jar test apparatus)	MBA/EDA - d<1mm (B2) MBA/EDA - 1mm<d<1mm (B2)	pH of water (6.5 - 8.5)	0.82 - 1.64 - 3.28 mg_{Cr}/L (16 - 32 - 64 µM)	0.5 L	6.7 - 3.3 - 1.67 - 0.83 g/L	6 to 7 values from 5 to 60 min	120 rpm
STIRRING RATE EXPERIMENTS - Cu(II) batch and dynamic conditions (jar test apparatus)	MBA/EDA - d<1mm (B1) MBA/EDA - 1mm<d<2mm (B1) MBA/CYS - d<1mm (B1) MBA/CYS - 1mm<d<2mm (B1)	pH of water (6.5 - 7.5)	2 mg_{Cu}/L (32 µM)	0.5 L	3.3 g/L	45 min for MBA/CYS; 15 min for MBA/EDA	4 to 5 values from 10 to 200 rpm
ISOTHERMS - Cu(II) batch and dynamic conditions (jar test apparatus)	MBA/EDA - d<1mm (B1)	pH of water (7.5 - 9.0)	3 mg_{Cu}/L (47 µM)	1 L	7 values from 0.4 to 3.3 g/L	120 min	120 rpm
ISOTHERMS - Cr(VI) batch and dynamic conditions (jar test apparatus)	MBA/EDA -d<1mm (B2)	pH of water (6.0 - 8.5)	1.64 mg_{Cr}/L (32 µM)	0.5 L	7 values from 0.4 to 6.7 g/L	45 min	120 rpm
pH EXPERIMENTS - Cu(II) batch and dynamic conditions (jar test apparatus)	MBA/EDA - d<1mm (B2) MBA/CYS - d<1mm (B2)	Fixed at: 4.0, 5.0, 6.0, 7.0, 8.0	2 mg_{Cu}/L (32 µM)	0.5 L	3.3 g/L	20 min 60 min	120 rpm
SELECTIVITY EXPERIMENTS - Cr(VI)/Cu(II) batch and dynamic conditions (jar test apparatus)	MBA/EDA - d<1mm (B2)	pH of water (6.5 - 8.5)	Cu: 1 - 2 mg_{Cu}/L (16 - 32 µM) Cr: 0.82 - 1.64 -3.28 mg_{Cr}/L (16 - 32 - 64 µM)	0.5 L	3.3 g/L	10 min 45 min	120 rpm
SELECTIVITY EXPERIMENTS - Cu(II)/Zn(II)/ Ni(II)/Cd(II) - batch and dynamic conditions (jar test apparatus)	MBA/EDA - d<1mm (B2) MBA/CYS - d<1mm (B2)	pH of water (6.5 - 8.5)	Cu: 2 mg_{Cu}/L (32 µM) Cd: 100 μg_{Cd}/L, Ni: 40 μg_{Ni}/L, Zn: 1.200 μg_{Zn}/L	0.5 L	3.3 g/L	24 hours	120 rpm

Table 2.4. Experimental plan on KGBM and corresponding conditions used for each type of experiment

TYPE OF TEST	EXPERIMENTAL CONDITIONS*			
	FIXED PARAMETER(S)	**VARIABLE PARAMETER(S)**	**Mixing Mode (and rate)**	**Contact Time**
pH EXPERIMENTS - Cu(II) batch and dynamic conditions	%[Cu^{2+}]	4 values of pH: 4.5 - 5.0 - 5.5 - 6.0	Magnetic Stirrer (700 rpm)	6 values from 5 to 60 min
INORGANIC LIGANDS EXPERIMENTS - Cu(II) batch and dynamic conditions	Type of ligand: hydroxides [OH^-]	4 percentages of [Cu-OH] (97% - 81% - 31% - 4%) corresponding to 4 pH values (6.0 - 6.5 - 7.0 - 7.5)	Magnetic Stirrer (700 rpm)	6 values from 5 to 60 min
	Type of ligand: carbonates [$CO_3^=$] pH = 5.0	7 concentrations of total carbonate $[CO_3]_{TOT}$ (0 - 0.1 - 0.3 - 0.5 - 0.7 - 1.0 mM)	Tumbler (15 rpm)	6 values from 5 to 60 min
	Type of ligand: carbonates [$CO_3^=$] pH = 6.0	9 percentages of [Cu-CO_3] (0% - 10% - 25% - 33% - 50% - 60% - 75% - 90% -100%)	Tumbler (15 rpm)	6 values from 5 to 60 min
ORGANIC LIGANDS EXPERIMENTS - Cu(II) batch and dynamic conditions	Type of ligand: EDTA pH = 6.0	7 values of ER (0.17 - 0.5 - 1.0 - 2.0 - 4.0 - 6.0 - 10 eq_{Cu}/eq_C)	Magnetic Stirrer (700 rpm)	6 values from 5 to 60 min
	Equivalent ratio: ER = 2.0 eq_{Cu}/eq_C pH = 6.0	3 organic compound tested (EDTA, SRFA, SRNOM)	Magnetic Stirrer (700 rpm)	6 values from 5 to 60 min
	Mass of organic compound: M_{OC} = 27 mg/L pH = 6.0	4 organic compound tested (HA, FA, SRFA, SRNOM)	Magnetic Stirrer (700 rpm)	6 values from 5 to 60 min
	Dissolved Organic Concentration: DOC = 6.3 mg_C/L pH = 6.0	4 organic compound tested (HA, FA, SRFA, SRNOM)	Magnetic Stirrer (700 rpm)	6 values from 5 to 60 min

**Parameters adopted for all type of test: Dose of KGBM: 5 g/L - Reactor Volume: 0.5 L - Initial Cu(II) concentration: 12 µM*

2.5 References

1. Calucci L., Forte C., Ranucci E. (2007). Water/polymer interactions in a poly(amidoamine) hydrogel studied by NMR spectroscopy. Biomacromolecules 8(9), 2936-2942.
2. Casolaro M., P. Ferruti, C. Bertoglio Riolo, T. Soldi, M. Pesavento, R. Barbucci, M. C. Beni (1982). Applied macroinorganics. II. Protonation and heavy metal ions complex-formation behavior of three crosslinked resins of poly(amido-amine) structure. Journal of Applied Polymer Science 27(6), 2239-2248.
3. Ferruti P., M. A. Marchisio, R. Duncan (2002). Poly(amido-amine)s: Biomedical Applications. Macromolecular Rapid Communications 23(5-6), 332-355.
4. Ferruti P., Ranucci E., Bianchi S., Falciola L., Mussini P.R., Rossi M. (2006). Novel polyamidoamine-based hydrogel with an innovative molecular architecture as a Co^{2+}, Ni^{2+}, and Cu^{2+} sorbing material: cyclovoltammetry and extended X-Ray absorption fine structure studies. Journal of Polymer Science, Part A: Polym. Chem. 44(7), 2316-2327.
5. Ferruti P., E. Ranucci, A. Manfredi, N. Mauro, E. Ferrari, R. Bruni, F. Colombo, P. Mussini, M. Rossi (2012). L-lysine and EDTA polymer mimics as resins for the quantitative and reversible removal of heavy metal ion water pollutants. Journal of Polymer Science, Part A: Polym. Chem. 50(24), 5000-5010.
6. http://www.kdfft.com/

3 Removal of copper from aqueous solutions by PolyAmidoAmine Hydrogels: kinetics, isotherms and influence of water constituents

3.1 Introduction

Heavy metals and metalloids can have severe implications on environmental and human health. Specifically, copper is mainly used to make utensils, alloys, electrical wires, munitions, coatings, pipes and valves and it is added in a large amount to fungicides, algicides, insecticides, wood preservatives, fertilizers and animal feeds (WHO, 2004). Besides the major sources of copper in drinking water are corrosion of household plumbing systems and erosion of natural deposits; human activities can release copper into the environment and its release into water occurs from weathering of soil, industrial discharge, sewage disposal and antifouling paints (Moore et al., 2013). As a result of variations in water characteristics, such as pH, hardness and copper presence in the distribution system, copper concentration in drinking water varies widely, from less than 0.005 to more than 30 mg/L (WHO, 2004).

More restrictive legal limits were recently defined and specifically-designed technologies are required to support and/or substitute conventional processes used for the removal of copper and, generally, heavy metals, such as chemical precipitation, coagulation/flocculation, ion exchange, adsorption, and membrane filtration (Kurniawan et al., 2006). All of these processes, in fact, lack specificity, resulting in several disadvantages: low removal capacity, low selectivity and long equilibrium. Much attention is being focused on innovative and specific water treatment technologies (AWWA, 1999; Liang et al. 2013).

Various kinds of new adsorbents for removing and recovering heavy metal ions have been reported. Among them, polymeric hydrogels are considered to be particularly effective because of their chemical stability and high selectivity (Fu and Wang, 2011; Bajpai and Johnson, 2005). Hydrogels containing amide, amine, carboxylic acid and ammonium groups can bind with heavy metal ions by virtue of the functional groups, and function as good adsorbents in water purification processes. However, hydrogels prepared from either natural or synthetic sources usually exhibit poor mechanical properties (Kara et al., 2004; Bekiari et al., 2008; Wang and Li, 2013). Up to now, the removal of various kinds of heavy metal ions, including Cd^{2+}, Pb^{2+}, Cu^{2+} and Mn^{2+} based on hydrogels has been reported (Essawy and Ibrahim, 2004).

PolyAmidoAmine Hydrogels (PAAHs) proved to be a suitable media for heavy metals removal from aqueous solutions: thanks to the complexing ability of their amine and, in some instances, carboxyl groups, they create coordination complexes with heavy metal ions such as Cu^{2+}, Ni^{2+} and Co^{2+} (Ferruti et al., 2006).

This paper reports about a laboratory scale research work pertaining the removal of Cu(II) by means of two samples of PAAHs, termed MBA/EDA and MBA/CYS, different in their chemical structures, since MBA/CYS is functionalized with disulphide groups -SS- in order to improve its removal abilities. Kinetic and isotherm tests, aimed at defining equilibrium parameters such as contact times, residual concentrations, amounts of copper removed per unit mass of hydrogels, were performed. Experiments at different pH values allowed to study the type of reaction involved in the removal of copper and possible changes in PAAH structure at varying H^+ concentration. Finally, the influence on the removal efficiency of PAAHs was evaluated by testing Cu(II) in the presence of other divalent heavy metal cations: Zn(II), Ni(II) and Cd(II).

3.2 Materials and Methods

3.2.1 Reagents, stock solutions, glassware and equipment

Copper nitrate ($Cu(NO_3)_2 \cdot 3H_2O$, 99% assay), zinc chloride ($ZnCl_2$, ≥99.0 %assay), nickel chloride ($NiCl_2 \cdot 6H_2O$, 99.0% assay), cadmium nitrate ($Cd(NO_3)_2 \cdot 4H_2O$, ≥99% assay), sodium hydroxide (NaOH, ACS reagent, ≥97.0%), hydrochloric acid (HCl, ACS reagent, 37% assay), nitric acid (HNO_3, ≥99.999% trace metals basis, 70% assay), hydroxylamine hydrochloride, ($NH_2OH \cdot HCl$, for AAS, ≥99.0% assay) and sodium citrate ($Na_3C_6H_5O_7 \cdot 2H_2O$, FG, ≥99% assay) were purchased from Sigma Aldrich; bathocuproinedisulfonic acid disodium salt ($C_{26}H_{18}N_2Na_2O_6S_2$, p.a. for spectrophotometric det. of Cu, Fe, ~90% assay) from Fluka. All reagents were used without further purification.
Copper, zinc, nickel and cadmium stock solutions (C_{Cu} = 1 $g_{Cu} \cdot L^{-1}$; C_{Zn} = 1.5 $g_{Zn} \cdot L^{-1}$ C_{Ni} = 1 $g_{Ni} \cdot L^{-1}$ C_{Cd} = 1 $g_{Cd} \cdot L^{-1}$) were prepared by dosing solid phase reagents in MilliQ water; the solutions were then stabilized at 5% HNO_3 and stored for all the experiments at room temperature.
Before use, all glassware was washed in an acidic bath (10% HCl), rinsed with MilliQ water and dried.
The contaminated solutions for kinetic, isotherm, selectivity and pH experiments were prepared spiking a defined volume of the metal stock solution into 500 mL (1 L for isotherm tests) tap water, previously filtered on a Millipore device equipped with 0.45 µm cellulose acetate membrane filters (Whatman), to obtain the selected starting metal concentration. A jar test equipment at the fixed stirring rate of 120 rpm was used to provide adequate turbulence into the reactor during the experiments.

3.2.2 PolyAmidoAmine Hydrogels (PAAHs)

Two samples of PAA hydrogels, MBA/EDA (753±56 kg/m^3) and MBA/CYS (709±28 kg/m^3), were synthesized by Laboratori Alchemia (Milan, IT) in the form of powders of diameter smaller than 1 mm: a particle size analysis provided the diameter corresponding to 60% finer in the particle-size distribution D_{60}, for MBA/EDA (D_{60} = 618 µm) and MBA/CYS (D_{60} = 686 µm). The two hydrogels are termed according to the starting polymers employed during the synthesis process and differ in functionalization: MBA/EDA (MethyleneBisAcrylamide/EthyleneDiAmine), besides aminic nitrogen, has no specific functional groups active for heavy metal complexation, while MBA/CYS (MethyleneBisAcrylamide/CYStamine) is further functionalized with disulphide groups -SS-. Chemical formulas are shown in par. 2.2.1.
The mass of hydrogel to be tested in kinetic, isotherm and interference experiments was previously washed to remove the residues of synthesis solutions and minimize alterations of water composition. Tap water filtered on a Millipore device equipped with 0.45 µm cellulose acetate membrane filters (Whatman) was used for this purpose. The number of steps in batch conditions (Solid/Liquid ratio, *S/L ratio* = 1/20 g·mL^{-1}; contact time, t_c: 5 minutes for each step) was previously determined (Appendix 1) in 10 steps for MBA/EDA and 5 steps for MBA/CYS, by monitoring changes in water pH, till negligible variations were observed. At the end of each step water was separated from the solid phase by using a centrifuge (IEC CL 10) at the rate of 2000 rpm for 5 minutes.

3.2.3 Evaluation of PAAH swelling ability

The volume expansion of hydrogels in tap water was evaluated in static conditions on both MBA/EDA and MBA/CYS. The swelling degree measured over time (SD_t) is defined by eq. 1, where $V_{SH,t}$ is the volume of the swelled hydrogel in tap water at time *t* and V_{DH} is the initial dry volume. Seven contact times were selected: 5 - 15 - 30 - 60 - 90 - 120 minutes and 1 day.

$$SD_t = \frac{(V_{SH,t} - V_{DH})}{V_{DH}} \quad (1)$$

3.2.4 Kinetic experiments

Batch kinetic tests, in duplicate, were performed on MBA/EDA and MBA/CYS. The contaminated solution to be tested had a starting copper concentration ($C_{Cu,0}$) of 2 mg_{Cu}/L. The *S/L ratio* adopted was of 1/300 g_{PAAH}/mL, corresponding to a mass of hydrogel used (M_{PAAH}) of 1.67 g_{PAAH}. At the end of each contact time (5 - 10 - 15 - 30 - 45 - 60 - 120 minutes

for MBA/EDA and 5 - 10 - 15 - 45 - 120 minutes, 6 - 16 hours for MBA/CYS), samples were collected for the detection of pH, electrical conductivity (EC), temperature (T) and copper concentration.

3.2.5 Isotherm experiments

Batch isotherm experiments were performed in duplicate on MBA/EDA at a starting copper concentration of 3 mg_{Cu}/L. An equilibrium contact time of 120 minutes was selected using the results of kinetic tests. Seven *S/L ratio* were tested: 1/150, 1/300, 1/1600, 1/1200, 1/1500, 1/2000 and 1/2500 g_{PAAH}/mL. Samples were collected for pH, EC, T and copper concentration detection.

3.2.6 pH experiments

Experiments at the fixed pH value of 4.0, 5.0, 6.0, 7.0 and 8.0 were performed in duplicate on both MBA/EDA and MBA/CYS, adopting two contact times (20 and 60 minutes), a *S/L ratio* of 1/300 g_{PAAH}/mL, a staring copper concentration of 2 mg_{Cu}/L. An automatic titrator (MARTINA) was used to maintain the fixed pH in the range ± 0.1 unit of pH. It operates by continuously measuring the pH and adding dilute acidic (HCl 0.1 M) or basic solution (NaOH 0.1 M) to the tested sample. Samples were collected for the detection of copper concentration.

3.2.7 Selectivity experiments

Selectivity tests were performed in duplicate on MBA/EDA and MBA/CYS in the form of powder, adopting a *S/L ratio* of 1/300 g_{PAAH}/mL, a contact time of 24 h and an initial copper concentration of 2 mg_{Cu}/L. As interfering metals, Cd(II) ($C_{Cd,0}$ = 100 μg_{Cd}/L), Ni(II) ($C_{Ni,0}$ = 40 μg_{Ni}/L) and Zn(II) ($C_{Zn,0}$ = 1.200 μg_{Zn}/L) were selected. Two types of experiments were performed: tests on copper in the presence of the single interfering metal; tests on copper in the presence of Cd(II), Ni(II) and Zn(II). In order to assess the reproducibility of metal removal efficiency upon consecutive spikes, a second loading step on the hydrogel samples with the mixture of interfering metals was performed adopting the same conditions as for the first step. Samples were collected for the detection of pH, EC, T and metal concentrations.

3.2.8 Analytical methods

Prior to analyses, the liquid phase of the collected samples was separated from the solid phase by vacuum filtration on a Millipore device with 0.45 μm cellulose acetate membrane filters (Whatman). Samples collected for pH, electrical conductivity, temperature were quickly analysed; samples collected for the detection of copper concentration were acidified with HCl and stored at 4°C for analyses. As for selectivity experiments, samples collected for the detection of metal concentrations were acidified at 2% HNO_3 and stored at 4°C for analyses.

A portable pH-meter, model Eutech pH 5+ (Eutech Instruments), was used for pH analysis (Method: IRSA 2080). EC (APAT-IRSA, 2003. Method 2030) and T (APAT-IRSA, 2003. Method 2100) were monitored using the conductivity meter model Eutech Cond 6+ (Eutech Instruments).

Concentrations of copper in samples collected from kinetic tests were analyzed using the Atomic Absorption Spectometer, (VARIA Spectra AA 55) and adopting the procedure explained in method APAT-IRSA 3250A (APAT-IRSA, 2003).

Concentrations of copper in samples collected from isotherm and pH tests were analyzed using the procedure explained in Standard Method 3500-Cu(C) for Bathocuproine Method: UNICAM VIS-UV 2 spectrophotometer was used for absorbance measurements at 484 nm wavelength (APHA, 2005).

Concentrations of copper, cadmium, nickel and zinc in samples collected from kinetic tests were analyzed using inductively coupled plasma mass spectrometry, ICP-MS (Agilent 7700) according to Standard Methods 3125-B (APHA, 2005).

3.3 Results and Discussion

3.3.1 Swelling degree

For both PAAH hydrogels, swelling degree trends over time are shown in Figure 3.1. MBA/EDA expands its volume in water almost twice as much as for MBA/CYS. Moreover the process of swelling is faster for MBA/EDA that achieves the asymptotic value of 220% in 30 minutes, while MBA/CYS needs more than 1 hour to get a swelling degree of 120%. Because of their structure, the two hydrogels behave differently in water: from a mechanical point of view, MBA/CYS structure, less flexible than that of MBA/EDA, is sturdier because chains in water open to a lower extent; however, since pores are less wide if compared to those of MBA/EDA, active groups on MBA/CYS chains are less accessible thus affecting the diffusion processes of solutes through the polymer matrix and, probably, the whole removal mechanisms. Nevertheless, at the same removal ability of copper per unit mass of hydrogel, the use of MBA/EDA in unit process involves greater volumes thus rendering MBA/CYS more suitable for field applications.

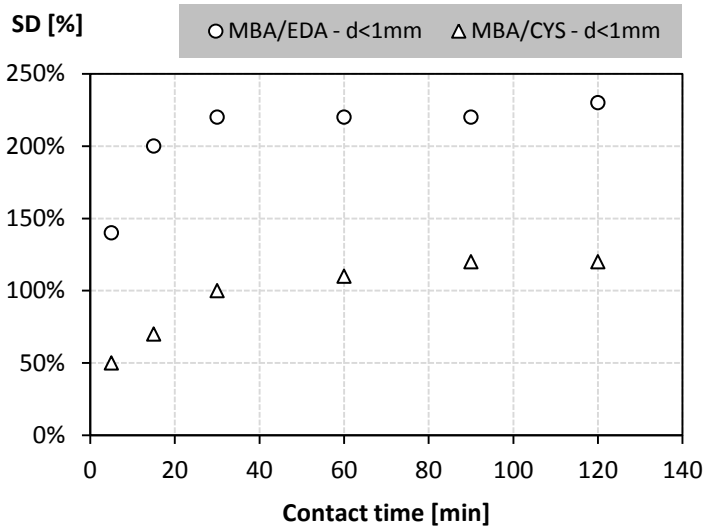

Figure 3.1. Swelling degree (*SD*) vs. contact time for MBA/EDA and MBA/CYS in the form of powder.

3.3.2 Kinetic experiments

pH and EC values are shown in Figure 3.2 for both MBA/EDA and MBA/CYS: pH is of interest since it influences both kinetics and the application of PAAHs in water treatment processes, especially if referring to drinking water; EC is of help in the understating of the interactions between hydrogels and aqueous solutions, and in determining if in-depth analysis is required through an ionic balance on water constituents.

Mean values and standard deviations of pH and EC measured on the contaminated solutions at the beginning of the experiments on both hydrogels were 8.1±0.1 and 714±14 µS/cm, respectively. Mean values and standard deviations of pH and EC measured at the end of the experiments were: 7.6±0.0 and 796±0 µS/cm for tests performed on MBA/EDA; 7.7±0.1 and 515±22 µS/cm for tests performed on MBA/CYS. pH was quickly lowered by MBA/EDA up to 1 pH unit, but then it slowly increased; MBA/CYS reduced pH up to 0.5 unit but no attempt to achieve again the starting conditions was observed. As for EC, MBA/EDA slightly increased the amount of ions dissolved in water (~ 80 µS/cm) contrarily to MBA/CYS that greatly reduced EC values of about 200 µS/cm.

The increase of H^+ concentrations into water and changes in the electrical conductivity of the solution are to be ascribed to two possible mechanisms: the release of residues from the synthesis process and the interactions between active groups on chains and the ions dissolved in water besides copper. Both polymers were rinsed before all experiments but residues of synthesis solutions can be released even during the tests: particularly, acids used at the end of the synthesis processes can determine the increase of H^+ concentrations that it's supposed to determine a rise in the value of EC, as suggested from results on MBA/EDA. However MBA/CYS behaves differently, since EC significantly decreased over time: other ions (positive or negative) are exchanged or complexed by the active groups, thus changing the composition of water: the presence of -SS- groups affects the mechanisms of interactions of

MBA/CYS structure with the compounds dissolved in water, possibly interfering with the removal ability of heavy metal ions.

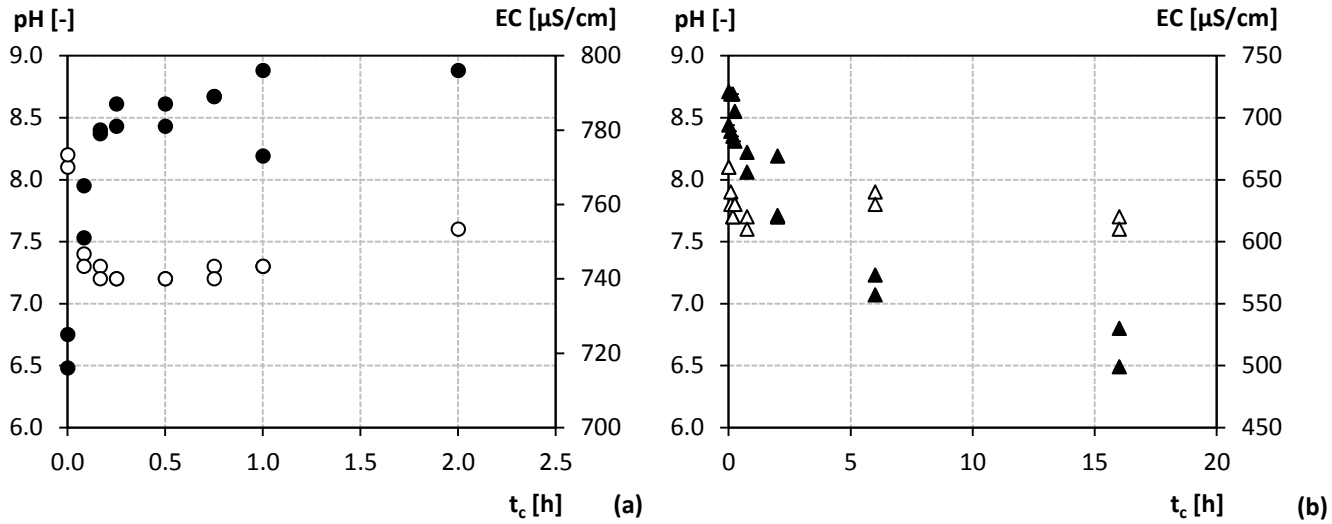

Figure 3.2. pH (white points) and EC (black points) values vs. contact time in kinetic tests on MBA/EDA (a) and MBA/CYS (b). Boundary conditions: *S/L ratio* = 1/300 g/mL; $C_{Cu,0}$ = 2.0 mg_{Cu}/L; jar test device at 120 rpm.

Copper residual concentrations ($C_{Cu,,t}$) over time (t_c) are reported in Figure 3.3 for MBA/EDA and MBA/CYS. Copper concentrations ($C_{Cu,t}$) falling outside the range [$\bar{C}_{Cu,t-1} \cdot (1+\%Err)$, $\bar{C}_{Cu,t+1} \cdot (1-\%Err)$] were considered as outliers, where $\bar{C}$ is the average value of concentrations on replicates. An error percentage value of 15% (*%Err*) was selected and adopted for the entire set of data in order to keep the percentage of removed data within the 10%.

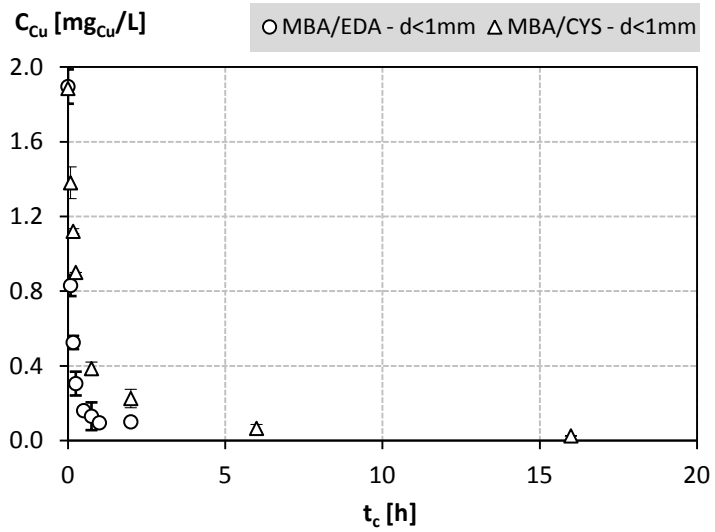

Figure 3.3. Average values of Cu concentrations vs. contact time for MBA/EDA (a) and MBA/CYS (b). Boundary conditions: *S/L ratio* = 1/300 g/mL; $C_{Cu,0}$ = 2.0 mg_{Cu}/L; jar test device at 120 rpm. Error bars are drawn using standard deviations.

Notwithstanding the low starting copper concentration, tested to simulate contaminated waters entering treatment plants for drinking waters or leakages due to corrosion of plumbing systems, removal percentages are high and above the 95%, thus revealing a good affinity of copper ions towards active groups and proving the efficacy of the dose adopted for both hydrogels (3.3 g_{PAAH}/L).

3.3.2.1 Evaluation of the equilibrium conditions

Equilibrium conditions are set when: a) the slope of the line interpolating copper residual concentrations at *t-1* and *t* is smaller than 10 degree; b) the $q_t/q_{t,max}$ ratio is at least the 85%, where q_t and q_{t-max} are the amount of copper removed

per unit mass of PAAH at the generic contact time *t* and at the final tested contact time *t-max*, respectively. Table 3.1 reports contact times t_{eq}, residual concentrations in water C_{Cueq} and hydrogel copper loads $q_{Cu,,eq}$ achieved in equilibrium conditions: for both MBA/EDA and MBA/CYS the starting mass of Cu(II) available for the removal process at the beginning of the experiments ($q_{Cu,0}$) was 0.60 mg_{Cu}/g_{PAAH}.

Copper removal abilities are similar for the two hydrogels, which remove almost the whole amount of copper dissolved in water. However equilibrium times are different: MBA/EDA is twice faster than MBA/CYS, despite the presence of disulphide groups that should improve the removal process. Two possible reasons may explain the slowing down of the removal process observed on MBA/CYS: from a chemical point of view, as previously asserted, interactions with water compounds besides copper can interfere and compete with the creation of copper-complexes that determine the removal of the metal ion, thus delaying the activation of disulphide groups towards copper. Otherwise, the mechanical structure of MBA/CYS, with its low swelling degree and its reduced accessibility towards active groups on chains, it's likely to affect the diffusion processes of solutes into polymer towards both amine and disulphide groups.

Since the presence of -SS- groups do not improve the removal ability of hydrogels, complicating also the synthesis process, experimental results suggests that MBA/EDA structure is more efficient and more advisable for applications in a unit process, thought its great volume expansion.

Table 3.1. Times t_{eq}, residual concentrations $C_{Cu,eq}$ and removal ability $q_{Cu,eq}$ at the equilibrium conditions for MBA/EDA and MBA/CYS from kinetic tests. Boundary conditions: *S/L ratio* = 1/300 g/mL; $C_{Cu,0}$ = 2.0 mg_{Cu}/L; jar test device at 120 rpm.

PAAH SAMPLE AND PARTICLE SIZE	t_{eq} [min]	$C_{Cu,eq}$ [mg_{Cu}/L]	$q_{Cu,eq}$ [mg_{Cu}/g_{PAAH}]
MBA/EDA d<1mm	45	0.13	0.53
MBA/CYS d<1mm	120	0.23	0.50

3.3.2.2 Cu(II) removal reactions

The creation of copper-complexes may be not the only process involved: ion exchange or physical adsorption due to the presence of charged groups on chains can occur and the identification of the prevailing mechanism is of importance in the study of the removal rate. Therefore, in order to define the removal mechanism of Cu(II) by means of MBA/EDA and MBA/CYS hydrogels, two models were tested against data.

Pseudo first order (eq. 2) and pseudo second order (eq. 3) models relate the rate of the process to the amount of solute removed per unit mass of media, $q_{Cu,t}$ (mg_{Cu}/g_{PAAH}). They describe the removal process as governed by the rate of the chemical reaction so that the transition from dissolved to solid state is the mechanism controlling the whole rate. The difference between the two models lies in the type of reactions involved: the first model well describes reversible reactions where, generally, the solute molecule/ion interacts with only one reactive site of the material; the pseudo second-order kinetic explains the mechanisms as controlled by the chemiosorption process, and by the reaction of two sites with the solute molecule/ion (Rudzinski and Plazinski, 2006; El-Naggar et al., 2012).

$$\frac{dq_{Cu,t}}{dt} = k_1 \cdot \left(q_{Cu,eq} - q_{Cu,t}\right) \quad (2)$$

$$\frac{dq_{Cu,t}}{dt} = k_2 \cdot \left(q_{Cu,eq} - q_{Cu,t}\right)^2 \quad (3)$$

Integrating and applying boundary conditions (t = 0 to $t = t$ and q_t = 0 to $q_t = q_t$) to eq. 2 and 3, linear form equations are obtained. Table 3.2 reports the correlation coefficients (R^2) and the estimated parameters of the two models: the rate constant of pseudo first-order kinetic (k_1), the rate constant of pseudo second-order kinetic (k_2) and the amount of copper removed per unit mass of media at the equilibrium ($q_{Cu,eq}$). Considering the pseudo second-order model, R^2 values are very high and theoretical estimates of $q_{Cu,eq}$ greatly agree with the experimental results on MBA/EDA and

MBA/CYS, as shown in Table 3.2. Results suggest that that the pseudo second-order kinetic describes better the process, thus the overall rate constant of the process is controlled by chemiosorption reactions.
Again, the different colouring of the two samples of hydrogels, after contacting copper solutions, suggests that both disulphide and amine groups concur in the formation of complexes: amine groups determine light-blue complexes while the mixed colour of amine and sulphuric complexes with copper appears brown/grey.

Table 3.2. Number of experimental data used (*N*), correlation coefficients (R^2) and estimates of parameters of the pseudo 1st and 2nd order kinetic models for MBA/EDA and MBA/CYS.
Boundary conditions: *S/L ratio* = 1/300 g/mL; $C_{Cu,0}$ = 2.0 mg_{Cu}/L; jar test device at 120 rpm

		PSEUDO 1st ORDER KINETIC			PSEUDO 2nd ORDER KINETIC		
PAAH SAMPLE AND PARTICLE SIZE	***N***	R^2	$q_{Cu,eq}$ [mg_{Cu}/g_{PAAH}]	k_1 [s^{-1}]	R^2	$q_{Cu,eq}$ [mg_{Cu}/g_{PAAH}]	k_2 [$mg_{Cu}/(g_{PAAH}\cdot s)$]
MBA/EDA d<1mm	16	0.965	0.26	$1.3\cdot10^{-3}$	1.000	0.55	$1.1\cdot10^{-2}$
MBA/CYS d<1mm	14	0.916	0.28	$1.5\cdot10^{-4}$	1.000	0.57	$2.1\cdot10^{-3}$

3.3.3 Isotherm experiments

MBA/EDA was selected for an in-depth analysis on both the removal mechanism and the surface properties of the hydrogel. Figure 3.4 shows experimental data where q_{eq} is the solid phase copper concentration at equilibrium (mol/g_{PAAH}) and C_{eq} is the molar concentration of the solute at equilibrium (mol/L). The graph shows that an asymptotic value is achieved, since MBA/EDA get saturated in the tested conditions: the amount of copper removed per unit mass of hydrogel is about $6.0\cdot10^{-5}$ mol_{Cu}/g_{PAAH} (3.8 mg_{Cu}/g_{PAAH}) and the residual concentration in water is $1.0\cdot10^{-5}$ mol_{Cu}/L (0.64 mg_{Cu}/L).

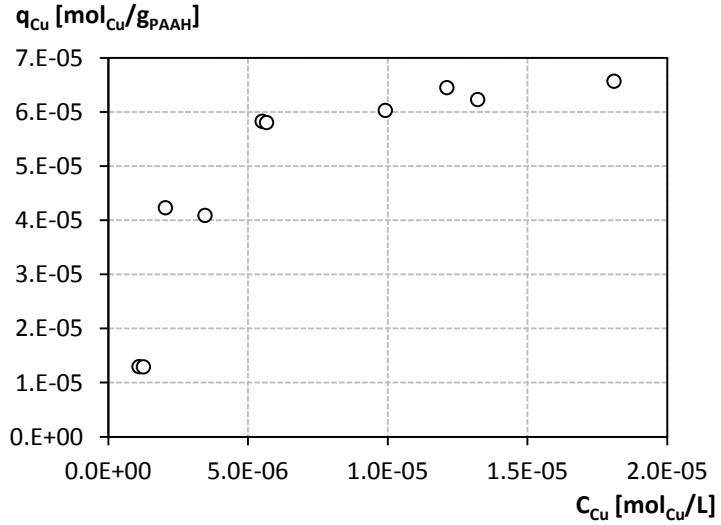

Figure 3.4. Amount of Cu(II) removed at equilibrium, q_{eq} (mol/g_{PAAH}) vs. residual Cu(II) concentration at equilibrium C_{eq} (mol/L) from isotherm tests on MBA/EDA. Boundary conditions: t_c = 120 min; $C_{Cu,0}$ = 3.0 mg_{Cu}/L; jar test at 120 rpm.

Three models of isotherm were used to fit data: Langmuir, Freundlich and Dubinin-Radushkevich. Equations are shown in Table 3.3 as well as the correlation coefficients (R^2), defined to verify the fitting of experimental data to the model, and the estimates of models parameters.
The Langmuir model describes a monolayer coverage of the sorbent with the sorbate: the removal process is due to chemical reactions involving a set of well-defined localized binding sites having the same sorption energies. Q_o is the maximum sorption capacity (mol/g_{PAAH}) while *b* is a constant related to the energy involved in the process (L/mol) (Brown et al., 2000; Hasany et al. 2001).
The Freundlich isotherm describes a heterogeneous media having an exponential distribution of active sites and energies. No saturation of the sorbent surface occurs so infinite surface coverage is predicted mathematically,

indicating reversible physisorption. Two constants define Freundlich's model: k_f, the sorption capacity and n, the sorption intensity: the numerical value of 1/n indicates that the sorption capacity is only slightly suppressed at lower equilibrium concentration (Ho et al., 2002; Hasany et al. 2001).
The Dubinin-Raduskevich isotherm describes sorbents as porous structures: q_m is the theoretical saturation capacity (mol/g); B is a constant related to the mean free energy of sorption per mole of sorbate as it is transferred to the surface of the solid from infinite distance; ϵ is the Polanyi potential, defined as shown in Table 3.3 where R ($J/mol^{-1} \cdot K^{-1}$) is the gas constant and T (K) is the absolute temperature (Ho et al., 2002; Namasivayam and Sureshkumar, 2008).

Table 3.3. Linearized equations for Langmuir, Freundich and Dubinin–Radushkevich isotherms. Correlation coefficients (R^2) and corresponding estimates of models' parameters evaluated on data from tests on MBA/EDA-d<1mm (*S/L ratio* = 1/300 g_{PAAH}/mL, $C_{Cu,0}$ = 2.0 mg_{Cr}/L, t_{eq} = 45 min).

ISOTHERM MODEL NAME	LINEARIZED EQUATION	CORRELATION COEFFICIENT (R^2)	ESTIMATES OF MODEL PARAMETERS
Langmuir	$\frac{C_{eq}}{q_{eq}} = \frac{1}{Q_o} b + \frac{C_{eq}}{Q_o}$	0.930	$Q_o = 8.4 \cdot 10^{-5}$ mol/g_{PAAH} $b = 2.4 \cdot 10^{+5}$ L/mol
Freundlich	$log_{10}(q_{eq}) = log_{10}(k_f) + \frac{1}{n} log_{10}(C_{eq})$	0.780	$k_f = 4.0 \cdot 10^{-2}$ $(L/mol)^{1/n} \cdot g^{-1}$ n = 1.78
Dubinin-Radushkevich	$\ln(q_{eq}) = \ln(q_m) - B\varepsilon^2$ where $\varepsilon = RT \cdot ln(1 + 1/C_{eq})$	0.801	$q_m = 1.3 \cdot 10^{-3}$ mol/g_{PAAH} $B = 3.9 \cdot 10^{-9}$ mol^2/J^2

Langmuir fits better than Freundlich model and this proves what stated in par. 3.3.2.2 about the prevailing occurrence of chemiosorption reactions (specifically, the creation of coordination complexes between copper and amine groups) on reversible physisorption.
Furthermore, Langmuir assumes a monolayer surface adsorption; however, hydrogels have a porous, cross-linked structure and a volume process should be taken into account when describing MBA/EDA removal mechanisms. Dubinin-Raduskevich model fit is good but not high (R^2 = 0.801): saturation is achieved only considering the tested conditions adopted, but MBA/EDA can be further loaded with larger amounts of copper: consequently, in the experiments performed, active groups reacting with copper ions are those quickly available on the external surface of particles, while those placed inside the porous structure of the hydrogel are likely react for higher copper loads. In fact, the maximum sorption capacity estimated with Langmuir model ($Q_o = 8.4 \cdot 10^{-5}$ mol/g_{PAAH}) is similar to that reported in Figure 3.4, while the theoretical saturation capacity defined by Dubinin-Raduskevich isotherm ($q_m = 1.3 \cdot 10^{-3}$ mol/g_{PAAH}) is greatly higher since the model takes into account the whole porous structure of the hydrogel.

3.3.4 pH experiments

Figure 3.5 reports the removal efficiency of copper ($\eta_{Cu(II)}$) at different pH values, evaluated on both MBA/EDA and MBA/CYS at two contact times, 20 and 60 minutes.
pH influences the removal mechanism for both hydrogels: MBA/EDA continuously increases the percentage of copper removed up to an asymptotic value occurring at the pH values of 7.0. MBA/CYS removal percentages rise up to 7.0 and then decrease at the pH value of 8. Furthermore, pH affects the copper removal kinetics for MBA/CYS only: in this case, the gap between removal efficiencies at 20 and 60 minutes changes on varying the pH while it remains constant for MBA/EDA (except in correspondence to 100% removal at pH values of 7.0 and 8.0). Finally, experiments at different pH values prove the overall reduced rate or ability in the removal of copper for MBA/CYS.
The use of an automatic titrator allowed to measure the volume of titrated HCl and NaOH: during tests on both MBA/EDA and MBA/CYS the acidic solution was used for tests from pH 4.0 to 7.0, while the basic solution for tests at pH 8.0.

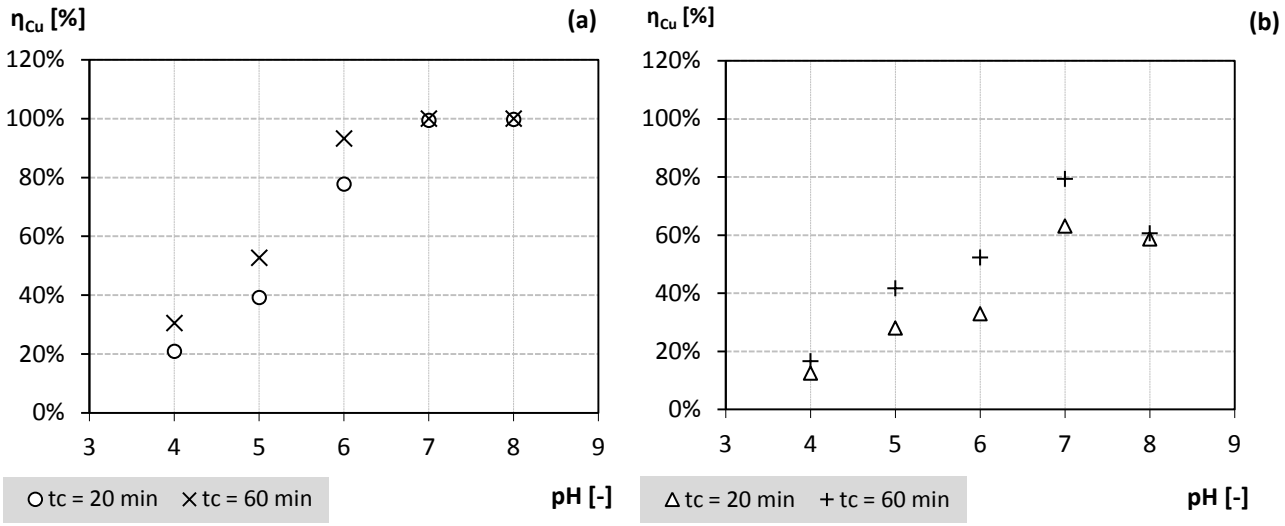

Figure 3.5. MBA/EDA (a) and MBA/CYS (b) copper removal efficiency, $\eta_{Cu(II}$ vs. pH values of aqueous solution. Boundary conditions: *S/L ratio* = 1/300 g/mL; $C_{Cu,0}$ = 3.0 mg_{Cu}/L; jar test device at 120 rpm.

The creation of coordination complexes between Cu(II) and amine nitrogen depends on the pH value and affects the concentration of H^+ in water. The presence of an acidic environment promotes the solubility of metals and the aminic nitrogen, a weak base, displays a low coordination ability. The creation of complexes is facilitated at pH greater than 6, as it can be observed in Figure 3.5. However, at the pH of 8.0 MBA/EDA and MBA/CYS behave differently since aminic nitrogen protonates: H^+ are released because of the occurrence of repulsive forces with divalent copper cations and the pH of bulk solution slows down, thus requiring the adding of a basic solution (0.1 M NaOH) in order to keep constant the selected pH value during the experiments.

3.3.5 Selectivity experiments

Selectivity tests were performed to evaluate the removal efficiency of copper in the presence of other metals and to preliminary assess the performance of hydrogels when in contact with complex aqueous factors.

The removal of copper is not significantly affected by the presence of a single interfering metal, especially for MBA/EDA which displays a copper removal efficiency of 93±4% with respect to MBA/CYS (88±3%). As reported in par. 3.3.2, copper removal efficiency in absence of other contaminants is 95±0.1% for MBA/EDA and 97±1% for MBA/CYS: a slightly efficiency decrease is thus observed for MBA/CYS. As for the interfering metals, Cd(II) and Zn(II) display negligible affinity towards both hydrogels (MBA/EDA: η_{Cd} = 15±1%; η_{Zn} = 6±2%; MBA/CYS: η_{Cd} = 4±3%; η_{Zn} = 1±1%), while Ni(II) removal efficiencies by MBA/EDA and MBA/CYS were 45±7% and 53±4%, respectively.

As for the experiments performed with the simultaneous presence of Cu(II), Ni(II), Cd(II) and Zn(II), Figure 3.6 summarizes the results for both hydrogels: the selectivity and removal efficiency obtained in the experiments in the presence of single metals are confirmed also when metals were present as mixture. Moreover, it can be noted the reproducibility of the removal efficiency values with respect to values obtained upon consecutive spikes. These results are probably related to the fact that hydrogel samples are far from saturation and consequently competition for active sites do not occur.

Table 3.4 shows overall removal abilities per unit mass of hydrogels in different loading conditions: the presence of copper alone, of a single interfering metal and of a mixture of interfering metals. Data show that the presence of multiple interfering metals acts in a slightly inhibitory way, since Q_{tot} is lower, if compared to the other two conditions tested, especially for MBA/CYS: this is predictable because of the presence of greater amounts of solute of different type that might increase the diffusive resistances into hydrogels structures. However, this behavior is restrained and should not affect significantly the use of this media in even more complex aqueous solution.

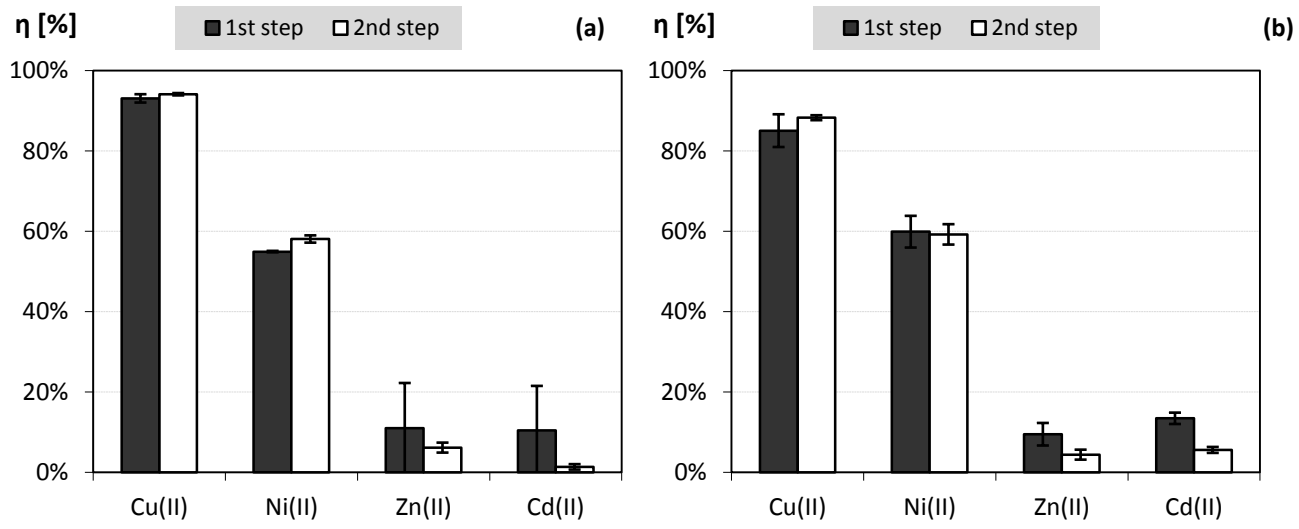

Figure 3.6. Average removal efficiencies and standard deviations for Cu(II), Ni(II), Zn(II) and Cd(II) tested simultaneously on MBA/EDA (a) and MBA/CYS (b).

Table 3.4. Overall removal abilities, expressed in terms of moles (μmol/g_{rPAAH}) and masses (μg/g_{rPAAH}) of contaminants, for MBA/EDA and MBA/CYS tested in different conditions: copper alone, single interference, mix of interferences.

PAAH SAMPLE AND PARTICLE SIZE	OVERALL REMOVAL ABILITY OF HYDROGEL (Q_{tot})		
	Cu(II)	Single interference Cu(II) + Zn(II) or Ni(II) or Cd(II)	Mix of interferences Cu(II)+Zn(II)+Ni(II)+Cd(II)
MBA/EDA d<1mm	540±25 μg/g_{PAAH} 8.5±0.4 μmol/g_{PAAH}	551±19 μg/g_{PAAH} 8.7±0.3 μmol/g_{PAAH}	519±11 μg/g_{PAAH} 8.2±0.2 μmol/g_{PAAH}
MBA/CYS d<1mm	546±8 μg/g_{PAAH} 8.6±0.1 μmol/g_{PAAH}	551±22 μg/g_{PAAH} 8.7±0.4 μmol/g_{PAAH}	480±9 μg/g_{PAAH} 7.5±0.1 μmol/g_{PAAH}

3.4 Conclusions

Coordination complexes bounds between the solute and active groups arranged along hydrogel chains allow the removal of copper from aqueous solutions: irreversible chemiosorption has been verified by fitting kinetic data with pseudo first-order and pseudo-second order kinetic models. The pH influences the charge and the activity of active sites, especially the amine nitrogen, thus affecting the amount and the kinetic of copper removal.

The different structure of the two tested hydrogels affects not only the chemical reactions involved in the process but also the diffusion mechanisms of the solute through the polymer matrix, towards active groups: the good fitting of experimental isotherm data on Dubinin-Raduskevich isotherm model allows to identify a volume process involving the diffusion of contaminants into pores.

As a result of both chemical reactions and diffusion processes, MBA/EDA removes copper twice faster than MBA/CYS, although both hydrogels display the same ability in the uptake of solutes. Specifically, copper and nickel are removed by both structures while no affinity with zinc and cadmium has been observed from experiments.

The swelling degree of hydrogels in water is relevant both at the small scale, for the definition of the kinetic parameters, and at the large scale, because of implications in the process design. Even though MBA/EDA greatly expands its volume in water (almost twice, compared to MBA/CYS), the chemical and physical structure of this hydrogel is more efficient and more advisable for applications in a unit process, because of ease of synthesis and lower equilibrium contact times at same removal ability.

Further investigations would be useful to clearly identify diffusion processes through polymer matrixes and process parameters affecting the overall removal rate, in order to improve the knowledge of PAA hydrogels and define their application field in the treatment of heavy metal contaminated waters.

3.5 References

1. American Public Health Association (APHA), American Water Works Association (AWWA) & Water Environment Federation (WEF). Standard Methods for the Examination of Water and Wastewater, 21st Edition, Washington DC, 2005.
2. American Water Works Association (AWWA), Water Quality and Treatment Handbook: A Handbook of Community Water Supplies, Fifth Edition, Irwin/McGraw-Hill, 1999.
3. APAT-IRSA, 2003. Metodi analitici per le acque. APAT Manuali e Linee Guida 29/2003.
4. Bajpai S.K., S. Johnson (2005). Superabsorbent hydrogels for removal of divalent toxic ions. Part I: Synthesis and swelling characterization. Reactive & Functional Polymers 62, 271-283.
5. Bekiari V., M. Sotiropoulou, G. Bokias, P. Lianos (2008). Use of poly(N,N-dimethylacrylamide-cosodium acrylate) hydrogel to extract cationic dyes and metals from water. Colloids and Surfaces A: Physicochemical and Engineering Aspects 312, 214-218.
6. Brown P.A., S.A. Gill, S.J. Allen (2000). Metal removal from wastewater using peat. Water Research 34(16), 3907-3916.
7. El-Naggar I.M., E.S. Zakaria, I.M. Ali, M. Khalil, M.F. El-Shahat (2012). Kinetic modeling analysis for the removal of cesium ions from aqueous solutions using polyaniline titanotungstate *Arabian Journal of Chemistry*, 5, 109–119.
8. Essawy H.A., H. S. Ibrahim (2004). Synthesis and characterization of poly(vinylpyrrolidone-co-methylacrylate) hydrogel for removal and recovery of heavy metal ions from wastewater. Reactive and Functional Polymers 61, 421-432.
9. Ferruti P., E. Ranucci, A. Manfredi, N. Mauro, E. Ferrari, R. Bruni, F. Colombo, P. Mussini, M. Rossi (2012). Llysine and EDTA polymer mimics as resins for the quantitative and reversible removal of heavy metal ion water pollutants. Journal of Polymer Science Part A: Polymer Chemistry, 50: 5000-5010.
10. Ferruti P., E. Ranucci, S. Bianchi, L. Falciola, P.R. Mussini, M. Rossi, Novel polyamidoamine-based hydrogel with an innovative molecular architecture as a Co^{2+}, Ni^{2+}, and Cu^{2+} sorbing material: cyclovoltammetry and extended x-ray absorption fine structure studies. Journal of Polymer Science Part A: Polymer Chemistry 44 (2006) 2316-2327.
11. Fu F., Q. Wang (2011). Removal of heavy metal ions from wastewaters: A review. Journal of Environmental Management 92, 407-418.
12. Hasany S.M., M.M. Saeed, M. Ahmed (2001). Sorption of traces of silver ions onto polyurethane foam from acidic solution. Talanta 54, 89-98.
13. Ho Y. S., J. F. Porter, G. McKay (2002). Equilibrium isotherm studies for the sorption of divalent metal ions onto peat: copper, nickel and lead single component systems. Water, Air, and Soil Pollution 141, 1-33.
14. Kara A., L. Uzun, N. Beşirli, A. Denizli (2004). Poly(ethylene glicol dimethacrylate- n-vinyl imidazole) beads for heavy metal removal. Journal of Hazardous Materials 106(2-3), 93-99.
15. Kurniawan T.A., G.Y.S. Chan, W.H. Lo, S. Babel (2006). Physicochemical treatment techniques for wastewater laden with heavy metals. Chemical Engineering Journal 118, 83-98.
16. Liang F.B., Song Y. L., Huang C. P., Li Y. X., Chen B. H. (2013). Synthesis of novel lignin-based ion-exchange resin and its utilization in heavy metals removal. Industrial and Engineering Chemistry Research, 52 (3), 1267-1274.
17. Moore L.R., J. R. Durand, F. Strickland (2013). Copper removal from mine effluents: from lab to field evaluations.

Mine Water Environ 32, 239-246.

18. Namasivayam C., M.V. Sureshkumar (2008). Removal of chromium(VI) from water and wastewater using surfactant modified coconut coir pith as a biosorbent. Bioresource Technology 99, 2218-2225.
19. Rudzinski W., W. Plazinski (2006). Kinetics of solute adsorption at solid/solution interfaces: a theoretical development of the empirical pseudo-first and pseudo-second order kinetic rate equations, based on applying the statistical rate theory of interfacial transport. J. Phys. Chem. B, 110, 16514-16525.
20. Wang J. and X. Li (2013). Ion-imprinted composite hydrogels with excellent mechanical strength for selective and fast removal of Cu^{2+}. Industrial & Engineering Chemistry Research 52, 572-577.
21. WHO (2004). Copper in Drinking-water. Background document for development of WHO Guidelines for Drinking-water Quality. World Health Organization, Geneva, 2003.

4 Kinetics, isotherms and interference tests on polyamidoamine hydrogels for the removal of hexavalent chromium

4.1 Introduction

The majority of toxic metal pollutants are waste products of industrial and metallurgical processes. According to the World Health Organization, the metals of most immediate concern are chromium, nickel, copper, lead, mercury and zinc (Bajpai and Johnson, 2005). Chromium compounds find their way into the environment mainly through tanning and electroplating industries. It essentially exists in two forms namely Cr(VI) and Cr(III). The distribution of compounds containing these two forms depends on the redox potential, the pH, the presence of oxidizing or reducing compounds, the kinetics of the redox reactions, the formation of Cr(III) complexes or insoluble Cr(III) salts, and the total chromium concentration. In the environment, Cr(VI) occurs mostly as CrO_4^{2-} or $HCrO^{4-}$ and Cr(III) as $Cr(OH)_n^{(3-n)+}$ (WHO, 2003; Sankararamakrishnan et al., 2006). Because of its negative impact on the aquatic ecosystem, the hexavalent state is more concerned by the research: it can diffuse as CrO_2^{4-} or $HCrO^{4-}$ through cell membranes, it is carcinogenic and mutagenic to living organisms, it has high water solubility and mobility, and because of its oxidizing properties it tends to accumulate in living organisms (Mahapatra et al. 2013).

The maximum permissible level of Cr(VI) in drinking water according to World Health Organization (WHO) is 50 µg/L. In general, concentrations of chromium in groundwater are low (<1 µg/L) even if levels up to 50 µg/L have been reported in the USA. Most surface waters contain between 1 and 10 µg/L, but levels up to 84 and 44 µg/L have been found in the USA and in central Canada (WHO, 2003).

Recently, considerable interest has been focused on the development of polymers and biopolymers, as a tool for removing and recovering heavy metal ions from polluted waters (Bajpai and Johnson, 2005; Kyzas et al. 2009; Aydın and Aksoy, 2009). Among them, polymeric hydrogels are considered to be particularly effective because of their chemical stability and high selectivity. Hydrogels containing amide, amine, carboxylic acid, and ammonium groups can bind with heavy metal ions by virtue of the functional groups, and act as good adsorbents in water purification processes. Up to now, the removal of various kinds of heavy metal ions, including Cr(VI), Cd^{2+}, Pb^{2+}, Cu^{2+}, and Mn^{2+} based on hydrogels has been reported (Chauhan and Mahajan, 2002; Bajpai and Johnson, 2005; Çavuş¸ and Gürdağ, 2009; Halim and Al-Deyab, 2011; Wang and Li, 2013).

PolyAmidoAmine Hydrogels (PAAHs) are able to absorbe large amounts of water, thus expanding in water, and to create coordination complexes with heavy metal ions such as Cu^{2+}, Ni^{2+}, Co^{2+}, because of the presence of amine and carboxyl groups able to create complexes (Ferruti et al., 2006; Ferruti et al., 2012). To our best knowledge, few results are found in literature about adsorption studies of heavy metals by means of PAA hydrogels: copper was tested in 1997 by Siyam et al., but no other contaminants were further investigated. In the current research, the removal of Cr(VI) by means of a sample of PAA hydrogel termed MBA/EDA is studied. Kinetic and isotherm tests were performed in order to define equilibrium parameters (contact time, residual concentration, chromium removed per unit mass of polymer) by varying the mass of hydrogel dosed and the initial chromium concentration adopted. Finally, the selective complexing abilities of the MBA/EDA structure was evaluated, by testing interferences of Cu^{2+} on Cr(VI) removal.

4.2 Materials and Methods

4.2.1 Reagents, stock solutions and glassware

Potassium dichromate ($K_2Cr_2O_7$, ACS reagent, ≥99.0% assay), copper nitrate ($Cu(NO_3)_2 \cdot 3H_2O$, 99% assay), hydrochloric acid (HCl, ACS reagent, 37% assay), hydroxylamine hydrochloride, ($NH_2OH \cdot HCl$, for AAS, ≥99.0% assay) and sodium citrate ($Na_3C_6H_5O_7 \cdot 2H_2O$, FG, ≥99% assay) were purchased from Sigma Aldrich; bathocuproinedisulfonic acid disodium salt ($C_{26}H_{18}N_2Na_2O_6S_2$, p.a. for spectrophotometric det. of Cu, Fe, ~90% assay) from Fluka. All reagents were used without further purification.

A chromium stock solution (1 $g_{Cr} \cdot L^{-1}$) and a copper stock solution (1 $g_{Cu} \cdot L^{-1}$), stored for all the experiments at room temperature, were prepared by dosing $K_2Cr_2O_7$ and $Cu(NO_3)_2 \cdot 6H_2O$, respectively, in MilliQ water. Copper stock solution was stabilized at 5% HNO_3.

Before use, all glassware was washed in an acidic bath (10% HCl), rinsed with MilliQ water and dried.

The contaminated solutions for kinetic, isotherm and selectivity experiments were prepared spiking a defined volume of metal stock solution into 500 mL tap water, previously filtered on a Millipore device equipped with 0.45 µm cellulose acetate membrane filters (Whatman), to obtain the selected starting metal concentration. A jar test equipment at the fixed stirring rate of 120 rpm was used to provide adequate turbulence into the reactor during the experiments.

4.2.2 PolyAmidoAmine Hydrogel (PAAH)

MBA/EDA PolyAmidoAmine Hydrogel is termed according to the starting polymers employed during the synthesis process (MethyleneBisAcrylamide/EthyleneDiAmine). The chemical formula is shown in par 2.2.1. The polymer was provided by Laboratori Alchemia (Milan, IT), into two different particle sizes: powder (d<1mm, 767±36 kg/m^3) and grain (1mm<d<2mm, 690±33 kg/m^3).

The mass of hydrogel to be tested in kinetic, isotherm and interference experiments, was previously washed to remove the residues of synthesis solutions. In order to minimize alterations of water composition, tap water filtered by Millipore on 0.45 µm cellulose acetate membrane filters (Whatman) was used. The number of steps in batch conditions (Solid/Liquid ratio, *S/L ratio* = 1/20 $g_{PAAH} \cdot mL^{-1}$; contact time, t_c: 5 minutes for each step) was previously determined (Appendix 1) in 10 steps by monitoring changes in water pH, till negligible variations were observed. At the end of each step water was separated from the solid phase by using: for powders, a centrifuge (IEC CL 10) at the rate of 2000 rpm for 5 minutes; for grains, gravity settlement in static conditions for 5 minutes.

4.2.3 Evaluation of PAAH swelling ability

The ability of MBA/EDA structure to expand its volume when in contact with water was evaluated in static conditions on both powders and grains. The swelling degree measured over time (SD_t) is defined by equation 1, where $V_{SH,t}$ is the volume of the swelled hydrogel in tap water at time *t* and V_{DH} is the initial dry volume. Seven contact times were selected: 5 - 10 - 15 - 30 - 60 - 120 minutes and 1 day.

$$SD_t = \frac{(V_{SH,t} - V_{DH})}{V_{DH}} \quad (1)$$

4.2.4 Kinetic experiments

Batch kinetic tests, in duplicate, were performed on MBA/EDA in the form of both powder and grain. Specifically, three initial hexavalent chromium concentrations $C_{Cr,0}$, were selected (0.82, 1.64, 3.28 mg_{Cr}/L) and four *S/L ratio* were adopted (1/150, 1/300, 1/600, 1/1200 g_{PAAH}/mL). MBA/EDA in the form of grain was tested at 1.64 mg_{Cr}/L and 1/300 g_{PAAH}/mL. MBA/EDA in the form of powder was tested at each combination of $C_{Cr,0}$ and *S/L ratio*, with the exception of the combination 0.82 mg_{Cr}/L and 1/150 g_{PAAH}/mL. At the end of each contact time (5 - 10 - 15 - 30 - 45 - 60 minutes for powders and 5 - 10 - 15 - 30 - 45 - 60 - 120 - 240 minutes for grains), samples were collected for the detection of pH, electrical conductivity (EC), temperature (T) and chromium concentration.

4.2.5 Isotherm experiments

Once selected the equilibrium contact time of 45 minutes from kinetic tests, batch isotherm experiments were performed on MBA/EDA in the form of powder adopting an initial chromium concentration of 1.64 mg_{Cr}/L. Seven *S/L ratio* were selected: 1/150, 1/300, 1/1600, 1/1200, 1/1500, 1/2000 and 1/2500 g_{PAAH}/mL. Samples were collected for the detection of pH, EC, T and chromium concentration.

4.2.6 Selectivity experiments

Selectivity experiments were performed on MBA/EDA in the form of powder, selecting two contact times (10 and 45 minutes) and a *S/L ratio* of 1/300 g_{PAAH}/mL. Specifically, three starting hexavalent chromium concentrations $C_{Cr,0}$, were selected (0.82, 1.64, 3.28 mg_{Cr}/L) and combined with two starting copper concentrations $C_{Cu,0}$ (1.0, 2.0 mg_{Cu}/L). Samples were collected for the detection of pH, EC, T, chromium and copper concentrations.

4.2.7 Analytical methods

Prior to analyses, the liquid phase of the collected samples was separated from the solid phase by vacuum filtration on a Millipore device with 0.45 μm cellulose acetate membrane filters (Whatman). Samples collected for the detection of pH, EC and T were quickly analysed; samples collected for the detection of chromium and copper concentrations were stored for analyses for no more than 24 hours, in the dark and at 4°C.
A portable pH-meter, model Eutech pH 5+ (Eutech Instruments), was used for pH analysis (Method: IRSA 2080). EC (APAT-IRSA, 2003. Method 2030) and T (APAT-IRSA, 2003. Method 2100) were monitored using the conductivity meter model Eutech Cond 6+ (Eutech Instruments).
Concentrations of Cr(VI) in water were analyzed using LCK313 cuvette test (Hach Lange), XION 500 (Dr Lange) spectrophotometer based on Diphenylcarbazide Method from Standard Method 3500-Cr(B) (APHA, 2012). As for copper residual concentrations, Bathocuproine Method from Standard Method 3500-Cu(C) was adopted (APHA, 2012) and UNICAM VIS-UV 2 spectrophotometer used for absorbance measurements at 484 nm wavelength (optical path, 1 cm).

4.3 Results and Discussion

In the following, residual chromium and copper concentration data ($C_{Me,t}$) falling outside the range [$\bar{C}_{Me,t-1} \cdot (1+\%Err)$, $\bar{C}_{Me,t+1} \cdot (1-\%Err)$] were considered as outliers, where $\bar{C}$ is the average value of concentrations on replicates and an error percentage value (*%Err*) of 15% is adopted.

4.3.1 Swelling degree

Swelling degree trends over time are shown in Figure 3.1 for both MBA/EDA particle sizes. Almost the same asymptotic value of 200% is achieved by both MBA/EDA samples, meaning that the volume expansion of an hydrogel is related to its chemical structure and not to the form it is provided; however particle size plays a key role in accelerating the process of expansion: powders swell quickly, getting about the 90% of the final *SD* in the first 10 minutes, while for grains 30 minutes are needed to achieve the equilibrium: because of particle dimensions, it takes more time for water to access all molecule pores and this feature is likely to affect the removal performances of the two MBA/EDA samples.

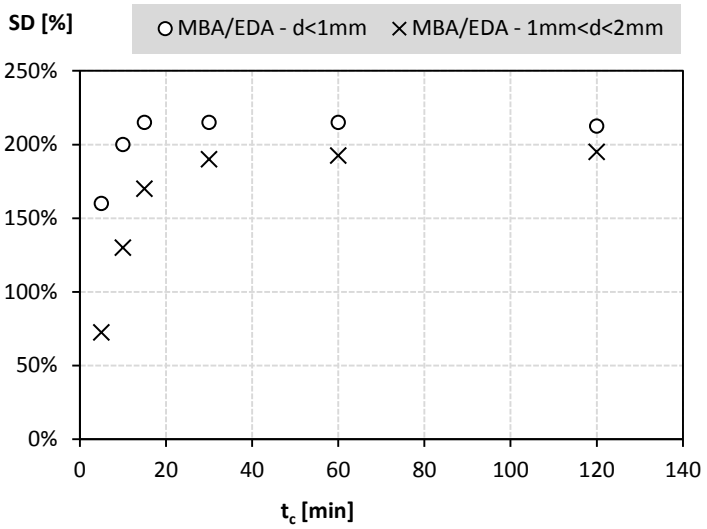

Figure 4.1. Swelling degree (*SD*) vs. contact time (t_c) for MBA/EDA hydrogel in the form of powder and grain.

4.3.2 Kinetic experiments

The ratio between the residual chromium concentrations at the generic time *t* and at the beginning of the experiments (C_t/C_0) over time (t_c) are reported in Figure 4.2 and Figure 4.3 for MBA/EDA in the form of powder, depending on the starting chromium concentration tested and the adopted value of S/L ratio. Removal percentages range from 53% to 96% and increase for high PAAH doses (low S/L ratios) as it can be seen in Figure 4.2, while the effect of $C_{Cr,0}$ is negligible as shown in Figure 4.3.

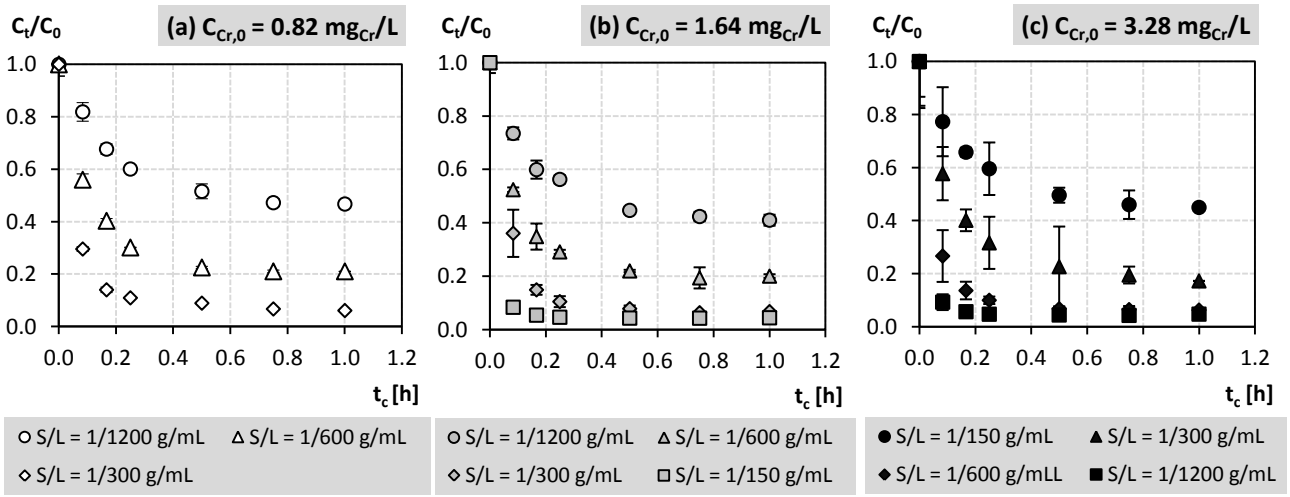

Figure 4.2. Average values of the ratio C_t/C_0 vs. contact time t_c for MBA/EDA - d<1mm, at varying of the *S/L ratio*. Each graph is shown for tests at the same starting chromium concentration $C_{Cr,0}$: (a) 0.82 mg_{Cr}/L; (b) 1.64 mg_{Cr}/L; (c) 3.28 mg_{Cr}/L. Error bars are drawn using standard deviations.

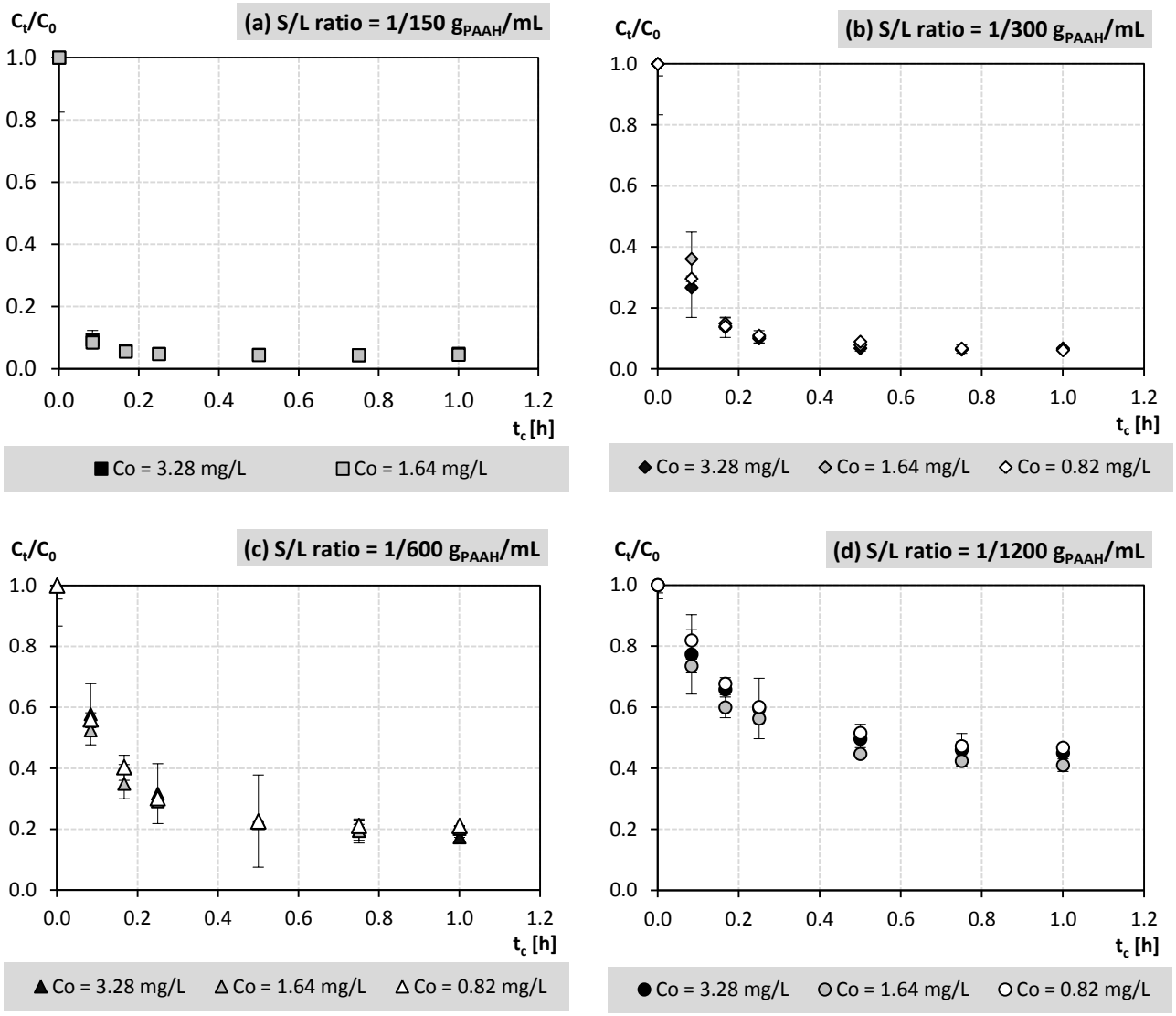

Figure 4.3. Average values of the ratio C_t/C_0 vs. contact time t_c for MBA/EDA-d<1mm, at varying of the starting chromium concentration $C_{Cr,0}$. Each graph is shown for tests at the same *S/L ratio*: (a) 1/150 g_{PAAH}/mL; (b) 1/300 g_{PAAH}/mL; (c) 1/600 g_{PAAH}/mL; (d) 1/1200 g_{PAAH}/mL. Error bars are drawn using standard deviations.

4.3.2.1 Evaluation of equilibrium conditions

Once defined the amount of chromium removed per unit mass of PAAH at the generic contact time *t* (q_t) and at the final tested contact time *t-max* ($q_{t\text{-}max}$), equilibrium conditions are set when: a) the slope of the line interpolating copper residual concentrations at *t-1* and *t* is smaller than 10 degree; b) the $q_t/q_{t,max}$ ratio is at least the 85%.

Contact times t_{eq}, residual concentrations in water $C_{Cr,eq}$ and chromium removal ability $q_{Cr,,eq}$ at the equilibrium, are reported in Table 4.1 for each combination of *S/L ratio* and $C_{Cr,0}$, corresponding to a specific mass of chromium available to the unit mass of hydrogel. In addition, Table 4.1 indicates the starting conditions of the studied system, since both the concentration and the amount of Cr(VI) available per unit mass of PAAH at the beginning of the experiments, given by the product between the S/L ratio and the initial concentration ($C_{Cr,0}$ and $q_{Cr,0}$ respectively), could affect the results.

At equivalent *S/L ratio*, the starting concentration of Cr(VI) influences equilibrium times that raise of just 15 minutes when passing from 1.64 to 3.28 mg_{Cr}/L, against a removal ability achieved ($q_{Cr,eq}$) almost doubled. This could be ascribed to the positive effect of the increased concentration gradient (Fick's first law) which accelerates the diffusion of chromium through the film layer surrounding the particle. Moreover, high chromium concentrations determine increased salinity and osmotic pressure, thus producing greater solution flow through hydrogel pores and enhancing the removal of chromium.

A different behavior is observed when passing from 0.82 to 1.64 mg_{Cr}/L: it's supposed to be that, in this case, negligible

differences in t_{eq} values are observed since the effect of the concentration gradient and osmotic pressure is too low to affect the removal process which involves, again, nearly doubled amounts of Cr(VI) removed per unit mass of PAAH.

Table 4.1. Equilibrium conditions achieved on MBA/EDA-d<1mm (equilibrium times t_{eq}, residual concentrations in water $C_{Cr,eq}$ and chromium removal ability $q_{Cr,,eq}$) as a function of the boundary conditions adopted (*S/L ratio*, $C_{Cr,0}$, $q_{Cr,0}$).

	STARTING CONDITIONS		EQUILIBIUM CONDITIONS		
S/L RATIO [g_{PAAH}/mL]	**$C_{Cr,0}$ [mg_{Cr}/L]**	**$q_{Cr,0}$ [mg_{Cr}/g_{PAAH}]**	**t_{eq} [min]**	**$C_{Cr,eq}$ [mg_{Cr}/L]**	**$q_{Cr,eq}$ [mg_{Cr}/g_{PAAH}]**
	0.82	-	-	-	-
1/150	1.64	0.25	15	0.08	0.24
	3.28	0.49	30	0.15	0.47
	0.82	0.25	30	0.07	0.22
1/300	1.64	0.49	30	0.13	0.44
	3.28	0.98	45	0.21	0.92
	0.82	0.49	45	0.16	0.37
1/600	1.64	0.98	45	0.32	0.80
	3.28	1.97	60	0.56	1.60
	0.82	0.98	45	0.37	0.49
1/1200	1.64	1.97	45	0.68	1.11
	3.28	3.94	60	1.49	2.18

As for the type of equilibrium established, Figure 4.4 shows $C_{Cr,eq}$ (a) and $q_{Cr,eq}$ (b) trends, as a function of the total amount of Cr(VI) available per unit mass of hydrogel at the beginning of the test ($q_{Cr,0}$). A good linear fit (R^2 = 0.978) is observed, especially for graph (a), meaning that the more the hydrogel is loaded the higher the residual concentration of chromium is, and that anyhow the hydrogel is loaded with Cr(VI) ($q_{Cr,0}$), the residual concentration achieved at equilibrium is the same though the different kinetic rate observed.

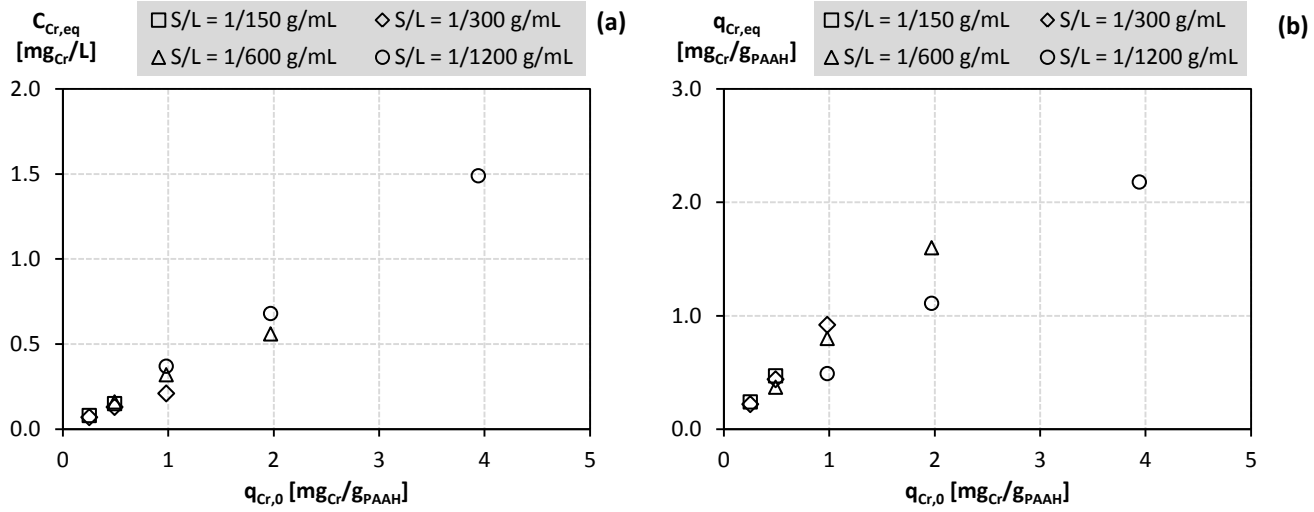

Figure 4.4. Chromium residual concentrations, $C_{Cr,eq}$ (a) and amounts removed per unit mass of PAAH, $q_{Cr,eq}$ (b) vs. the total amount of chromium available per unit mass of PAAH at the beginning of the test, $q_{Cr,0}$, at varying the *S/L ratio*.

The amount of Cr(VI) removed is well fitted too (R^2 = 0.926 for graph (b) in Figure 4.4), but results from tests performed at the S/L ratio of 1/1200 g_{PAAH}/mL, slightly deviate from all the others: this highlights the effect of the *S/L ratio* on the hydrodynamic condition of the system, apparent, but at a lower extent, on the other tested values too. At same conditions of $q_{Cr,0}$, if less amounts of PAAH are dispersed in the same volume of water, contacts between the solute molecules and the hydrogel particles are reduced, thus lowering the amount of Cr(VI) removed per unit mass of MBA/EDA.

4.3.2.2 Effect of particle size

A comparison between the removal ability of MBA/EDA powders (d<1mm) and grains (1mm<d<2mm) was carried out at the S/L ratio of 1/300 g_{PAAH}/mL and at the starting chromium concentration of 1.64 mg_{Cr}/L. Results are shown in Figure 4.5: equilibrium conditions achieved for MBA/EDA 1mm<d<2mm are: t_{eq} = 45 min, $C_{Cr,eq}$ = 0.14 mg_{Cr}/L, $q_{Cr,,eq}$ = 0.45 mg_{Cr}/L. Residual concentrations and amounts of chromium removed are the nearly same for both MBA/EDA forms, but, as expected, it takes more time for grains to achieve equilibrium. This suggests the occurrence of a volume process, involving not only the surface of particles but their entire volume, since more time is needed for the solute to penetrate particles with high size dimensions.

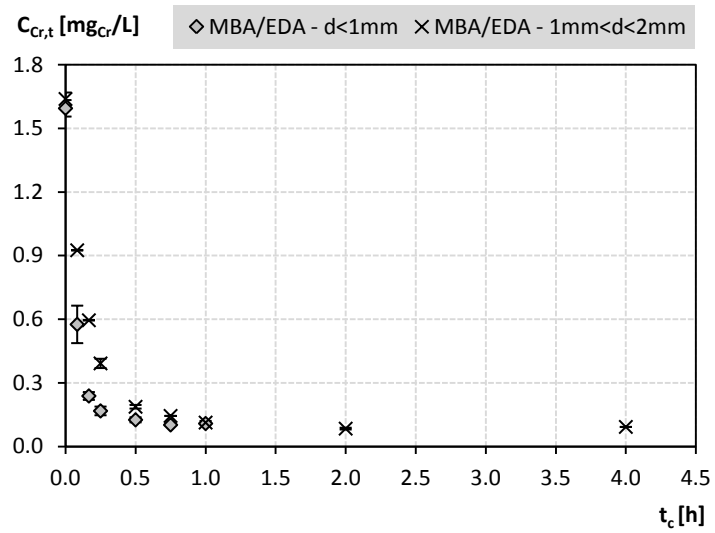

Figure 4.5. Average values of the residual chromium concentrations in water vs. contact time for MBA/EDA - d<1mm and MBA/EDA - 1mm<d<2mm. Boundary conditions: *S/L ratio* = 1/300 g_{PAAH}/mL, $C_{Cr,0}$ = 1.64 mg_{Cr}/L. Error bars are drawn using standard deviations.

4.3.2.3 Cr(VI) removal reaction

In order to define the removal mechanism characterizing Cr(VI) uptake by MBA/EDA, two models were tested against data: the pseudo first-order kinetic (eq. 2) which describes reversible reactions where, generally, the solute molecule/ion interacts with only one reactive site of the material; the pseudo second-order kinetic (eq. 3) which explains the mechanisms as controlled by the chemiosorption process, and by the reaction of two sites with the solute molecule/ion (Rudzinski and Plazinski, 2006; El-Naggar et al., 2012).

$$\frac{dq_{Cr,t}}{dt} = k_1 \cdot \left(q_{Cr,eq} - q_{Cr,t}\right) \quad (2)$$

$$\frac{dq_{Cr,t}}{dt} = k_2 \cdot \left(q_{Cr,eq} - q_{Cr,t}\right)^2 \quad (3)$$

The left-hand member of the two equations defines the variation over time of the amount of solute removed per unit mass of PAAH at the generic time t ($q_{Cr,t}$). By integrating eq. 2 and 3 and applying boundary conditions (t = 0 to t = t and $q_{Cr,t}$ = 0 to $q_{Cr,t}$ = $q_{Cr,t}$), linear equations are obtained and a linear regression was used to estimate the parameters of the two models. Table 4.2 reports the rate constant of the pseudo first-order kinetic (k_1), the rate constant of the pseudo second-order kinetic (k_2), the amount of copper removed per unit mass of media at the equilibrium ($q_{Cr,eq}$) and correlation coefficients (R^2).

Results suggest that that the pseudo second-order kinetic well describes the process, thus the overall rate constant of the process is controlled by chemiosorption reactions. In fact, R^2 values are very high and theoretical estimates of $q_{Cr,eq}$ greatly agree with the experimental results as shown in Table 4.1.

Table 4.2. Number of experimental data used (*N*), correlation coefficients (R^2) and estimates of parameters for the pseudo 1st and 2nd order kinetic models. MBA/EDA-d<1mm tested at different values of $C_{Cr,0}$ and *S/L ratio*.

			PSEUDO 1st ORDER KINETIC			PSEUDO 2nd ORDER KINETIC		
S/L RATIO [g_{PAAH}/mL]	$C_{Cr,0}$ [mg_{Cr}/L]	***N***	R^2	$q_{Cr,eq}$ [mg_{Cr}/g_{PAAH}]	k_1 [s^{-1}]	R^2	$q_{Cr,eq}$ [mg_{Cr}/g_{PAAH}]	k_2 [$g_{PAAH}/(mg_{Cr}\cdot s)$]
	0.82	-	-	-	-	-	-	-
1/150	1.64	13	0.957	0.14	$6.6\cdot10^{-3}$	1.000	0.24	$5.0\cdot10^{-1}$
	3.28	14	0.968	0.37	$7.7\cdot10^{-3}$	1.000	0.47	$2.6\cdot10^{-1}$
	0.82	12	0.888	0.10	$1.6\cdot10^{-3}$	1.000	0.24	$4.8\cdot10^{-2}$
1/300	1.64	14	0.921	0.27	$2.4\cdot10^{-3}$	0.999	0.46	$2.2\cdot10^{-2}$
	3.28	14	0.943	0.41	$2.2\cdot10^{-3}$	1.000	0.95	$1.5\cdot10^{-2}$
	0.82	14	0.997	0.33	$2.2\cdot10^{-3}$	0.999	0.40	$1.1\cdot10^{-2}$
1/600	1.64	14	0.981	0.62	$2.0\cdot10^{-3}$	0.999	0.85	$6.1\cdot10^{-3}$
	3.28	13	0.971	1.15	$1.3\cdot10^{-3}$	1.000	1.74	$1.9\cdot10^{-3}$
	0.82	14	0.978	0.55	$1.6\cdot10^{-3}$	0.995	0.59	$2.8\cdot10^{-3}$
1/1200	1.64	14	0.992	0.97	$1.4\cdot10^{-3}$	0.999	1.28	$1.8\cdot10^{-3}$
	3.28	14	0.997	2.08	$1.4\cdot10^{-3}$	0.999	2.52	$7.8\cdot10^{-4}$

4.3.2.4 Effect on pH and EC

Averages and standard deviations of pH and EC measured on the contaminated solution at the beginning of the experiments were 8.2±0.1 and 377±11 µS/cm, respectively. During tests changes in the values of pH and EC were observed: results strongly depend on the S/L ratio used but not on the starting chromium concentration or on the amount of solute removed at the equilibrium ($q_{Cr,eq}$). Averages and standard deviations of pH and EC measured at the end of the experiments wwere: 5.9±0.1 and 472±8 µS/cm for tests performed at 1/150 g_{PAAH}/mL; 6.8±0.1 and 433±8 µS/cm for tests performed at 1/300 g_{PAAH}/mL; 7.5±0.1 and 398±15 µS/cm for tests performed at 1/600 g_{PAAH}/mL; 8.0±0.1 and 380±8 µS/cm for tests performed at 1/1200 g_{PAAH}/mL. Data suggest that the reaction between the active groups on MBA/EDA and the solute have a negligible effect on the variation of water composition, which is likely to be affected by the hydrogel dose adopted: hydrogel were rinsed before all experiments but residues of synthesis solutions are released even during the test and the more the S/L ratio is high (1/150 g_{PAAH}/mL) the more the composition of water is influenced by the presence of the hydrogel itself.

4.3.3 Isotherm experiments

Isotherms can be greatly useful in the design of adsorption systems since they often provide some insight into both the sorption mechanism and the surface properties and affinity of the sorbent (Ho et al., 2002; Namasivayam and Sureshkumar, 2008). Figure 4.6 shows experimental data where q_{eq} is the solid phase metal ion concentration at equilibrium (mol/g_{PAAH}) and C_{eq} is the molar concentration of chromium solution at equilibrium (mol/L). The use of moles instead of masses is required in order to interpret data with some specific isotherm models.

Table 4.3 reports the linearized equations of the three models of isotherms used to fit experimental data: Langmuir, Freundlich and Dubinin-Radushkevich. The correlation coefficients (R^2) are calculated as indicators of fitting of the experimental data, and estimates of model parameters give information on the type of interactions involved between chromium and MBA/EDA hydrogel.

The Langmuir and Freundlich adsorption models are widely used because they describe experimental results in a wide range of concentrations (Perić et al., 2004).

The Langmuir model represents chemisorption on a set of well-defined localized binding sites having the same sorption energies independent of surface coverage and no interaction between sorbed molecules. Q_o is a constant related to the maximum sorption capacity (mol/g_{PAAH}) and indicates monolayer coverage of sorbent with sorbate; *b* is

related to the energy, specifically the enthalpy, of sorption and it is independent of temperature (L/mol) (Brown et al., 2000; Hasany et al. 2001).

The Freundlich isotherm gives an expression encompassing the surface heterogeneity of the media and the exponential distribution of active sites and their energies. This isotherm does not predict any saturation of the sorbent surface; thus, infinite surface coverage is predicted mathematically, indicating reversible physisorption on the surface. Freundlich's constants k_f and n indicate sorption capacity and intensity, respectively: the numerical value of 1/n indicates the sorption capacity is only slightly suppressed at lower equilibrium concentration (Ho et al., 2002; Hasany et al. 2001).

Dubinin-Raduskevich isotherm is related to the porous structure of the sorbent, assuming the existence of an adsorption space close to the sorption surface: in the equation, ϵ is the Polanyi potential, calculated as shown in Table 4.3 where R (J/mol^{-1}·K^{-1}) is the gas constant and T (K) is the absolute temperature. B is a constant related to the mean free energy of sorption per mole of sorbate as it is transferred to the surface of the solid from infinite distance in the solution (mol^2/J^2) and q_m is the theoretical saturation capacity (mol/g) (Ho et al., 2002; Namasivayam and Sureshkumar, 2008).

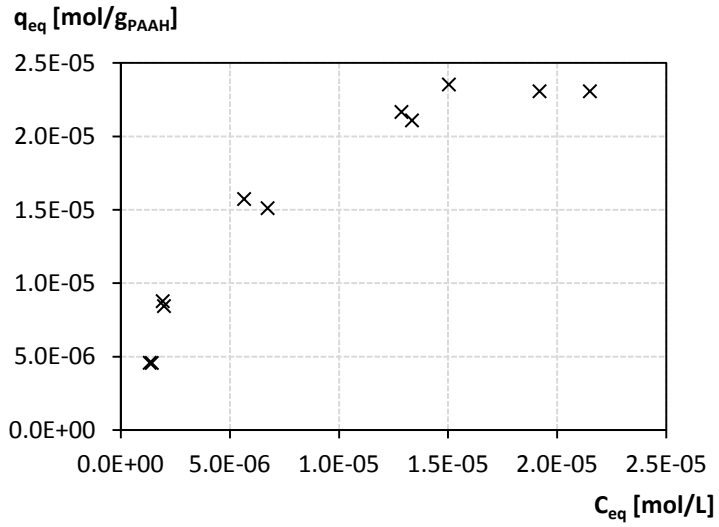

Figure 4.6. Moles of Cr(VI) removed at equilibrium per unit mass of MBA/EDA, q_{eq} (mol/g$_{PAAH}$) vs. residual molar concentration of chromium at equilibrium C_{eq} (mol/L).

Table 4.3. Linearized equations for Langmuir, Freundich and Dubinin–Radushkevich isotherms. Correlation coefficients (R^2) and corresponding estimates of models' parameters evaluated on data from tests on MBA/EDA-d<1mm (*S/L ratio* = 1/300 g$_{PAAH}$/mL, $C_{Cr,0}$ = 1.64 mg$_{Cr}$/L, t_{eq} = 45 min).

ISOTHERM MODEL NAME	LINEARIZED EQUATION	CORRELATION COEFFICIENT (R^2)	ESTIMATES OF MODEL PARAMETERS
Langmuir	$\frac{C_{eq}}{q_{eq}} = \frac{1}{Q_o} b + \frac{C_{eq}}{Q_o}$	0.981	Q_o = 3.1·10^{-5} mol/g$_{PAAH}$ b = 1.6·10^{+5} L/mol
Freundlich	$\log_{10}(q_{eq}) = \log_{10}(k_f) + \frac{1}{n}\log_{10}(C_{eq})$	0.937	k_f = 9.7·10^{-3} (L/mol)$^{1/n}$·g^{-1} n = 1.82
Dubinin–Radushkevich	$\ln(q_{eq}) = \ln(q_m) - B\varepsilon^2$ where $\varepsilon = RT \cdot \ln(1 + 1/C_{eq})$	0.946	q_m = 3.6·10^{-4} mol/g$_{PAAH}$ B = 3.8·10^{-9} mol^2/J^2

All the three isotherms can be used to describe chromium removal with MBA/EDA. Langmuir fits better than Freundlich model probably because it describes a process controlled by chemiosorption reactions, while Freundlich deals with physicochemical adsorption. Furthermore, the agreement of data with these two models implies that both monolayer adsorption (Langmuir) and heterogeneous surface conditions (Freundlich) co-exist: this is also proved by

the good fit on Dubinin-Raduskevich model that implies the presence of a porous structure, as it is for MBA/EDA. However, the adsorption capacity predicted with this model is higher compared to that of Langmuir and of experimental results; in fact, experimental conditions cannot determine the saturation of the media, while Dubinin-Raduskevich predict a removal process and a removal ability that involves the whole volume of particles and this can determine the increase of the predicted value of q_m, the theoretical saturation capacity.

4.3.4 Selectivity experiments

Selectivity tests were performed using defined ratios between copper and chromium molar concentrations [Cu]/[Cr], obtained by combining two Cu(II) molar concentrations (16 and 32 $\mu mol_{Cu}/L$) and three Cr(VI) molar concentrations (16, 32, 64 $\mu mol_{Cr}/L$). Removal percentages of chromium are shown in Figure 4.7 at two different contact times, 10 and 45 minutes, selected to gain information about the removal process at a generic time corresponding to an intense removal phase and at the time corresponding to an equilibrium phase, respectively.

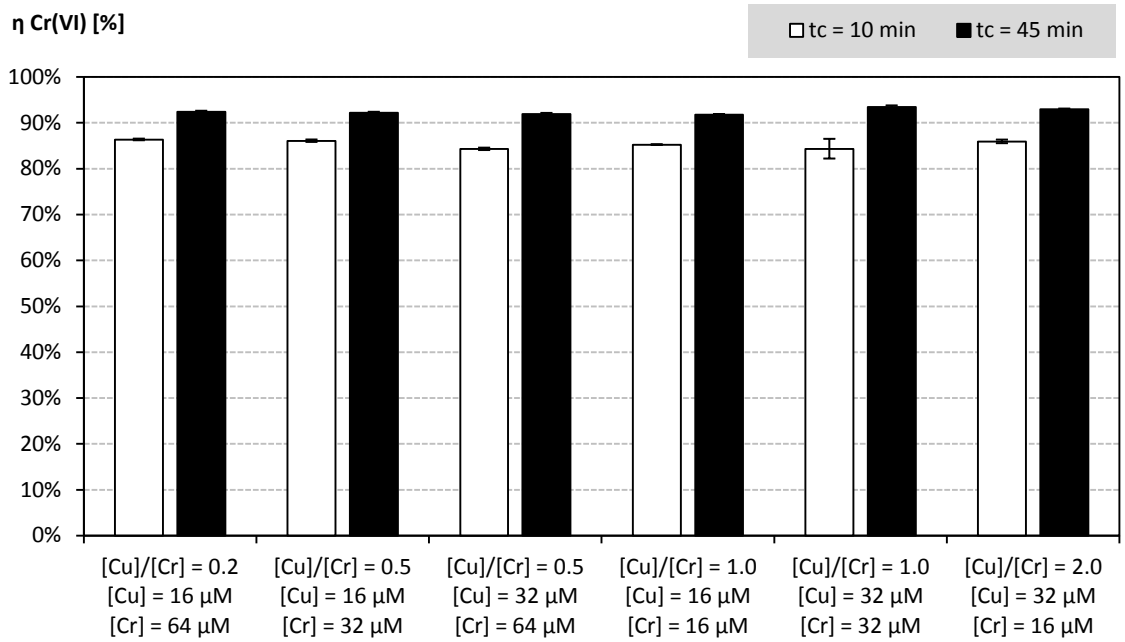

Figure 4.7. Average values of chromium removal efficiencies ($\eta_{Cr(VI)}$) at 10 and 45 minutes contact times, for the six combinations of Cu(II) and Cr(VI) molar concentrations for (MBA/EDA-d<1mm, *S/L ratio* = 1/300 g_{PAAH}/mL). Error bars are drawn using standard deviations.

Cr(VI) was previously tested individually on MAB/EDA-d<1mm at the *S/L ratio* of 1/300 and at the three starting concentrations and results are weakly affected by $C_{Cr,0}$: the percentage of Cr(VI) removal after 10 and 45 minutes are 85.8±0.6% and 93.5±0.2%, respectively. As for copper, only tests at the starting concentration of 32 $\mu mol_{Cu}/L$ were performed (par. 3.3.2), resulting in removal percentages of 77.9% after 10 minutes and 96% after 45 minutes.
Figure 4.7 shows that hexavalent chromium removal is negligibly affected by both the starting concentration and the presence of different concentrations of copper: no differences are observed in MBA/EDA behavior when the polluted solution contains both copper and chromium, regardless the *[Cu]/[Cr] ratio* adopted. This could explained considering that, copper is a cation while hexavalent chromium is dissolved in water as an anion that, at the pH values measured during the experiments (from 8.0±0.2 to 6.7±0.02 after 45 minutes), can be in the form of both chromate (CrO_4^{2-}) and dichromate ($Cr_2O_7^{2-}$). Consequently, active groups involved in the complexation of copper and hexavalent chromium are supposed to be different. In 1995 in their study concerning the removal of Cu(II) and Cr(VI) with moss, Lee et al. assessed the possibility that Cu(II) ions, if held firmly at the sorption sites, may act as anion exchange sites in aqueous phase with relatively high affinities towards anions with a strong ligand characteristic. Other authors (Ramana & Sengupta, 1992) report about chelating polymers with immobilized Cu(II) at the sorption sites able to enhance sorption abilities towards arsenates and selenites. The occurrence of similar processes towards Cr(VI) could explain the results reported in Figure 4.7. Positive or negative interferences between Cu(II) and Cr(VI) are to be taken into

account but more data and focused tests for the identification of the active groups and the mechanisms involved in copper and chromium complexation are needed.

4.4 Conclusions

PAA hydrogels remove Cr(VI) from water solutions creating complexes between the solute and its active groups: by fitting kinetic data with pseudo first-order and pseudo-second order models it's been possible to verify this statement, thus describing the Cr(VI) removal reaction as controlled by irreversible chemiosorption.
Boundary conditions adopted during tests greatly influence hexavalent chromium removal by MBA/EDA: if varying the *S/L ratio* from 1/150 to 1/1200 g_{PAAH}/mL and $C_{Cr,0}$ from 0.82 to 3.28 mg_{Cr}/L, equilibrium contact times and the amounts of Cr(VI) in the solid phase at equilibrium results to be in the range of 15-60 minutes and 0.22-2.18 mg_{Cr}/g_{PAAH} respectively. Particle size too determines the achievement of equilibrium conditions, and a good fitting of isotherm experimental data with the Dubinin-Raduskevich model allowed to postulate a volume process involving the diffusion of contaminants into pores.
MBA/EDA it is likely to be a useful polymer to be used in water treatment process: the simultaneous removal of both Cr(VI) and Cu(II) was tested and low interference phenomena were detected even when modifying copper/chroumium molar ratio and solute's starting concentrations. Further investigations are needed in order to define, on the one hand, the affinity of MBA/EDA towards other relevant heavy metals, and on the other hand, the reactions involved in the removal of cations and anions, since experimental evidences and other studies reported in literature let think as possible that Cu(II) ions, held on the hydrogel structure, act as anion exchange sites.

4.5 References

1. Abdel-Halim E.S., S.S. Al-Deyab (2011). Hydrogel from crosslinked polyacrylamide/guar gum graft copolymer for sorption of hexavalent chromium ion. Carbohydrate Polymers 86, 1306-1312.
2. American Public Health Association (APHA), American Water Works Association (AWWA) & Water Environment Federation (WEF). Standard Methods for the Examination of Water and Wastewater, 22st Edition, Washington DC, 2012.
3. APAT-IRSA, 2003. Metodi analitici per le acque. APAT Manuali e Linee Guida 29/2003.
4. Aydın Y.A., N.D. Aksoy (2009). Adsorption of chromium on chitosan: optimization, kinetics and thermodynamics. Chemical Engineering Journal 151, 188-194.
5. Bajpai S.K. and S. Johnson (2005). Superabsorbent hydrogels for removal of divalent toxic ions. Part I: Synthesis and swelling characterization Reactive & Functional Polymers 62, 271-283.
6. Brown P.A., S.A. Gill, S.J. Allen (2000). Metal removal from wastewater using peat. Water Research 34(16), 3907-3916.
7. Çavuş S., G. Gürdağ (2009). Noncompetitive removal of heavy metal ions from aqueous solutions by poly[2-(acrylamido)-2-methyl-1-propanesulfonic acid-co-itaconic acid] hydrogel. Industrial & Engineering Chemistry Research 48, 2652-2658.
8. Chauhan G.S., S. Mahajan (2002).Use of novel hydrogels based on modified cellulosics and methacrylamide for separation of metal ions from water systems. Journal of Applied Polymer Science 86, 667-671.
9. El-Naggar I.M., E.S. Zakaria, I.M. Ali, M. Khalil, M.F. El-Shahat (2012). Kinetic modeling analysis for the removal of cesium ions from aqueous solutions using polyaniline titanotungstate Arabian Journal of Chemistry, 5, 109–119.

10. Ferruti P., E. Ranucci, A. Manfredi, N. Mauro, E. Ferrari, R. Bruni, F. Colombo, P. Mussini, M. Rossi (2012). Llysine and EDTA polymer mimics as resins for the quantitative and reversible removal of heavy metal ion water pollutants. J. Polym. Sci. A Polym. Chem., 50: 5000-5010.

11. Ferruti P., E. Ranucci, S. Bianchi, L. Falciola, P.R. Mussini, M. Rossi, Novel polyamidoamine-based hydrogel with an innovative molecular architecture as a Co^{2+}, Ni^{2+}, and Cu^{2+} sorbing material: cyclovoltammetry and extended x-ray absorption fine structure studies. J. Polym. Sci., Part A: Polym. Chem. 44 (2006) 2316-2327.

12. Hasany S.M., M.M. Saeed, M. Ahmed (2001). Sorption of traces of silver ions onto polyurethane foam from acidic solution. Talanta 54, 89-98.

13. Ho Y. S., J. F. Porter, G. McKay (2002). Equilibrium isotherm studies for the sorption of divalent metal ions onto peat: copper, nickel and lead single component systems. Water, Air, and Soil Pollution 141, 1-33.

14. Kyzas G.Z., M. Kostoglou, N.K. Lazaridis (2009). Copper and chromium(VI) removal by chitosan derivatives. Equilibrium and kinetic studies. Chemical Engineering Journal 152, 440-448.

15. Lee C. K., K. S. Low, K. L. Kek (1995). Removal of chromium from aqueous solution. Bioresource Technology 54, 183-189.

16. Mahapatra A., B.G. Mishra, G. Hota (2013). Studies on electrospun alumina nanofibers for the removal of chromium(VI) and fluoride toxic ions from an aqueous system. Industrial & Engineering Chemistry Research 52, 1554-1561.

17. Namasivayam C., M.V. Sureshkumar (2008). Removal of chromium(VI) from water and wastewater using surfactant modified coconut coir pith as a biosorbent. Bioresource Technology 99, 2218-2225.

18. Perić J., M. Trgo, N. Vukojević Medvidović (2004) Removal of zinc, copper and lead bynatural zeolite- a comparison of adsorption isotherms. Water Research 38, 1893-1899.

19. Ramana, A., A. Sengupta (1992). Removing selenium(IV) and arsenic(V) oxyanions with tailored chelating polymers. Journal of Environmental Engineering 118(5), 755-775.

20. Rudzinski W., W. Plazinski (2006). Kinetics of solute adsorption at solid/solution interfaces: a theoretical development of the empirical pseudo-first and pseudo-second order kinetic rate equations, based on applying the statistical rate theory of interfacial transport. J. Phys. Chem. B, 110, 16514-16525.

21. Sankararamakrishnan N., A. Dixit, L. Iyengar, R. Sanghi (2007). Removal of hexavalent chromium using a novel cross linked xanthated chitosan. Bioresource Technology 97, 2377-2382.

22. Siyam T., Youssef H.A., El-Naggar I.M. (1997). Adsorption studies of copper sulfate on hydrogels of Poly(amido-amines). Journal of macromolecular science, Pure Appl. Chem. 34(11), 2379-2388.

23. Wang J. and X. Li (2013). Ion-imprinted composite hydrogels with excellent mechanical strength for selective and fast removal of Cu^{2+}. Industrial & Engineering Chemistry Research 52, 572-577.

24. WHO (2003). Chromium in Drinking-water. Background document for development of WHO Guidelines for Drinking-water Quality. World Health Organization, Geneva, 1996.

5 Kinetic models and removal mechanisms of copper by PolyAmidoAmine Hydrogels

5.1 Introduction

Heavy metals and metalloids can have severe implications on environmental and human health. More restrictive legal limits were recently defined and conventional processes, such as chemical precipitation, coagulation/flocculation, ion exchange, adsorption, and membrane filtration, generally lack specificity thus resulting in several disadvantages: low removal capacity, low selectivity and long equilibrium. Much attention is to be focused on innovative and specific water treatment technologies in order to improve process removal efficiency and selectivity (AWWA, 1999; Kurniawan et al., 2006; Liang et al. 2013).

PolyAmidoAmine Hydrogels (PAAHs) proved to be a suitable media for heavy metals removal from aqueous solutions: the complexing ability of their amine and, in some instances, carboxyl groups, enables the creation of coordination complexes with heavy metal ions such as Cu^{2+}, Ni^{2+}, Co^{2+} (Ferruti et al., 2006). Moreover, PAAH specific properties, related to the chemical structure of hydrogels and their ability of absorbing large amounts of water leading to a volumetric expansion, determine differences in the behavior of PAAHs if compared to common granular media used for water treatment (Casolaro et al. 1982; Ferruti et al., 2012). Few research works have been found in literature dealing with the investigation on the basic features of kinetic and mass transfer characteristic of hydrogels and no engineering applications of PAA hydrogels in this field have been reported so far.

Literature suggests a lot of techniques for the characterization of porous materials (Satoh et al., 2008; Sonetaka et al., 2009; Fujiki et al., 2010; Xie et al., 2011) starting from equilibrium isotherms and kinetic experiments. Broadly speaking, the determination of kinetic processes and parameters has two main objectives: (a) the description of the actual solute removal process; (b) the achievement of information for the selection and design of water treatment process (Kumar, 2006; Mousavi et al., 2012; Valderrama et al., 2008).

Models for the interpretation of kinetics for activated carbon or ion exchange resins generally include: the pseudo first-order and the pseudo second-order models, the intraparticle diffusion model and the Homogeneous Particle Diffusion Model, HPDM (Rudzinski and Plazinski, 2006; Caetano et al., 2009; Xie et al., 2011; El-Naggar et al., 2012).

Batch kinetic experiments for the removal of copper from fresh water were then designed and performed on two samples of hydrogels, different in their structure and functional groups and termed MBA/EDA and MBA/CYS. In order to study the effect of experimental boundary conditions and hydrogels physical characteristics, three different PAAH doses or solid to liquid ratios (*S/L ratio*) were tested on hydrogels provided into two different particle sizes: powders ($d<1mm$) and grains ($1mm<d<2mm$). Experimental results were fitted with kinetic models in order to obtain information about the physical and chemical mechanisms involved in copper uptake with PAAHs.

5.2 Materials and Methods

5.2.1 Reagents, stock solutions and glassware

Copper nitrate ($Cu(NO_3)_2 \cdot 3H_2O$, 99% assay), hydrochloric acid (HCl, ACS reagent, 37% assay) and nitric acid (HNO_3, ≥99.999% trace metals basis, 70% assay) were purchased from Sigma Aldrich. All reagents were used without further purification.

A copper stock solution at 1 $g_{Cu} \cdot L^{-1}$ was prepared by dosing $Cu(NO_3)_2 \cdot 6H_2O$ in MilliQ water; the solution was stabilized at 5% HNO_3 and stored for all the experiments at room temperature.

Before use, all glassware was washed in an acidic bath (10% HCl), rinsed with MilliQ water and dried.

5.2.2 PolyAmidoAmine Hydrogel (PAAH)

Two samples of PAA hydrogels, MBA/EDA (623±56 kg/m^3) and MBA/CYS (697±28 kg/m^3), were provided by the Department of Organic and Industrial Chemistry (Università degli Studi di Milano, IT), both into two different particle size: powder (d<1mm; D_{60} = 686 µm for MBA/EDA; D_{60} = 618 µm for MBA/CYS) and grains (1mm<d<2mm; D_{60} = 1.40 mm for MBA/EDA and MBA/CYS). They are termed according to the starting polymers employed during the synthesis process and differ in functionalization: MBA/EDA (MethyleneBisAcrylamide/EthyleneDiAmine), besides aminic nitrogen, has no specific functional groups active for heavy metals complexation, while MBA/CYS (MethyleneBisAcrylamide/CYStamine) is further functionalized with disulphide groups -SS-. Chemical formulas are reported in par. 2.2.1.

The mass of hydrogel to be tested in kinetic, isotherm and interference experiments, was previously washed to remove the residues of synthesis reagents and minimize alterations to water composition. Tap water filtered on Millipore with 0.45 µm cellulose acetate membrane filters (Whatman) was used for this purpose. The number of steps in batch conditions (Solid/Liquid ratio, *S/L ratio* = 1/20 $g \cdot mL^{-1}$; contact time, t_c: 5 minutes for each step) was previously determined (Appendix 1) in 10 steps for MBA/EDA and 5 steps For MBA/CYS, by monitoring changes in water pH, till negligible variations were observed. At the end of each step water was separated from the solid phase by using a centrifuge (IEC CL 10) at the rate of 2000 rpm for 5 minutes.

5.2.3 Evaluation of PAAH swelling ability

The volume expansion of hydrogels in tap water was evaluated in static conditions on both MBA/EDA and MBA/CYS. The swelling degree measured over time (SD_t) is defined by eq. 1, where $V_{SH,t}$ is the volume of the swelled hydrogel in tap water at time *t* and V_{DH} is the initial dry volume. Ten contact time were selected: 5 - 15 - 30 minutes, 1 - 1.5 - 2 - 4 - 4.5 - 5 hours and 1 day.

$$SD_t = \frac{(V_{SH,t} - V_{DH})}{V_{DH}} \quad (1)$$

5.2.4 Kinetics experiments

Batch kinetic tests, in duplicate, were performed on MBA/EDA and MBA/CYS in both particle sizes. Three different *S/L ratios* were used (1/150, 1/300, 1/600 $g \cdot mL^{-1}$) and up to 9 contact times (t_c) were selected over 72 hours as reported in Table 5.1.

In order to prepare a contaminated solution to be tested at the starting copper concentration ($C_{Cu,0}$) of 2 mg_{Cu}/L, a defined volume of copper stock solution was spiked into 500 mL tap water filtered on Millipore with 0.45 µm cellulose acetate membrane filters (Whatman). A mechanical shaker at a fixed shaking speed (150 swinging per minute) was used to provide adequate turbulence into the reactor; at the end of each contact time the liquid phase was separated from the solid phase by vacuum filtration on Millipore with 0.45 µm cellulose acetate membrane filters (Whatman): samples collected for the detection of pH, electrical conductivity (EC), temperature (T) were quickly analysed; samples collected for the detection of copper concentration were acidified at 2% HNO_3 and stored at 4°C for analyses.

Table 5.1 Contact times adopted for kinetics tests, as a function of the *S/L ratio* and particle size.

S/L RATIO	PARTICLE SIZE	CONTACT TIME							
		15 min	45 min	2 h	6 h	16 h	24 h	48 h	72 h
1/150 g·mL^{-1}	d<1 mm	×	×	×	×	×	×		
	1 mm<d<2 mm	×	×	×	×	×	×		
1/300 g·mL^{-1}	d<1 mm	×	×	×	×	×	×		
	1 mm<d<2 mm	×	×	×	×	×	×	×	
1/600 g·mL^{-1}	d<1 mm	×	×	×	×	×	×	×	
	1 mm<d<2 mm	×	×	×	×	×	×	×	×

5.2.5 Analytical methods

A portable pH-meter, model Eutech pH 5+ (Eutech Instruments), was used for pH analysis (Method: IRSA 2080). EC (APAT-IRSA, 2003. Method 2030) and T (APAT-IRSA, 2003. Method 2100) were monitored using the conductivity meter model Eutech Cond 6+ (Eutech Instruments).
The concentrations of copper were analyzed using the Atomic Absorption Spectometer, (VARIA Spectra AA 55) and adopting the procedure explained in method APAT-IRSA 3250A (APAT-IRSA, 2003).

5.3 Results and Discussion

5.3.1 Swelling degree

Hydrogels have a tri-dimensional molecular architecture and are insoluble in water; however, they can absorbe and store large amounts of water leading to a volumetric expansion. Swelling degree trends over time are shown in Figure 5.1 for the four tested media. Both hydrogels, regardless of particle size, achieve an asymptotic value: however, MBA/EDA expands its volume twice as much than MBA/CYS and swells rapidly, getting about the 80-90% of the final *SD* in the first 5-30 minutes, contrarily to MBA/CYS that needs 4-5 hours.

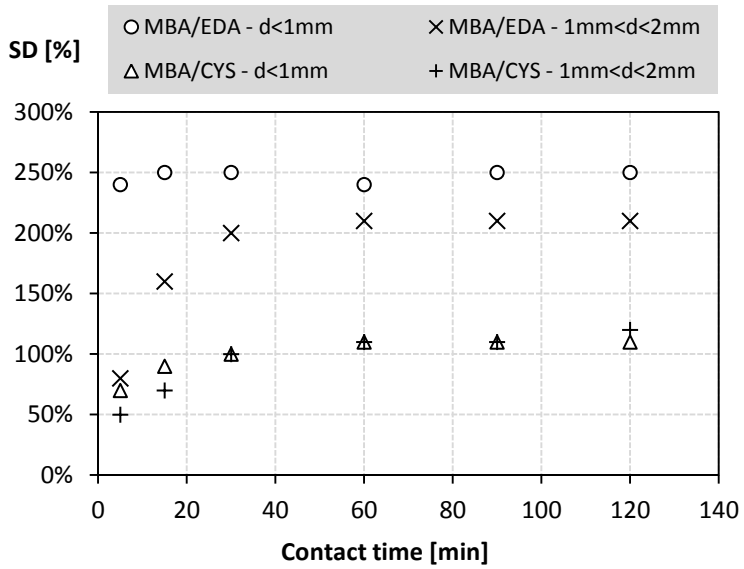

Figure 5.1. Swelling degree (*SD*) vs. contact time for MBA/EDA and MBA/CYS hydrogels

Furthermore few differences are observed between the swelling behavior of MBA/CYS powders and grains, proving that its molecule structure is stiffer than that of MBA/EDA. When water gets into the hydrogels, MBA/CYS polymer chains extend slower and less than that of MBA/EDA, thus suggesting that pores and therefore functional groups are less accessible for water molecules: this is likely to affect the removal performances and mechanisms of the two hydrogels in a different way.

5.3.2 Kinetic experiments

In the following, residual copper concentration data ($C_{Cu,t}$) falling outside the range [$\bar{C}_{Cu,t-1} \cdot (1+\%Err)$, $\bar{C}_{Cu,t+1} \cdot (1-\%Err)$] were considered as outliers, where $\bar{C}$ is the average value of concentrations on replicates. An error percentage value of 15% (*%Err*) was selected and adopted for the entire set of data in order to keep the percentage of removed data within the 10%.
In Figure 5.2 the residual coper concentrations ($C_{Cu,t}$) is shown as a function of contact time (t_c) for the two hydrogels MBA/EDA and MBA/CYS (b) in both particle sizes at the three tested S/L ratios. Regardless S/L ratio, powders are faster than grains but the two hydrogels behave differently because of the presence of distinct mechanisms for the diffusion of copper towards functional groups, as suggested by SD results.

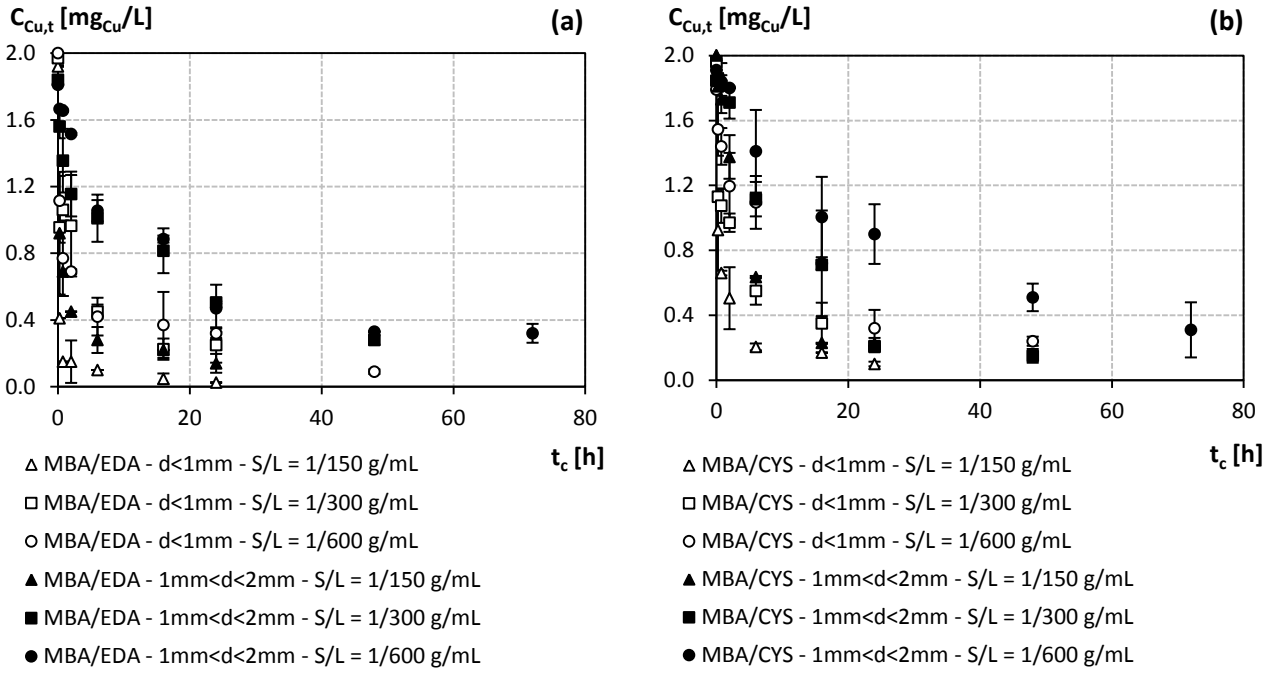

Figure 5.2. Average values for residual copper concentrations in water ($C_{Cu,t}$) vs. contact time (t_c) for MBA/EDA (a) and MBA/CYS (b). Error bars are drawn using standard deviations.

A generic contact time *t* is defined as the equilibrium contact time t_{eq}, when two conditions are satisfied at the same time: a) the slope of the line interpolating copper residual concentrations at *t-1* and *t* is less than 10 degree; b) the $q_t/q_{t,max}$ ratio is above the 85%, where q_t and $q_{t\text{-}max}$ are the amount of copper removed per unit mass of hydrogel at the generic contact time *t* and at the final tested contact time *t-max*. Equilibrium conditions, t_{eq} and the corresponding amount of copper removed per unit mass of hydrogel q_{eq}, are shown in Table 5.2.
When decreasing *S/L ratio*, contact times range from 6 to 24 hours for powder and from 6 to 48 hours for grains, while copper uptake per unit mass of hydrogel (mg_{Cu}/g_{PAA}) varies from 0.26±0.02 for 1/150 g/mL, to 0.46±0.04 for 1/300 g/mL, to 0.88±0.08 for 1/600 g/mL. No significant differences due to particles size or hydrogel chemical structure are observed for data concerning copper removal abilities, while equilibrium contact times are affected by PAAH physical and chemical characteristics, reproducing what previously observed as for the swelling behavior.

Table 5.2. Equilibrium conditions for MBA/CYS and MBA/EDA as a function of particle size and S/L ratio.

		MBA/CYS		MBA/EDA	
PARTICLE SIZE	**S/L RATIO [g_{PAAH}/mL]**	**t_{eq} [h]**	**q_{eq} [mg_{Cu}/g_{PAAH}]**	**t_{eq} [h]**	**q_{eq} [mg_{Cu}/g_{PAAH}]**
d<1mm	1/150	6	0.269	6	0.273
d<1mm	1/300	16	0.483	6	0.456
d<1mm	1/600	24	0.882	16	0.978
1mm<d<2mm	1/150	16	0.266	6	0.234
1mm<d<2mm	1/300	24	0.491	24	0.401
1mm<d<2mm	1/600	48	0.840	24	0.804

5.3.2.1 Selection and description of the kinetic models

There are essentially 3 consecutive steps in the removal process of contaminants by porous media such as PAA hydrogels: (a) the diffusion of the solute through the liquid film surrounding the particle or "liquid film diffusion", (b) the diffusion of the solute through the polymeric matrix of the resin or "pore diffusion", (c) the chemical reaction of the solute with the functional groups linked to the matrix (the creation of "metal complexes" in this case). These three steps determine the overall rate of the reaction; however, when the chemical reaction may be explained as a chemisorption process, it is usually assumed to be too fast to affect the overall rate (Caetano et al., 2009; Xie et al., 2011).

Data collected from kinetic tests on MBA/EDA and MBA/CYS hydrogels were analyzed using four different models: pseudo first order, pseudo second order, intraparticle diffusion and homogeneous particle diffusion model (HPDM). Models are based on different hypothesis as for the mechanisms of interactions between the media and the solute: specifically pseudo first and second order models describe the removal process as governed by the rate of the chemical reaction so that the transition from dissolved to solid state is the mechanism controlling the whole rate (El-Naggar et al., 2012). The homogeneous particle diffusion model hypothesizes the chemical reaction as a chemisorption process; in this case the third step is usually assumed to be too fast to affect the overall removal rate and two equations were developed in order to separately describe conditions of "liquid film diffusion" and "particle diffusion" controlling the overall process (Xie et al., 2011). The intraparticle diffusion model focuses on the description of the second diffusion mechanism, the diffusion through pores (Weber and Morris, 1963; Valderrama et al., 2008).

In the following the fitting of experimental data is assessed by means of the correlation coefficient (R^2), in order to evaluate the suitability of a model to kinetic mechanisms characterizing PAAHs.

Pseudo first-order and pseudo second-order models

Pseudo first order (eq. 2) and pseudo second order (eq. 3) models relate the rate of the process to the amount of solute removed per unit mass of media, q_t (mg_{Cu}/g_{PAAH}). The two models describes two different types of chemical reactions: the first one well describe reversible reactions where, generally, the solute molecule/ion interacts with only one reactive site of the material; the pseudo second-order kinetic explains the mechanisms as controlled by the chemiosorption process, and by the reaction of two sites with the solute molecule/ion (Rudzinski and Plazinski, 2006; El-Naggar et al., 2012).

$$\frac{dq_{Cu,t}}{dt} = k_1 \cdot \left(q_{Cu,eq} - q_{Cu,t}\right) \quad (2)$$

$$\frac{dq_{Cu,t}}{dt} = k_2 \cdot \left(q_{Cu,eq} - q_{Cu,t}\right)^2 \quad (3)$$

Integrating and applying boundary conditions (t = 0 to t = t and q_t = 0 to q_t = q_t) to eq. 2 and 3, linear form equations are obtained. Table 5.3 reports the correlation coefficients (R^2) and the estimated parameters for the two models: the rate constants of pseudo first-order (k_1) and pseudo second-order (k_2) kinetics and the amount of copper removed per unit mass of media at the equilibrium (q_e). Results suggest that that the pseudo second order kinetic well describe the process and that the overall rate constant of the process is controlled by chemiosorption reaction: Table 4.2 shows

extremely high values of the correlation coefficients resulting from fitting data with the model in eq. 3. Furthermore theoretical estimates of q_{eq} greatly agree with the corresponding experimental values: experimental q_{eq} are weakly influenced by the tested hydrogel and its particle size, whereas they are affected by the tested S/L ratio: data varies from 0.26±0.02 mg_{Cu}/g_{PAAH} for 1/150 g/mL, to 0.46±0.04 mg_{Cu}/g_{PAA} for 1/300 g/mL, to 0.88±0.08 mg_{Cu}/g_{PAA} for 1/600 g/mL. As for PAAHs, the creation of copper-complexes may be not the only chemical process involved and ion exchange or physical adsorption due to the presence of charged groups on chains may occur. However results prove that the prevailing mechanism involved in the chemical reaction of Cu(II) with MBA/EDA and MBA/CYS structures can be classified as a chemiosorption process, detrmining the creation of complexes between metal divalent ions and active groups along molecule chains, that are amine groups for MBA/EDA and both amine and disulphide groups for MBA/CYS.

Table 5.3. Number of experimental data used (*N*), correlation coefficients (R^2) and estimates of parameters for the pseudo 1st and 2nd order kinetic models. Values for MBA/EDA and MBA/CYS as a function of particle size and S/L ratio.

			PSEUDO 1st ORDER KINETIC			PSEUDO 2nd ORDER KINETIC		
PAAH SAMPLE AND PARTICLE SIZE	**S/L RATIO [g_{PAAH}/mL]**	***N***	R^2	q_{eq} [mg_{Cu}/g_{PAAH}]	k_1 [s^{-1}]	R^2	q_{eq} [mg_{Cu}/g_{PAAH}]	k_2 [$mg_{Cu}/(g_{PAAH}\cdot s)$]
MBA/EDA d<1mm	1/150	11	0.843	0.03	$4.0\cdot10^{-5}$	1.000	0.28	$7.5\cdot10^{-3}$
	1/300	13	0.920	0.28	$6.7\cdot10^{-5}$	0.997	0.54	$6.3\cdot10^{-4}$
	1/600	15	0.779	0.42	$1.5\cdot10^{-5}$	0.995	1.14	$2.0\cdot10^{-4}$
MBA/EDA 1mm<d<2mm	1/150	10	0.829	0.08	$3.6\cdot10^{-5}$	0.999	0.26	$2.5\cdot10^{-3}$
	1/300	16	0.941	0.34	$1.7\cdot10^{-5}$	0.973	0.48	$1.5\cdot10^{-4}$
	1/600	16	0.976	0.95	$2.8\cdot10^{-5}$	0.988	0.99	$3.9\cdot10^{-5}$
MBA/CYS d<1mm	1/150	13	0.808	0.08	$4.1\cdot10^{-5}$	1.000	0.29	$2.5\cdot10^{-3}$
	1/300	14	0.969	0.27	$3.3\cdot10^{-5}$	0.995	0.54	$4.7\cdot10^{-4}$
	1/600	15	0.902	0.84	$2.9\cdot10^{-5}$	0.974	0.99	$6.2\cdot10^{-5}$
MBA/CYS 1mm<d<2mm	1/150	10	0.984	0.34	$1.0\cdot10^{-4}$	0.988	0.32	$2.3\cdot10^{-4}$
	1/300	15	0.903	0.61	$3.5\cdot10^{-5}$	0.967	0.66	$5.0\cdot10^{-5}$
	1/600	17	0.992	0.92	$1.2\cdot10^{-5}$	0.933	1.23	$1.0\cdot10^{-5}$

Homogeneous particle diffusion model (HPDM)

In this model, the rate-determining step of sorption is normally described by either film diffusion or particle diffusion mechanisms. Assuming spherical particles with average radius *r* and the Vermeulen approximation for the whole range *0<X(t)<1*, a solution of the simultaneous set of differential and algebraic equations has been proposed, once defined *X(t)*, the fractional attainment of equilibrium at time *t*, obtained from eq. 4 (Caetano et al., 2009; Xie et al., 2011).

$$X(t)=\frac{q_t}{q_e} \qquad (4)$$

If the diffusion of ions through the sorbent particles is the slowest step, the particle diffusion will be the rate-determining step and the particle diffusion model could be applied to calculate the diffusion coefficients. Then, the rate equation is expressed by eq. 5, where $D_{e,p}$ (m^2/s) is the particle diffusion coefficient indicating the diffusion of solute in the solid phase (El-Naggar et al., 2012).

$$-\ln(1-X^2(t))=K_P\cdot t \qquad \text{where} \quad K_P=\frac{\pi^2\cdot D_{e.p}}{r^2} \qquad (5)$$

If the diffusion of ions from the solution to the sorbent particles is the slowest step, rate-determining step, the liquid film diffusion model controls the rate of sorption. In this case, the relation in eq. 6 can be used, where *C* and C_r are the equilibrium concentrations of the ion in solution and in the solid phase, respectively, $D_{e,l}$ the diffusion coefficient in the liquid phase (m/s) and δ (m) the thickness of the liquid film (El-Naggar et al., 2012).

$$-\ln(1-X(t)) = K_L \cdot t \qquad \text{where} \quad K_L = \frac{3 \cdot D_{e,l} \cdot C}{r \cdot C_r} \tag{6}$$

The two previous models (eq. 5 and 6) were tested against the kinetic data of MBA/EDA and MBA/CYS, by plotting the functions of *-ln(1- X^2(t))* and *-ln(1-X(t))* against contact time *t* (Valderrama et al., 2008). Table 5.4 shows the number of data used (*N*), correlation coefficients (R^2) and the estimated parameters of the two models: among them, the intercept of the straight lines with the y-axis (*a*) is of great importance in the interpretation of results. The more the straight lines pass next to the origin the more the model is well interpreting the actual diffusion mechanisms involved (El-Naggar et al., 2012). The absolute value of the intercept *a* for both MBA/EDA and MBA/CYS is greater than zero, thus indicating that, in the experimental conditions adopted, both film diffusion and pore diffusion take place, without displaying a specific mechanism controlling the overall rate copper removal. However, if comparing both correlation coefficients and intercept values, at same PAAH sample and particle size, the particle diffusion control model provides on average a better fitting, particularly in the case of grains. This result is predictable because of the greater volume of grains compared to that of powders, that makes the diffusion of solutes through pores more significant than the diffusion through the liquid film. The slope values of the straight lines obtained using eq. 5 on PAAH samples in the form of grain were used to calculate the particle diffusion coefficients ($D_{e,p}$): $3.9 \cdot 10^{-13}$ m^2/s for MBA/EDA and $7.1 \cdot 10^{-13}$ m^2/s for MBA/CYS.

On the other hand, few differences are observed on powders of both PAAH structures between the fitting with PDC and LFDC models, meaning that in this case both particle and liquid film diffusion mechanisms are to be taken into account in the description of copper removal.

In order to provide more reliable values of the particle diffusion coefficients, modified experimental conditions can be adopted to control and reduce the influence of the transport of the solute through the liquid film. Specifically, improving the contact mode and providing sufficient turbulence into the reactor, the transport of the solute within the porous media controls the uptake rate and the HPD Model under PDC condition can be used to measure $D_{e,p}$.

Table 5.4 Number of experimental data used (*N*), correlation coefficients (R^2) and estimates of parameters for the Homogeneous Particle Diffusion Model in both conditions: particle diffusion control (PDC) and liquid film diffusion control (LFDC). Values for MBA/EDA and MBA/CYS hydrogels as a function of particle size and S/L ratio.

			Particle Diffusion Control				**Liquid Film Diffusion Control**			
PAAH SAMPLE AND PARTICLE SIZE	**S/L RATIO [g_{PAA}/mL]**	***N***	***R^2***	***a***	***K_P* [s^{-1}]**	***$D_{e,p}$* [m^2/s]**	***R^2***	***a***	***K_L* [s^{-1}]**	***$D_{e,l}/\delta$* [m/s]**
MBA/EDA d<1mm	1/150	11	0.855	1.59	$3.9 \cdot 10^{-05}$	$1.5 \cdot 10^{-13}$	0.843	2.22	$4.0 \cdot 10^{-05}$	$2.5 \cdot 10^{-10}$
	1/300	13	0.921	0.21	$5.8 \cdot 10^{-05}$	$2.3 \cdot 10^{-13}$	0.920	0.62	$6.7 \cdot 10^{-05}$	$2.3 \cdot 10^{-9}$
	1/600	15	0.806	0.52	$1.3 \cdot 10^{-05}$	$5.0 \cdot 10^{-14}$	0.779	1.00	$1.5 \cdot 10^{-05}$	$3.8 \cdot 10^{-10}$
MBA/EDA 1mm<d<2mm	1/150	10	0.850	0.66	$3.3 \cdot 10^{-05}$	$5.5 \cdot 10^{-13}$	0.829	1.18	$3.6 \cdot 10^{-05}$	$1.5 \cdot 10^{-9}$
	1/300	16	0.928	0.04	$1.3 \cdot 10^{-05}$	$2.2 \cdot 10^{-13}$	0.941	0.31	$1.7 \cdot 10^{-05}$	$1.5 \cdot 10^{-9}$
	1/600	16	0.952	-0.25	$2.5 \cdot 10^{-05}$	$4.1 \cdot 10^{-13}$	0.976	-0.06	$2.8 \cdot 10^{-05}$	$2.3 \cdot 10^{-9}$
MBA/CYS d<1mm	1/150	13	0.820	0.70	$3.8 \cdot 10^{-05}$	$1.2 \cdot 10^{-13}$	0.808	1.22	$4.1 \cdot 10^{-05}$	$4.8 \cdot 10^{-10}$
	1/300	14	0.979	0.25	$2.9 \cdot 10^{-05}$	$9.3 \cdot 10^{-14}$	0.969	0.66	$3.3 \cdot 10^{-05}$	$7.4 \cdot 10^{-10}$
	1/600	15	0.855	-0.11	$2.3 \cdot 10^{-05}$	$7.5 \cdot 10^{-14}$	0.902	0.10	$2.9 \cdot 10^{-05}$	$6.4 \cdot 10^{-10}$
MBA/CYS 1mm<d<2mm	1/150	10	0.964	-0.42	$9.3 \cdot 10^{-05}$	$1.5 \cdot 10^{-12}$	0.984	-0.24	$1.0 \cdot 10^{-04}$	$3.1 \cdot 10^{-9}$
	1/300	15	0.842	-0.21	$2.8 \cdot 10^{-05}$	$4.7 \cdot 10^{-13}$	0.903	-0.09	$3.5 \cdot 10^{-05}$	$1.1 \cdot 10^{-9}$
	1/600	17	0.980	-0.06	$8.3 \cdot 10^{-06}$	$1.4 \cdot 10^{-13}$	0.992	0.04	$1.2 \cdot 10^{-05}$	$1.0 \cdot 10^{-9}$

Intraparticle diffusion model

Intraparticle diffusion mechanism involves pores of different size: when the macroporous structure reaches saturation, solute molecules or ions diffuses in the internal surface pores within the particle (micropore structure). The intraparticle diffusion model developed by Weber and Morris (Weber and Morris, 1963) can be used as a first approach to identify the rate limiting step of the overall kinetic: the mathematical dependence of uptake q_t of copper

on $t^{1/2}$ is shown in eq. 7. Table 5.5 reports the correlation coefficients (R^2) and the estimated parameters of the model: k_{ad} is the rate constant of intraparticle transport and D the boundary layer diffusion coefficient, a constant that gives an indication of the thickness of the boundary layer: the higher the value of *C is*, the greater the boundary layer effect are (Valderrama et al., 2008; El-Naggar et al., 2012).

$$q_t = k_{ad} \cdot t^{1/2} + D \quad (7)$$

As expected because of the results on homogenous particle diffusion model, the intraparticle diffusion model better describes (see R^2) grain sized PAAH samples than powder. Furthermore, for both hydrogels, D values are higher for powder (0.38 ± 0.22 mg_{Cu}/g_{PAA} for MBA/EDA; 0.17 ± 0.05 mg_{Cu}/g_{PAA} for MBA/CYS) if compared to that of grains (0.11 ± 0.04 mg_{Cu}/g_{PAA} for MBA/EDA; -0.01 ± 0.03 mg_{Cu}/g_{PAA} for MBA/CYS). In the tested experimental conditions, the rate limiting step of the overall kinetic is different for powders and grains. Results further prove that neither liquid film nor particle diffusion mechanisms can be neglected in the description of the copper removal kinetic by means of PAAH samples in the form of powders; however, if using grains, the size of particles gain more influence and the intraparticle diffusion mechanism is supposed to control to a greater extent the process. If considering grain sized particles, the rate constants of intraparticle diffusion for MBA/EDA and MBA/CYS are comparable, since average k_{ad} values result to be $1.1 \cdot 10^{-3}$ and $1.5 \cdot 10^{-5}$ $mg_{Cu}/(g_{PAAH} \cdot s)$, respectively.

In general, higher absolute values of D are observed for MBA/EDA, thus suggesting that the resistance opposed by liquid film diffusion is lower for MBA/CYS besides the mixing conditions adopted. It is supposed that the polymer structure and the corresponding charges due to the presence of active groups along chains determine in a way the thickness of the liquid film surrounding particles attracting and keeping water molecules adherent to particles. However, MBA/EDA results to be faster than MBA/CYS in the removal of copper. It should be considered that D is just a parameter indicating the thickness of the boundary layer and not the kinetic of the process: the mass of copper inside the boundary layer is experimentally removed from the bulk solution (since analyzed samples are taken from the bulk solution) even if copper is still in the form of dissolved ion in the film surrounding the particle and the chemical reaction with active groups is yet to occur.

Table 5.5. Number of experimental data used (N), correlation coefficients (R^2) and estimates of parameters for the intraparticle diffusion model. Values for MBA/EDA and MBA/CYS hydrogels as a function of particle size and S/L ratio.

PAAH SAMPLE AND PARTICLE SIZE	S/L RATIO [g_{PAAH}/mL]	N	R^2	k_{ad} [$mg_{Cu}/(g_{PAAH} \cdot s)$]	D [mg_{Cu}/g_{PAAH}]
MBA/EDA d<1mm	1/150	11	0.627	$1.5 \cdot 10^{-04}$	0.244
	1/300	13	0.883	$1.0 \cdot 10^{-03}$	0.252
	1/600	15	0.842	$1.3 \cdot 10^{-03}$	0.638
MBA/EDA 1mm<d<2mm	1/150	10	0.811	$3.8 \cdot 10^{-04}$	0.154
	1/300	16	0.964	$9.4 \cdot 10^{-04}$	0.095
	1/600	16	0.912	$1.9 \cdot 10^{-03}$	0.075
MBA/CYS d<1mm	1/150	13	0.822	$4.2 \cdot 10^{-04}$	0.177
	1/300	14	0.966	$1.1 \cdot 10^{-03}$	0.219
	1/600	15	0.950	$2.1 \cdot 10^{-03}$	0.125
MBA/CYS 1mm<d<2mm	1/150	10	0.924	$9.9 \cdot 10^{-04}$	0.010
	1/300	15	0.937	$1.5 \cdot 10^{-03}$	0.002
	1/600	17	0.980	$2.1 \cdot 10^{-03}$	-0.038

5.3.2.2 Saturation kinetic model

A saturation kinetic model has been used to fit experimental data by means of the integral linear method. The equation of the model (eq. 8) describes the rate by which dissolved copper concentration decreases in water over time, and uses two parameters, k_{MAX} and K_C that are the maximum removal velocity and the concentration by which the removal velocity is equal to k_{MAX} /2, respectively.

$$\frac{dC}{dt} = -k_{MAX} \cdot \frac{C}{K_C + C} \quad (8)$$

Table 5.6 reports the correlation coefficients and the estimates of parameters evaluated on experimental results for both PAAH samples in both particle sizes. As shown from R^2 values, the saturation kinetic well describes copper removal with the two hydrogels for each combination of PAAH samples, particle size and S/L ratio. In the following, a physical interpretation of results fitted with the saturation kinetic model is reported and a comparison between the behavior of the two hydrogel samples in the form of powder and grains enables to define and, at a first approximation, to quantify the influence of layer and pore diffusion on the overall rate of the process.

Table 5.6. Number of experimental data used (*N*), correlation coefficients (R^2) and estimates of parameters for the saturation kinetic model. Values for MBA/EDA and MBA/CYS hydrogels as a function of particle size and S/L ratio.

PAAH SAMPLE AND PARTICLE SIZE	S/L RATIO [g_{PAAH}/mL]	*N*	R^2	K_C [mg_{Cu}/L]	k_{MAX} [mg_{Cu}/(L·h)]
MBA/EDA d<1mm	1/150	11	0,977	0,98	0,29
	1/300	13	0,999	1,43	0,05
	1/600	15	0,995	1,52	0,11
MBA/EDA 1mm<d<2mm	1/150	10	0,996	1,36	0,16
	1/300	16	0,999	1,73	0,04
	1/600	16	0,996	1,84	0,03
MBA/CYS d<1mm	1/150	13	0,997	1,43	0,19
	1/300	14	1,000	1,56	0,07
	1/600	15	0,999	1,74	0,04
MBA/CYS 1mm<d<2mm	1/150	10	0,961	2,39	0,17
	1/300	15	0,967	2,23	0,07
	1/600	17	0,978	2,17	0,03

In Figure 5.3 (a) K_C values are reported as a function of the mass of copper provided during the trials to the mass of hydrogel (M_{Cu}/M_{PAAH} = 2 mg_{Cu}/L · $(S/L)^{-1}$), which increases when decreasing the *S/L ratio*. Small values of K_C mean that the maximum value of the rate constant k_{MAX} is halved at a lower value of the residual concentration. In this sense, small values of K_C imply faster processes even at low residual concentrations. Similar trends of K_C are observed for powder, for both hydrogels, while grains behave differently, suggesting a volume process for the removal of copper which involves pore diffusions through two different polymer matrixes.

K_C can be considered as the sum of two terms: K_L, which takes into account the "film diffusion", and K_P, which describes "pore diffusion". According to previous considerations and in order to quantify the film diffusion and the pore diffusion for the two PAAH samples, in this case as for powder, the contribution of K_P is assumed as negligible to the overall removal rate, thus enabling to calculate K_P as the difference between K_C and K_L, where K_L has the same value of the half-saturation constant (K_C) evaluated for powder. Figure 5.3 (b) reports K_L and K_P values as a function of M_{Cu}/M_{PAAH} for both MBA/EDA and MBA/CYS.

Except for MBA/EDA corresponding to 0.3 mg_{Cu}/g_{PAAH}, averagely K_L values are comparable for both hydrogels: the liquid film diffusion resistance applied to the system in the tested conditions is the same for both hydrogels and for all tested *S/L ratio*.

As for K_P, a different behavior for the two hydrogels is observed in Figure 5.3 (b). In general the diffusion through MBA/EDA pores is faster than that of MBA/CYS. Furthermore MBA/EDA is characterized by constant K_P values when M_{Cu}/M_{PAAH} increases, suggesting that the mass of copper provided does not affect the pore diffusion mechanism. This implies that the saturation of the pores is not achieved in the tested conditions and no significant variation occurs in the geometry of MBA/EDA structure when creating complexes: this is probably related also to its high and fast swelling degree, as shown in Figure 5.1. MBA/CYS behaves differently: it would be expected a reduction of the pore diffusion due to the saturation of pores when increasing M_{Cu}/M_{PAAH}; however, a decrease of K_p values is observed in

Figure 5.3 (b), which implies faster processes even at low residual concentrations. The only difference between the two hydrogels lies in the presence of functional groups: it is possible that, when loading the mass of MBA/CYS with larger amounts of copper that determine the creation of complexes with both amine and disulphide groups, a modification in the geometry of the molecule occurs. Complex formation between copper and disulphide groups could result in opening chains and making pores more accessible for the solute. Concluding, compared to MBA/EDA, it is much more difficult for the liquid phase to penetrate MBA/CYS, most likely because of the presence of disulphide bonds between the molecule chains.

Figure 5.4 shows k_{MAX} values as a function of M_{Cu}/M_{PAAH}. The maximum velocity of the whole process decreases rapidly for both hydrogels when decreasing the *S/L ratio* (higher M_{Cu}/M_{PAAH}), and its variation due to particle size is negligible especially for MBA/CYS. It's supposed that variations of k_{MAX} are mainly related to "film diffusion" rather than "pore diffusion". Film diffusion, as described by the Fick's first law for diffusion across the film layer (MWH, 2005), depends upon 3 factors: the molecular diffusion of the solute in a stagnant layer, the film thickness and the concentration gradient across the film layer. Assuming the first two terms invariable with the operating conditions, the third parameter influences K_L. As for the concentration gradient, namely the difference between the concentration in the bulk solution and the concentration at the interface, the process is slower when the concentration at the interface is higher, i.e. when the loading of the hydrogel in terms of M_{Cu}/M_{PAAH} increases and the available functional groups on particles surface decrease.

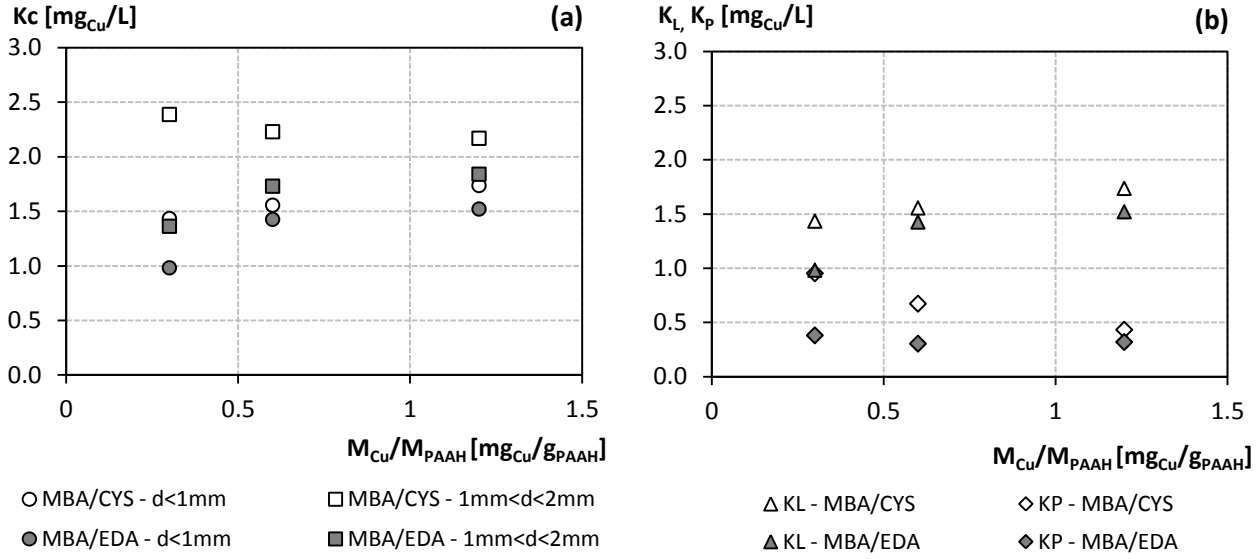

Figure 5.3. K_C (a), K_P and K_L (b) values vs. the mass of copper provided to the unit mass of hydrogel (M_{Cu}/M_{PAAH}). Data are shown for MBA/EDA and MBA/CYS.

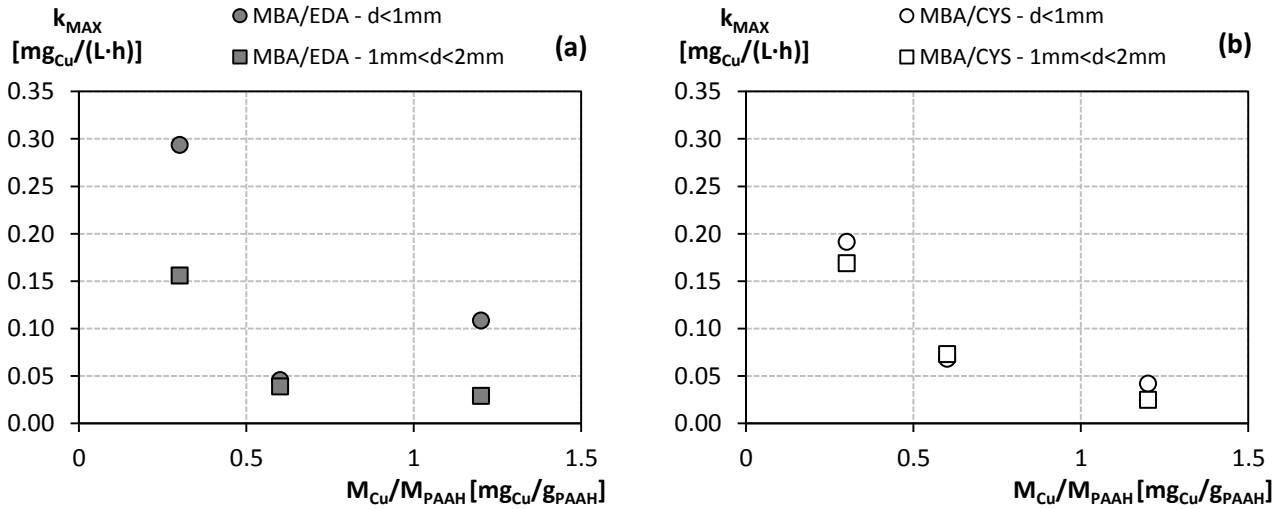

Figure 5.4. k_{MAX} values vs. the mass of copper provided during the trials to the unit mass of hydrogel (M_{Cu}/M_{PAAH}). Data are shown for MBA/EDA (a) and MBA/CYS (b).

5.4 Conclusions

The kinetic modeling analysis implemented on experimental data from batch kinetic tests, allowed deepen the knowledge of mechanisms involved during copper removal with PAAH samples: data were fitted with different models in order to derive different types of information and prove statements pertaining the diffusion processes involved. Firstly the measure of the swelling degree enable to hypothesize that the different chemical structure of MBA/EDA and MBA/CYS, resulting in different physical properties, affects the removal performances and mechanisms of the two hydrogels: MBA/CYS pores and functional groups are supposed to be less accessible for water than that of MBA/EDA, since polymer chains extend slower and less. This could explain the lower values of equilibrium contact times as for MBA/EDA tests.

Results from fitting kinetic data with the pseudo first and second order models, prove that the prevailing mechanism characterizing the chemical reaction is to be considered as a chemiosorption process, namely the creation of complexes between divalent copper ions and active groups along molecule chains: amine groups for MBA/EDA and both amine and disulphide groups for MBA/CYS.

Under conditions of chemiosorption removal mechanisms, the HPDM and the intraparticle diffusion models were used to study the influence of both liquid film and pore diffusion processes. The two kinetic models prove that, as for hydrogels in the form of powder, both particle and liquid film diffusion mechanisms are to be taken into account in the description of copper removal while, as for grains, the size of particles gain more influence along with the pore diffusion mechanism. Anyway, copper removal by means of PAAH samples of both particle sizes is affected by the diffusion through the liquid film in a way that depends upon the relative influence of particle diameter.

In order to provide more reliable results about the particle diffusion processes, modified experimental conditions can be used to control and reduce the influence of the solute transport through the liquid film: if sufficient turbulence is provided into the reactor, the diffusion of the solute within the porous media controls the overall removal rate and a comparison between MBA/EDA and MBA/CYS pore systems would enable to verify what stated in relation to swelling degree results.

The saturation kinetic model has been finally tested: it well describes experimental data of copper removal for both hydrogels and particle sizes. Based on the study of the saturation kinetic model parameters, an in-depth analysis enabled to attempt a physical explanation of the different removal kinetics observed on MBA/EDA and MBA/CYS. It's been found that the polymer matrixes of the two hydrogels behave differently because of functional groups linked to the main structure, particularly the presence of disulphide groups on MBA/CYS. It's supposed that the particle diffusion mechanism involves pore of different size; furthermore, pore size and shape can be modified during the creation of complexes between active groups and copper ions, thus further affecting diffusion mechanisms. A deep study on this two topics, the presence of macro- and micro- pores and their change over time, could be useful to improve the description of PAAH diffusion processes and to define parameters useful to predict the removal rate of hydrogels and design suitable water treatment unit processes.

5.5 References

1 American Water Works Association (AWWA), Water Quality and Treatment Handbook: A Handbook of Community Water Supplies, Fifth Edition, Irwin/McGraw-Hill, 1999.

2 APAT-IRSA, 2003. Metodi analitici per le acque. APAT Manuali e Linee Guida 29/2003.

3 Caetano M., Valderrama C., Farrán A., Cortina J.L (2009). Phenol removal from aqueous solution by adsorption and ion exchange mechanisms onto polymeric resins. Journal of Colloid and Interface Science, 338(2), 402-409.

4 Casolaro M., P. Ferruti, C. Bertoglio Riolo, T. Soldi, M. Pesavento, R. Barbucci, M. C. Beni (1982) Applied macroinorganics. II. Protonation and heavy metal ions complex-formation behavior of three crosslinked resins of poly(amido-amine) structure. J. Appl. Polymer Sci. 27, 2239-2248.

5 El-Naggar I.M., E.S. Zakaria, I.M. Ali, M. Khalil, M.F. El-Shahat (2012). Kinetic modeling analysis for the removal of

cesium ions from aqueous solutions using polyaniline titanotungstate Arabian Journal of Chemistry, 5, 109–119.

6 Ferruti P., E. Ranucci, A. Manfredi, N. Mauro, E. Ferrari, R. Bruni, F. Colombo, P. Mussini, M. Rossi (2012). Llysine and EDTA polymer mimics as resins for the quantitative and reversible removal of heavy metal ion water pollutants. J. Polym. Sci. A Polym. Chem., 50: 5000–5010.

7 Ferruti P., Ranucci E., Bianchi S., Falciola L., Mussini P.R., Rossi M. (2006). Novel polyamidoamine-based hydrogel with an innovative molecular architecture as a Co^{2+}, Ni^{2+}, and Cu^{2+} sorbing material: cyclovoltammetry and extended x-ray absorption fine structure studies. Journal of Polymer Science, Part A: Polym. Chem., 44(7), 2316-2327.

8 Fujiki J., Sonetaka N., Ko K.P., Furuya E. (2010). Experimental determination of intraparticle diffusivity and fluid film mass transfer coefficient using batch contactors. Chemical Engineering Journal, 160 (2), 683-690.

9 Kumar K. V. (2006). Linear and non-linear regression analysis for the sorption kinetics of methylene blue onto activated carbon. Journal of Hazardous Materials, 137(3), 1538-1544.

10 Kurniawan T. A., G. Y.S. Chan, W. H. Lo, S. Babel (2006). Physico–chemical treatment techniques for wastewater laden with heavy metals. Chemical Engineering Journal, 118: 83-98.

11 Liang F.B., Song Y. L., Huang C. P., Li Y. X., Chen B. H. (2013). Synthesis of novel lignin-based ion-exchange resin and its utilization in heavy metals removal. Industrial and Engineering Chemistry Research, 52 (3), 1267-1274.

12 Mousavi S.F., Esteki M., Mostafazadeh-Fard B., Dehghani S., Khorvash M. (2012). Linear and nonlinear modeling for predicting nickel removal from aqueous solutions. Environmental Engineering Science, 29 (8), 765-775.

13 MWH (2005). Water treatment: principles and design, 2nd edn. Wiley, Hoboken (N.J.), USA.

14 Rudzinski W., W. Plazinski (2006). Kinetics of solute adsorption at solid/solution interfaces: a theoretical development of the empirical pseudo-first and pseudo-second order kinetic rate equations, based on applying the statistical rate theory of interfacial transport. J. Phys. Chem. B, 110, 16514-16525.

15 Satoh K., Fan H.J., Hattori H., Tajima K., Furuya E. (2008). Simultaneous determination of intraparticle diffusivities from ternary component uptake curves using the shallow bed technique. Journal of Hazardous Materials, 155, 397-402.

16 Sonetaka N., Fan H.J., Kobayashi S., Chang H.N., Furuya E. (2009). Simultaneous determination of intraparticle diffusivity and liquid film mass transfer coefficient from a single-component adsorption uptake curve. Journal of Hazardous Materials, 164(2-3), 1447-1451.

17 Valderrama C., Gamisans X., de las Heras X., Farrán A., Cortina J.L. (2008). Sorption kinetics of polycyclic aromatic hydrocarbons removal using granular acrivated carbon: intraparticle diffusion coefficients. Journal of Hazardous Materials, 157(2-3), 386-396.

18 Weber W.J. and J.C. Morris (1963). Kinetics of Adsorption on Carbon from Solution, *Journal* of the Sanitary *Engineering* Division, American Society of Chemical Engineering 89, 31-59.

19 Xie Y., Jing K.J., Lu Y. (2011). Kinetics, equilibrium and thermodynamic studies of L-tryptophan adsorption using a cation exchange resin. Chemical Engineering Journal, 171(3), 1227-1233.

6 Investigation on particle diffusion of heavy metal ions into PolyAmidoAmine Hydrogel structures

6.1 Introduction

The kinetics of solute removal at the solid/liquid interfaces is of great importance for the use of granular media in the water treatment field. Kinetics explain how fast the rate of processes occur and enable to identify the factors affecting the reaction rate. The nature of removal mechanisms will therefore depend on physical and/or chemical characteristics of the solute/media system and on the system conditions (Kumar, 2006). The optimization of costs and performances of these processes needs for a deep study into the efficiency of the selected media, including not only the equilibrium features but also to the kinetics mechanisms. When using granular media in field applications such as water treatment units, a sorbent and a solution are brought into contact for a limited period of time: the understanding of the nature of the kinetic process and its theoretical description are crucial for practical applications, in order to improve the equipment and the conditions for the achievement of an optimum efficiency (Rudzinski and Plazinski, 2007).

Heterogeneous processes between solids and fluids can be explained through several consecutive steps determining the rate of reaction: a) the diffusion of solute through the liquid film surrounding the particle (liquid film diffusion, LFD); b) the diffusion of solute through the polymeric matrix of the resin (particle diffusion, PD) and c) the chemical reaction (CR) (Xie et al., 2011). One of these steps usually offers much greater resistance than the others and may thus be considered as the rate-limiting step of the process. The definition of the step which controls the overall rate is largely dependent on the method by which the granular media is contacted with water. For a batch reactor which provides a high degree of turbulence, pore diffusion is often rate-limiting. For continuous flow systems, such as columns, film diffusion is most likely rate-limiting for normal flow rates (Weber, 1972).

Furthermore, when the chemical reaction may be explained as a chemisorption process, it is usually assumed to be too fast to affect the overall rate, unless chemical modifications occur during the reaction (Xie et al., 2011). In this case, only the rates of liquid film transfer and particle diffusion determine the overall rate of the process, since the last step can be neglected. Specifically, particle diffusion includes pore and surface diffusions. For pore diffusion, the solute moves within the pores before reacting onto the surface of the pores: this mainly occurs into macro-pores, at the beginning of the removal process, and the solute movement is controlled by the concentration difference in the liquid-phase. On the other hand, surface diffusion occurs along the pore surface of the media, after initial adsorption has taken place and mainly involve micro-pores. The driving force for the surface diffusion is the difference in the amount adsorbed on the pore surface (Furuya et al., 1996; Sonetaka et al., 2009a).

In order to reduce the overall rate and thus improve removal processes, liquid film diffusion can be, in a way, controlled and reduced by selecting the appropriate contact mode and conditions between the solute and the media. However, particle diffusion is specific for each combination of solute/reactive media, and the identification of its features is significant in the water treatment field. The particle diffusivity can be experimentally determined by reducing diffusion resistance at fluid-to-solid film at very high fluid flow rate, thus making liquid film resistance surrounding the particle is negligible, thus. However, When relatively small adsorbent particles are employed, contribution due to liquid film resistance to overall adsorption rate might be significant (Valderrama et al., 2008, Caetano et al., 2009; Sonetaka et al., 2009b).

PolyAmidoAmine Hydrogels (PAAH) are synthetic polymers particle-shaped, able to create complexes with specific heavy metal ions (Ferruti et al., 2006). PD control conditions in batch experiments were selected for two PAAH samples, termed MBA/EDA and MBA/CYS and different in their chemical structure. Kinetics of copper and chromium removal were thus performed under such conditions, and data fitted on two kinetic models (the Homogeneous

Particle Diffusion Model, HPDM, and the Intraparticle Diffusion Model) in order to study particle diffusion processes (El-Naggar et al., 2012).

6.2 Materials and Methods

6.2.1 Reagents, stock solutions and glassware

Copper nitrate ($Cu(NO_3)_2 \cdot 3H_2O$, 99% assay), Potassium dichromate ($K_2Cr_2O_7$, ACS reagent, ≥99.0% assay), hydrochloric acid (HCl, ACS reagent, 37% assay) and nitric acid (HNO_3, ≥99.999% trace metals basis, 70% assay) were purchased from Sigma Aldrich. All reagents were used without further purification.
A chromium stock solution (1 $g_{Cr} \cdot L^{-1}$) and a copper stock solution (1 $g_{Cu} \cdot L^{-1}$), stored for all the experiments at room temperature, were prepared by dosing $K_2Cr_2O_7$ and $Cu(NO_3)_2 \cdot 6H_2O$, respectively, in MilliQ water. Copper stock solution was stabilized at 5% HNO_3.
Before use, all glassware was washed in an acidic bath (10% HCl), rinsed with MilliQ water and dried.
The contaminated solutions for stirring rate and kinetic experiments were prepared spiking a defined volume of metal stock solution into 500 mL tap water, previously filtered on a Millipore device equipped with 0.45 µm cellulose acetate membrane filters (Whatman), to obtain the selected starting metal concentration.

6.2.2 PolyAmidoAmine Hydrogels (PAAHs)

Two samples of PAA hydrogels, MBA/EDA (753±56 kg/m^3) and MBA/CYS (709±28 kg/m^3), were synthesized by Laboratori Alchemia (Milan, IT) in the form of powders (diameter smaller than 1 mm) and grains of: a particle size analysis provided the diameter corresponding to 60% finer in the particle-size distribution D_{60}, for MBA/EDA (D_{60} = 686 µm) and MBA/CYS (D_{60} = 618 µm). The two hydrogels are termed according to the starting polymers employed during the synthesis process and differ in functionalization: MBA/EDA (MethyleneBisAcrylamide/EthyleneDiAmine), besides aminic nitrogen, has no specific functional groups active for heavy metal complexation, while MBA/CYS (MethyleneBisAcrylamide/CYStamine) is further functionalized with disulphide groups -SS-. Chemical formulas are shown in par. 2.2.1.
The mass of hydrogel to be tested in kinetic, isotherm and interference experiments, was previously washed to remove the residues of synthesis solutions and minimize alterations of water composition. Tap water filtered on a Millipore device equipped with 0.45 µm cellulose acetate membrane filters (Whatman) was used for this purpose. The number of steps in batch conditions (Solid/Liquid ratio, *S/L ratio* = 1/20 g·mL^{-1}; contact time, t_c: 5 minutes for each step) was previously determined (Appendix 1) in 10 steps for MBA/EDA and 5 steps for MBA/CYS, by monitoring changes in water pH, till negligible variations were observed. At the end of each step water was separated from the solid phase by using a centrifuge (IEC CL 10) at the rate of 2000 rpm for 5 minutes.

6.2.3 Evaluation of PAAH swelling ability

The ability of MBA/EDA and MBA/CYS structures to expand its volume when in contact with water was evaluated in static conditions on both powders and grains. The swelling degree measured over time (SD_t) is defined by eq. 1, where $V_{SH,t}$ is the volume of the swelled hydrogel in tap water at time t and V_{DH} is the initial dry volume. Seven contact times were selected: 5 - 15 - 30 - 60 - 90 - 120 minutes and 1 day.

$$SD_t = \frac{(V_{SH,t} - V_{DH})}{V_{DH}} \quad (1)$$

6.2.4 Stirring rate experiments

Tests in duplicate on both particle sizes of MBA/CYS and MBA/EDA were performed on a magnetic stirrer, selecting different rates of stirring (ω): 10, 30, 60, 120, 150 rpm for MBA/CYS; 10, 30, 60, 90, 120 rpm for MBA/EDA-d<1mm. Batch conditions were adopted using a *S/L ratio* of 1/300 g·mL^{-1} and a starting copper concentration of 2 $mg_{Cu} \cdot L^{-1}$.

Contact times of 15 minutes for MBA/EDA and 45 minutes for MBA/CYS were selected in order to observe variations of the residual copper concentration. Samples were collected for pH, electrical conductivity (EC), temperature (T) and copper concentration detection.

6.2.5 Kinetics experiments

Batch kinetic tests, in duplicate, were performed using a a jar test equipment at the fixed stirring rate of 120 rpm to provide adequate turbulence into the reactor so that PD control conditions were achieved.
Copper was tested on MBA/EDA and MBA/CYS in the form of powder, at the fixed solid to liquid ratio (*S/L ratio*) of 1/300 g/mL and initial copper concentration ($C_{Cu,0}$) of 2.0 $mg_{Cu} \cdot L^{-1}$. Chromium was tested on MBA/EDA in the form of powder and grain. Specifically, three initial chromium concentrations ($C_{Cr,0}$) were selected (0.82, 1.64, 3.28 mg_{Cr}/L) and four *S/L ratio* were adopted (1/150, 1/300, 1/600, 1/1200 g_{PAAH}/mL). MBA/EDA in the form of grain was tested at 1.64 mg_{Cr}/L and 1/300 g_{PAAH}/mL. MBA/EDA in the form of powder was tested at each combination of $C_{Cr,0}$ and *S/L ratio*, with the exception of the combination 0.82 mg_{Cr}/L and 1/150 g_{PAAH}/mL. Table 6.1 summarizes contact times used during tests. Samples were collected for pH, EC, T chromium and copper concentrations detection.

Table 6.1. Contact times selected for kinetics tests on MBA/EDA and MBA/CYS with copper and chromium.

HEAVY METAL	PAAH SAMPLE AND PARTICLE SIZE	CONTACT TIME								
		5 min	10 min	15 min	30 min	45 min	1 h	2 h	4 h	6 h
Cu(II)	MBA/EDA - d<1 mm	×	×	×	×	×	×	×		
	MBA/CYS - d<1 mm	×	×	×		×		×		×
Cr(VI)	MBA/EDA - d<1 mm	×	×	×	×	×	×			
	MBA/EDA - 1mm<d<2mm	×	×	×	×	×	×	×	×	

6.2.6 Analythical methods

At the end of each contact time the liquid phase was separated from the solid phase by vacuum filtration on Millipore with 0.45 μm cellulose acetate membrane filters (Whatman): samples collected for the detection of pH, EC and T were quickly analyzed; samples collected for the detection of copper concentrations were acidified at 2% HNO_3 and stored at 4°C for analysis; samples collected for the detection of chromium concentrations were stored for analysis for no more than 24 hours, in the dark and at 4°C.
A portable pH-meter, model Eutech pH 5+ (Eutech Instruments), was used for pH analysis (Method: IRSA 2080). EC (APAT-IRSA, 2003. Method 2030) and T (APAT-IRSA, 2003. Method 2100) were monitored using the conductivity meter model Eutech Cond 6+ (Eutech Instruments).
Concentrations of copper in water were analyzed using the Atomic Absorption Spectometer, (VARIA Spectra AA 55) and adopting the procedure explained in method APAT-IRSA 3250A (APAT-IRSA, 2003). Concentrations of Cr(VI) in water were analyzed using LCK313 cuvette test (Hach Lange), XION 500 (Dr Lange) spectrophotometer based on Diphenylcarbazide Method from Standard Method 3500-Cr(B) (APHA, 2012). As for copper residual concentrations, Bathocuproine Method from Standard Method 3500-Cu(C) was adopted (APHA, 2012) and UNICAM VIS-UV 2 spectrophotometer used for absorbance measurements at 484 nm wavelength (optical path, 1 cm).

6.3 Results and Discussion

In the following, residual chromium and copper concentrations data ($C_{Me,t}$) falling outside the range [$\bar{C}_{Me,t-1} \cdot (1+\%Err)$, $\bar{C}_{Me,t+1} \cdot (1-\%Err)$] were considered as outliers where $\bar{C}$ is the average value of concentrations on replicates. An error

percentage value of 15% (*%Err*) was selected and adopted for the entire set of data in order to keep the percentage of removed data within the 10%.

6.3.1 Swelling degree

Swelling degree values are shown as a function of contact time in Figure 6.1: both hydrogels, regardless of particle size, achieve an asymptotic value, almost double for MBA/EDA compared to MBA/CYS. Furthermore, MBA/EDA swells rapidly, getting about the 80-90% of the final *SD* in the first 5-35 minutes, contrarily to MBA/CYS that needs 60-90 minutes: in general grains are slower than powders. When water gets into the hydrogels, MBA/CYS polymer chains extend slower and less than that of MBA/EDA, thus suggesting the presence of a stiffer structure and of pores and functional groups less accessible to water and solutes. Possible influences of this physical property on the removal performances and mechanisms of the two hydrogels in the two forms should be considered when analyzing kinetic results.

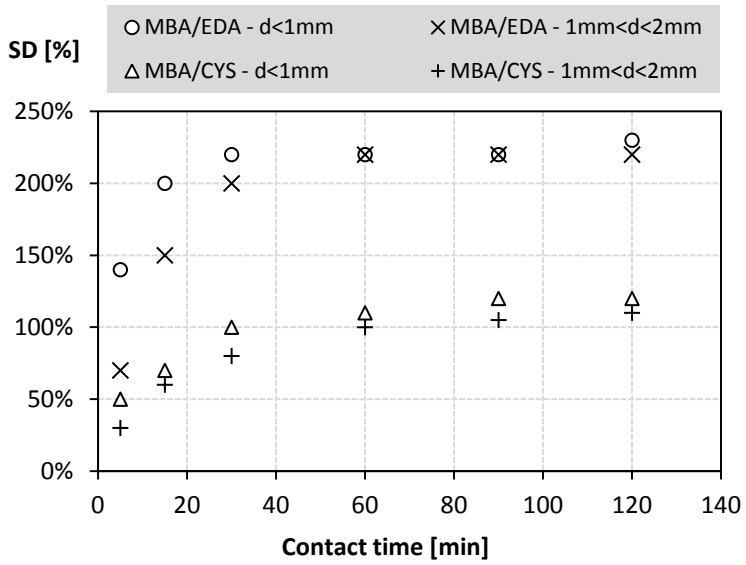

Figure 6.1. Swelling degree (*SD*) vs. contact time for MBA/EDA and MBA/CYS in the form of powders and grains.

6.3.2 Stirring rate experiments

Results of experiments at different stirring speeds (ω) are shown in Figure 6.2, where the amount of copper removed per unit mass of hydrogel ($q_{Cu,\omega}$) is related to ω. Figure 6.2 can be interpreted as a "picture" of the copper loading for MBA/EDA and MBA/CYS at the fixed contact times of 15 and 45 minutes, respectively. Equilibrium conditions were established when the ratio between $q_{Cu,\omega}$ and the maximum amount of copper removed during trials $q_{Cu,max}$ is at lowest the 0.9: the equilibrium state achieved defines the minimum speed above which liquid film diffusion has no longer influence on the overall removal rate of hydrogels, and thus stirring conditions for particle diffusion control can be adopted for experiments aimed at the study and comparison of PAAH structures.

Both MBA/EDA and MBA/CYS in the form of powder achieve PD control conditions above 60 rpm and the amounts of copper removed are comparable (0.55 and 0.52 mg_{Cu}/g_{PAAH} for MBA/EDA and MBA/CYS, respectively). However grains behave differently: MBA/EDA and MBA/CYS PD control conditions are set, respectively at 90 and 120 rpm, displaying different copper removal abilities (0.34 mg_{Cu}/g_{PAAH} for MBA/EDA and 0.21 mg_{Cu}/g_{PAAH} for MBA/CYS).

At same contact time for each hydrogel, it can be stated that, once achieved equilibrium/particle diffusion conditions, the resistance opposed by MBA/CYS structure is greater than that of the other PAAH sample, since the difference in the amounts of copper removed by grains and powder is higher for the functionalized hydrogel ($\Delta q_{MBA/CYS}$ = 0.31 mg_{Cu}/g_{PAAH}) compared to that of MBA/EDA ($\Delta q_{MBA/EDA}$ = 0.21 mg_{Cu}/g_{PAAH}), as shown in Figure 6.2.

As for the influence of liquid film diffusion on different PAAH structure having different particle dimensions, assuming a first order process, the slopes (*m*) of the straights line defined by data within the equilibrium were evaluated. Stirring conditions greatly affect both hydrogels in the form of powder, resulting in comparable m values: 0.009 and 0.008 $mg_{Cu}/(g_{PAAH}\cdot rpm)$ for MBA/EDA and MBA/CYS, respectively: the thickness of the liquid film layer is thus

supposed not to be affected by the type of hydrogel. However, it is surely influenced by particle dimensions, and differences between hydrogels become more significant if considering results obtained on grains: 0.003 and 0.001 $mg_{Cu}/(g_{PAAH}\cdot rpm)$ for MBA/EDA and MBA/CYS, respectively. Concluding, the liquid film diffusion process affects more small than big particles (more powders than grains) and more MBA/EDA than MBA/CYS, probably because of the formation of a thicker liquid film due to the presence of free charges on polymer chains that attract water molecules. As an example, under certain conditions of pH values, amine nitrogen protonates in water and, because of their structure, the percentage of amine groups on MBA/EDA is greater than that on MBA/CYS.

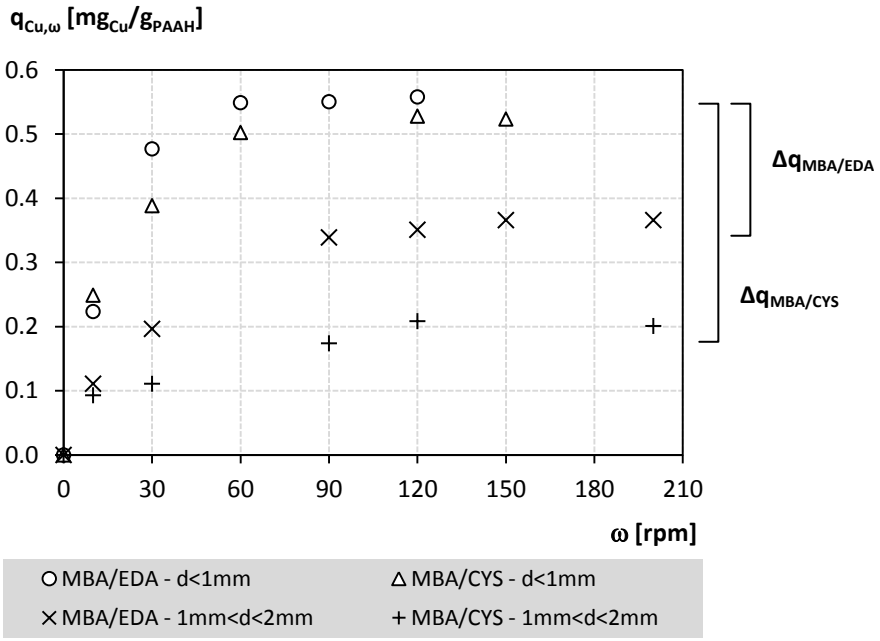

Figure 6.2. Amounts of copper removed per unit mass of PAAH ($q_{Cu,\omega}$) vs. stirring speed (ω) for MBA/EDA and MBA/CYS at the fixed contact times of 15 and 45 minutes, respectively.
Boundary conditions: *S/L ratio* = 1/300 g/mL; $C_{Cu,0}$ = 2.0 mg_{Cu}/L.

6.3.3 Kinetic experiments

In order to study particle diffusion processes of two different polymer structures towards two differently charged and sized ions, kinetics of copper and chromium removal were performed. Specifically, copper was tested on MBA/EDA and MBA/CYS samples in the form of powders (d<1mm) while chromium was tested on MBA/EDA in the form of both powder and grains (1mm<d<2mm) in order to compare different particle sized samples. Furthermore, the influence of the PAAH dose (solid to liquid ratio, S/L ratio) and of starting solute concentration (C_0) was tested on chromium experiments .

6.3.3.1 Evaluation of equilibrium conditions

Figure 6.3 and Figure 6.4 reports results of copper and chromium kinetic tests as the ratio between residual solute concentration at the generic time *t* and at the beginning of the experiment (C_t/C_0) over time (t_c). Once defined the amounts of chromium removed per unit mass of PAAH at the generic contact time *t* (q_t) and at the final tested contact time *t-max* ($q_{t\text{-}max}$), equilibrium conditions are set when: a) the slope of the line interpolating copper residual concentrations at *t-1* and *t* is smaller than 10 degree; b) the $q_t/q_{t,max}$ ratio is at least the 85%.
As for copper, about the 90% is removed at equilibrium: MBA/EDA is faster and achieves equilibrium conditions in 45 minutes, while MBA/CYS needs about 2 hours. Average copper loadings $q_{Cu,eq}$ at the equilibrium for MBA/EDA and MBA/CYS are, respectively, 0.530 and 0.498 mg_{Cu}/g_{PAAH}.
As for tests on chromium removal percentages and equilibrium contact times t_{eq} range from 53% to 96% and from 15 to 60 minutes: values increase for high PAAH doses (low S/L ratios), while the effect of $C_{Cr,0}$ is almost negligible. Chromium removal abilities $q_{Cr,eq}$ at the equilibrium, depend upon both $C_{Cr,0}$ and *S/L ratio* and range from 0.22 to 2.18 mg_{Cr}/g_{PAAH}.

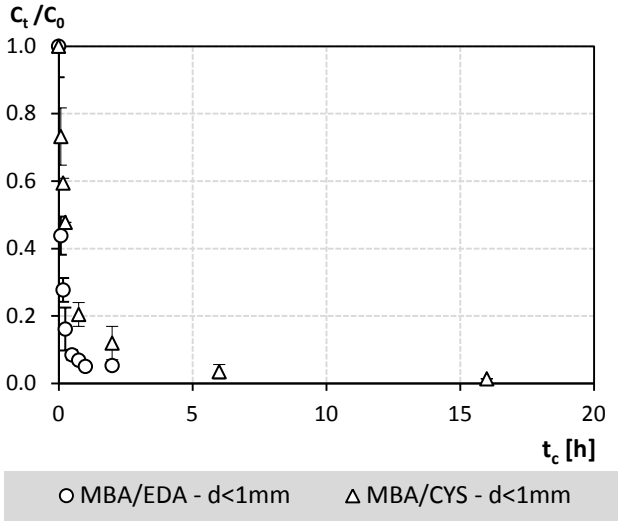

Figure 6.3. Average values of C_t/C_0 vs. contact time t_c from copper kinetic tests on MBA/EDA and MBA/CYS in the form of powder. Boundary conditions: *S/L ratio* = 1/300 g/mL; $C_{Cu,0}$ = 2.0 mg_{Cu}/L; jar test device at 120 rpm. Error bars are drawn using standard deviations.

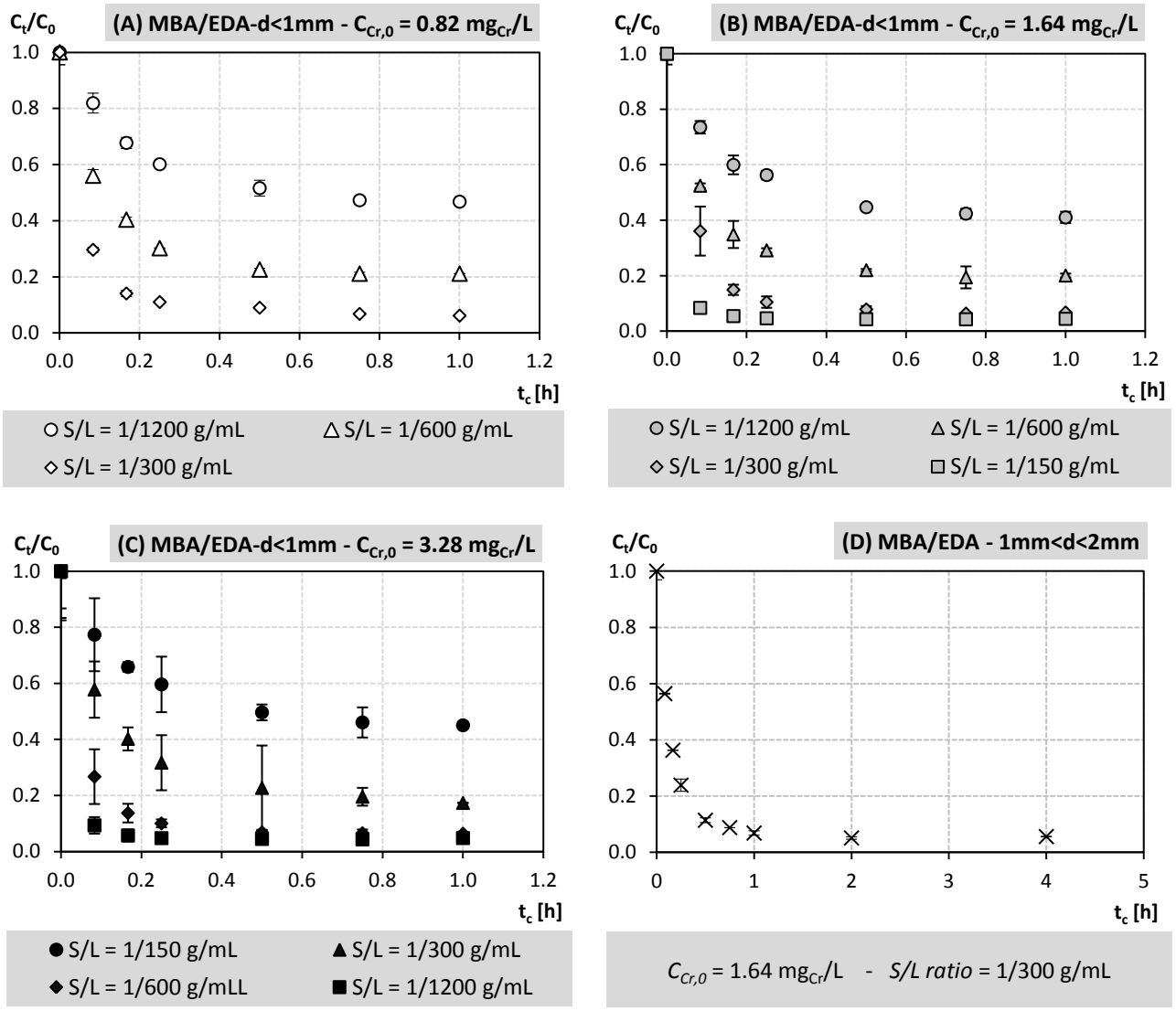

Figure 6.4. Average values of C_t/C_0 vs. contact time t_c from chromium kinetic tests on jar test device at 120 rpm: results for MBA/EDA in the form of powder (A, B and C: each graph is shown for tests at the same starting chromium concentration) and for MBA/EDA in the form of grain (D). Error bars are drawn using standard deviations.

6.3.3.2 Removal kinetics modelling

Since the chemical reactions occurring between hydrogels active groups and copper (par. 3.3.2.2) or chromium (par. 4.3.2.3) can be explained as a chemisorption process, it is usually assumed to be too fast to affect the overall rate (Ho et al., 2000; Xie et al., 2011).

Moreover, since tests were performed at a stirring rate of 120 rpm, the hydrodynamic conditions applied to the reactor guarantee the prevailing of particle diffusion mechanisms. A comparison between the behaviors of the polymer structure of the two hydrogels is proposed in the following. Experimental kinetic data on MBA/EDA and MBA/CYS hydrogels were fitted using the homogeneous particle diffusion model (HPDM) under for PD control conditions and the intraparticle diffusion model equations.

Homogeneous particle diffusion model (HPDM)

The homogeneous particle diffusion model is used when the chemical reaction rate is negligible in determining the overall reaction rate. In this model, the rate-determining step of sorption is normally described by either the liquid film diffusion, or the particle diffusion mechanism. HPDM equations are based on Nernst-Plank equation, which takes into account both concentration and electrical gradients into the flux equation. Two different models are proposed, describing both conditions: liquid film diffusion and particle diffusion rate-determining step (Shenata et al., 2010).

Kinetic experiments on PAAH were performed under particle diffusion control conditions: assuming particles as spherical and defining *X(t)* as the fractional attainment of equilibrium at time *t* (the ratio between q_t and q_{eq}, the solute loadings on hydrogels at time *t* and when equilibrium is attained, respectively, expressed in mg/g_{PAAH}), equation 2 has been used to fit experimental data and derive the particle diffusion coefficient in the solid phase or particle diffusivity D_p (m^2/s) (Valderrama et al. 2008).

$$-\ln(1-X^2(t)) = K_P \cdot t \qquad \text{where} \quad K_P = \frac{\pi^2 \cdot D_p}{r^2} \qquad (2)$$

By plotting the function *-ln(1- X^2(t))* against contact time *t*, correlation coefficients (R^2), slopes (K_P) and intercepts (*m*) were derived and are shown in Table 6.2. If observing *m* values, straight lines do not pass through the origin as they should: a slight deviation from linearity near this point can be due to the fact that at the beginning of the reaction, the liquid film resistance is comparable to that of the particle, since the thickness of the reacted layer is still very small and thus similar to that of the liquid film surrounding the particle.

Correlation coefficients are high for each set of experiment, thus suggesting that model hypothesis are satisfied and that it is possible to calculate particle diffusion coefficients, D_p, shown in Table 6.2.

Focusing on MBA/EDA in the form of powder, few differences are observed between the removal of the positive divalent ion of copper and the negatively charged hexavalent chromium: D_p in the case of copper and chromium, averagely results to be $5.0 \cdot 10^{-12}$ and $7.5 \cdot 10^{-12}$ m^2/s, respectively. Differently charged and sized ions have few influence on the rate of the solute diffusion through hydrogel particles and its porosity. Furthermore, starting concentrations and S/L ratios too have negligible influence on D_p values. Such results are of importance, since it's supposed to be that differences in removal percentages observed from experiments on the removal of copper and chromium by means of MBA/EDA are to be ascribed not to the physical structure of the hydrogel (pore size, shape and frequency), but more likely to the presence of enough active groups able to react with the solute. In order to improve removal efficiencies, higher PAAH doses or, a better solution, hydrogels with greater amounts of active groups, should be used or designed, respectively.

As for MBA/EDA in the form of grains, its D_p value describes faster particle diffusion mechanism: this is apparently in contrast to what experimentally observed from data (at same *S/L ratio* of 1/300 g_{PAAH}/mL and C_0 of 1.64 mg_{Cr}/L, equilibrium contact times are 30 and 45 minutes for powder and grains, respectively and chromium loadings at equilibrium are comparable and equal to 0.441 and 0.448 mg_{Cr}/g_{PAAH}, respectively); it is convenient to remark that D_p describes the diffusion through the hydrogel structure itself irrespective of the radius of particles, which is instead taken into account when evaluating K_P and thus the overall rate of the process. In this sense D_p obtained on grains and powders should be considered as the same coefficient describing particle diffusion through MBA/EDA structure.

As for copper removal, MBA/EDA particle diffusion process is of one order of magnitude faster than that of MBA/CYS, practically resulting in a more than halved equilibrium contact time for the unfunctionalized sample. It can be stated that chemical structure of the two hydrogels are of influence in the kinetic process: as confirmed by data in Figure 6.1, because of the presence of disulphide links between the chains of the molecule, it's harder for the solute to penetrate MBA/CYS towards active groups. As a consequence, it's supposed that the particle diffusion mechanism for PAA

hydrogels involves different steps: an "external" instantaneous uptake on macro-pores surfaces and a gradual removal step, involving micro-pores; furthermore, pore size and shape, and therefore the hydrogel geometry, are likely to be modified during the complex formation between copper and disulphide groups. An interesting description concerning this feature of the particle diffusion is drawn using the intraparticle diffusion model, developed by Weber and Morris (Weber and Morris, 1963).

Table 6.2. Correlation coefficients (R^2), intercepts (m), slopes (K_P) and particle diffusivities (D_p) evaluated for different test conditions by fitting experimental data with HPDM in condition of particle diffusion control.

HEAVY METAL	PAAH SAMPLE AND PARTICLE SIZE	C_0 [mg/L]	S/L RATIO [g/mL]	N	R^2	m	K_P [s^{-1}]	D_p [$m^2 \cdot s^{-1}$]
Cu(II)	MBA/EDA - d<1mm	2.0	1/300	16	0,973	0,21	$1.3 \cdot 10^{-3}$	$5.0 \cdot 10^{-12}$
	MBA/CYS - d<1mm	2.0	1/300	14	0,947	0,30	$1.4 \cdot 10^{-4}$	$4.5 \cdot 10^{-13}$
Cr(VI)	MBA/EDA - d<1mm	0.82	1/300	12	0.941	0.80	$1.3 \cdot 10^{-3}$	$5.1 \cdot 10^{-12}$
			1/600	14	0.998	-0.27	$2.0 \cdot 10^{-3}$	$7.8 \cdot 10^{-12}$
			1/1200	14	0.959	-0.51	$1.5 \cdot 10^{-3}$	$6.1 \cdot 10^{-12}$
	MBA/EDA - d<1mm	1.64	1/150	13	0.999	1.03	$4.8 \cdot 10^{-3}$	$1.9 \cdot 10^{-11}$
			1/300	14	0.933	0.42	$2.0 \cdot 10^{-3}$	$7.8 \cdot 10^{-12}$
			1/600	14	0.997	-0.01	$1.7 \cdot 10^{-3}$	$6.8 \cdot 10^{-12}$
			1/1200	14	0.995	-0.16	$1.2 \cdot 10^{-3}$	$4.8 \cdot 10^{-12}$
	MBA/EDA - d<1mm	3.28	1/150	14	*NA	NA	NA	NA
			1/300	14	0.972	0.69	$1.9 \cdot 10^{-3}$	$7.6 \cdot 10^{-12}$
			1/600	13	0.994	0.08	$1.1 \cdot 10^{-3}$	$4.3 \cdot 10^{-12}$
			1/1200	14	0.990	-0.30	$1.3 \cdot 10^{-3}$	$5.1 \cdot 10^{-12}$
	MBA/EDA - 1mm<d<2mm	1.64	1/300	16	0.989	0.06	$1.0 \cdot 10^{-3}$	$1.7 \cdot 10^{-11}$

**NA: Not Available*

Intraparticle diffusion model

Particle diffusion mechanism involves pores of different size: when the macro-porous structure achieves saturation, solute molecules or ions diffuses into the inner structure of particles (micro-pore structure). The possibility of intra-particle diffusion was explored by the intra-particle diffusion model given by Weber and Morris (Weber and Morris, 1963; Ho et al., 2000) represented by the mathematical dependence of copper uptake at time t, q_t on $t^{1/2}$ (eq. 3): k_P is the rate constant of intraparticle transport (mg/($g_{PAAH} \cdot min^{½}$)), and D (mg/g_{PAAH}) is a constant that roughly describes the thickness of the boundary layer surrounding the particle: the higher the value of *D is*, the greater the boundary layer effects are (El-Naggar et al., 2012).

$$q_t = k_P \cdot t^{1/2} + D \qquad (3)$$

Experimental results of copper removal kinetics on MBA/EDA and MBA/CYS in the form of powder were fitted by using equation 3. Scarce correlation was observed with R^2 values of 0.646 and 0.654, respectively and Figure 6.5 shows that a linear interpretation of equation 3 on data badly describes the process.

A multi-linear (in this case bi-linear) approach in q_t on $t^{1/2}$ plot can be used to interpret data, thus meaning that two steps with two different rates are involved in the particle diffusion process: the external and faster macro-pore diffusion (1st step) and the internal and slower micro-pore diffusion (2nd step) (Valderrama et al., 2008). Based on equilibrium contact times corresponding to a change in the slope of data, experimental kinetic results were divided into two groups and then interpolated with eq. 3: $k_{p,1}$ was derived from data in the range $0 < t < t_{eq}$, while data in the range $t_{eq} \leq t \leq t_{max}$ were used to evaluate $k_{p,2}$. Intraparticle diffusion rate constants through macro-pores ($k_{p,1}$) and micro-pores ($k_{p,2}$), and the corresponding R^2 values are shown in Table 6.3.

The two-steps diffusion process through macropores and micropores well describes MBA/CYS hydrogel (Figure 6.5). It's likely to be that when active groups on macro-pores get saturated, copper ions slowly try to diffuse into the

internal micro-pores: here the diffusion resistance increases and causes the diffusion rate to decrease. Furthermore, since copper concentration is decreased, the diffusion rate lowers because of Fick's Law and the diffusion processes reaches the final equilibrium stage. Changes in $k_{p,1}$ and $k_{p,2}$ values of more than one order of magnitude, are to be ascribed both to the resistance opposed into the macro- and micro-porous structures and to the equilibrium approach because of low gradient concentration. This behavior is consistent with data reported in Figure 6.1: probably because of the presence of -SS- groups on MBA/CYS structure, its polymer chains open to a lesser extent, thus maintaining a micro-porous structure besides the macro-porous one, and resulting in two different intraparticle diffusion rates, $k_{p,1}$ and $k_{p,2}$.

MBA/EDA behaves differently and the R^2 value corresponding to $k_{p,2}$ (Table 6.3) is very low. In this case and for the tested conditions in fact, there's no micro-porous structure opposing resistance to the diffusion of solutes: this is proved by results pertaining the swelling degree: MBA/EDA greatly expands in water and, when considering the overall kinetic rate, the potential presence of micro-pores can be neglected. It can be concluded that in this case only the diffusion through macro-pores determine the overall rate of particle diffusion and that the final equilibrium stage is achieved in this part of the hydrogel structure.

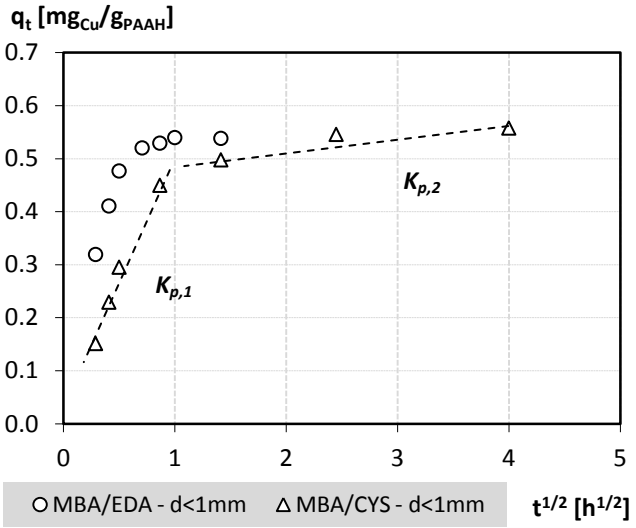

Figure 6.5. Experimental data of copper removal kinetics MBA/EDA and MBA/CYS in the form of powder, linearized with the intraparticle diffusion model. Boundary conditions: *S/L ratio* = 1/300 g/mL; $C_{Cu,0}$ = 2.0 mg_{Cu}/L; jar test device at 120 rpm.

Table 6.3. Number of experimental data used (*N*), correlation coefficients (R^2) and intraparticle diffusion rates for the first ($k_{p,1}$) and second ($k_{p,2}$) steps. Copper removal kinetics on MBA/EDA and MBA/CYS in the form of powder.

		1st STEP OF INTRAPARTICLE DIFFUSION		2nd STEP OF INTRAPARTICLE DIFFUSION	
PAAH SAMPLE AND PARTICLE SIZE	***N***	R^2	$k_{p,1}$ [s^{-1}]	R^2	$k_{p,2}$ [s^{-1}]
MBA/EDA - d<1mm	16	0,918	$2.1 \cdot 10^{-4}$	0,345	$3.2 \cdot 10^{-6}$
MBA/CYS - d<1mm	14	0,984	$1.4 \cdot 10^{-4}$	0,812	$6.1 \cdot 10^{-6}$

Results pertaining chromium removal verify the effectiveness of the multi-linear approach in the description of particle diffusion through MBA/EDA structure. Correlation coefficients and corresponding intraparticle diffusion rate constants for the overall rate of intraparticle diffusion and for the diffusion through macro-pores ($k_{p,1}$) are shown in Table 6.4 for MBA/EDA in the form of powder and grains and for different *S/L ratio* and C_0 values.

If using the intraparticle diffusion model to fit the whole set of data, the fit worsens at higher the *S/L ratio* and lower C_0, thus for low amounts of chromium provided to the mass of hydrogel. This is consistent to the fact that, especially when decreasing the amount of chromium provided, only macro-pores are involved in the diffusion processes. Estimates of the intraparticle diffusion rate constants through macro-pores ($k_{p,1}$) are shown in Table 6.4 along with

correlation coefficients that demonstrate the improvement in the description of the particle diffusion process if considering a process involving only macropores.

Table 6.4. Number of experimental data used (*N*), correlation coefficients (R^2) and corresponding particle diffusion coefficients for the intraparticle diffusion model (k_P) and for the 1st step of intraparticle diffusion ($k_{p,1}$). Results pertain to chromium removal kinetics on MBA/EDA in the form of powder and grains at varying the *S/L ratio* and C_0.

				INTRAPARTICLE DIFFUSION MODEL		1st STEP OF INTRAPARTICLE DIFFUSION	
PAAH SAMPLE AND PARTICLE SIZE	**C_0 [mg/L]**	***S/L RATIO* [g/mL]**	***N***	**R^2**	**k_P[s^{-1}]**	**R^2**	**$k_{p,1}$ [s^{-1}]**
MBA/EDA - d<1mm	0.82	1/300	12	0.680	$1.1\cdot10^{-3}$	0.916	$3.7\cdot10^{-3}$
		1/600	14	0.790	$3.5\cdot10^{-3}$	0.904	$6.0\cdot10^{-3}$
		1/1200	14	0.877	$7.2\cdot10^{-3}$	0.927	$1.1\cdot10^{-2}$
MBA/EDA - d<1mm	1.64	1/150	13	0.551	$1.8\cdot10^{-4}$	0.940	$7.5\cdot10^{-4}$
		1/300	14	0.606	$2.6\cdot10^{-3}$	0.703	$4.9\cdot10^{-3}$
		1/600	14	0.778	$6.7\cdot10^{-3}$	0.864	$1.1\cdot10^{-2}$
		1/1200	14	0.893	$1.4\cdot10^{-2}$	0.942	$2.7\cdot10^{-2}$
MBA/EDA - d<1mm	3.28	1/150	14	0.509	$4.0\cdot10^{-4}$	0.939	$1.8\cdot10^{-4}$
		1/300	14	0.672	$3.9\cdot10^{-3}$	0.791	$7.2\cdot10^{-3}$
		1/600	13	0.854	$1.7\cdot10^{-2}$	*NA*	*NA*
		1/1200	14	0.910	$2.9\cdot10^{-2}$	0.943	$3.5\cdot10^{-2}$
MBA/EDA - 1mm<d<2mm	1.64	1/300	16	0.539	$1.9\cdot10^{-3}$	0.932	$8.6\cdot10^{-3}$

**NA: Not Available*

6.4 Conclusions

An in-depth analysis on the diffusion mechanisms involved in the removal processes of copper and chromium by means of two different PAAH chemical structures has been carried on. Swelling degree and kinetic data from experiments in conditions of particle diffusion control were used to this purpose.

Swelling degree data prove that when water, and thus solute, gets into the hydrogels, MBA/CYS polymer chains extend slower and less than that of MBA/EDA, thus suggesting the presence of a stiffer structure and of pores and functional groups less accessible to water and solutes. This is to be ascribed to the presence of disulphide groups able to cross-link polymer chains to a greater extent.

Starting from experiments performed at different stirring rates specific contact modes and conditions were identified I order to perform experiments in conditions of particle diffusion control. Furthermore, it can be drawn from results of such experiments that the liquid film diffusion process have more influence on small particles (more on powders than on grains) and on MBA/EDA structure than on MBA/CYS: this is probably due to the formation of a thicker liquid film determined by the presence of free charges on MBA/EDA polymer chains that attract water molecules.

As for the particle diffusion mechanisms, by fitting data with the Homogeneous Particle Diffusion Model (HPDM) it's been verified that differently charged and sized ions have few influence on the rate of particle diffusion of the solute. Operating conditions too, such as starting concentrations and S/L ratios, have negligible influence on the overall rate of particle diffusion. However, the different chemical structure of MBA/EDA and MBA/CYS determine the pore diffusion process.

The intraparticle diffusion model analysis, suggests a two-steps approach for the description of particle diffusion into MBA/CYS structure: an "external" instantaneous uptake on macro-pores surfaces and a gradual removal step,

involving micro-pores. When active groups on macro-pores surfaces get saturated, solutes slowly try to diffuse into the internal micro-pores: this mechanism is more visible for MBA/CYS, compared to MBA/EDA, since the presence of disulphide groups impedes polymer chains to widely open, thus maintaining a micro-porous structure and resulting in two different intraparticle diffusion rates. Otherwise, the influence of the micro-porous structure on MBA/EDA diffusion processes is negligible considering the operating conditions adopted. This result proves what physically observed on the swelling degree of MBA/EDA that greatly expands in water thus making the diffusion through macro-pores the effective mechanism determining the overall rate of the process.

6.5 References

1. American Public Health Association (APHA), American Water Works Association (AWWA) & Water Environment Federation (WEF). Standard Methods for the Examination of Water and Wastewater, 22st Edition, Washington DC, 2012.
2. APAT-IRSA, 2003. Metodi analitici per le acque. APAT Manuali e Linee Guida 29/2003.
3. Caetano M., Valderrama C., Farrán A., Cortina J.L (2009). Phenol removal from aqueous solution by adsorption and ion exchange mechanisms onto polymeric resins. Journal of Colloid and Interface Science, 338(2), 402-409.
4. El-Naggar I.M., E.S. Zakaria, I.M. Ali, M. Khalil, M.F. El-Shahat (2012). Kinetic modeling analysis for the removal of cesium ions from aqueous solutions using polyaniline titanotungstate Arabian Journal of Chemistry, 5, 109–119.
5. Ferruti P., Ranucci E., Bianchi S., Falciola L., Mussini P.R., Rossi M. (2006). Novel polyamidoamine-based hydrogel with an innovative molecular architecture as a Co2+, Ni2+, and Cu2+ sorbing material: cyclovoltammetry and extended x-ray absorption fine structure studies. Journal of Polymer Science, Part A: Polym. Chem., 44(7), 2316-2327.
6. Furuya E.G., H.T. Chang, Y. Miura, H. Yokomura, S. Tajima, S. Yamashita, K. E. Noll (1996). Intraparticle mass transport mechanism in activated carbon adsorption of phenols. Journal of Environmental Engineering 122(10), 909-916.
7. Ho Y.S., J.C.Y. Ng, G. McKay (2000). Kinetics of pollutant sorption by biosorbents: review. Separation and purification methods 29(2), 189-232.
8. Kumar K. V. (2006). Linear and non-linear regression analysis for the sorption kinetics of methylene blue onto activated carbon. Journal of Hazardous Materials, 137(3), 1538-1544.
9. Rudzinski W., W. Plazinski (2006). Kinetics of solute adsorption at solid/solution interfaces: a theoretical development of the empirical pseudo-first and pseudo-second order kinetic rate equations, based on applying the statistical rate theory of interfacial transport. J. Phys. Chem. B, 110, 16514-16525.
10. Shehata F.A., M.F. Attallah, E.H. Borai, M.A. Hilal, M.M. Abo-Aly (2010). Sorption reaction mechanism of some hazardous radionuclides from mixed waste by impregnated crown ether onto polymeric resin. Applied Radiation and Isotopes 68, 239-249.
11. Sonetaka N., Fan H.J., Kobayashi S., Chang H.N., Furuya E. (2009a). Simultaneous determination of intraparticle diffusivity and liquid film mass transfer coefficient from a single-component adsorption uptake curve. Journal of Hazardous Materials, 164(2-3), 1447-1451.
12. Sonetaka N., Fan H.J., Kobayashi S., Chang H.N., Furuya E. (2009b). Characterization of adsorption uptake curves for both intraparticle diffusion and liquid film mass transfer controlling systems, 165, 232-239.
13. Valderrama C., Gamisans X., de las Heras X., Farrán A., Cortina J.L. (2008). Sorption kinetics of polycyclic aromatic hydrocarbons removal using granular acrivated carbon: intraparticle diffusion coefficients. Journal of Hazardous Materials, 157(2-3), 386-396.
14. Weber W.J. (1972). Physicochemical Processes for Water Quality Control. Wiley Interscience, New York, USA.

15. Weber W.J. and J.C. Morris (1963). Kinetics of Adsorption on Carbon from Solution, Journal of the Sanitary Engineering Division, American Society of Chemical Engineering 89, 31-59.

16. Xie Y., Jing K.J., Lu Y. (2011). Kinetics, equilibrium and thermodynamic studies of L-tryptophan adsorption using a cation exchange resin. Chemical Engineering Journal, 171(3), 1227-1233.

7 Kinetics of copper removal from aqueous solution using KDF Granular Brass Media: influence of pH and dissolved inorganic complexes

7.1 Introduction

Techniques currently used to remove heavy metals from aqueous solutions include chemical precipitation and ion exchange often coupled with oxidation (Kurniawan et al., 2006; Barakat, 2011), membrane processes mainly reverse osmosis, ultra- and nano-filtration (Qdais and Moussa, 2004), complexing or reactive media (Kocabaş-Ataklı and Yurum, 2013), adsorption onto materials of mineral, organic or biological origin (Babel and Kurniawan, 2003) and biosorption (Terry and Stone, 2002). Depending on starting concentrations, water characteristics and the removal efficiency required, all these technologies can lack selectivity or be ineffective, expensive and maintenance intensive (Li et al., 2011).

Copper concentrations in US surface waters range from 0.0005 to 1 mg/L (median value: 0.01 mg/L), and it is primarily present as complex or particulate matter. Although the current MCL (Maximum Contamination Level) of copper in potable water, as set by the USEPA, is 1.3 mg/L (2 mg/L for WHO and EU standards), copper amounts in drinking water vary widely (0.005 - 30 mg/L), due to water characteristics such as pH and hardness and to copper presence in the distribution system: corrosion of pipes, faucets and household plumbing systems is in fact one of the primary sources of copper (WHO, 2004). At the same time, as a result of increasing industry activities such as copper mining and smelting, brass manufacture, petroleum refineries and electroplating, serious copper contamination into local waterways is produced by wastewater discharge into the environment (Kocabaş-Ataklı and Yurum, 2013; Li et al., 2011).

Due to low production costs and high efficiency for the removal of a wide range of contaminants, redox processes are widely studied, especially based on metallic iron (Fe^0) namely Zero Valent Iron (ZVI) [Scott et al., 2011], and used for environmental applications, both for soil (Puls et al., 1999; Singh et al., 2012) and water remediation (Nikolaidis et al., 2003; Leupin and Hug, 2005). In fact, in redox reactions contaminants with positive Standard Electrode Potential (E_0) values are reduced by the electron donor. Therefore, the electrochemical process of corrosion of ZVI involves the reduction at the cathode of the primary components available in natural waters, O_2 and H_2O, and the oxidation of Fe^0 at the anode. The dissolution of ferrous iron (Fe^{2+}) and the local chemically reductive conditions achieved promote the removal of contaminants (Noubactep and Schöner, 2009; Crane and Scott, 2012). Because of the occurrence of multiple interactions such as reduction, (co)precipitation, complexation and sorption, ZVI particles result to be effective for the removal of organic or inorganic contaminants (Dries et al., 2005; Li and Zhang, 2007). However, drawbacks related to leakages of dissolved iron should be taken into account. Iron filing filters can leach significant (70%) quantities of iron: if the process is used in a drinking water facility, an iron removal treatment unit after the ZVI process is needed to reduce iron concentration below the legal limit: the USEPA sets the MCL for iron at 0.3 mg/L (Nikolaidis et al., 2003).

Conceptually similar to ZVI particles, KDF/granular brass media are high purity copper-zinc granules that reduce contaminants in water using oxidation/reduction reactions. The exchange of electrons allows to effectively reduce and remove contaminants such as chlorine, iron, hydrogen sulfide, heavy metals, and to control microorganisms without the use of chemicals. The interest and the advantages in using KDF media lies in the replacement of iron with zinc leakages: zinc MCL is higher (5.0 mg/L) than that of iron. Compared to iron, zinc is a highly reductant species (E_0(Fe) = -0.44 V at 25°C for ZVI particles, E_0(Zn) = -0.76 V at 25°C for KDF media) and the reaction proceeds easier from a

thermodynamic point of view (Snoeynk and Jenkins, 1980; Morel and Hering, 1993). Specifically heavy metals such as mercury, copper and nickel are removed simply by bonding to the KDF media.
Corrosion processes are involved in the study of heavy metals removal from water with redox media. Both Zn^0 and Cu^0, the constituents of brass media, can be oxidized by the main oxidants available in natural waters, O_2 and H_2O, by combining anode and cathode reactions (eq. 2 - 6) when standard potential values E^0 make it thermodynamically possible ($\Delta G^0 < 0$) as shown in eq. 1: ΔG^0 is the standard free energy, n is the number of electrons transferred from reductant to oxidant species, F is the Faraday constant (96,497 kJ/volt), subscripts "red" and "ox" refer to the reductant and oxidant species involved in the overall reaction (Butler and Cogley, 1998).

$$\Delta G^0 = -n \cdot F \cdot (E^0_{red} - E^0_{ox}) < 0 \quad (1)$$

Anode reactions:

$$Zn^{2+} + 2e^- \rightleftarrows Zn^0_{(s)} \qquad E^0 = -0.76\ V \quad (2)$$

$$Cu^{2+} + 2e^- \rightleftarrows Cu^0_{(s)} \qquad E^0 = +0.34\ V \quad (3)$$

$$Cu^{+} + e^- \rightleftarrows Cu^0_{(s)} \qquad E^0 = +0.52\ V \quad (4)$$

Cathode reactions:

$$O_{2(aq)} + 4H^+ + 4e^- \rightleftarrows 2H_2O \qquad E^0 = +1.27\ V \quad (5)$$

$$H^+ + e^- \rightleftarrows \tfrac{1}{2}H_{2(g)} \qquad E^0 = 0\ V \quad (6)$$

Zinc is oxidized to Zn^{2+} by O_2 and H^+ ions, while for copper only the reaction with O_2 is spontaneous producing monovalent or divalent ions. Products of corrosion in the form of divalent cations can react with OH^- and $CO_3^{=}$ species, if present in water, giving rise to hydroxides, carbonates and hydroxycarbonates; depending on water characteristics, they will dissolve in water or precipitate on the surface of the media thus creating a deposit. As for Cu^+, a very slightly soluble compound that usually deposits, cuprous oxide, is formed (eq. 7) in the presence of oxygen as a consequence of the combination of reactions in eq. 4 and 5 (Legrand and Leory, 1990; AWWA, 1985).

$$\tfrac{1}{2}O_2 + H_2O + 4Cu^0 \rightleftarrows 2Cu_2O + 2H^+ + 2e^- \quad (7)$$

In this paper kinetic tests of copper removal with brass media were performed in order to identify and quantify sequestration mechanisms as a function of water characteristics: the pH and the presence of dissolved inorganic constituents that could result in copper complexes, specifically hydroxides [OH^-] and carbonates [$CO_3^{=}$].

7.2 Materials and Methods

7.2.1 Reagents, stock solutions and glassware

Copper chloride ($CuCl_2$), hydrochloric acid (HCl), sodium hydroxide (NaOH) and sodium bicarbonate ($NaHCO_3$), were purchased from Fisher Scientific.
A copper stock solution of 250 mg_{Cu}/L, stabilized at 5% HNO_3, was prepared using ultrapure water and then stored at 4°C.
Before use, all glassware was washed in an acid bath (10% HCl) for 12 hours, then thoroughly rinsed with ultrapure water (≥17.8 MΩ·cm) and dried.

7.2.2 Granular brass media

KDF55 (Kinetic Degradation Fluxion Fluid Treatment, Inc, Three Rivers, MI) was used as granular brass media and pretreated: granules were rinsed with ultrapure water in two steps, stirring for 5 minutes and using a S/L (solid to liquid) ratio of 200 and 100 g_{brass}/L, respectively. Batch conditions were adopted and grains were recovered by vacuum

filtration on paper filters. Brass media was then dried and stored under N_2 atmosphere in a desiccator for at most two months.
Prior to use, the amount of brass needed for a single test was rinsed for 60 minutes adopting the same experimental conditions used in kinetic tests, reported in Table 7.1.

7.2.3 Kinetic tests

Two types of batch kinetic tests were performed on granular brass media, according to the tested parameters influencing the kinetic behavior:

- *pH tests.* Different pH values but at the same dissolved Cu^{2+} percentages in water.
- *Inorganic ligands tests.* Hydroxides [OH^-] and carbonates [$CO_3^{=}$] tested individually and at different concentrations corresponding to different dissolved Cu^{2+} percentages in water.

All kinetic tests were performed at room temperature (22±2°C) using the experimental conditions reported in Table 7.1, a brass media dose (D_{brass}) of 5 g_{brass}/L and 500 mL of test solution having an initial copper concentration $[Cu]_0$ of 12 µM. Details on parameters adopted for each set of experiments and the corresponding number of replicates are summarized in Table 7.2. For each kinetic test, samples of 5 mL of the test solution at different contact times (0, 5, 10, 15, 20, 30, 60 minutes) were extracted from the same batch. Samples were filtered through a 0.2 µm Polyethersulfone (PES) membrane, collected into Polystyrene-copolymer (PS) centrifuge tubes, acidified at 2% HNO_3 and stored at 4°C for analysis.

Table 7.1. Reference solution and experimental conditions adopted for kinetic batch experiments.

		EXPERIMENTAL CONDITIONS				
	REFERENCE SOLUTION	**Reactor type**	**Mixing mode**	**pH test value(s)**	**pH adjustment while mixing**	**N_2 blown on water surface**
pH tests	Ultrapure water	500 mL flask (in the dark)	Magnetic stirring (700 rpm)	4.5; 5.0; 5.5; 6.0 (±0.10)	Yes**	yes
[OH^-] ligand tests	Ultrapure water	500 mL flask (in the dark)	Magnetic stirring (700 rpm)	6.0; 6.5; 7.0; 7.5 (±0.10)	Yes**	yes
[$CO_3^{=}$] ligand tests	Ultrapure water at the tested $[CO_3]_{tot}$*	500 mL amber bottles	Tumbler (15 rpm)	6.0 (±0.25) 5.0 (±0.25)	No	no

** Total concentrations of carbonates in water $[CO_3]_{tot}$, were obtained by dissolving $NaHCO_3$ in ultrapure water.*
***pH was manually adjusted with acidic (HCl 0.1 M and 1 M) and basic (NaOH 0.1 M and 1 M) solutions during both procedures of rinse and test.*

Table 7.2. Adopted parameters and number of replicates (into branches) for each set of experiments.

pH tests	4 tested pH values: 4.5 (2); 5.0 (2); 5.5 (2); 6.0 (2)
[OH^-] ligand tests	4 tested [OH^-] concentrations [M]: $10^{-7.5}$ (1); $10^{-7.0}$ (1); $10^{-6.5}$ (1); $10^{-6.0}$ (2)
[$CO_3^{=}$] ligand tests	9 tested $[CO_3]_{tot}$ concentrations (total carbonates dissolved in water) [mM] at pH = 6.0: 0 (1); 0.13 (1); 0.48 (3); 1.0 (1); 1.5 (1); 3.2 (1); 4.7 (3); 14 (1); 50 (2)
	7 tested $[CO_3]_{tot}$ concentrations (total carbonates dissolved in water) [mM] at pH = 5.0: 0 (1); 0.10 (1); 0.30 (1); 0.5 (1); 0.7 (1); 1.0 (2)

7.2.4 Analytical methods

Dissolved copper and zinc concentrations were measured using inductively coupled plasma mass spectrometry (Agilent 7500cx, Agilent Technologies, Santa Clara, CA) and standard method 3125-B (APHA, 2005).
A pH meter was used to monitor pH (Accumet AB15).

7.2.5 Data analysis

Copper removal by brass media can be described as a first order reaction with respect to dissolved copper molar concentration *[Cu]*, and the brass dose, C_{brass}: since C_{brass} is constant for a single experiment, it can be included in the whole kinetic constant of copper removal, k_{Cu} (eq. 8). It's been proved that the zinc release kinetic is first order with respect to brass dose: as C_{brass} is constant for a single experiment, zinc release can be described with eq. 9 (Chuan et al., 20XX).

$$\frac{d[Cu]}{dt} = -k'_{Cu} \cdot [Cu] \cdot C_{brass} = -k_{Cu} \cdot [Cu] \quad (8)$$

$$\frac{d[Zn]}{dt} = k'_{Zn} \cdot C_{brass} = k_{Zn} \quad (9)$$

In the following, copper removal and zinc release rates, k_{Cu} and k_{Zn} respectively, were obtained from linear regressions on eq. 8 and 9, setting the intercept to zero and considering data collected up to 30 minutes included. This value of contact time was selected since it guarantees both significant removal percentages and small changes in the composition of the tested samples of brass media.
Moreover, copper trends are shown as the ratio between the dissolved copper molar concentration at time *t* and the starting copper concentration, unvaried for each experiments and equal to 12 µM; since the starting concentration of zinc is almost equal to zero, zinc releases are displayed as zinc dissolved molar concentrations at time *t*.
Then, a multiple regression analysis was used on SPSS (Statistical Package for Social Science) software to correlate the kinetic rates of copper removal and zinc release to those parameters defining the composition of water. In order to select the best set of predictors, a stepwise method was used to identify the smallest possible set of predictor variables able to effectively describe experimental data. The procedure stops when no more variables met the entry or removal criteria or when the current model is the same as the previous (Afifi and Clark, 1996).

7.3 Results and Discussion

A definite amount of copper has been dosed into water as Cu^{2+} in order to study its removal through the redox reaction resulted by the combination of eq. 2 at the anode and eq. 3 at the cathode. This reaction contributes to the corrosion of zinc, therefore in the following, k_{Zn} includes the contributions of all the active mechanisms for zinc release, while k_{Cu} is the algebraic sum of copper removal from water and copper release from brass.

7.3.1 Effect of pH

Figure 7.1 reports the reduction of copper and increase of zinc as a function of time. It is possible to observe that copper removal efficiency increases with a pH increase, contrarily to zinc release that is higher for lower pH, as highlighted in Figure 7.2 where trends for copper and zinc kinetic rates are shown: points and error bars stand for averages and standard deviations calculated on replicates.
Given the experimental conditions, dissolved oxygen concentrations are negligible and unvaried, and copper in water is almost totally dissolved as a divalent ion Cu^{2+}, directly available for the redox reaction with Zn^0 on brass surface. The concentration of H^+ ions is the only varying parameter of the system, hence pH has an influence in the processes of copper uptake and zinc release from the brass media. Two redox reactions, eq. 10 and 11, are spontaneous and thermodynamically favorite, and involve Zn^0, Cu^{2+} and H^+. Molar concentrations of H^+ (ranging from 1 to 32 µM) and Cu^{2+} (12 µM) are of the same order of magnitude, and so both ions compete in the reaction with Zn^0. Zinc release at low pH values it's supposed to be fast, because of higher H^+ concentrations influencing this process as shown in eq. 11. This can in turn affect copper removal kinetics: the amount of Zn^0 available on brass surface for the reaction with Cu^{2+} (eq. 10) decreases quickly at low pH values, thus reducing k_{Cu} values.

$$Cu^{2+}_{(aq)} + Zn^0_{(s)} \rightleftarrows Cu^0_{(s)} + Zn^{2+}_{(aq)} \qquad \Delta G = -n \cdot F \cdot (1.10V) < 0 \quad (10)$$

$$2H^+_{(aq)} + Zn^0_{(s)} \rightleftarrows H_{2\,(g)} + Zn^{2+}_{(aq)} \qquad \Delta G = -n \cdot F \cdot (0.76V) < 0 \quad (11)$$

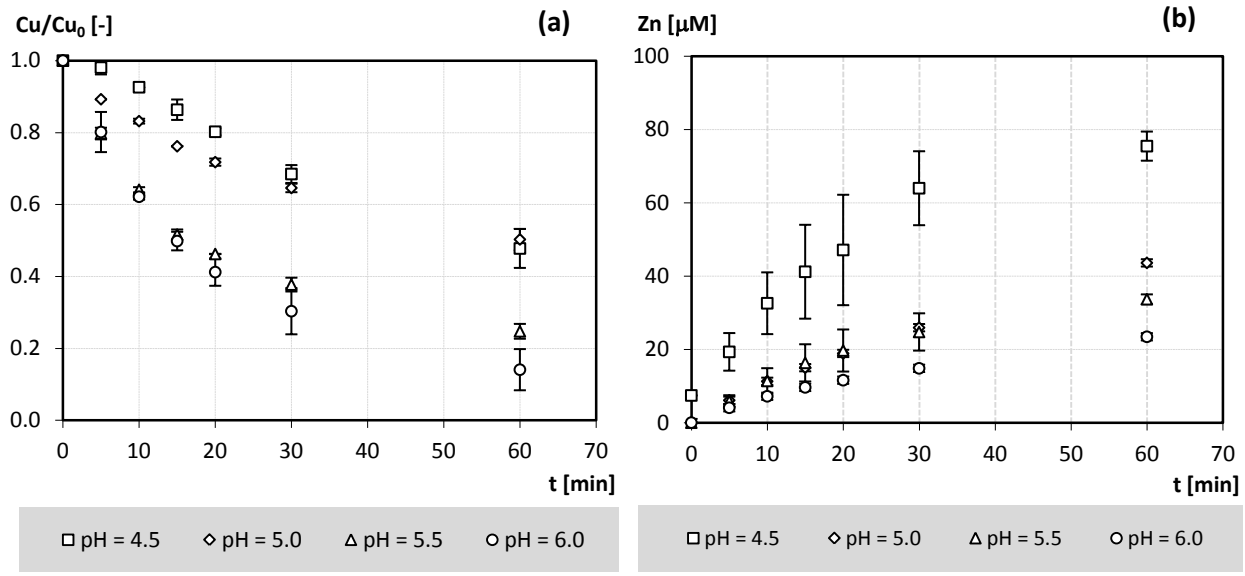

Figure 7.1. Reduction of dissolved copper (a) and increase of dissolved zinc (b) concentrations as a function of time for tests at different pH values but at the same percentage of copper dissolved as Cu^{2+} (~ 100%).

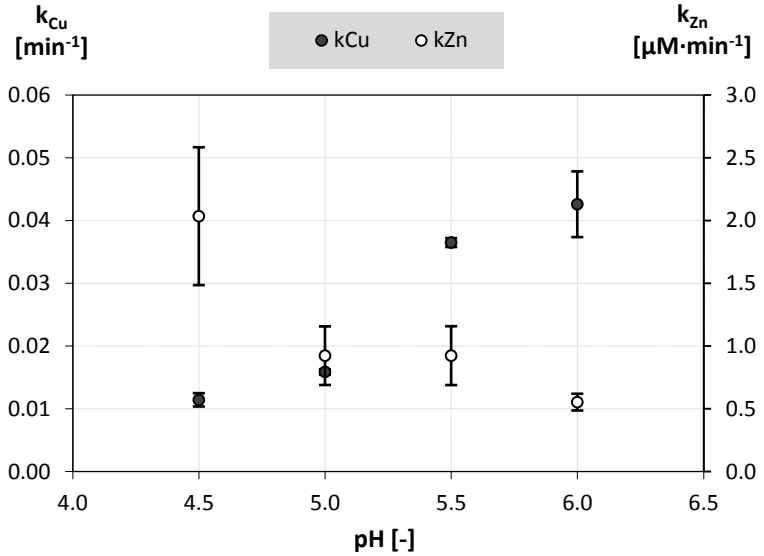

Figure 7.2. Averages and standard deviations (error bars) of k_{Cu} and k_{Zn} vs. pH. Copper is almost totally dissolved as Cu^{2+} for all pH values. Boundary conditions: $[Cu]_0$ = 12 µM; D_{brass} = 5 g/L; magnetic stirrer at 700 rpm.

7.3.2 Effect of inorganic complexes

7.3.2.1 [OH^-] complexes

Four values of pH were tested, corresponding to different percentages of copper dissolved in water as hydroxides complexes, in the following *%[Cu-OH]*, as explained in Supplementary Material. Given the adopted experimental conditions, since no other complexes in significant percentages are formed, the complement to 100 of the *%[Cu-OH]* is the percentage of dissolved copper as divalent ions (%Cu^{2+}). Figure 7.3 reports the reduction of copper and increase of zinc as a function of time. As already observed for Figure 7.1, the release of zinc decreases increasing the pH, even if in this case copper removal decreases too.

Figure 7.4 shows that both k_{Cu} and k_{Zn} values increase when high concentrations of H^+ and Cu^{2+} are dissolved in water. Error bars are drawn using the standard deviation value calculated on replicates at the pH value of 6.0. The trend of k_{Zn} is consistent with what explained as for the effect of pH on zinc release: from a quantitative point of view, compared to the results reported in Figure 7.2, smaller variations of k_{Zn} values are observed in the pH range of 6.0 - 7.5. This could be ascribed to the decreasing amounts of Cu^{2+} and, especially, H^+ (because of the pH Log scale) directly

available in water for the redox reactions with Zn^0. As a consequence, because of low H^+ concentrations, the reaction in eq. 10 is supposed to be the main process acting for the oxidation of Zn^0 to Zn^{2+} over pH 6. This explains also the trend of k_{Cu} since, for high pH values, less free Cu^{2+} is available to be directly reduced and removed from water by brass granules. Also, at pH values higher than 7.0, precipitation of copper and zinc hydroxides can occur, thus creating a deposit on brass media which prevents Cu^{2+} from reacting with Zn^0.

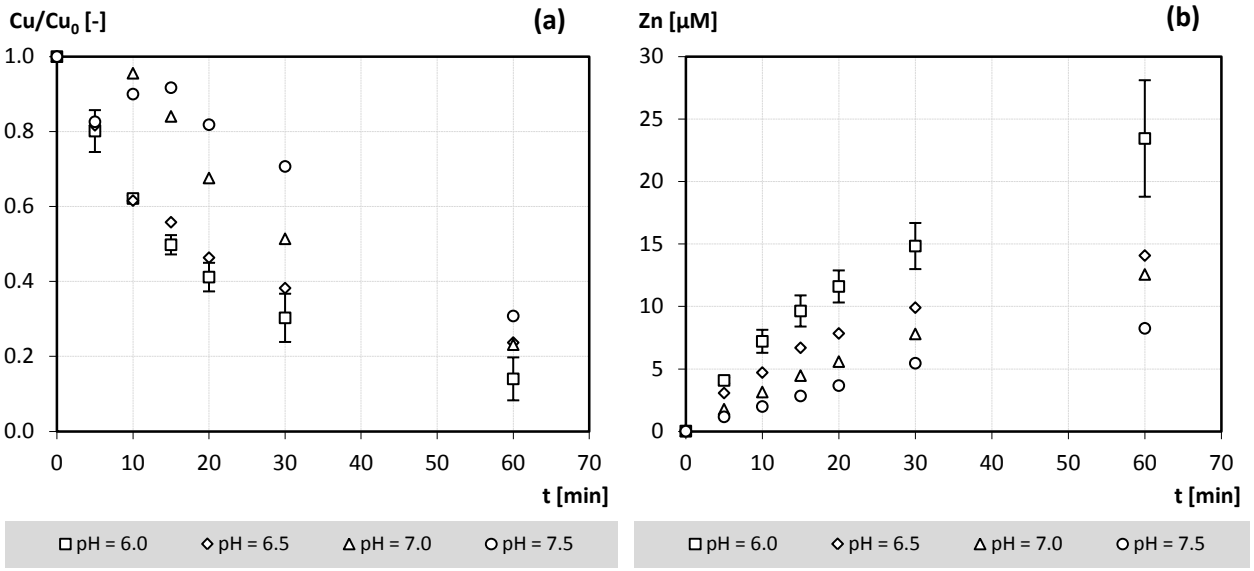

Figure 7.3. Reduction of dissolved copper (a) and increase of dissolved zinc (b) concentrations as a function of time for tests at different pH values and corresponding different percentages of copper dissolved as Cu^{2+}.

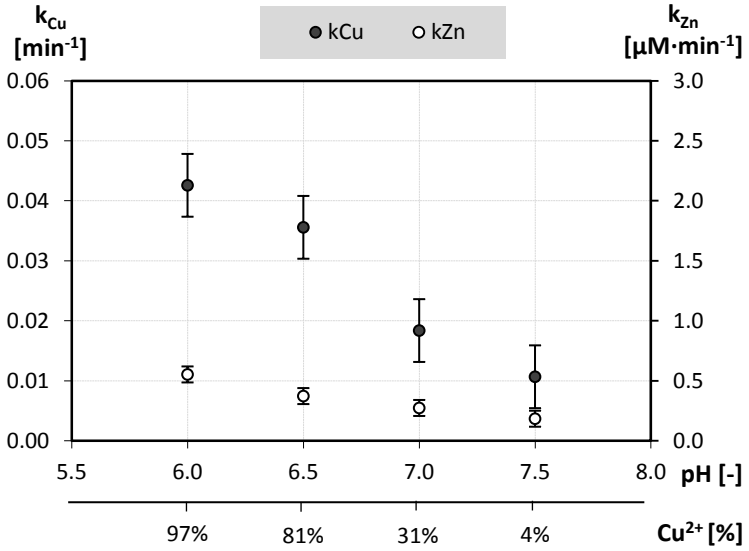

Figure 7.4. Averages and standard deviations (error bars) of k_{Cu} and k_{Zn} vs. pH and the corresponding percentages of dissolved Cu^{2+}. Boundary conditions: $[Cu]_0$ = 12 µM; D_{brass} = 5 g/L; magnetic stirrer at 700 rpm.

7.3.2.2 $[CO_3^{=}]$ complexes

Nine percentages of dissolved copper-carbonate complexes, in the following *%[Cu-$CO_3^{=}$]* (see Supplementary Material), were tested at the fixed pH value of 6.0, by dosing different amounts of $NaHCO_3$ in water. No other complexes in significant percentages are dissolved, and the one hundred's complement of *%[Cu-$CO_3^{=}$]* results to be the percentage of dissolved copper in the form of divalent ion (%Cu^{2+}). In order to minimize air-water exchanges that could modify the total carbonate concentration during the tests, different experimental conditions were adopted (Table 7.1): results of a test at the pH of 6.0 and in absence of copper complexes allow to define the rate of the tumbler (15 rpm) that recreates the turbulence provided by the magnetic stirrer at 700 rpm resulting in comparable

kinetic constants (tumbler: k_{Cu} = 0.046 min^{-1} and K_{Zn} = 0.462 µM·min^{-1}; magnetic stirrer: k_{Cu} = 0.043 min^{-1} and K_{Zn} = 0.554 µM·min^{-1}).

Figure 7.5 shows copper and zinc concentrations as a function of time. Average values of k_{Cu} and K_{Zn}, are shown in Figure 7.7(a) as a function of the percentage of Cu^{2+}. Error bars are drawn using standard deviations: the value calculated at 25% Cu^{2+} is extended to results at 10%, 33% and 50%; the value at 75% Cu^{2+} to results at 60% 90% and 100%.

The presence of dissolved carbonate complexes in water results in different k_{Cu} and K_{Zn} trends, compared to data on hydroxides complexes. If decreasing %Cu^{2+}, k_{Cu} remains constant with a no definite trend, while K_{Zn} clearly increases, contrarily to what observed for Cu-OH complexes. Also, since the pH is the same for all tests, neither equation 9 nor 10 fully explain the mechanisms of interactions between the solution and the brass media.

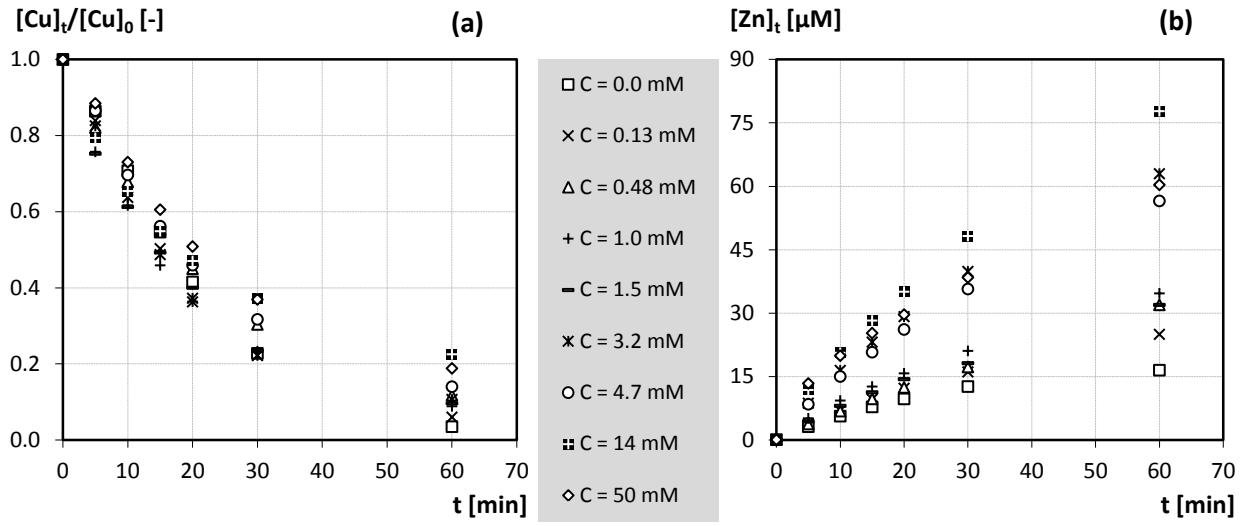

Figure 7.5. Reduction of dissolved copper (a) and increase of dissolved zinc (b) concentrations as a function of time for tests at different $NaHCO_3$ concentrations (*C*) and at the fixed pH value of 6.0.

A set of experiment at the pH of 5.0 were designed in order to maintain in water low percentages of Cu-CO_3 complexes (%Cu^{2+} ranging from 93% to 100%), while changing the amount of $NaHCO_3$ used from 0 to 1.0 mM: results are shown in Figure 7.6, where dissolved copper and zinc concentrations are reported as a function of time. By plotting k_{Cu} and k_{Zn} as a function of the concentrations of $NaHCO_3$ and by comparing results at the pH values of 5.0 and 6.0 as shown in Figure 7.7(b), kinetic constants and their trends are quantitatively similar: this is in line with what stated about the scarce significance of H^+ and Cu^{2+} in explaining the mechanisms involved.

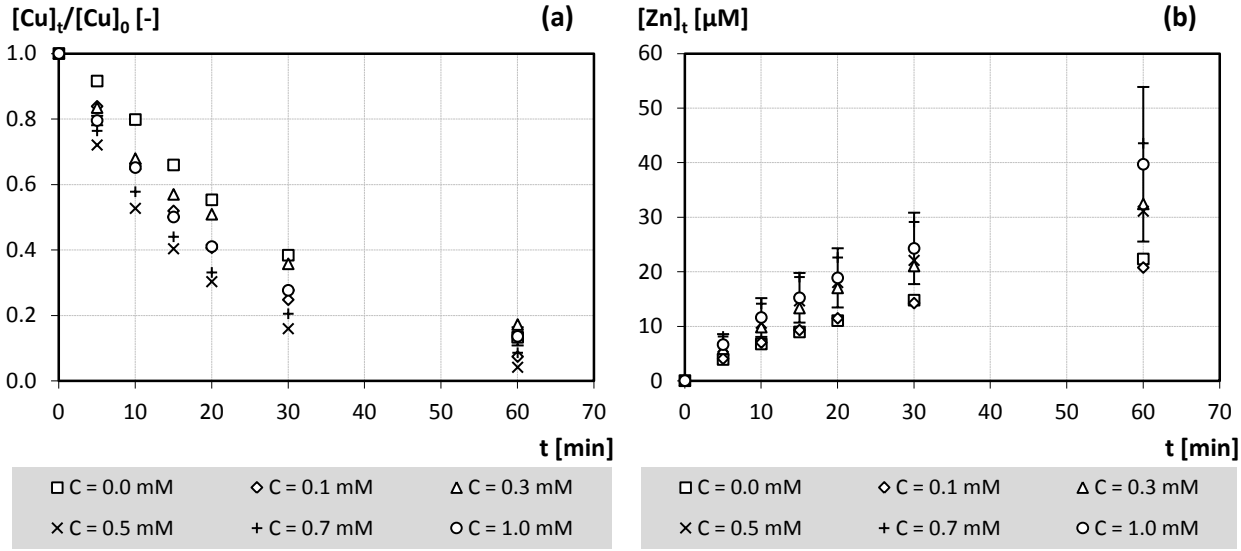

Figure 7.6. Reduction of dissolved copper (a) and increase of dissolved zinc (b) concentrations as a function of time for tests at different $NaHCO_3$ concentrations (C) and at the fixed pH value of 5.0.

The different concentrations of $NaHCO_3$ dissolved in water are supposed to play a key role for both copper removal and zinc release. Sodium bicarbonate dissolves into water producing the three carbonate forms (H_2CO_3, HCO_3^-, $CO_3^{=}$) and monovalent sodium (Na^+). Since no redox reactions between Na^+ and the brass media are thermodynamically spontaneous, the species of the carbonic acid are supposed to be of great influence. At low $\%Cu^{2+}$ the presence of carbonate species is high, and concentrations of both H_2CO_3 and HCO_3^- cannot be neglected, ranging from $3.5 \cdot 10^{-2}$ M to $1 \cdot 10^{-6}$ M and from $1.5 \cdot 10^{-2}$ M to $4 \cdot 10^{-6}$ M respectively. The presence of carbon dioxide in aqueous solutions appreciably increases the corrosion rate of brass: on the one hand, the reduction of carbonic acid ($H_2CO_3 \rightleftarrows H^+ + HCO_3^-$) serves as an additional source of H^+ ions which can be subsequently reduced by Zn^0, according to eq. 10; on the other hand, the corrosion products are soluble in water and may not have an opportunity, therefore, to create a deposit and stifle the corrosive action [Uhlig, 1948].
As for copper removal rate, a behavior similar to what observed in Figure 7.1 would be expected, with small values of k_{Cu} where there's less Zn^0 and Cu^{2+} available (corresponding to high dissolved carbonate concentrations); however, in this case, the rate of copper removal is weakly affected by the presence of dissolved carbonate complexes in water.

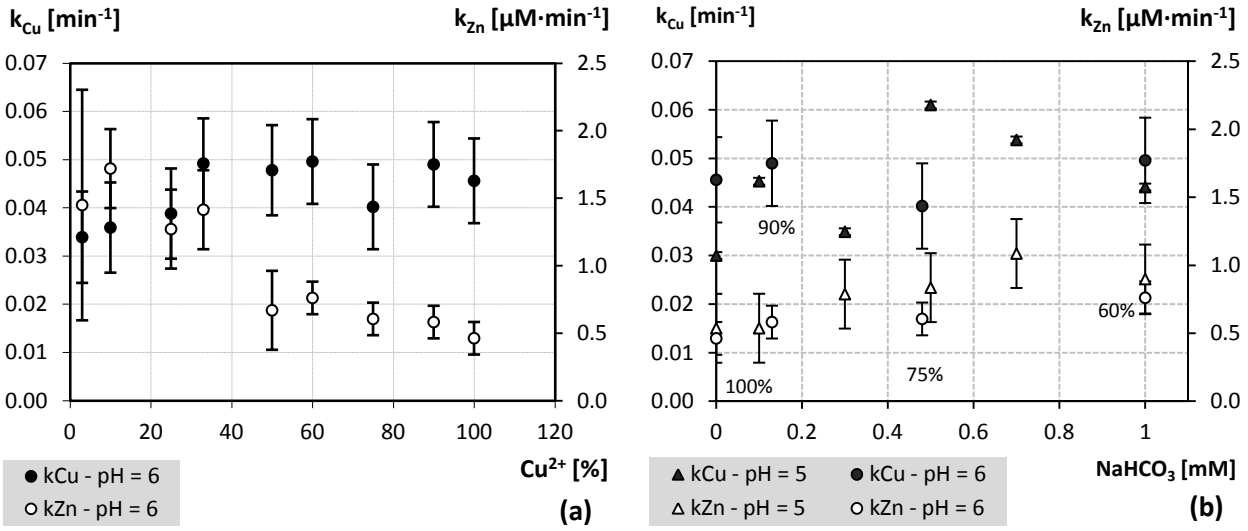

Figure 7.7. Averages and standard deviations (error bars) of k_{Cu} and k_{Zn} at pH 5.0 and 6.0 vs. (a) percentages of dissolved Cu^{2+}, (b) $NaHCO_3$ concentrations and pH values where labels on data at pH 6 are $\%Cu^{2+}$. Boundary conditions: $[Cu]_0$ = 12 µM; D_{brass} = 5 g/L; tumbler at 15 rpm.

7.3.3 Statistical Analysis on SPSS

The dataset used in the stepwise multiple regression consists of 14 variables describing conditions and results of the 32 kinetic tests performed on brass media. The list of variables includes: the two kinetic rates of copper removal (k_{Cu}, min^{-1}) and zinc release (k_{Zn}, $\mu M \cdot min^{-1}$); the measured copper concentration at the beginning of the experiments ($[Cu_0]$, µM) and the sodium bicarbonate dosed in water ($[NaHCO_3]$, µM); the pH of water expressed in terms of molar concentration ($[H^+]$, µM), the resulting amounts of carbonate species ($[H_2CO_3]$, $[HCO_3^-]$, $[CO_3^{=}]$, µM), the concentration of the corresponding species of copper dissolved in water ($[Cu^{2+}]$, $[Cu\text{-}OH]$, $[Cu\text{-}Cl]$, $[Cu\text{-}CO_3]$, µM), the amounts of sodium and chloride due to the use of acidic and basic solutions for the adjustment of pH ($[Cl^-]$, $[Na^+]$, µM). Two analysis were performed, selecting k_{Zn} and k_{Cu} as dependent variables, respectively.
In the first case, where zinc release kinetic rate is the dependent (or criterion) variable and k_{Cu}, along with all the others, are possible predictors of the model, the stepwise analysis stopped after 3 steps and selected $[H^+]$, $[Cu\text{-}CO_3]$ and $[Cu\text{-}Cl]$ as the strongest predictors, resulting in the model described by eq. 12.

$$k_{Zn} = a \cdot [H^+] + b \cdot [Cu - CO_3] + c \cdot [Cu - Cl] + q \qquad (12)$$

The regression on the three selected variables explains the 74.5% of the variance of k_{Zn} (R^2 = 0.745; *Adjusted* R^2 = 0.718; *Std. Error of the Estimate* = 0.278 $\mu M \cdot min^{-1}$). Table 7.3 reports the estimated values of the regression coefficients (B) and their standard errors. The standardized β coefficients give a measure of the contribution of each variable to the model and their sign, positive or negative, refers to direct or inverse proportionality: $[Cu\text{-}CO_3]$ is the

first strongest predictor followed by $[H^+]$ and these results are consistent with the explanations based on chemistry knowledge. Moreover the concentration of copper complexes with chlorides, which effect is not experimentally investigated in this work, it's supposed to be of influence in determining k_{Zn}. *Tolerance* values are closer to one, so the independent variables do not depend linearly on each other.

In the second case, considering k_{Cu} as the criterion variable, the stepwise analysis stopped after 5 steps outlining the following predictors: *[Cu-Cl]*, *[Cu-OH]*, $[H^+]$, $[NaHCO_3]$ and $[CO_3^=]$. However, as expected, *Tolerance* values were close to zero for $[CO_3^=]$ and $[NaHCO_3]$, confirming that these two variables are strongly correlated and one of them had to be removed. The model that includes 4 predictors (eq. 13) explains only the 60.4% of the variance of k_{Cu} (R^2 = 0.604; *Adjusted* R^2 = 0.546; *Std. Error of the Estimate* = 0.009 min^{-1}), but gains reliability in the description of k_{Cu}. Table 7.4 reports the estimated values of the regression coefficients (*B*) and their standard errors. All predictors included in this model have comparable standardized coefficients, slightly higher for *[Cu-OH]*.

$$k_{Cu} = d \cdot [Cu\text{-}Cl] + e \cdot [Cu - OH] + f \cdot [H^+] + g \cdot [CO_3^=] + z \qquad (13)$$

Table 7.3. Zinc release model from stepwise multiple regression. Regression coefficients and collinearity check.

Predictors	Unstandardized coefficients		Standardized coefficients	t	Sig(p)	Collinearity statistics
	B	Std. Error	β	Zero-order	Partial	Tolerance
constant	0.124	0.112	-	1.101	0.280	-
$[H^+]$	0.041	0.007	0.619	5.890	0.000	0.824
$[Cu\text{-}CO_3]$	0.120	0.016	0.901	7.354	0.000	0.607
[Cu-Cl]	95.056	31.010	0.389	3.065	0.005	0.564

Table 7.4. Copper removal models from stepwise multiple regression. Regression coefficients and collinearity check.

Predictors	Unstandardized coefficients		Standardized coefficients	t	Sig(p)	Collinearity statistics
	B	Std. Error	β			Tolerance
constant	0.049	0.003	-	18.684	0.000	-
[Cu-Cl]	-2.560	0.852	-0.411	-3.006	0.006	0.786
[Cu-OH]	-0.004	0.001	-0.574	-4.552	0.000	0.923
$[H^+]$	-0.001	0.000	-0.430	-3.153	0.004	0.787
$[CO_3^=]$	-0.024	0.010	-0.311	-2.409	0.023	0.879

Comparing the two selected models, both *[Cu-Cl]* and $[H^+]$ are included as predictors but affect k_{Cu} and k_{Zn} displaying inverse and direct proportionality respectively. Therefore further experiments should be designed to define the effect of copper-chloride complexes, especially in the range 0.002-0.004 µM for which few observations are available, as observed in Figure 7.8(a), where a partial regression plot on k_{Cu} and *[Cu-Cl]* is shown. Moreover, as for *[Cu-OH]*, Figure 7.8(b) shows that two cases of study, corresponding to tests at the pH of 7.0 and 7.5, strikingly affect this correlation: more data in the range 2-8 µM of copper hydroxides are needed to assess the accuracy of the model that interprets k_{Cu}. A relationship between k_{Cu} and k_{Zn} is explained both chemically and statistically, but neither of the two models includes the kinetic rate: if considering the model on k_{Cu}, this fact is to be ascribed to the strong correlation existing between k_{Zn} and predictors already selected by the stepwise procedure to describe k_{Cu}: this prevents zinc release rate to be included as a predictor for k_{Cu}.

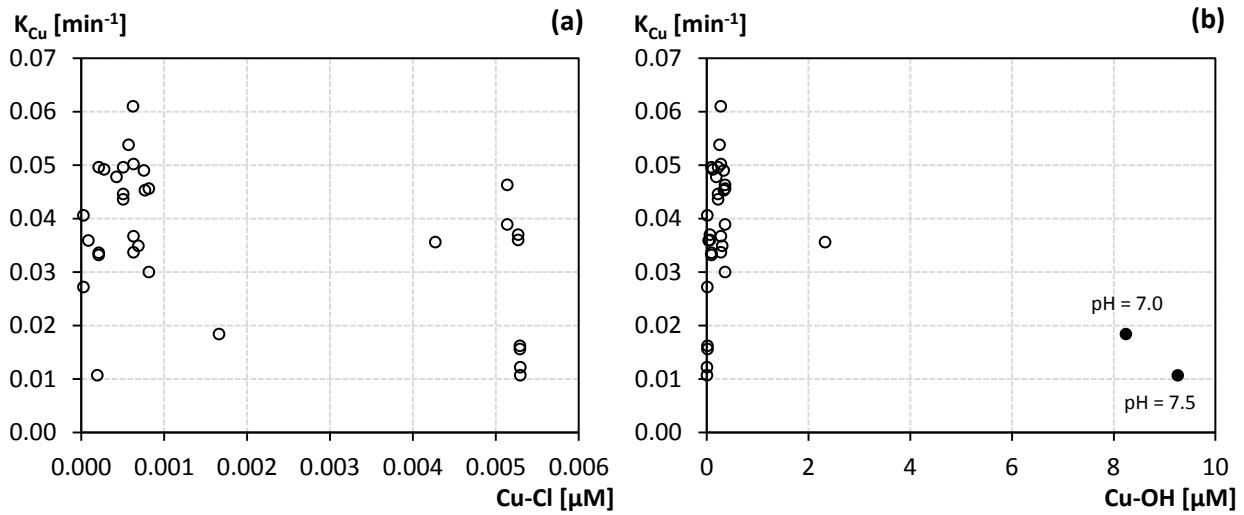

Figure 7.8. k_{Cu} partial regression plots on copper-chlorides (a) and copper-hydroxides (b) molar concentrations.

7.4 Conclusions

Chemical reactions involved in the removal process of copper by granular brass media and their relative relevance when changing the characteristic of water were identified in the present work.

From results on pH and OH^- complexes tests, it can be stated that copper is mainly removed in the form of divalent ion, by reducing its oxidation state from Cu^{2+} to Cu^0 and thus moving from the liquid to the solid phase. k_{Cu} increases from 0.01 to 0.04 min^{-1} for low and high percentages of Cu^{2+} (respectively the 4% and the 97%). Variations in the pH are supposed not to have a direct effect on the removal rate of copper; however $[H^+]$ concentration modifies the rate of zinc release, actually the passage of zinc from Zn^0 to dissolved Zn^{2+}. This process indirectly influences copper removal, because of the slowed down reaction between Zn^0 and Cu^{2+}: at a pH value of 4.5 and 100% of dissolved Cu^{2+}, k_{Cu} decreases to a value comparable to that obtained at the pH of 7.5, almost in absence of free Cu^{2+}. Furthermore, both copper removal and zinc release rates are necessary to be quantitatively defined when designing filters or other process units, as they allow the selection of contact times, volumes and flow rates that can be treated.

The presence of other dissolved inorganic ligands in water, such as carbonates, greatly affects the mechanisms of interactions between the brass media and copper or zinc: the system becomes more complex, since the presence of dissolved carbon dioxide influences brass corrosion, especially for Zn^0. Furthermore other chemical reactions and processes can gain influence in the evaluation of the overall kinetic. A more detailed study is needed to fully explain how the brass media behaves when in contact with the different species of carbonates generally found in natural water. Also, the stepwise multiple regression points out the influence of copper dissolved as chloride complexes.

7.5 References

1. Afifi, A., Clark, V., 1996. Computer-Aided Multivariate Analysis. Texts in Statistical Science, fourth ed. Chapman & Hall./CRC Press.

2. American Public Health Association (APHA), American Water Works Association (AWWA) & Water Environment Federation (WEF). Standard Methods for the Examination of Water and Wastewater, 21st Edition, Washington DC, 2005.

3. AWWA Research Foundation. Internal corrosion of water distribution systems: Cooperative research report.

AWWA, 1985

4. Babel S., T. A. Kurniawan (2003). Low-cost adsorbents for heavy metals uptake from contaminated water: a review. Journal of Hazardous Materials B97, 219-243.

5. Barakat M.A. (2011). New trends in removing heavy metals from industrial wastewater. Arabian Journal of Chemistry 4, 361-377.

6. Butler J.N., D.R. Cogley. Ionic Equilibrium: solubility and pH calculations. New York: John Wiley & Sons, 1998.

7. Chuan W., D. Holcomb, P.C. Singer, O. Coronell (20XX). Removal of Copper and Lead Ions From Aqueous Solution Using Granular Brass Media. In preparation for submission.

8. Crane R.A., T.B. Scott (2012). Nanoscale zero-valent iron: future prospects for an emerging water treatment technology. *Journal of Hazardous Materials* 211-212, 112-125.

9. Dries J., L. Bastiaens, D. Springael, S. N. Agathos, L. Diels (2005). Combined removal of chlorinated ethenes and heavy metals by zerovalent iron in batch and continuous flow column systems. *Environmental Science & Technology* 39 (21), 8460-8465.

10. Kocabaş-Ataklı Z. Ö., Y. Yurum (2013). Synthesis and characterization of anatase nanoadsorbent and applicationin removal of lead, copper and arsenic from water. Chemical Engineering Journal 225, 625-635.

11. Kurniawan T. A., G. Y.S. Chan, W. H. Lo, S. Babel (2006). Physico–chemical treatment techniques for wastewater laden with heavy metals. Chemical Engineering Journal, 118: 83-98.

12. Legrand L., P.Leory. Prevention of corrosion and scaling in water supply systems. New York: Horwood, 1990

13. Leupin O. X., S. J. Hug (2005). Oxidation and removal of arsenic (III) from aerated groundwater by filtration through sand and zero-valent iron. *Water Research* 39, 1729-1740.

14. Li X., W. Zhang (2007). Sequestration of metal cations with zerovalent iron nanoparticles. A study with high resolution X-ray Photoelectron Spectroscopy (HR-XPS). *Journal of Physical Chemistry C* 111, 6939-6946.

15. Li Y., B. X., Q. Zhao, F. Liu, P. Zhang, Q. Du, D. Wang, D. Li, Z. Wang, Y. Xia (2011). Removal of copper ions from aqueous solution by calcium alginate immobilized kaolin. Journal of Environmental Sciences, 23(3) 404-411.

16. Morel F.M.M., J.G. Hering. Principles and applications of aquatic chemistry. New York: Wiley, 1993.

17. Nikolaidis N. P., G. M. Dobbs, J. A. Lackovic (2003). Arsenic removal by zero-valent iron: field, laboratory and modeling studies. *Water Research* 37, 1417-142.

18. Noubactep C., A. Schöner (2009). Fe0-based alloys for environmental remediation: thinking outside the box. *Journal of Hazardous Materials* 165, 1210-1214.

19. Puls R. W., C. J. Paul, R. M. Powell (1999). The application of in situ permeable reactive (zero-valent iron) barrier technology for the remediation of chromate- contaminated groundwater: a field test. *Applied Geochemistry* 14, 989-1000.

20. Qdais H. A., H. Moussa (2004). Removal of heavy metals from wastewater by membrane processes: a comparative study. Desalination 164, 105-110.

21. Scott T.B., I.C. Popescu, R.A. Crane, C. Noubactep (2011). Nano-scale metallic iron for the treatment of solutions containing multiple inorganic contaminants. *Journal of Hazardous Materials* 186, 280-287.

22. Singh R., V. Misra, R. P. Singh (2012). Removal of Cr(VI) by nanoscale zero-valent iron (nZVI) from soil contaminated with tannery wastes. *Bulletin of Environmental Contamination and Toxicology* 88, 210-214.

23. Snoeynk V.L., D. Jenkins. Water chemistry. New York: Wiley, 1980.

24. Terry P.A., W. Stone (2002). Biosorption of cadmium and copper contaminated water by Scenedesmus abundans. Chemosphere 47, 249-255.

25. Uhlig H.H.. Corrosion handbook. New York: John Wiley & Sons, 1948.

26. World Health Organization (2004). Copper in Drinking-water. Background document for development of WHO Guidelines for Drinking-water Quality.

8 Influence of natural organic matter in the copper removal kinetics by granular brass media

8.1 Introduction

Granular brass media is widely used in water treatment units for the removal of heavy metals; when in water, it undergoes a chemical oxidation-reduction reaction where electrons are transferred between molecules. Copper, lead, mercury, and other heavy metals react to plate out onto the medium's surface, thus effectively being removed from waters (http://www.kdfft.com/index.html). As an example, divalent copper removal through the redox reaction on brass media results by the combination of eq. 1 at the anode and eq. 2 at the cathode: Cu^{2+} reduces to its zero valent form, Cu^0 and the zero valent zinc, Zn^0 on the surface of brass media oxidizes to Zn^{2+} and dissolves into water (AWWA, 1985).

$$Zn^{2+} + 2e^- \rightleftarrows Zn^0_{(s)} \quad (1)$$

$$Cu^{2+} + 2e^- \rightleftarrows Cu^0_{(s)} \quad (2)$$

Corrosion is essential in the study of heavy metals removal from water with redox processes, since both Zn^0 and Cu^0, the constituents of brass media, can be oxidized by the main oxidants available in natural waters, O_2 and H_2O (Crane and Scott, 2012). When waters contains natural organic matter (NOM), its effect on the corrosion of copper-based alloys might be substantial and it has been shown that NOM significantly affects the corrosion of copper in potable water (Korshin et al., 2000; Uhlig, 1948). Again, since NOM contains a large number of weak metal-binding groups, such as carboxyl and phenolic, and a smaller number of strong metal-binding nitrogen or sulfur containing sites, the extent of metal complexation in natural waters can be close to 100% for reactive metals such as copper, thus dominating the speciation of trace metals (Lu and Allen, 2002).

NOM is ubiquitous in global aquatic systems and its concentration range from 0.5 to 100 mg/L of organic carbon (Frimmel, 1998). NOM is a complex mixture of organic compounds with different size, molecular weight, polarity, acid/base properties and functional groups; it includes humic and fulvic acids as well as many types of carbohydrates, proteins, and lipids. The chemical composition of NOM may vary considerably between aquatic systems depending on the input source of organic matter (Richards et al., 2001). Humic substances, namely humic and fulvic acids, represent dominating forms of organic carbon in soils and natural waters and have a key influence in relation to water treatment and the corrosion processes (Broo et al., 1998). The characteristic features of organic solution chemistry are determined by high heterogeneity of functional groups and broad molecular weight distribution. Specifically, the surface charge of organic compounds determines their activity in organo-mineral complexes, adsorption on mineral surfaces, interactions with oppositely charged polyelectrolytes (Bratskaya et al., 2008).

This paper reports upon batch kinetic experiments on granular brass media designed to define, both qualitatively and quantitatively, how different types and amounts of organics dissolved in water influence copper removal. Five organic compounds were selected: ETDA because of its well-known complexing ability towards copper; two generic fulvic and humic acids, FA and HA respectively; two organics, a fulvic acid (SRFA) and a natural organic matter (SRNOM) coming from a specific location, the Suwannee River basin, pervading from the Okefenokee Swamp in south Georgia (USA) to the Gulf of Mexico (Averett et al. 1994). Aimed at both the design of the kinetic experiments and the interpretation of data, charge densities were previously evaluated by means of direct potentiometric titration on selected organics. Then, a stepwise linear regression on data was carried out to select the predictors that best explain copper removal rate, and to define the order of significance among those selected.

8.2 Materials and Methods

8.2.1 Reagents, stock solutions and glassware

Copper chloride ($CuCl_2$), hydrochloric acid (HCl), sodium hydroxide (NaOH), Ethylenediaminetetraacetic acid (EDTA) and Fulvic Acid (FA) were purchased from Fisher Scientific. Humic Acid (HA) from Sigma Aldrich. Suwanee River Fulvic Acid (SRFA) and Suwanee River Natural Organic Matter (SRNOM) from the International Humic Substances Society. All reagents were used without further purification.
Stock solutions of copper (250 mg_{Cu}/L), EDTA (200 mg_C/L), FA (500 mg_C/L), HA (200 mg_C/L), SRFA (200 mg_C/L) and SRNOM (200 mg_C/L) were prepared using ultrapure water and then stored at 4°C. Copper stock solution was stabilized at 5% HNO_3 and used for all the experiments; organic stock solutions were discarded after 14 days of storage.
Before use, all glassware was washed in an acid bath (10% HCl) for 12 hours, then rinsed with ultrapure water (≥17.8 MΩ·cm) and dried.

8.2.2 Granular brass media

KDF55 (Kinetic Degradation Fluxion Fluid Treatment, Inc, Three Rivers, MI) or granular brass media was tested. The pretreatment comprised two steps in which grains were rinsed with ultrapure water in batch conditions, stirring for 5 minutes and using a *S/L ratio* of 200 and 100 g_{brass}/L, respectively. Brass media was then dried, and stored under N_2 atmosphere in a desiccator for at most two months.
Prior to use, the mass of granular brass media needed for a single test (2.5 g_{brass}) was rinsed again for 60 minutes in batch conditions on a magnetic stirrer (700 rpm), in the dark. Adopting a *S/L* (solid to liquid) *ratio* of 5 g_{brass}/L, the 500 mL of rinsing solution were prepared starting from ultrapure water adjusted at pH 6.0. While stirring, N_2 was blown on the surface of water and the pH of the solution was maintained in the range 6.0±0.10, by using acidic (HCl 0.1 M and 1 M) and basic (NaOH 0.1 M and 1 M) solutions.

8.2.3 Evaluation of carbon content and charge density for organics

Carbon content (*%C*) for EDTA was calculated using its molecular formula; as for HA and FA it was evaluated analyzing DOC concentration. SRFA and SRNOM elemental analyses (Huffman Laboratories, Wheat Ridge, CO, USA) already reported the carbon content of the two organics.
Charge density (*CD*) was determined by titration of 50 mL NOM stock solution at 300 mg/L, using a 0.04 N NaOH titrant solution. The ionic strength of the stock solution was adjusted to 0.1 with 4 M KCl solution and the solution was stirred for 30 min while insufflating nitrogen gas, according to the procedure described by Yi-Pin et al. (2005). Titrations were performed in duplicate for EDTA, SRFA and SRNOM and FA, in the pH range of about 3 - 11. The charge density was calculated based on a charge balance of the solution as shown in eq. 3, where ion concentrations are in meq/L, C_{NOM} is the carbon concentration of the NOM stock solution in g_C/L and $[K^+]$ and $[Cl^-]$ were not included since they were opposite in charge and equal in concentration (Yi-Pin et al., 2005; Boyer, 2008).

$$CD\,[meq \cdot g_C^{-1}] = \frac{[H^+] + [Na^+] - [OH^-]}{C_{NOM}} \qquad (3)$$

Specifically, since SRNOM had problem to completely dissolve, the second test on SRNOM was performed adding 0.10 mL of a 1 M NaOH solution; in order to neglect these term in the calculation of charge density, the same molar quantity of HCl (0.10 mL of a 1 M HCl solution) was added to the solution. As for FA, when dissolving the reagent into water the starting pH was of about 5.5: two tests were performed, with and without the addition of 0.6 mL of a 0.1 M HCl solution in order to lower the pH. Both for SRNOM and FA, the different procedure used for replicates resulted in negligible differences in the calculated titration curves (Ritchie and Perdue, 2003; Bratskaya et al., 2008).

8.2.4 Definition of the equivalent ratio

The equivalent ratio, *ER* (eq_{Cu}/eq_C) between the equivalents of copper and carbon is used to analyze and compare data. It is obtained by eq. 4, where, at the numerator M_{Cu} (mol_{Cu}/L) is the copper molar concentration in water and OV_{Cu} (eq_{Cu}/mol) its operative valence; at the denominator, M_{LIG} (g_{OC}/L) is the concentration of the organic compound

in water, %C (g_C/g_{OC}) its carbon content, *DOC* (g_C/L) the concentration of dissolved organic carbon in water, CD_C (eq_C/g_C) and CD_{OC} (eq_C/g_{OC}) the charge densities expressed as previously explained.

$$ER = \frac{M_{Cu} \cdot OV_{Cu}}{M_{OC} \cdot \%C \cdot CD_C} = \frac{M_{Cu} \cdot OV_{Cu}}{DOC \cdot CD_C} = \frac{M_{Cu} \cdot OV_{Cu}}{M_{OC} \cdot CD_{OC}} \quad (4)$$

8.2.5 Kinetic tests

The experiments were organized as follows where the number of replicates is reported into brackets:

- EDTA was tested at 7 different equivalent ratios, *ER* (see eq. 4, par. 8.3.1) expressed in eq_{Cu}/eq_C: 0.17 (2); 0.5 (1); 1.0 (2); 2.0 (2); 4.0 (2); 6.0 (1); 10 (2)
- 3 organics were tested at the same equivalent ratio of 2 eq_{Cu}/eq_C: EDTA (2); SRFA (2); SRNOM (2)
- 4 organics were tested at the same mass of organic of 27 mg/L: FA (2); HA (2); SRFA (2); SRNOM (2)
- 4 organics were tested at the same DOC concentration of 6.3 mg_C/L: FA (2); HA (1); SRFA (1); SRNOM (2)

Batch kinetic tests were performed in the dark, at room temperature (22±2°C) and on a magnetic stirrer at 700 rpm. A 500 mL flask was used as reactor to put in contact 500 mL test solution and the brass media using a dose (D_{brass}) of 5 g_{brass}/L. A volume of 520 mL of test solution was prepared, diluting into ultrapure water a definite volume of organic and copper stock solution, and 20 mL collected at first into amber vials and store at 4°C for DOC analysis. . An initial copper concentration $[Cu]_0$ of 12 µM was selected. The pH of the test solution was initially adjusted to 6.0, by using acidic (HCl 0.1 M and 1 M) and basic (NaOH 0.1 M and 1 M) solutions. During the tests, N_2 was blown on the surface of water and the pH was kept in the range 6.0±0.10. For each kinetic test, samples of 5 mL of the test solution at different contact times (0-5-10-15-20-30-60 minutes) were collected from the same batch. Samples were filtered through a 0.2 µm Polyethersulfone (PES) membrane, collected into Polystyrene-copolymer (PS) centrifuge tubes, acidified at 2% HNO_3 and stored at 4°C for residual copper and zinc concentration analysis.

8.2.6 Analytical methods

Dissolved copper and zinc concentrations were measured using inductively coupled plasma mass spectrometry (Agilent 7500cx, Agilent Technologies, Santa Clara, CA) and standard method 3125-B (APHA, 2005).
A pH meter was used to monitor pH (Accumet AB15).
Dissolved organic concentrations were performed using a TOC analyzer (Shimadzu TOC-VCPH Total Organic Carbon Analyzer - Shimadzu Corp., Atlanta, GA).

8.2.7 Data analysis

According to Chuan et al., 20XX, copper removal by means of granular brass media can be described as a first order reaction with respect to the dissolved copper molar concentration, *[Cu]* and to the brass dose, C_{brass}: since C_{brass} is constant for a single experiment, it can be included in the whole kinetic constant of copper removal (eq. 5). As for data concerning zinc a first order kinetic with respect to the brass dose can be adopted; again, when C_{brass} is constant for a single experiment, zinc release can be described with eq. 6.

$$\frac{d[Cu]}{dt} = -k'_{Cu} \cdot [Cu] \cdot C_{brass} = -k_{Cu} \cdot [Cu] \quad (5)$$

$$\frac{d[Zn]}{dt} = k'_{Zn} \cdot C_{brass} = k_{Zn} \quad (6)$$

In the following, copper removal rates (k_{Cu}) and zinc release rates (k_{Zn}) result from linear regressions on equations 5 and 6, setting the intercept to zero and considering data collected up to 30 minutes included. The selection of this contact time guarantees both significant removal percentages and small changes in the composition of the tested samples of brass media. Copper trends are shown as the ratio between the dissolved copper molar concentration at time *t* and the starting copper concentration, unvaried for each experiments and equal to 12 µM; as for zinc, since its starting concentration is almost equal to zero, zinc releases are displayed as zinc dissolved molar concentrations at time *t*.
Using SPSS (Statistical Package for Social Science) software, a multiple regression analysis was run to correlate the kinetic rates of copper removal and zinc release to those parameters defining the composition of water. In order to select the smallest and best set of predictors, a stepwise method was used: each predictor is tested for entry into the

model based on the significance level of the score statistic and its value is assessed. The procedure stops when no more variables met the entry or removal criteria or when the current model is the same as the previous (Afifi and Clark, 1996).

8.3 Results and Discussion

8.3.1 Carbon content and charge density of the selected organics

Figure 8.1 shows potentiometric titration curves obtained on EDTA, SRFA, SRNOM, FA and HA. Charge density is expressed in milliequivalent per unit mass of carbon, by using the percentages of carbon content (*%C*) reported in Table 8.1. Positive values of the surface *CD* refers to electronegative ligands able to create complexes with Cu^{2+}: since it is difficult to predict the speciation of copper in presence of organic compounds dissolved into water, *CD* can be of help in quantitatively defining the amounts of organo-complexes created with Cu and Zn. EDTA is a strong complexing agent and its *CD* profile is above those of all the other organics. Suwannee river compounds have similar carbon content percentages but SRFA is more electronegative than SRNOM; this could be ascribed to the presence of humic acids or other substances in SRNOM which lower its charge density. Positive or negative values, close to zero for all the pH range, were recorded for FA and HA. Based on these information, a pH of 6.0 was selected for batch kinetic experiments, since at this value it is possible to test the removal of copper at positive (EDTA, SRFA, SRNOM), zero (FA) and slightly negative (HA) charge densities, corresponding to different organic compounds. Table 8.1 shows *CD* values at the pH of 6.0 for each organic compound.

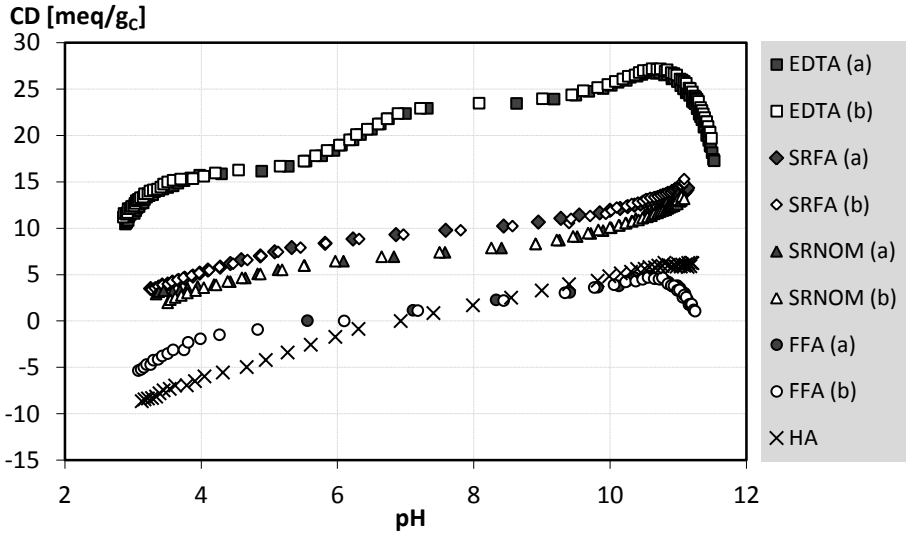

Figure 8.1. Charge density profiles as a function of pH. Duplicates for EDTA, SRFA, SRNOM and FA are shown using the same graphic symbol with different colors.

Table 8.1. Organics carbon contents (*%C*) and charge densities defined per unit mass of both carbon (CD_C) and organic compound (CD_{OC}) at the pH value of 6.0.

LIGANDS	CARBON CONTENT %C [g_C/g_{OC}]	CHARGE DENSITY AT pH = 6	
		CD_C [meq/g_C]	CD_{OC} [meq/g_{OC}]
EDTA	41.1%	18.74	7.70
SRFA	52.4%	8.55	4.49
SRNOM	52.5%	6.42	3.37
FA	23.0%	0.15	0.03
HA	29.9%	-1.63	-0.49

8.3.2 Effect of the equivalent ratio

Because of its strong complexing ability towards copper, EDTA was selected to test the influence of the *ER* in the redox processes involved in the removal of copper, and thus the influence of the speciation of copper itself. Copper dissolved in organic solutions can be found in the form of both divalent ions Cu^{2+} and copper complexes Cu-EDTA.
Figure 8.2 reports the reduction of copper and increase of zinc as a function of time for tests on EDTA.
Figure 8.3(a) shows average values for k_{Cu} resulted from tests performed on EDTA: error bars are drawn using standard deviations when replicates are available. Below the value of about 0.5-1.0 eq_{Cu}/eq_C, no copper removal is observed: it is supposed that almost all dissolved copper creates complexes with EDTA, and that Cu-EDTA complexes are barely removed by granular brass media. At the same time, since the amount of organic compounds dissolved in water is higher when low values of *ER* are tested, it is possible that the corrosion of copper from brass media prevails on its removal. Conversely, the percentage of Cu-EDTA complexes slows down in correspondence to high values of the *ER*, thus increasing the copper kinetic constant: when ER is above the value of 6.0 eq_{Cu}/eq_C, k_{Cu} profile achieves an horizontal asymptote of about 0.04 min^{-1}; this value is similar to the kinetic constant obtained from previous experiments in absence of organic compounds when copper is entirely dissolved in water as Cu^{2+} (par.7.3.1). It can be stated that above a definite value of *ER*, the system behaves as if no EDTA is dissolved in water.

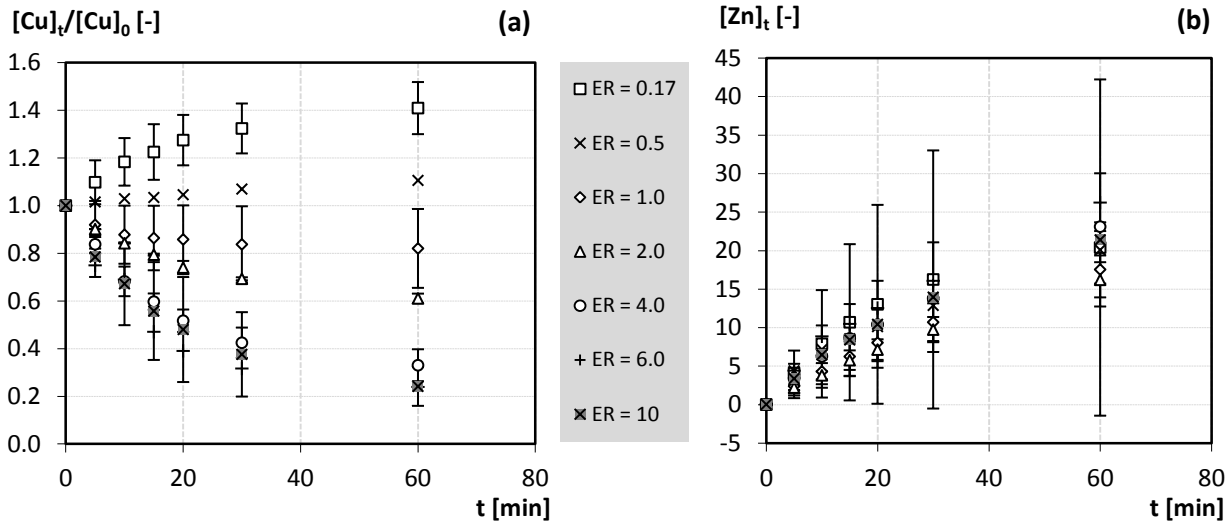

Figure 8.2. Reduction of dissolved copper (a) and increase of dissolved zinc (b) concentrations as a function of time for tests on EDTA at different equivalent ratios (*ER*) reported as eq_{Cu}/eq_C. Boundary conditions: $[Cu]_0$ = 12 µM; D_{brass} = 5 g/L; magnetic stirrer at 700 rpm.

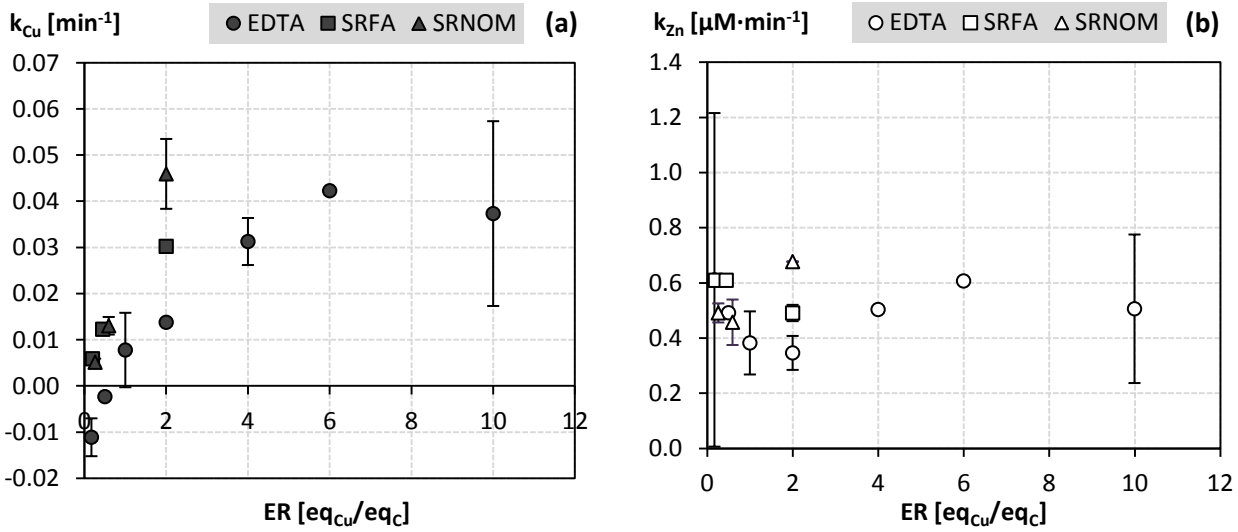

Figure 8.3. Averages and standard deviations (error bars) of k_{Cu} (a) and k_{Zn} (b) vs. equivalent ratio (*ER*) for EDTA, SRFA and SRNOM. Boundary conditions: $[Cu]_0$ = 12 µM; D_{brass} = 5 g/L; magnetic stirrer at 700 rpm.

As for zinc release, k_{Zn} are shown in Figure 8.3(b) as a function of the equivalent ratio adopted for each test. Considering results on EDTA, a minimum value is achieved at about 2.0 eq_{Cu}/eq_C. The release of zinc for ER values below this value is not related to the redox reaction between copper and zinc, as previously explained. However, k_{Zn} increases up to a value of about 0.6 $\mu M \cdot min^{-1}$, both when adopting values of *ER* greater and smaller than 2.0 eq_{Cu}/eq_C. Corrosion of Zn^0 because of the presence of high amounts of dissolved EDTA could explain high k_{Zn} at low *ER* values; this process turns to be negligible with respect to copper-zinc redox reaction when the presence of dissolved organic in water decreases. The kinetic constant for zinc release from previous experiments in absence of organic compounds when copper is entirely dissolved in water as Cu^{2+} (par.7.3.1) is comparable to the asymptotic value of about 0.6 $\mu M \cdot min^{-1}$ obtained above 6.0 eq_{Cu}/eq_C, thus confirming the interpretation given for both copper removal and zinc release.

8.3.3 Effect of the organic charge density

Figure 8.4 shows copper and zinc concentrations as a function of time for tests performed at the same equivalent ratio of 2 eq_{Cu}/eq_C on EDTA, SRFA and SRNOM.

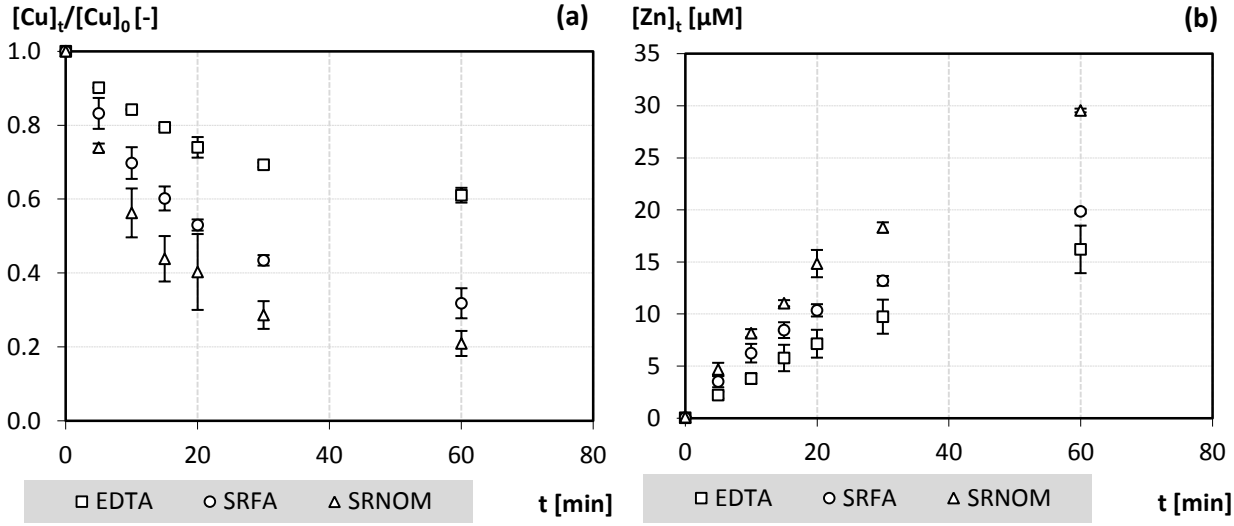

Figure 8.4. Reduction of dissolved copper (a) and increase of dissolved zinc (b) concentrations as a function of time for tests on EDTA, SRFA and SRNOM at the same equivalent ratio of 2 eq_{Cu}/eq_C. Boundary conditions: $[Cu]_0$ = 12 µM; D_{brass} = 5 g/L; magnetic stirrer at 700 rpm.

If comparing EDTA with results on SRFA and SRNOM at *ER* values equal or lower than 2.0 (Figure 8.3), k_{Cu} results in higher values: it is supposed to be that, since Suwannee River organics are less electronegative than EDTA (lower values of *CD*, see Table 8.1), higher concentrations of Cu^{2+} are dissolved in water and the kinetic constant of copper removal is positively affected.

As for zinc release kinetic constants, results agree with what previously stated: at 2.0 eq_{Cu}/eq_C SRFA and SRNOM creates less copper complexes with organics than EDTA, thus increasing k_{Cu} and consequently k_{Zn}. Besides no tests were performed on SRFA and SRNOM adopting higher *ER* values, it is supposed to be that asymptotic conditions for both copper removal and zinc release kinetic constants are achieved at lower *ER* values than EDTA: charge densities of organics are thus of great importance in this process, and the lower *CD* is, the lower *ER* values are to be used in order to achieve asymptotic k_{Cu} and k_{Zn} values.

8.3.4 Tests at the same DOC and organic concentrations

Table 8.2 shows, for each organic compound tested at the same DOC concentration and at the same organic concentration, the corresponding values of *ER* and, respectively M_{OC} and *DOC*. Figure 8.5 and Figure 8.6 report the reduction of copper and increase of zinc as a function of time for tests performed, respectively, at the same DOC concentration and at the same mass of ligand. Figure 8.7 reports k_{Cu} and k_{Zn} obtained on HA, FA, SRNOM and SRFA from tests at the same DOC concentration of 6.3 mg_C/L and at the same organic compound concentration of 27 mg_{OC}/L.

If comparing results in Figure 8.7(a) for the three compounds with positive *CD*, copper kinetic constant of FA is higher than those of SRNOM and SRFA, as expected given the high value of *ER* applied (26 eq_{Cu}/eq_C). However, especially considering the differences in k_{Cu} values obtained on both SRNOM and SRFA, when moving from 0.26 and 0.20 eq_{Cu}/eq_C to 0.59 and 0.45 eq_{Cu}/eq_C, the increase of k_{Cu} for FA is lower than what expected. This could be ascribed to the high amount of FA dissolved in water (27 mg_{OC}/L) if compared to that of Suwannee River organics (12 mg_{OC}/L): it probably covers and protects brass media grains, thus lowering both copper removal and zinc release. This is confirmed by results of k_{Cu} from tests at the same organic concentration on SRFA and SRNOM: at 27 mg_{OC}/L, the kinetic rate is lowered more than what expected if considering only the influence of *ER*.
As for the negatively charged organic compound selected, the humic acid HA, the system behaves differently: because of its electropositive character at the pH of 6.0, it is likely to be that few/no Cu-HA complexes are created in water; however, since high amounts of HA are dissolved in water, the possibility for Cu^{2+} to be effectively reduced by Zn^0 on granular brass media is reduced and both k_{Cu} and k_{Zn} are affected by the mass of HA dissolved.

Table 8.2. Equivalent ratios, DOC concentrations and organic compound concentrations calculated for each organic in experiments at DOC = 6.3 mgC/L and for test at M_{OC} = 27 mg_{OC}/L.

ORGANIC COMPOUND	SAME DOC CONCENTRATION DOC = 6.3 mgC/L		SAME ORGANIC CONCENTRATION M_{OC} = 27 mg_{OC}/L	
	M_{OC} [mg_{LIG}/L]	ER [eq_{Cu}/eq_C]	DOC [mg_C/L]	ER [eq_{Cu}/eq_C]
HA	21	-2.34	8.2	-1.79
FA	27	26	6.3	25.8
SRNOM	12	0.59	14	0.26
SRFA	12	0.45	14	0.20

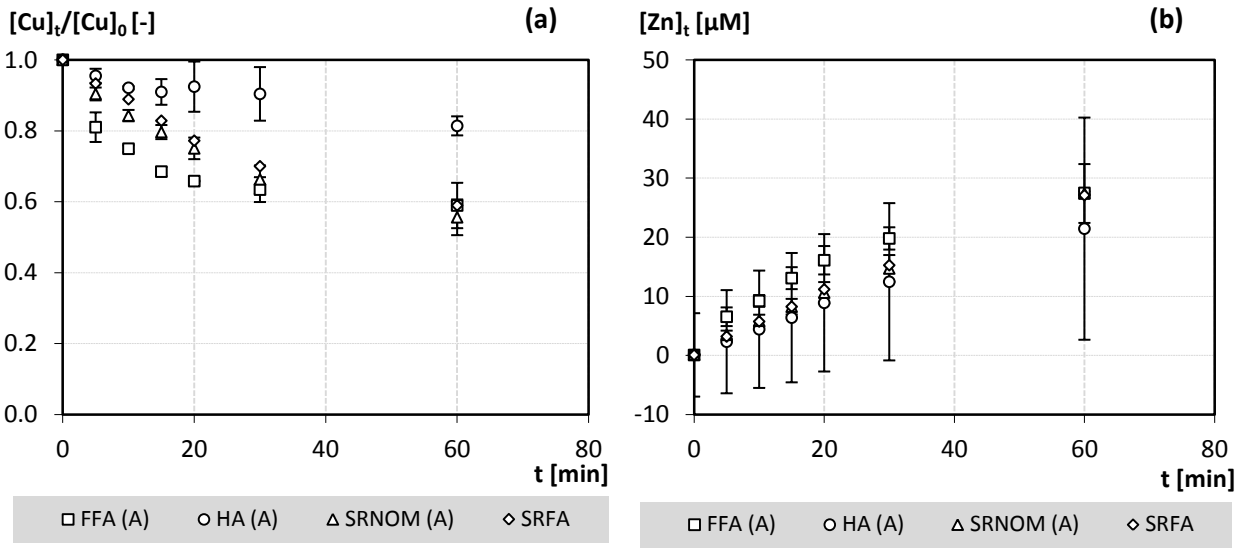

Figure 8.5. Reduction of dissolved copper (a) and increase of dissolved zinc (b) concentrations as a function of time for tests on FFA, HA, SRNOM and SRFA at the same DOC concentration of 6.3 mg_C/L. Boundary conditions: $[Cu]_0$ = 12 µM; D_{brass} = 5 g/L; magnetic stirrer at 700 rpm.

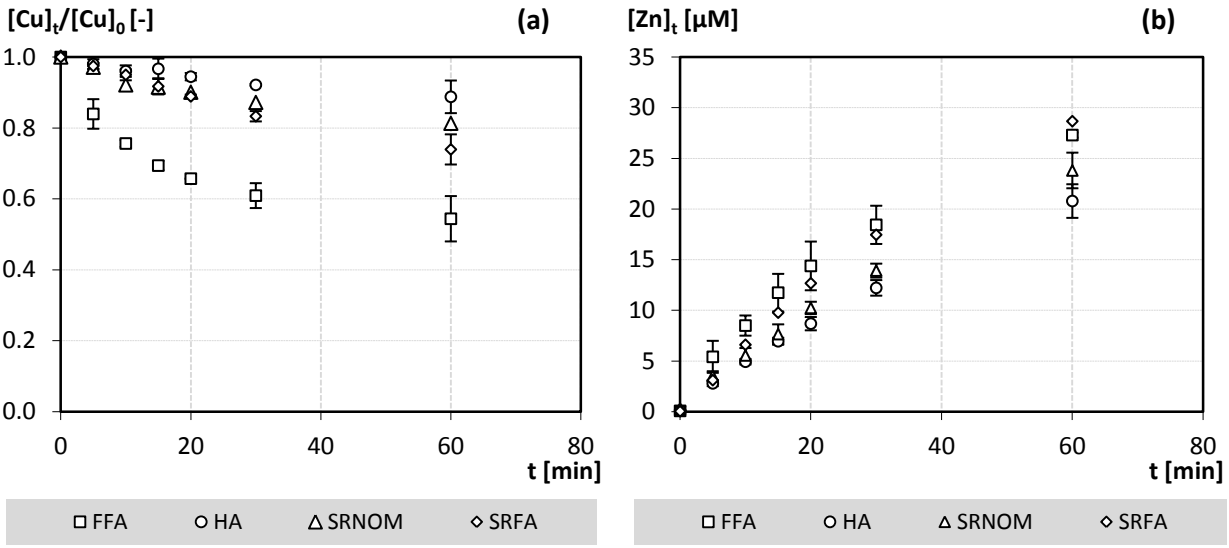

Figure 8.6. Reduction of dissolved copper (a) and increase of dissolved zinc (b) concentrations as a function of time for tests on FFA, HA, SRNOM and SRFA at the same mass of ligand of 27 mg/L. Boundary conditions: $[Cu]_0$ = 12 µM; D_{brass} = 5 g/L; magnetic stirrer at 700 rpm.

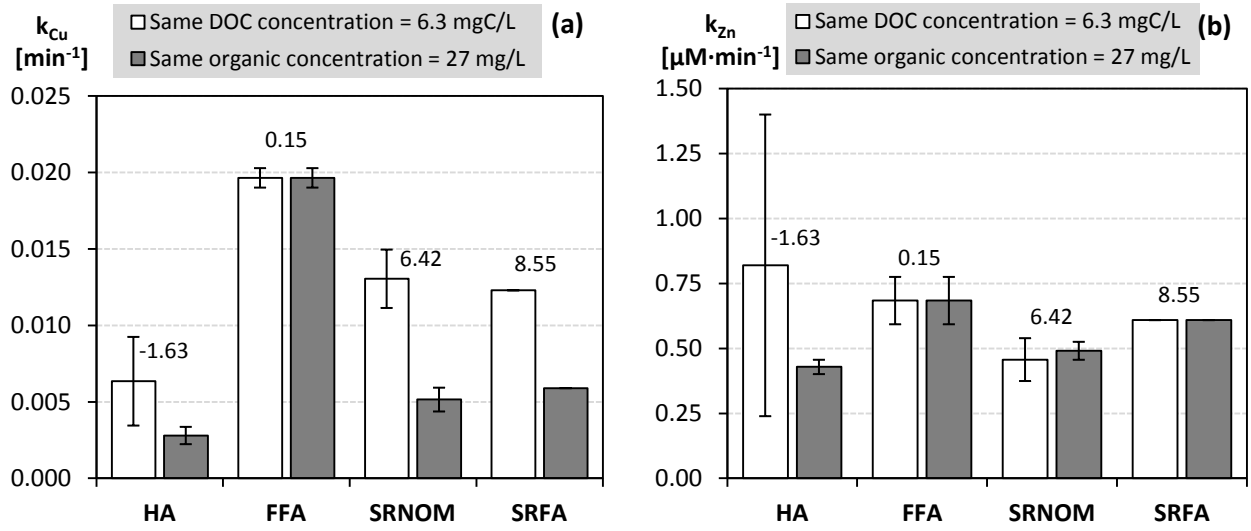

Figure 8.7. Averages and standard deviations (error bars) of k_{Cu}(a) and k_{Zn} (b) for HA, FA, SRNOM and SRFA, tested at the same DOC and M_{OC}. Labels into boxes are the charge density values (meq/g_C) at the pH of 6.0. Boundary conditions: $[Cu]_0$ = 12 µM; D_{brass} = 5 g/L; magnetic stirrer at 700 rpm.

8.3.5 Statistical Analysis on SPSS

The dataset used in the stepwise multiple regression consists of 8 variables describing conditions and results of the 28 kinetic experiments. The list of variables includes: the two kinetic rates of copper removal (k_{Cu}, min^{-1}) and zinc release (k_{Zn}, µM·min^{-1}); the measured copper concentration at the beginning of the experiments ([Cu_0], µM) and the mass of organic compound dosed in water (M_{OC}, mg_C/L); the properties of the organic compounds: charge density at the pH of 6.0 (CD_{OC}, meq/g_{OC}) and the percentage of carbon per unit mass of compound (*%C*, g_C/g_{OC}); the values of equivalent ratio (*ER*, eq_{Cu}/eq_C) and DOC (*DOC*, mg_C/L) selected for each test.

By choosing k_{Cu} as the dependent (or criterion) variable, a predictive model on the kinetic rate was obtained. Two approaches were adopted for the analysis of the dataset: in both cases, $[Cu_0]$ and *DOC* turned out to be strongly correlated to the other variables thus impeding them to be selected as predictors: for this reason they were removed from dataset.

Using all the 28 observations, the stepwise analysis stopped after 4 steps and selected M_{OC}, CD_{OC}, *ER* and %C as the strongest predictors, resulting in the model (MODEL 1) described by eq. 7. The regression on the four selected variables explains the 72% of the variance of k_{Cu} (R^2 = 0.720; *Adjusted* R^2 = 0.671; *std. error of estimate* = 0.0097 min^{-1}).

$$k_{Cu} = a \cdot M_{OC} + b \cdot CD_{OC} + c \cdot ER + d \cdot \%C + q \quad (7)$$

Since it is known that k_{Cu} and k_{Zn} are related one each other, in order to verify the possibility for k_{Zn} to be included among predictors, a linear regression on k_{Cu} and k_{Zn} (Figure 8.8) data allowed SPSS to identify and remove two outliers from the dataset. A stepwise regression was implemented on the new dataset made of 26 observations: the model achieved includes 3 predictors, k_{Zn}, M_{OC} and *ER* as shown in eq. 8 (MODEL 2): compared to MODEL 1, this model explains more variance of k_{Cu} (R^2 = 0.775; *Adjusted* R^2 = 0.745; *std. error of estimate* = 0.0085 min^{-1}).

$$k_{Cu} = n \cdot k_{Zn} + m \cdot M_{OC} + p \cdot ER + z \quad (8)$$

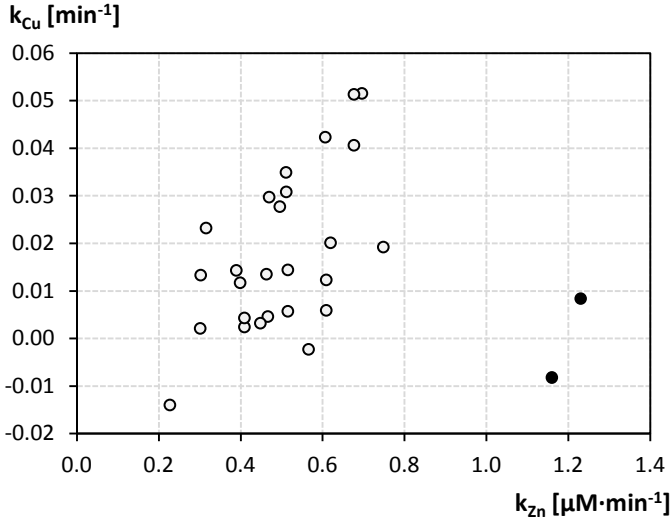

Figure 8.8. Linear regression on k_{Zn} and k_{Cu} data. Outliers are highlighted in black.

Significant variables for the two models described by eq. 7 and 8 are reported in Table 8.3. The standardized coefficients *β* measure the contribution of each variable to predict k_{Cu} and their positive or negative sign pertains to direct or indirect proportionality: both models are greatly influenced by the mass of organic compounds dissolved in water. k_{Zn} in MODEL 2 results to be a strong predictor of k_{Cu}, meaning that the corrosion of zinc greatly influences copper removal. When k_{Zn} is not included in the regression analysis, the rate of copper removal is influenced by the chemical properties of the organic compound (CD_{OC} and *%C*) and by the characteristics of water contamination due to the presence of dissolved organic compounds and copper (M_{OC} and *ER*). Since in MODEL 2, the equivalent ratio and the percentage of carbon per unit mass of organics are not included among predictors by the stepwise procedure, they are supposed to strongly affect k_{Zn}.

Table 8.3. Copper removal models from stepwise multiple regression: regression coefficients and collinearity check. MODEL 1 and MODEL 2 are obtained using 28 and 26 observations, respectively.

Model	Predictors	Unstandardized coefficients		Standardized coefficients	t	Sig(p)	Collinearity statistics
		Estimate	Std. Error	β			Tolerance
MODEL 1	constant	0.021	0.012	-	1.646	0.113	-
	M_{OC}	-0.001	0.000	-0.975	-6.025	0.000	0.465
	CD_{OC}	-0.003	0.001	-0.652	-3.995	0.001	0.457
	ER	0.001	0.000	0.495	3.947	0.001	0.774
	%C	0.062	0.024	0.344	2.540	0.018	0.665
MODEL 2	constant	0.007	0.011	-	0.684	0.501	-
	M_{OC}	-0.001	0.000	-0.889	5.235	0.000	*NA**
	k_{Zn}	0.070	0.013	0.561	-5.581	0.000	*NA*
	CD_{OC}	-0.002	0.001	-0.363	-2.199	0.039	*NA*

**NA: Not Available*

8.4 Conclusions

Five organic compounds were studied in order to define their influence in the redox reactions mechanisms involving the removal of copper by means of granular brass media and the corresponding zinc release. Three parameters determine the rate of the process: the charge density of the organic at the pH of water, the equivalent ratio between copper and carbon adopted, and the mass of organic dissolved in water being the most important.

The first parameter pertains to the intrinsic characteristics of the organic compound, specifically its activity in terms of charges to be exchanged; the pH of the tested solution identifies the value of the charge density from titration curves. Charge density influences the creation of copper complexes, actually the percentage of Cu^{2+} dissolved in water and probably the interactions between organic compounds and the brass media. An increase in the charge density value from 6.42 (SRNOM) to 18.74 (EDTA) meq/g_C, nearly doubles k_{Cu} which increases from 0.014 to 0.030 min^{-1} at the tested equivalent ratio of 2.0 eq_{Cu}/eq_C.

The equivalent ratio applied is also of importance since it determines the amount of copper-organic complexes dissolved in water, thus influencing the removal kinetic constant. Referring to tests with EDTA, an asymptotic value of k_{Cu} is achieved at high *ER* values, probably corresponding to the presence of copper almost entirely dissolved as Cu^{2+} directly available for the reaction with the brass media. It's likely to be that the asymptotic value is achieved at low or high values of *ER* depending on the charge density features of the organic compound.

Finally, the amount of organic dissolved in water is supposed to inhibit the processes of both copper removal and zinc release by covering grains and making them less accessible for the interactions with copper and the other compounds present in the aqueous solution.

8.5 References

1. Afifi, A., Clark, V., 1996. Computer-Aided Multivariate Analysis. Texts in Statistical Science, fourth ed. Chapman & Hall./CRC Press.
2. American Public Health Association (APHA), American Water Works Association (AWWA) & Water Environment Federation (WEF). Standard Methods for the Examination of Water and Wastewater, 21st Edition, Washington DC, 2005.
3. Averett, R.C., J.A. Leenheer, D.M. McKnight, K.A. Thorn (1994). Humic substances in the Suwannee River, Georgia; interactions, properties, and proposed structures. US Geological Survey - Water Supply Paper: 2373.
4. AWWA Research Foundation. Internal corrosion of water distribution systems: Cooperative research report. AWWA, 1985
5. Boyer T.R.H., P.C. Singer (2008). Stoichiometry of Removal of Natural Organic Matter by Ion Exchange. Environ. Sci. Technol. 42, 608-613.
6. Bratskaya S., A. Golikov, T. Lutsenko, O. Nesterova, V. Dudarchik (2008). Charge characteristics of humic and fulvic acids: Comparative analysis by colloid titration and potentiometric titration with continuous pK-distribution function model. Chemosphere 73, 557-563.
7. Broo A.E., B. Berghult, T. Hedberg (1997). Copper corrosion in water distribution systems – The influence of natural organic matter (NOM) on the solubility of copper corrosion products. Corrosion Science 39 (8), 1479-1489.
8. Chuan W., D. Holcomb, P.C. Singer, O. Coronell (20XX). Removal of Copper and Lead Ions From Aqueous Solution Using Granular Brass Media. In preparation for submission.
9. Crane R.A.,T.B. Scott (2012). Nanoscale zero-valent iron: future prospects for an emerging water treatment technology. Journal of Hazardous Materials 211-212, 112-125.
10. Frimmel F.H. (1998). Characterization of natural organic matter as major constituents in aquatic systems. Journal of Contaminant Hydrology 35, 201-216.

11. Korshin G.V., J.F. Ferguson, A.N. Lancaster (2000).Influence of natural organic matter on the corrosion of leaded brass in potable water Corrosion Science 42 (1), 53-66.

12. Lu Y., H.E. Allen (2002). Characterization of copper complexation with natural dissolved organic matter (DOM)-link to acidic moieties of DOM and competition by Ca and Mg. Water Research 36, 5083-5101.

13. Richards J.G., P.J. Curtis, B.K. Burnison, R.C. Playle (2001). Effects of natural organic matter source on reducing metal toxicity to rainbow trout (Oncorhynchus Mykiss) and on metal binding to their gills. Environmental Toxicology and Chemistry 20 (6), 1159-1166.

14. Ritchie J.D., E.M. Perdue (2003). Proton-binding study of standard and reference fulvic acids, humic acids, and natural organic matter. Geochimica et Cosmochimica Acta 67(1), 85-96.

15. Uhlig H.H.. Corrosion handbook. New York: John Wiley & Sons, 1948

16. Yi-Pin L., P.C. Singer, G.R. Aiken (2005). Inhibition of calcite precipitation by Natural Organic Material: kinetics, mechanism, and thermodynamics. Environ. Sci. Technol. 39, 6420-6428.

17. http://www.kdfft.com/index.html

Appendix 1

Preliminary tests for the assessment of the washing procedure for MBA/EDA and MBA/CYS samples

A washing procedure for the hydrogel mass used during experiments was adopted to remove the residues of synthesis solutions and minimize alterations of water composition during tests. Tap water filtered on Millipore equipped with 0.45 µm cellulose acetate membrane filters (Whatman) was used for this purpose. The number of steps was determined by monitoring changes in water pH, till negligible variations were observed.

Batch conditions were adopted:

- Solid/Liquid ratio, *S/L ratio* = 1/20 $g \cdot mL^{-1}$;
- contact time, t_c: 5 minutes (for each step).

At the end of each step water was separated from the solid phase by using:

- for hydrogels in the form of powders (d<1mm): a centrifuge (IEC CL 10) at the rate of 2000 rpm for 5 minutes;
- for hydrogels in the form of grains (1mm<d<2mm): gravity settlement in static conditions for 5 minutes.

Tests were performed separately on powders and grains of MBA/EDA and MBA/CYS samples. Results are shown in par. A (Table 4 and Figure 9) for hydrogels provided by the Department of Organic and Industrial Chemistry (Università degli Studi di Milano, IT) and in par. B (Table 5 and Figure 10) for hydrogels provided by Laboratory Alchemia (IT).
The Washing Volume (WV) corresponding to each step, indicates the cumulated volume of water per unit mass of hydrogel tested, used in the washing procedure. The Bed Volume (BV) is defined for each step as the volume of water used to wash a specific volume of hydrogel; since it depends upon the specific weight of the samples, two different BVs are reported as for MBA/EDA and MBA/CYS.
Based on results obtained from preliminary tests, the number of washing steps used for experiments has been averagely set in 10 for MBA/EDA samples (both powders and grains) and 5 for MBA/CYS (both powders and grains), irrespective of the supplier, corresponding to 200 and 100 mL/g_{PAAH} washing volumes, respectively.

A. MBA/EDA and MBA/CYS provided by the University of Milan

Table 4. Number of steps, corresponding washing volumes (WV) and bed volumes (BV), and pH values of water after batch contact with hydrogels (*S/L ratio* = 1/20 g·mL^{-1}; t_c: 5 minutes) for MBA/EDA and MBA/CYS in the form of powder and grain.

				pH OF WATER			
STEP NUMBER	**WV [mL/g_{PAHH}]**	**$BV_{MBA/EDA}$ [-]**	**$BV_{MBA/CYS}$ [-]**	**MBA/EDA d<1mm**	**MBA/EDA 1mm<d<2mm**	**MBA/CYS d<1mm**	**MBA/CYS 1mm<d<2mm**
0	0	0	0	8.03	7.92	7.79	7.79
1	20	12	14	3.34	2.40	6.79	7.40
2	40	25	28	5.05	2.46	6.99	7.56
3	60	37	42	3.36	2.68	7.07	7.68
4	80	50	56	5.23	2.93	7.34	7.76
5	100	62	70	5.08	3.51	7.46	7.72
6	120	75	84	5.34	4.93	7.47	7.66
7	140	87	98	6.07	5.48	7.34	7.56
8	160	100	112	6.41	5.90	7.51	7.71
9	180	112	125	6.27	6.06	7.30	7.75
10	200	125	139	6.60	6.21	7.49	7.77
11	220	137	153	6.51	6.41	*NA**	*NA*
12	240	150	167	6.81	6.54	*NA*	*NA*
13	260	162	181	6.91	6.64	*NA*	*NA*
14	280	174	195	6.51	6.81	*NA*	*NA*
15	300	187	209	6.34	6.91	*NA*	*NA*
16	320	199	223	6.42	6.94	*NA*	*NA*
17	340	212	237	6.89	7.01	*NA*	*NA*
18	360	224	251	6.53	7.08	*NA*	*NA*
19	380	237	265	6.74	7.12	*NA*	*NA*
20	400	249	279	7.02	7.18	*NA*	*NA*

**NA: Not Available*

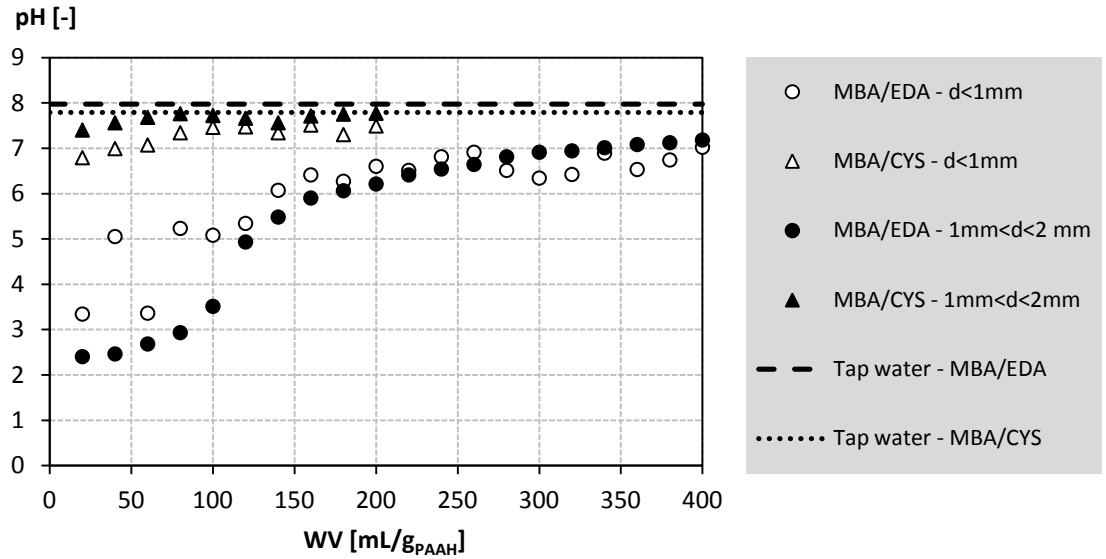

Figure 9. pH of water after batch contact with hydrogels (*S/L ratio* = 1/20 g·mL^{-1}; t_c: 5 minutes) vs. WV for MBA/EDA and MBA/CYS in the form of powders and grains. Dotted lines indicate the initial pH of tap water used for tests.

B. MBA/EDA and MBA/CYS provided by Laboratori Alchemia

Table 5. Number of steps, corresponding washing volumes (WV) and bed volumes (BV), and pH values of water after batch contact with hydrogels (*S/L ratio* = 1/20 g·mL^{-1}; t_c: 5 minutes) for MBA/EDA and MBA/CYS in the form of powder and grain.

				pH OF WATER			
STEP NUMBER	**WV [mL/g_{PAHH}]**	**$BV_{MBA/EDA}$ [-]**	**$BV_{MBA/CYS}$ [-]**	**MBA/EDA d<1mm**	**MBA/EDA 1mm<d<2mm**	**MBA/CYS d<1mm**	**MBA/CYS 1mm<d<2mm**
0	0	0	0	7.81	7.81	7.70	7.7
1	20	15	14	5.89	7.11	7.21	7.48
2	40	30	28	5.72	6.62	7.11	7.32
3	60	45	43	NA	6.87	7.19	7.39
4	80	60	57	6.43	5.82	7.10	7.42
5	100	75	71	6.49	6.63	7.32	7.58
6	120	90	85	6.53	6.72	7.34	7.62
7	140	105	99	6.52	6.89	7.38	7.51
8	160	120	113	6.58	6.98	7.29	7.49
9	180	136	128	6.63	6.99	7.33	7.44
10	200	151	142	6.64	7.02	7.34	7.48
11	220	166	156	6.71	7.04	*NA**	*NA*
12	240	181	170	6.79	*NA*	*NA*	*NA*
13	260	196	184	6.81	*NA*	*NA*	*NA*
14	280	211	199	6.83	*NA*	*NA*	*NA*
15	300	226	213	6.84	*NA*	*NA*	*NA*
16	320	241	227	6.88	*NA*	*NA*	*NA*
17	340	256	241	6.91	*NA*	*NA*	*NA*

**NA: Not Available*

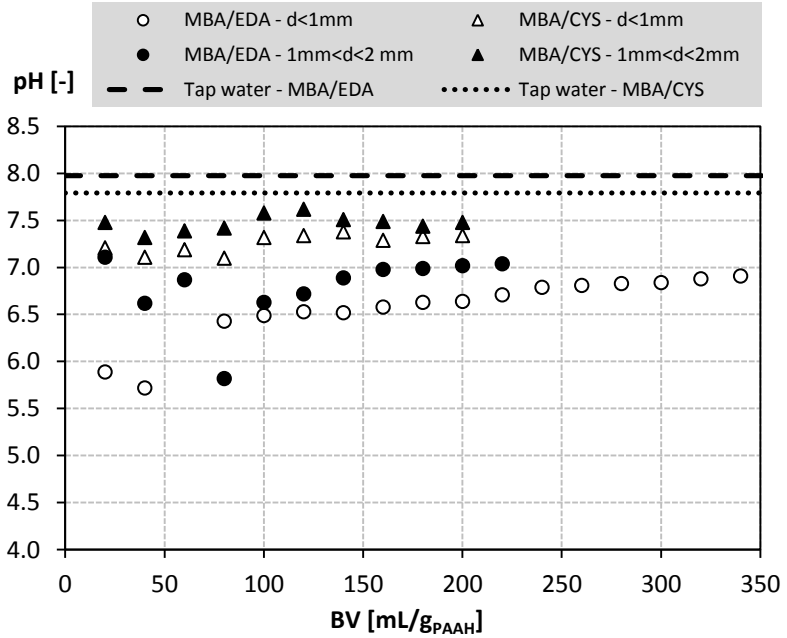

Figure 10. pH of water after batch contact with hydrogels (*S/L ratio* = 1/20 g·mL^{-1}; t_c: 5 minutes) vs. WV for MBA/EDA and MBA/CYS in the form of powders and grains. Dotted lines indicate the initial pH of tap water used for tests.

Appendix 2

Preliminary tests to assess the applicability of PAAH in water treatment units

Two main processes have been identified as possible full scale application units for PAA hydrogels: filtration on membranes and filtration in column systems. In order to define the suitability of these two processes, tests to evaluate the specific resistance to filtration (SRF) and the operational suitability of column filtration were performed on PAAH samples; results are briefly described in sections A and B of this Appendix, respectively.

A. Membrane filtration: evaluation of the Specific Resistance to Filtration (SRF)

The Specific Resistance to Filtration (SRF) was evaluated on MBA/CYS - d<1mm by using tap water on a Millipore device (filtering diameter D_F = 3.9 cm) connected to a vacuum pump operating at about -0.9 bar. Three tests, as shown in Table 6, were performed at varying the mass of hydrogel used (M_{PAAH}) and thus the thickness of the panel (h). Each test consisted in filtering for a specific number of steps (N) a definite volume of water (V_{step}): the whole volume of water filtered at the end of the test (V_{tot}) is shown in Table 6 along with all the other experimental conditions. The first step for all of the three tests was performed at a V_{step} of 300 mL in order to create the panel that was subsequently covered with a paper filter to avoid the re-suspension of PAAH particles during the experiment. The volume of filtered water (V_F) was monitored as a function of time for each step: specifically, filtration times (t_F) were measured after filtering 25 mL of water for test A and 100 mL for tests B and C.

Table 6. Solubility product constants for the selected ionic compounds.

TEST	M_{PAAH} [g]	h [cm]	N [-]	V_{step} [mL]	V_{tot} [L]
A	1	0.22	20	300	6
B	1	0.22	50	300	15
C	2	0.44	11	1000	10.3

The equation of Carman-Kozeny (1) describes the volume of filtered water (V) as a function of time (t), once defined the pressure drop across the filter (ΔP), the surface of the filter (A), the thickness of the panel (h) and the dynamic viscosity of the filtrate (μ), in this case water at 20°C ($1.002 \cdot 10^{-3}$ Pa·s). R^* and R_f are the resistance to filtration of the panel per unit of thickness and the resistance to filtration of the membrane, respectively.

$$\frac{dV}{dt} = \frac{A \cdot \Delta P}{\mu \cdot (h \cdot R^* + R_f)} \quad (1)$$

The thickness of the panel can be expressed as shown in equation 2 where v_p and p_p are the volume and the dried mass of the panel.

$$h = \frac{p_p \cdot V}{A} \cdot \frac{v_p}{p_p} \quad (2)$$

The Specific Resistance to Filtration, SRF is thus evaluated by using equation 3.

$$SRF = \frac{v_p}{p_p} \cdot R^* \quad (3)$$

By assuming ΔP as a constant and integrating equation 1 from time 0 to a generic time t, a linear equation in $t/V_t - V_t$ can be used to evaluate its slope (m) and use it in equation 4 to derive the SRF.

$$SRF = \frac{2 \cdot m \cdot A^2 \cdot \Delta P}{\mu \cdot (p_p)} \quad (4)$$

As shown in Figure 11 results are comparable since filtration times increase when increasing the volume of filtered water, thus suggesting that a compression of the panel occurs during filtration. Results from test B slightly deviate from that of test A and C, since a heterogeneous thickness of the panel originated during this test: for this reason, only results from tests A and C were used to evaluate the SRF.

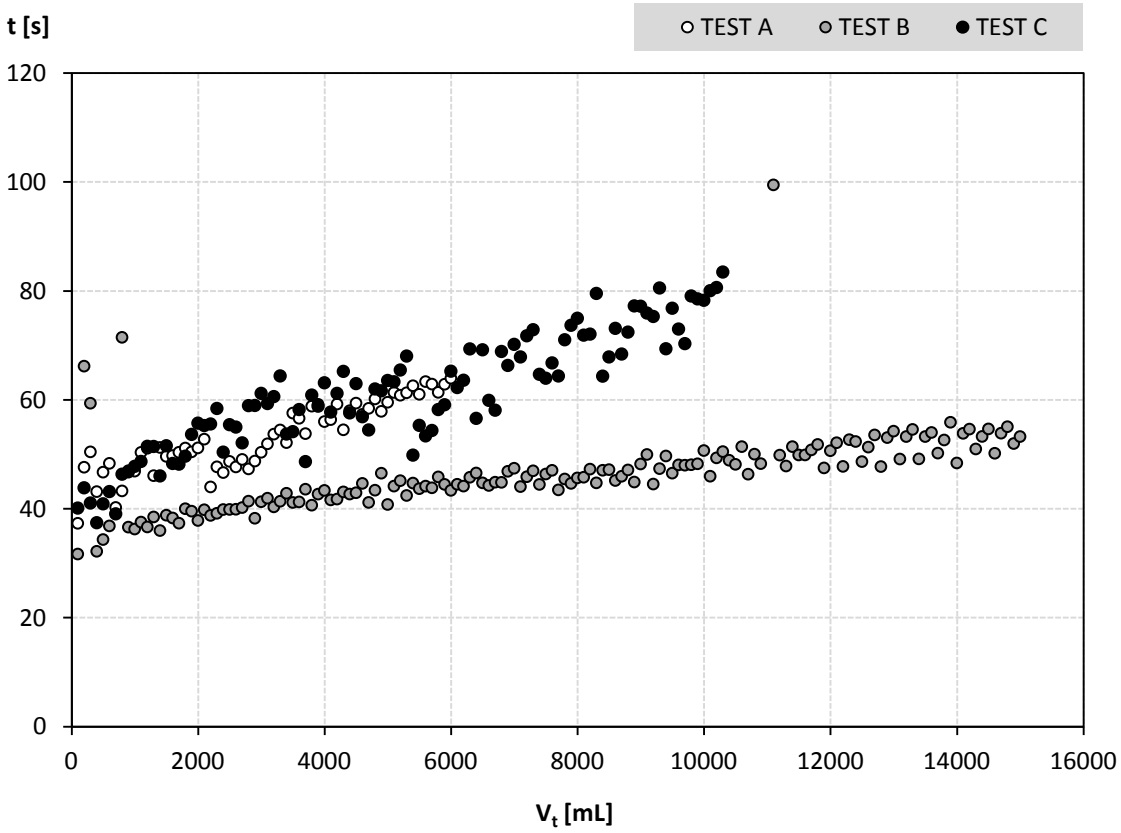

Figure 11. Filtration time t as a function of the corresponding volume of filtered water (V_t) for the three testing conditions.

By plotting t/V_t as a function of V (Figure 12) it is possible to state that, following to a first filtrate volume needed for the panel to be created and stabilized, as expected from theory the two curves assume a linear trend. This suggests the occurrence of a progressive compression of the panel, probably a slow phase since filtration proceeds, without stopping, along all the duration of both tests. A "relaxation test" on both panels was performed by interrupting the experiments and thus the steps of filtration for about one hour: two areas termed "A" and "C" are shown in Figure 12, and represent the time needed for PAAH panels of tests A and C to gain the compression degree achieved till the starting of the relaxation period. This suggests that reversible deformations occur on PAAH samples under the tested filtering conditions; this phenomenon is probably due to the flexible structure of PAAH and to the ability of hydrogels to expand their volume in water and swell again after a relaxation time.

In order to obtain the SRF values, the slope of the t/V_t - V_t curve was evaluated by using the method of least squares for linear regression on data collected after the relaxation time needed to the curve to achieve again a linear shape: Table 2 summarizes the initial and final values of volumes (V_0 and V_f) and times (t_0 and t_f) used for the linear regressions on data from tests A and C, the corresponding slopes (m) and correlation coefficients (R^2) and the two values of SRF. The specific resistances to filtration of MBA/CYS in both tested conditions are comparable and greatly

lower than what reported in literature[1] for other kind of filtering media: mixed sludge (10^{13}-10^{14} m/kg), conditioned mixed sludge (~10^{11} m/kg), primary sludge from paper factories (10^{8}-10^{9} m/kg), petrochemical sludge (~10^{16} m/kg), calcium carbonate suspensions (~10^{10} m/kg). To a mechanical point of view, PAAHs could be used in membrane filtering unit processes.

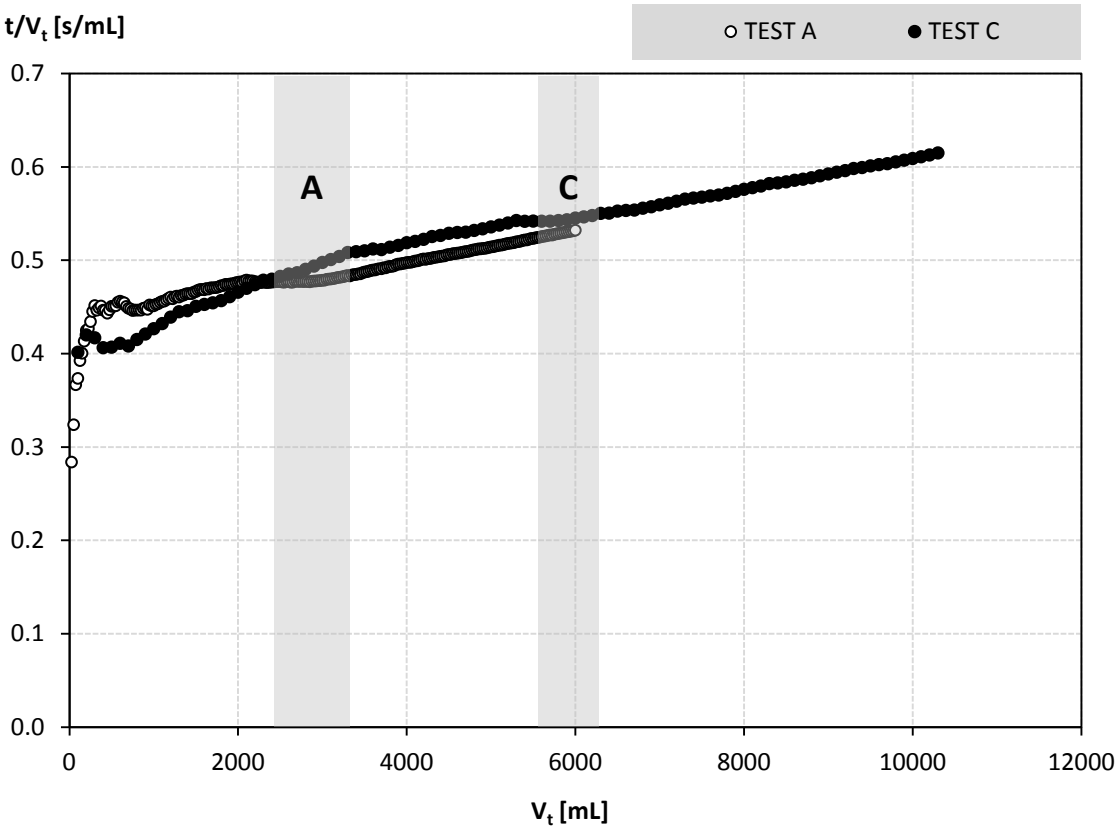

Figure 12. Filtration time *t* as a function of the volume of filtered water (V_t) for the experimental conditions "A" and "C". Relaxation areas "A" and "C" are highlighted in grey and correspond to test A and C, respectively.

Table 7. Linear regression parameters and *SRF* values evaluated on MBA/CYS-d<1mm in the experimental conditions "A" and "C".

TEST	LINEAR REGRESSION						*SRF* [m/kg]
	V_0 [mL]	V_f [mL]	t_0 [s]	t_f [s]	*m*	R^2	
A	3000	6000	1436	3194	$1.79 \cdot 10^{-5}$	0.999	0.027
C	6000	10300	3272	6335	$1.63 \cdot 10^{-5}$	0.999	0.021

B. Column filtration: evaluation of the breakthrough curve and of PAAH volume filtration abilities

Column tests on MBA/EDA, designed by using the Rapid Small Scale Column Tests (RSSCT) methodology, were performed in order to evaluate the shape of the breakthrough curve for copper removal, and thus the maximum loading ability of PAAH samples. The advantages of RSSCTs are that breakthrough curves can be obtained in a fraction of the time, with a fraction of the water, required for pilot tests. Theoretically, a RSSCT and full-scale adsorbent would have identical breakthrough curves, but in reality they differ based upon water quality, biological processes, or RSSCT

[1] Bonomo L. (2008). Trattamento delle acque reflue. McGraw-Hill.

scaling assumptions. RSSCT method utilizes dimensionless mathematical equations to scale down a full-scale adsorbent based upon similitude between solute transport mechanisms. The selection of the hydraulic loading (*v*) and of the Empty Bed Contact Time (*EBCT*) of the RSSCT is determined by considering those mechanisms that cause spreading in the mass transfer zone of a breakthrough curve (Crittenden et al, 1987; Westerhoff et al., 2005)[2]:

1) external mass transfer resistance or film transfer;
2) axial mixing resulting from dispersion;
3) internal or intraparticle mass transfer resistances (pore and surface diffusion).

The *EBCT* is determined by intraparticle mass transfer resistances and equation 5 can be used to scale down the *EBCT* of a Small Column (subscripts: "SC") from that of a Large Column (subscripts: "LC"); $d_{p,SC}$ and $d_{p,LC}$ are the adsorbent particle sizes of the media used for the small and the large column respectively, while t_{SC} and t_{LC} are the corresponding breakthrough times (Crittenden et al, 1991)[2].

$$\frac{EBCT_{SC}}{EBCT_{LC}} = \left[\frac{d_{p,SC}}{d_{p,LC}}\right]^{2-X} = \frac{t_{SC}}{t_{LC}} \qquad (5)$$

The exponent *X* defines the dependence of the intraparticle diffusion coefficient on particle size and two equations can be written based on different hypothesis (Crittenden et al, 1986; Crittenden et al, 1991)[2]:

- CONSTANT DIFFUSIVITY: if the intraparticle diffusivity do not change with particle size (X = 0), then exact similarity between small and large column effluent profiles can be maintained, and equation 6 assures that the amounts of spreading caused by intraparticle mass transfer resistances in the two column are identical in relation to the adsorbent length.

$$\frac{EBCT_{SC}}{EBCT_{LC}} = \left[\frac{d_{p,SC}}{d_{p,LC}}\right]^{2} = \frac{t_{SC}}{t_{LC}} \qquad (6)$$

- PROPORTIONAL DIFFUSIVITY: if the intraparticle diffusivity is proportional to particle size (X = 1), then the use of equation 7 assures that the amounts of spreading in the mass transfer zones of the RSSCTs and pilot columns caused by intraparticle diffusion resistances are identical.

$$\frac{EBCT_{SC}}{EBCT_{LC}} = \left[\frac{d_{p,SC}}{d_{p,LC}}\right] = \frac{t_{SC}}{t_{LC}} \qquad (7)$$

As for the evaluation of the hydraulic loading at the small scale (v_{SC}) once defined that at the large scale (v_{LC}), external mass transfer resistances and axial mixing caused by dispersion should be accounted in the spreading of the mass transfer zone. The Reynolds number is a dimensionless ratio of the inertial forces over the viscous forces in a fluid and the Schmidt number is a dimensionless ratio of the diffusion of momentum over the diffusion of mass. The product of the Reynolds number (*Re*) and the Schmidt number (*Sc*) can be used to determine the minimum Reynolds number for the RSSCT such that the effects of dispersion are not important. Dispersion is not important if the product of the Reynolds number and the Schmidt number is in the mechanical dispersion region from 200000-200 (Westerhoff et al., 2005)[2].

[2] Crittenden, J.C. (1986). Design of Rapid Small-Scale Adsorption Tests for a constant diffusivity. Journal of Water Pollution Control Federation 58(4), 312-319.

Crittenden J.C., J.K. Berrigan, D.W. Hand (1987). Design of rapid fixed-bed adsorption tests for non-constant diffusivities. Journal of Environmental Engineering 113(2), 243-259.

Crittenden J.C., S.R. Parimi, H. Arora, J. Trynoski, D.W. Hand, D.L. Perram, R.S. Summers (1991). Predicting GAC performance with rapid Small-Scale Column Tests. Journal of the American Water Works Association (AWWA) 83(1), 77-87.

Westerhoff P., D. Highfield, M. Badruzzaman, Y. Yoon (2005). Rapid Small-Scale Column Tests for arsenate removal in iron oxide packed bed columns. Journal of Environmental Engineering 131(2), 262-271.

If the Reynolds numbers for the small and large particles are set equal, an equal amount of spreading in the mass transfer zone caused by external mass transfer and dispersion in relation to the adsorbent length can be assured, as described in equation 8 (Crittenden et al, 1991)[2]:

$$\frac{v_{SC}}{v_{LC}} = \frac{d_{p,LC}}{d_{p,SC}} \quad (8)$$

However, it is difficult to maintain a similar amount of spreading, resulting from dispersion and external mass transfer between RSSCT and pilot columns. Since intraparticle diffusion resistance usually causes most of the spreading in the mass transfer zone, the amount of spreading caused by dispersion and external mass transfer can be reduced in the selection of the RSSCT hydraulic loading without affecting the RSSCT results. In order to reduce the pressure drop and RSSCT column length, equation 9 may be used to calculate v_{SC}, where $Re_{SC,min}$ is the minimum Reynolds number that guarantees the effects of dispersion and external mass transfer will not be greater in the RSSCT than in the large column (Crittenden et al, 1991; Westerhoff et al., 2005)[2].

$$\frac{v_{SC}}{v_{LC}} = \frac{d_{p,LC}}{d_{p,SC}} \cdot \frac{\mathrm{Re}_{SC,\min} \cdot Sc}{\mathrm{Re}_{LC} \cdot Sc} \quad (9)$$

Based on the knowledge achieved from results of previous experiments, equations 7 and 9 were used to derive $EBCT_{SC}$ and v_{SC} for pilot and laboratory scale column tests. As for equation 9, based on literature results, the two terms $Re_{SC,min} \cdot Sc$ and $Re_{LC} \cdot Sc$ were assumed to be 3300 and 10000 respectively.

PILOT SCALE COLUMN TEST

A pilot scale test (D_{SC} = 200 mm) was performed on MBA/EDA - 1mm<d<2mm (d_{SC} = 1.4 mm) in order to assess the possibility to use PAAH granular media in column processes, and to quantify the alteration of water parameters occuring during filtration. The experimental conditions for the small column were derived hypothesizing a large column (D_{LC} = 1500 mm), working in the following operating conditions:

- $EBCT_{LC}$ = 6 min;
- v_{LC} = 6 m/h;
- d_{LC} = 1.6 mm;

Starting from these data and using equations 7 and 9, the pilot scale column operated as follows:

- Empty bed contact time: $EBCT_{SC}$ = 5.3 min;
- Hydraulic loading: v_{SC} = 2.3 m/h;
- Water rate: Q = 71 L/h;
- Dried mass of MBA/EDA used: M_{PAAH} = 1693 kg;
- Effective height of the expanded bed in column: H_{eff} = 20 cm;
- Breakthrough time: t_B = 4 d (minimum duration of the test).

Water from a well located in the district of Lodi (IT) was used for the pilot test and water parameters were monitored on influent and effluent samples at different filtration times (t) in order to asses:

- the modification of the ionic balance: *pH*, electrical conductivity (*EC*), carbonate (CO_3^{2-}), bicarbonate (HCO_3^-), nitrate (NO_3^-), sulfate (SO_4^{2-}), chloride (Cl^-), potassium (K^+), sodium (Na^+), calcium (Ca^{2+}) and magnesium (Mg^{2+});
- the possible release of monomers or other chemical structures from MBA/EDA: Total Organic Carbon (*TOC*), total nitrogen (N_{TOT}), ammonium nitrogen (NH_4^+).

Results are shown in Table 8 along with the analytical methods used to quantify concentrations of parameters in water. it can be observed that no significant variations of water quality occurs during the process, except for sulfate and chloride ions that increase and decrease respectively, probably because of ion exchange reactions with MBA/EDA active groups.

Table 8. Water parameters measured on influent and effluent samples from a pilot scale column test. Analytical methods used are reported in footnotes.

PARAMETER	ANALYTICAL METHOD*	INFLUENT WATER	EFFLUENT WATER AFTER *t* HOURS						
			***t* = 2 h**	***t* = 18 h**	***t* = 20 h**	***t* = 22 h**	***t* = 64 h**	***t* = 68 h**	**t = 70 h**
pH [-]	1	7.11	7.13	7.12	7.28	7.27	7.32	7.42	7.48
EC at 20°C [µS/cm]	2	399	363	371	381	381	391	382	394
NO_3^- [mg/L]	3	<0.5	< 0.5	< 0.5	< 0.5	< 0.5	< 0.5	< 0.5	< 0.5
$SO_4^=$ [mg/L]	3	44.2	85.3	82.3	86.3	68.9	79.8	69.3	74.0
Cl^- [mg/L]	3	44.9	19.8	19.6	19.5	10.8	11.2	15.9	11.6
K^+ [mg/L]	4	2.84	2.83	2.82	2.88	2.85	2.88	2.85	2.79
Na^+ [mg/L]	4	8.57	8.44	8.39	8.42	8.42	8.49	8.51	8.30
Ca^{2+} [mg/L]	4	63.1	65.7	63.7	65.5	61.9	66.4	70.4	59.2
Mg^{2+} [mg/L]	4	14.9	15.0	14.8	15.0	15.0	14.8	15.2	14.6
TOC [mgC/L]	5	5.0	4.8	5.5	6.8	8.9	6.6	5.6	*NA***
NH_4^+ [mgN/L]	6	<0.01	< 0.01	< 0.01	< 0.01	< 0.01	< 0.01	< 0.01	< 0.01
N_{TOT} [mgN/L]	7	<1	< 1	< 1	< 2	< 1	< 1	< 1	NA
HCO_3^- [mg_{HCO3-}/L]	8	130	149	142	138	152	146	186	156
$CO_3^=$ [$mg_{CO3=}$/L]	8	<0.1	< 0.1	< 0.1	< 0.1	< 0.1	< 0.1	< 0.1	< 0.1

**Analytical methods: 1) APA- IRSA 2060, 2003; 2) APAT-IRSA 2030, 2003; 3) APAT-IRSA 4020, 2003; 4) APAT-IRSA 3010, 2003 + APAT-IRSA 3020, 2003; 5) APAT-IRSA 5040, 2003; 6) APA -IRSA 4030 A1, 2003; 7) APAT-IRSA 4020, 2003 + APAT-IRSA 4050, 2003 + APAT-IRSA 5030, 2003; 8) APAT- IRSA 2010 B, 2003*

*** NA: Not Available*

LABORATORY SCALE COLUMN AND BATCH TESTS

A laboratory scale column test on a glass chromatografy column (D_{SC} = 20 mm) was performed on MBA/EDA - d<1mm (d_{SC} = 0.686 mm) in order to derive the breakthrough curve for copper and thus the maximum copper loading per unit mass of hydrogel. Experimental conditions for the small column were derived assuming a large column (D_{LC} = 1500 mm) working in the following operating conditions:

- d_{LC} = 1.6 mm;
- $EBCT_{LC}$ = 6 min;
- v_{LC} = 5 m/h;

The small scale column was designed to operate in gravity, feeded with tap water at the starting copper concentration of 2 mg_{Cu}/L by means of a peristaltic pump and regulated downstream with the valve of the chromatografy column. Using equations 7 and 9, the operating parameters resulted to be:

- Empty bed contact time: $EBCT_{SC}$ = 2.6 min;
- Hydraulic loading: v_{SC} = 3.8 m/h;
- Water rate: Q = 20 mL/min;
- Dried mass of MBA/EDA used: M_{PAAH} = 14 g;
- Effective height of the expanded bed in column: H_{eff} = 15 cm;
- Breakthrough time: t_B = 1.8 d (minimum duration of the test).

The low permeability of the expanded media impeded the establishment of a regular flux of water through the bed of the column, thus resulting in the impossibility to run out the experiment.

For this reason, batch multi-step experiments were designed and performed on MBA/EDA in both particle sizes, powders (d<1mm) and grains (1mm<d<2mm); in fact it is possible to simulate, in batch condition, the continuous-flow conditions to which a unit volume of hydrogel is submitted when placed in a column system, thus determining the breakthrough curves for both MBA/EDA samples, as a function of bed volumes.
The batch multi-step procedure consisted in a sequence of trials during which the hydrogel sample is placed in contact (on jar test device at 120 rpm) with water (volume, V = 500 mL; solid to liquid ratio, S/L = 1/300 g_{PAAH}/mL) having the same contamination characteristics for each step (starting concentration, $C_{Cu,0}$ = 2 mg_{Cu}/L). At the end of each step equilibrium conditions were achieved (contact time, t_c = 60 minutes); then the hydrogel was separated by filtration (cellulose acetate filters, 0,45 µm) and re-suspended in a new contaminated solution following the same procedure of the previous step; 29 and 19 steps were conducted on MBA/EDA in the form of powders and grains was, corresponding, respectively, to a number of bed volumes (*BV*) of about 3000 and 10000. The separated solutions after each step were analyzed for the residual copper concentration[3], pH[4] and electrical conductivity[5].
Both samples were able to remove the almost the whole amount of copper provided to the mass of hydrogel along all steps; therefore saturation conditions were never achieved. The two tests were stopped because of the progressive increase in the turbidity of water, that negatively affected the separation of the mass of hydrogel at the end of each step. This phenomenon is probably related to precipitation reactions occurring during tests and involving ions and cations naturally occurring in tap water. An improvement in the experimental conditions adopted could enable the effective assessment of the breakthrough curve for both samples of MBA/EDA.

[3] Analytical method: Bathocuproine Method from Standard Method 3500-Cu(C); UNICAM VIS-UV 2 spectrophotometer used for absorbance measurements at 484 nm wavelength.

[4] Analytical method: IRSA 2080; pH-meter, model Eutech pH 5+ (Eutech Instruments).

[5] Analytical method: APAT-IRSA, 2003. Method 2030; conductivity meter model Eutech Cond 6+ (Eutech instruments).

Appendix 3

Methodology used for the prediction of Copper speciation in aqueous systems

In order to plot diagrams describing copper species distribution as a function of pH values, pH is set as the variable parameter and copper speciation is evaluated from 0 to 14 by using an incremental step of 0.25 pH units.
Different water models containing well-defined amounts of total copper, inorganic carbon and chloride are selected as for experiments described in Chapter 7; the following concentrations are thus fixed:

- Total copper molar concentration: *[Cu]*
- Total inorganic carbon molar concentration: $[CO_3]_{TOT}$
- Total chloride molar concentration: $[Cl^-]$

Since ultrapure water is used for tests and N_2 is blown on the surface of water during the experiments, the presence of dissolved oxygen $[O_2]$ is assumed to be negligible (specifically, it is used for computations a value of $1 \cdot 10^{-30}$ M).

A. Dissociation, solubility and complexation constants for species considered

Considering the divalent metal Cu^{2+}, and the aqueous systems selected for experiments reported in Chapter 7, the inorganic ligands that may form important ionic compounds or complexes are: OH^-, $CO_3^{=}$ and Cl^-. Once identified all the species considered, dissociation, solubility and complexation constants are listed.

Water dissociation constant: $K_w = [H^+] \cdot [OH^-] = 1 \cdot 10^{-14}$ $pK_w = 14$

First dissociation constants of carbonic acid: $K_{a1} = \frac{[H^+] \cdot [HCO_3^-]}{[H_2CO_3^*]} = 4.3 \cdot 10^{-7}$ $pK_{a1} = 6.37$

Second dissociation constant of carbonic acid: $K_{a2} = \frac{[H^+] \cdot [CO_3^=]}{[HCO_3^-]} = 4.7 \cdot 10^{-11}$ $pK_{a2} = 10.33$

Solubility product constants ($K_{sp,j}$) for the generic ionic compound *j*. Table 6 reports constants values for the main ionic compound of interests.

$$M_xA_{y(s)} \rightleftarrows x \cdot M^{y+}_{(aq)} + y \cdot A^{x-}_{(aq)}$$

$$K_{sp,j} = [M^{y+}]^x \cdot [A^{x-}]^y$$

Table 9. Solubility product constants for the selected ionic compounds.

IONIC COMPOUND *(j)*	$K_{sp,j}$	$pK_{sp,j}$
$Cu(OH)_2$	$4.4 \cdot 10^{-20}$	19.36
CuO	$4.2 \cdot 10^{-21}$	20.38
$CuCO_3$	$2.3 \cdot 10^{-10}$	9.63
$Cu_2(OH)_2CO_3$	$6.6 \cdot 10^{-34}$	33.18

Stability constants for the formation of complexes are reported in Table 10: β_i is referred to the generic metal-ligand complexation reaction in which the complex containing *i* ligands is formed from the metal ion, *i* ligands L and, eventually, *h* hydrogen ions H^+.

$$m \cdot M + i \cdot L + h \cdot H \rightleftarrows M_m L_i H_h$$

$$\beta_i = \frac{[M_m L_i H_h]}{[M]^m \cdot [L]^i \cdot [H^+]^h}$$

Table 10. Complexation constants for the creation of Cu-complexes.

Ligand	Number of Ligands (*i*)	Number of $[H^+]$ (*h*)	β_i	$Log(\beta_i)$
$[OH^-]$	1	0	$1.0 \cdot 10^{6}$	6.00
	2	0	$2.1 \cdot 10^{14}$	14.32
	3	0	$1.3 \cdot 10^{15}$	15.10
	4	0	$2.5 \cdot 10^{16}$	16.40
$[CO_3^=]$	1	0	$5.4 \cdot 10^{6}$	6.73
	2	0	$6.8 \cdot 10^{9}$	9.83
	1	1	$4.0 \cdot 10^{13}$	13.60
$[Cl^-]$	1	0	2.7	0.43
	2	0	1.5	0.16
	3	0	$5.1 \cdot 10^{-3}$	-2.29
	4	0	$2.6 \cdot 10^{-5}$	-4.59

B. System of equations implemented

EVALUATION OF FREE LIGAND CONCENTRATIONS FOR EACH pH VALUE

Since, in aqueous solutions, the amounts of hydroxide and carbonate species is determined by the presence of hydrogen ions $[H^+]$, concentrations are estimated for each value of pH; the total chloride molar concentration $[Cl^-]$ is fixed for each experiments and not affected by pH values.

Hydroxide molar concentration:

$$[OH^-] = \frac{[K_w]}{[H^+]} = \frac{[K_w]}{[10^{-pH}]}$$

Total carbonate molar concentration:

$$[CO_3]_{TOT} = [H_2CO_3] + [HCO_3^-] + [CO_3^=]$$

Fraction of carbonic acid:

$$\alpha_0 = \frac{[H_2CO_3]}{[CO_3]_{TOT}} = \frac{[H^+]^2}{[H^+]^2 + K_{a1} \cdot [H^+] + K_{a1} \cdot K_{a2}}$$

Carbonic acid molar concentration:

$$[H_2CO_3] = \alpha_0 \cdot [CO_3]_{TOT}$$

Fraction of carbonate ion:

$$\alpha_1 = \frac{[HCO_3^-]}{[CO_3]_{TOT}} = \frac{K_{a1} \cdot [H^+]}{[H^+]^2 + K_{a1} \cdot [H^+] + K_{a1} \cdot K_{a2}}$$

Carbonate ion molar concentration: $[HCO_3^-] = \alpha_1 \cdot [CO_3]_{TOT}$

Fraction of hydrogen carbonate ion: $\alpha_2 = \frac{[CO_3^=]}{[CO_3]_{TOT}} = \frac{K_{a1} \cdot K_{a2}}{[H^+]^2 + K_{a1} \cdot [H^+] + K_{a1} \cdot K_{a2}}$

Hydrogen carbonate ion molar concentration: $[CO_3^=] = \alpha_2 \cdot [CO_3]_{TOT}$

EVALUATION OF COPPER SOLUBILITY LIMIT FOR EACH pH VALUE

Maximum dissolved copper ion concentrations $[Cu^{2+}]_j$ above which precipitation occurs for a specific ionic compounds *j* are evaluated at varying of pH values.

Maximum Cu^{2+} concentrations for $Cu(OH)_2$ $[Cu^{2+}]_{Cu(OH)_2} = \frac{K_{sp,Cu(OH)_2}}{[OH^-]^2}$

Maximum Cu^{2+} concentrations for CuO $[Cu^{2+}]_{CuO} = \frac{K_{sp,CuO}}{[O_2]}$

Maximum Cu^{2+} concentrations for $CuCO_3$ $[Cu^{2+}]_{Cu(CO)_3} = \frac{K_{sp,Cu(CO)_3}}{[CO_3^=]}$

Maximum Cu^{2+} concentrations for $Cu_2(OH)_2CO_3$ $[Cu^{2+}]_{Cu_2(OH)_2CO_3} = \sqrt{\frac{K_{sp,Cu_2(OH)_2CO_3}}{[OH^-]^2 \cdot [CO_3^=]}}$

The maximum dissolved copper ion concentration $[Cu^{2+}]_{LIM,SOL}$ above which precipitation occurs considering all the ionic compounds, is defined for each pH values by selecting the minimum value among maximum Cu^{2+} concentrations, evaluated for each selected compound.

EVALUATION OF COPPER COMPLEXES SPECIATION FOR EACH pH VALUE

Considering the generic copper complexes listed in par. A and their corresponding constants, the ratio between the copper complexes molar concentration and the total dissolved copper molar concentration $[Cu^{2+}]$, is evaluated for each selected ligand L, at varying of pH values.

$$\frac{[Cu-L]}{[Cu^{2+}]} = \sum_i \beta_{L,i} \cdot [L]^i$$

Factor *f* is then defined as the sum of all dissolved copper species (complexes and divalent ion) molar concentrations divided by $[Cu^{2+}]$, that can be thus evaluated for each pH value.

$$f = 1 + \frac{[Cu-OH] + [Cu-CO_3] + [Cu-Cl]}{[Cu^{2+}]}$$

$$[Cu^{2+}] = \frac{[Cu]}{f}$$

By selecting, for each pH value, the minimum value between $[Cu^{2+}]_{LIM,SOL}$ and $[Cu^{2+}]$, the effective dissolved copper concentration $[Cu^{2+}]_{EFF}$ that take into account the solubility of copper compounds is evaluated.

Molar concentrations of copper complexes are thus recalculated using the effective dissolved copper concentration; the total dissolved copper concentration $[Cu^{2+}]_{DISS}$, and the precipitated copper concentration $[Cu^{2+}]_{PREC}$, can be also evaluated.

Chloride complexes molar concentration: $$[Cu-Cl] = [Cu^{2+}]_{EFF} \cdot \sum_i \beta_{Cl,i} \cdot [Cl^-]^i$$

Hydroxide complexes molar concentration: $$[Cu-OH] = [Cu^{2+}]_{EFF} \cdot \sum_i \beta_{OH,i} \cdot [OH^-]^i$$

Carbonate complexes molar concentration: $$[Cu-CO_3] = [Cu^{2+}]_{EFF} \cdot \sum_i \beta_{CO_3,i} \cdot [CO_3^=]^i$$

Total dissolved copper concentration: $$[Cu^{2+}]_{DISS} = [Cu^{2+}]_{EFF} + [Cu-Cl] + [Cu-OH] + [Cu-CO_3]$$

Total precipitated copper concentration: $$[Cu^{2+}]_{PREC} = [Cu] - [Cu^{2+}]_{DISS}$$